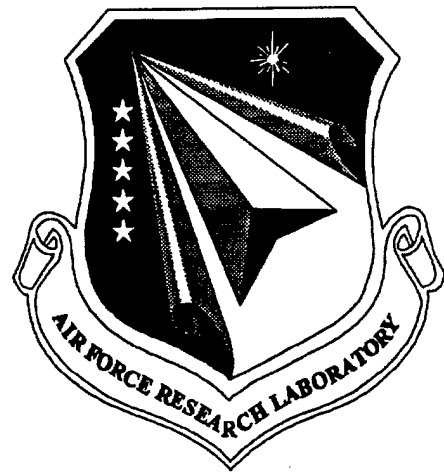


AFRL-VA-WP-TR-1999-3057

**MODULAR CONTROL LAW DESIGN FOR
THE INNOVATIVE CONTROL
EFFECTORS (ICE) TAILLESS FIGHTER
AIRCRAFT CONFIGURATION 101-3**



JAMES M. BUFFINGTON

**AIR FORCE RESEARCH LABORATORY
AIR VEHICLES DIRECTORATE
WRIGHT-PATTERSON AFB, OH 45433-7542**

JUNE 1999

FINAL REPORT FOR 05/01/1997 – 05/01/1999

APPROVED FOR PUBLIC RELEASE; DISTRIBUTION UNLIMITED

**AIR VEHICLES DIRECTORATE
AIR FORCE RESEARCH LABORATORY
AIR FORCE MATERIEL COMMAND
WRIGHT-PATTERSON AIR FORCE BASE OH 45433-7542**

DTIC QUALITY INSPECTED 3

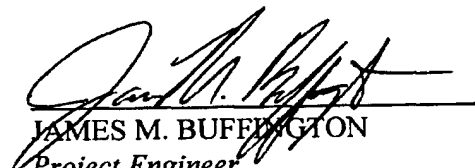
20000322 089


NOTICE


WHEN GOVERNMENT DRAWINGS, SPECIFICATIONS, OR OTHER DATA ARE USED FOR ANY PURPOSE OTHER THAN IN CONNECTION WITH A DEFINITE GOVERNMENT-RELATED PROCUREMENT, THE UNITED STATES GOVERNMENT INCURS NO RESPONSIBILITY OR ANY OBLIGATION WHATSOEVER. THE FACT THAT THE GOVERNMENT MAY HAVE FORMULATED OR IN ANY WAY SUPPLIED THE SAID DRAWINGS, SPECIFICATIONS, OR OTHER DATA, IS NOT TO BE REGARDED BY IMPLICATION, OR OTHERWISE IN ANY MANNER CONSTRUED, AS LICENSING THE HOLDER, OR ANY OTHER PERSON OR CORPORATION; OR AS CONVEYING ANY RIGHTS OR PERMISSION TO MANUFACTURE, USE, OR SELL ANY PATENTED INVENTION THAT MAY IN ANY WAY BE RELATED THERETO.

THIS REPORT IS RELEASABLE TO THE NATIONAL TECHNICAL INFORMATION SERVICE (NTIS). AT NTIS, IT WILL BE AVAILABLE TO THE GENERAL PUBLIC, INCLUDING FOREIGN NATIONALS.

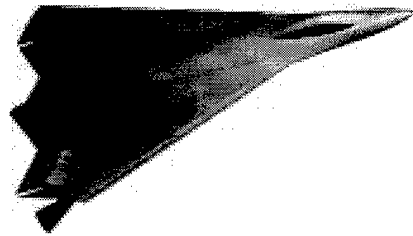
THIS TECHNICAL REPORT HAS BEEN REVIEWED AND IS APPROVED FOR PUBLICATION.


JAMES M. BUFFINGTON
Project Engineer
Flight Dynamics and Control Branch


DIETER MULTHOPP, Actg Chief
Flight Dynamics and Control Branch
Aeronautical Sciences Division


JAMES L. RUDD, Chief
Aeronautical Sciences Division
Air Vehicles Directorate

REPORT DOCUMENTATION PAGE			Form Approved OMB No. 0704-0188	
<small>Public reporting burden for this collection of information is estimated to average 1 hour per response, including the time for reviewing instructions, searching existing data sources, gathering and maintaining the data needed, and completing and reviewing the collection of information. Send comments regarding this burden estimate or any other aspect of this collection of information, including suggestions for reducing this burden, to Washington Headquarters Services, Directorate for Information Operations and Reports, 1215 Jefferson Davis Highway, Suite 1204, Arlington, VA 22202-4302, and to the Office of Management and Budget, Paperwork Reduction Project (0704-0188), Washington, DC 20503.</small>				
1. AGENCY USE ONLY (Leave blank)	2. REPORT DATE JUNE 1999	3. REPORT TYPE AND DATES COVERED FINAL REPORT FOR 05/01/1997 - 05/01/1999		
4. TITLE AND SUBTITLE MODULAR CONTROL DESIGN FOR THE INNOVATIVE CONTROL EFFECTORS (ICE) TAILLESS FIGHTER AIRCRAFT CONFIGURATION 101-3		5. FUNDING NUMBERS C IN-HOUSE PE 61102 PR 2304 TA N2 WU 01		
6. AUTHOR(S) JAMES M. BUFFINGTON				
7. PERFORMING ORGANIZATION NAME(S) AND ADDRESS(ES) AIR FORCE RESEARCH LABORATORY AIR VEHICLES DIRECTORATE WRIGHT-PATTERSON AFB, OH 45433-7542		8. PERFORMING ORGANIZATION REPORT NUMBER		
9. SPONSORING/MONITORING AGENCY NAME(S) AND ADDRESS(ES) AIR VEHICLES DIRECTORATE AIR FORCE RESEARCH LABORATORY AIR FORCE MATERIEL COMMAND WRIGHT-PATTERSON AFB, OH 45433-7542 POC: SIVA S. BANDA, AFRL/VAAD, 937-255-8677		10. SPONSORING/MONITORING AGENCY REPORT NUMBER AFRL-VA-WP-TR-1999-3057		
11. SUPPLEMENTARY NOTES				
12a. DISTRIBUTION AVAILABILITY STATEMENT APPROVED FOR PUBLIC RELEASE, DISTRIBUTION UNLIMITED.			12b. DISTRIBUTION CODE	
13. ABSTRACT (Maximum 200 words) A modular flight control system is developed for a tailless fighter aircraft with innovative control effectors. Dynamic inversion control synthesis is used to develop a full envelope flight control law. Minor dynamic inversion command variable revisions are required due to the tailless nature of the configuration studied to achieve nominal stability and performance. Structured singular value and simulation analysis shows that robust stability is achieved and robust performance is slightly deficient due to modeling errors. A multi-branch linear programming-based method is developed and used for allocation of redundant limited control effectors.				
14. SUBJECT TERMS Tailless Fighter, Flight Control, Control Allocation, Dynamic Inversion			15. NUMBER OF PAGES 150	
			16. PRICE CODE	
17. SECURITY CLASSIFICATION OF REPORT UNCLASSIFIED	18. SECURITY CLASSIFICATION OF THIS PAGE UNCLASSIFIED	19. SECURITY CLASSIFICATION OF ABSTRACT UNCLASSIFIED	20. LIMITATION OF ABSTRACT SAR	



Modular Control Law Design
for the
Innovative Control Effectors (ICE)
Tailless Fighter Aircraft
Configuration 101-3

James M. Buffington
Aerospace Engineer
Air Force Research Laboratory
AFRL/VAAD
Wright Patterson AFB, OH
james.buffington@va.af.mil
937-255-3734

20 May 99

Contents

1	Introduction	2
2	Background	4
2.1	ICE Configuration 101-3	4
2.1.1	Control Effectors	4
2.1.2	Simulation Model	4
2.2	Dynamic Inversion Flight Control Theory	6
3	Flight Control Structure	9
3.1	Command Shaping	10
3.1.1	Stick Gradient	10
3.1.2	Command Limiter	10
3.1.3	Command Filter	10
3.2	Feedback and Feedforward Augmentation	11
3.3	Control Allocation	12
3.3.1	Single-branch Control Allocation	13
3.3.2	Multi-branch Control Allocation	14
3.4	On-board Model	17
3.4.1	Requirements Model	17
3.4.2	Configuration Model	21
3.5	Model Error Compensation	42
4	Flight Control Law Analysis	43
4.1	Nominal Stability	44
4.2	Flying qualities	47
4.3	Robustness	49
4.4	Batch simulation	52
4.4.1	Control Allocation Mode Verification Analysis	54
4.4.2	Final control law analysis	97
4.5	Piloted simulation	146
5	Conclusions	147

Chapter 1

Introduction

The main objectives of this study were to develop a re-usable flight control law, advance control allocation technology and apply the control law to a challenging configuration. A modular flight control architecture is designed that will maximize software reusability for future control law development efforts and allow efficient advanced technology insertion as it becomes available. A control allocation method is developed that optimally utilizes all available control power without violating actuator limits. A tailless fighter configuration was chosen for application due to the operational benefits and flight control law development challenges inherent in a tailless configuration [6].

A modular flight control system design approach is used so that promising technologies from feedback control synthesis and control allocation may be evaluated interchangeably without complete control system re-design. The control law is based upon feedback linearization or dynamic inversion control theory and follows closely with the MACH control philosophy in the MCT guidelines [25].

Control allocation algorithms must efficiently use nonlinear multi-axes control effectors to achieve current maneuverability requirements of fighter aircraft. The control allocation method should exploit control effector redundancy to optimize mission segment objectives such as minimize drag or wing loads. The control allocation must also optimize large command response and prevent departures. Although not specifically addressed in this study, low computational requirements is a very important characteristic of the control allocation method. A tradeoff exists between control allocation computational efficiency and performance, and tools exist to analyze this tradeoff [24]. Computational efficiency provisions have been added to existing methods [16] at the expense of performance. The control allocation method developed in this study is a refined version a linear program based method [10] which optimally exploits effector redundancy, optimizes large command aircraft response and uses all the available control power.

Tailless aircraft configurations have gained recent support due to inherent increase in stealth and decreases in weight and drag. Flight control challenges for this configuration include multi-axes instabilities and nonlinear control effectors. The operational advantages and the flight control challenges drove the current study toward a tailless fighter configuration

[23, 6].

This document is organized as follows. Chapter 2 describes background material regarding the aircraft configuration and dynamic inversion control theory as it applies to flight control. Chapter 3 contains a modular flight control law that is applied to the tailless aircraft configuration in Chapter 2. Chapter 4 provides a detailed analysis of the tailless aircraft flight control law. Chapter 5 summarizes the most important results and conclusions of the flight control development and analysis.

Chapter 2

Background

2.1 ICE Configuration 101-3

The vehicle in this study is a tailless fighter configuration developed under the Innovative Control Effectors (ICE) program [15]. Although there were multiple configurations studied in the ICE program, only configuration 101-3 was chosen in the current study to evaluate an advanced control law. Configuration 101-3 was the most promising from an aerodynamic perspective while being the most challenging from a control law development perspective. The ICE configuration 101-3 is shown in Figure 2.1.

2.1.1 Control Effectors

The control effectors for configuration 101-3 include elevons, pitch flaps, all moving tips, thrust vectoring, spoiler slot deflectors, and outboard leading edge flaps. The conventional control effectors are defined as the elevons, pitch flap and leading edge flaps. The innovative control effectors are defined as the thrust vectoring, all moving tips and spoiler slot deflectors. Pitch and yaw thrust vector coupling results from the non-rectangular nature of the thrust vector limits. The challenges of the all moving tips and spoiler slot deflectors are zero lower deflection limits, strong multi-axes effects and effector interactions.

2.1.2 Simulation Model

A generic simulation environment is used for ICE configuration simulation model development. The simulation model contains ordinary differential equations of the aircraft dynamics of the following form

$$\dot{X} = f(X, u^c) \quad (2.1)$$

where X are the aircraft states, including actuator states, and u^c are the control effector commands. The right hand side of the differential equations ($f(X, u)$) is computed using the aerodynamic model developed from Phase I wind tunnel experiments, a static engine model, actuator models and a standard atmosphere model. Although sensor noise, turbulence and

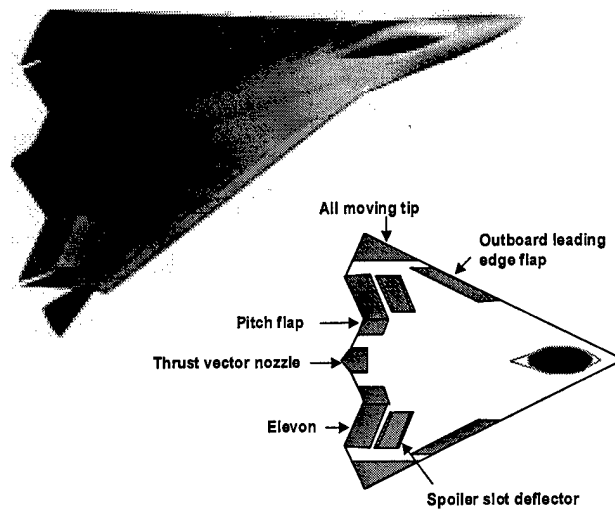


Figure 2.1: ICE Configuration 101-3

Table 2.1: Actuator data

Effector	Upper deflection limit	Lower deflection limit	No-load rate limit	Phase crossover frequency
δ_{elev}	30 deg	-30 deg	150 $\frac{deg}{sec}$	62 $\frac{rad}{sec}$
δ_{pflap}	30 deg	-30 deg	50 $\frac{deg}{sec}$	62 $\frac{rad}{sec}$
δ_{amt}	60 deg	0 deg	150 $\frac{deg}{sec}$	62 $\frac{rad}{sec}$
δ_{tv}	15 deg	0 deg	60 $\frac{deg}{sec}$	30 $\frac{rad}{sec}$
δ_{ssd}	60 deg	0 deg	150 $\frac{deg}{sec}$	62 $\frac{rad}{sec}$
$\delta_{obl f}$	40 deg	0 deg	40 $\frac{deg}{sec}$	62 $\frac{rad}{sec}$

gusts are also modeled, no results are presented since only a cursory analysis was completed with these effects.

The ICE program [15] developed hinge moment data which was used to size the actuators. However, simulation analysis showed that maximum hinge moments were exceeded during high speed maneuvering. The all moving tip pivot axis was initially located such that effector hard-overs resulted if maximum hinge moments were exceeded. The hinge moment effects were neglected in this study due to the need of a more rigorous actuator sizing and all moving tip pivot location analysis. The simulation model of each control effector actuator included fourth order dynamical models with deflection and rate limits. The properties of each actuator are given in Table 2.1.

The thrust vector nozzle deflection limits are conical about the zero deflection engine centerline. Note the low phase crossover frequency of the thrust vector nozzle actuator.

2.2 Dynamic Inversion Flight Control Theory

The aircraft rigid body equations of motion in eq.(2.1) may be approximated by ordinary differential equations that are affine in the control if actuator dynamics and control effector interactions are neglected

$$\dot{x} = a(x) + b(x)u \quad (2.2)$$

where $x \in \mathbb{R}^{n_x}$ are the states (excluding actuator states), $u \in \mathbb{R}^m$ are the control effector deflections (or actuator states) and $a(x)$ and columns of $b(x)$ are smooth vector fields on \mathbb{R}^n . All rigid body states are typically measured and available for feedback control.

A set of feedback control command variables is defined as a generally nonlinear function of the states

$$y = c(x) \quad (2.3)$$

where $y \in \mathbb{R}^{n_y}$ is the vector of command variables. It is assumed that there are at least as many controls as command variables, i.e. $m \geq n_y$. There are typically at least 3 controls for the 3 command variables for manual flight control. It is assumed that the command variables in eq.(2.3) for the system in eq.(2.2) have a well-defined vector relative degree with unity

elements $\{r_1, \dots, r_{n_y}\} = \{1, \dots, 1\}$. Typically each manual flight control command variable has unity relative degree, however the theory is easily extended for other than unity relative degree. Given these assumptions, there always exists a diffeomorphic state transformation to the following convenient form

$$\begin{bmatrix} \dot{z} \\ \dot{y} \end{bmatrix} = \begin{bmatrix} a_z(z, y) \\ a_y(z, y) \end{bmatrix} + \begin{bmatrix} b_z(z, y) \\ b_y(z, y) \end{bmatrix} u \quad (2.4)$$

where z are the uncommanded states. A well-defined vector relative degree implies that time derivatives of all command variables are affected by at least one control and that b_y has rank equal to n_y . It is further assumed that each control affects at least one command variable time derivative which is typical for manual flight control.

The feedback linearization or dynamic inversion control law has two main parts listed below

$$\begin{aligned} u &= \rho(d_y) \\ d_y &= -a_y(z, y) + v(y, y^{cmd}). \end{aligned} \quad (2.5)$$

The first part is the control allocation (ρ) which is a mapping from generalized controls (d_y) to actual controls (u) such that the following relationship holds

$$b_y(z, y)\rho(d_y) = d_y. \quad (2.6)$$

The second part is the generalized control law. This part consists of deaugmentation of the natural command variable dynamics ($-a_y(z, y)$) and augmentation of some desired command variable dynamics ($v(y, y^{cmd})$) that depend on the control system requirements. The reference command vector is y^{cmd} .

The nominal closed loop is defined by the following system with a cascade structure

$$\begin{aligned} \begin{bmatrix} \dot{z} \\ \dot{y} \end{bmatrix} &= \begin{bmatrix} f_z(z, y) \\ v(y, y^{cmd}) \end{bmatrix} \\ f_z(z, y) &\equiv a_z(z, y) + b_z(z, y)\rho(-a_y(z, y) + v(y, y^{cmd})) \end{aligned} \quad (2.7)$$

It may be shown [26] that this system is asymptotically stable if the command variable subsystem (y) is asymptotically stable and the complementary subsystem (z) is asymptotically stable on the zero command variable manifold which is equivalent to asymptotic stability of the following system

$$\dot{z} = a_z(z, 0) + b_z(z, 0)\tilde{u}(z) \quad (2.8)$$

where $\tilde{u}(z)$ is the control that maintains zero command variables

$$\tilde{u}(z) = \{u | a_y(z, 0) + b_y(z, 0)u = 0\}. \quad (2.9)$$

Note that the system in eq.(2.8) is often referred to as the zero dynamics, and asymptotic stability of the zero dynamics is equivalent to the minimum phase property. Further note

that asymptotic stability of the command variable dynamics is guaranteed by choosing a stabilizing $v(y, y^{cmd})$.

Stability of the zero dynamics depends on the choice of command variables in eq.(2.3). There are methods to choose the command variables to optimize stability robustness of the zero dynamics [27]. However, the choice of the command variables also affect disturbance rejection and robustness. A command variable choice that optimally rejects disturbances in the presence of uncertainties may result in unstable zero dynamics. In flight control, the zero dynamics are typically stable for an optimal robust disturbance rejection choice of the command variables.

Chapter 3

Flight Control Structure

The proposed flight controller (MODCON) for the ICE aircraft in Section 2.1 is shown in Fig. 3.1.

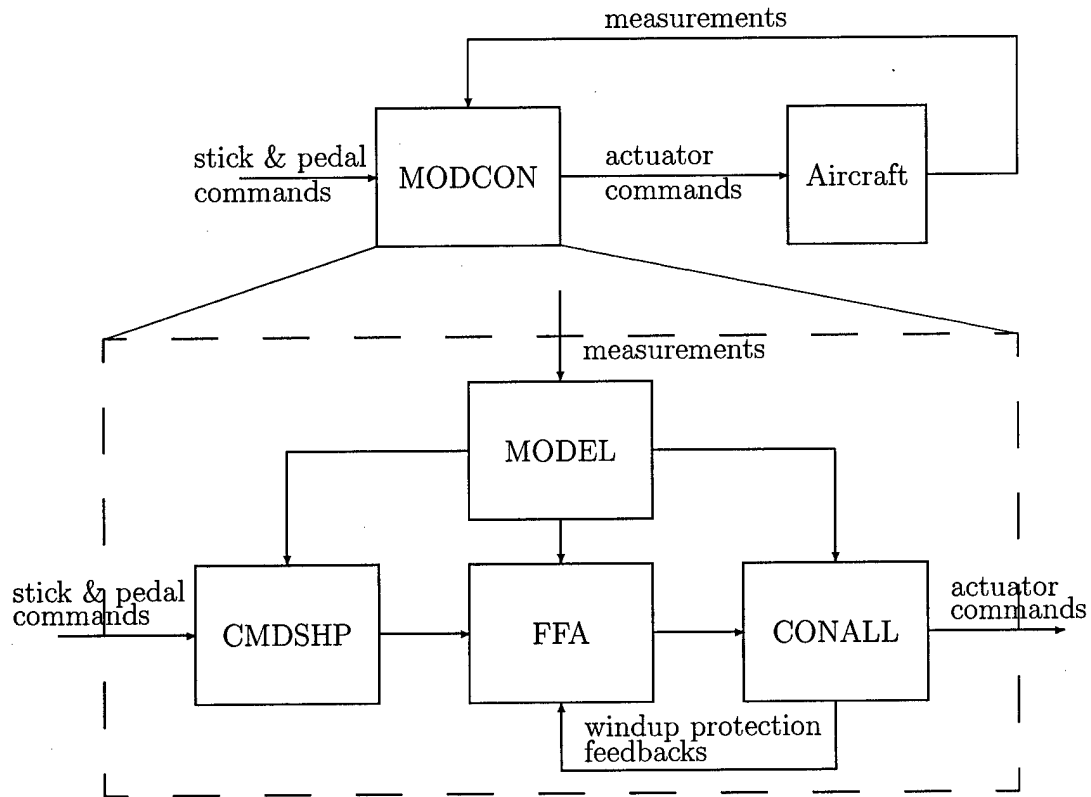


Figure 3.1: Controller Structure

It has a modular structure that encourages insertion of independent technology advances

in feedback control, modeling and control allocation. The aircraft MODEL module provides vehicle specific data, such as stability and control derivatives, and requirements data, such as desired bandwidths, to all other control law modules. The feedback and feedforward augmentation (FFA) module generates control law commands that provide desired stability and flying qualities properties in a manner that is robust to uncertainties. The control allocation (CONALL) module computes actuator commands that optimize a mission segment objective for achievable control law commands and optimally limits unachievable control law commands. The command shaping (CMDSP) module provides proper feedforward characteristics such as stick force gradients, command limiters and command filters.

3.1 Command Shaping

The command shaping module provides appropriate command augmentation properties. The F-16 was used as a requirements baseline. Therefore, a similar side stick shaping structure to the F-16 was used for the ICE aircraft. The command shaping module consists of three sub-modules: stick gradient, command limiter and command filter. The stick force gradient maps force inputs in pounds to CV commands in degrees per second. The command limiter restricts the CV commands to help prevent departure. The command filter provides desired transient command response.

3.1.1 Stick Gradient

The stick gradient provides desirable mappings between pilot stick/pedal forces and flight control commands. The piece-wise linear structure for the stick and pedal gradients is shown in Fig.(3.2). The gradient parameters for each axis are supplied by the on-board model and are given in Section 3.4.

3.1.2 Command Limiter

Only a cursory design of the command limiter was completed due to time limitations. The command limits were chosen to be of the following form

$$CV_{max} = \min(k_1 \bar{q}, k_2) \quad (3.1)$$

where \bar{q} is the dynamic pressure. The command limit parameters (k_1, k_2) for each axis are supplied by the on-board model and are given in Section 3.4.

3.1.3 Command Filter

The command filter in each control channel has the following first-order form

$$y = \frac{\frac{2}{\omega_c} s + 1}{\frac{1}{\omega_{fq}} s + 1} y^{cmd} \quad (3.2)$$

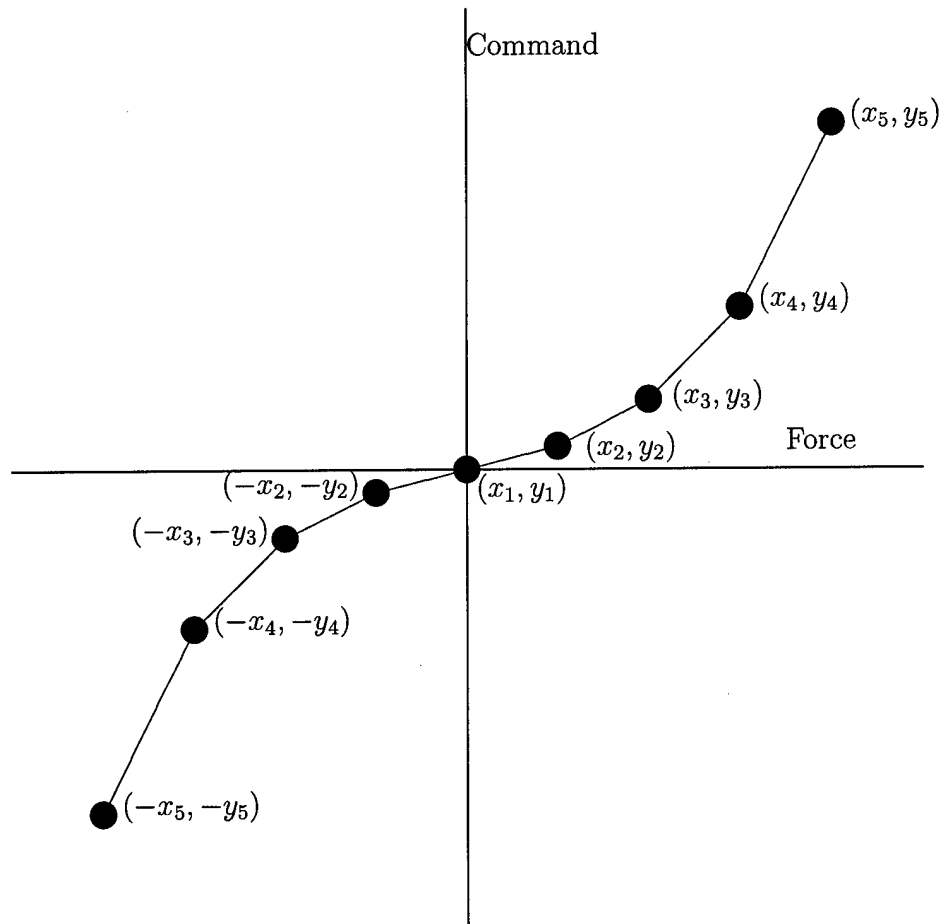


Figure 3.2: Stick Gradient Structure

where ω_c is the desired feedback control bandwidth and ω_{fq} is the desired flying qualities command bandwidth. The command bandwidth ω_{fq} allows the capability of fast command response without sacrificing closed loop stability margins. The command filter parameters for each axis are supplied by the on-board model and are given in Section 3.4.

3.2 Feedback and Feedforward Augmentation

Dynamic inversion synthesis [10, 22] is used for feedback and feedforward augmentation. Dynamic inversion consists of deaugmentation of the natural dynamics of a specified set of command variables followed by robust feedback stability augmentation and feedforward command variable augmentation. The generalized dynamic inversion control law is developed

in Section 2.2 and is given by

$$\begin{aligned} d_y^{des} &= -a_y(x) + v(y, y^{cmd}) \\ v(y, y^{cmd}) &= \omega_c x_i - \omega_c y + \omega_c f_c y^{cmd} \\ \dot{x}_i &= -\omega_c f_i y + \omega_c f_i y^{cmd} \end{aligned} \quad (3.3)$$

where y are the command variables, d_y^{des} are the generalized control commands, $-a_y(x)$ is the deaugmentation part and $v(y, y^{cmd})$ represents the augmentation part which consists of proportional-integral stability augmentation and command augmentation. Dynamic inversion inverts the command variable dynamics and proportional/integral feedback generates a desired robust loop shape. Proportional gains are used in the feedforward path to obtain desirable flying qualities. Note that y^{cmd} is the reference command that is to be tracked by the command variables. The augmentation parameters are supplied by the on-board model and are given in Section 3.4.

3.3 Control Allocation

By design, the control law in eq.(3.3) provides desired loop and command response properties in terms of d_y^{des} , however the reduced dimension controls (d_y^{des}) must still be resolved into actual control effector commands (u^c). The control allocation function in eq.(2.5) provides the mapping from reduced dimension controls to actual control commands, $u^c = \rho(d_y^{des})$. The control allocation module computes actuator commands that achieve the desired control law command if possible, or a limited control law command if necessary, to satisfy actuator limits.

The control allocation problem has been stated many times in various forms [18, 30, 11, 25, 10, 20]. The unlimited control allocation problem is to find u such that $B_y u = d_y^{des}$ for all d_y^{des} . For redundant control effector suites, there are many solutions to this unlimited control allocation problem. A unique solution is found by introducing a performance index that forces the redundant effectors to satisfy additional objectives such as minimal radar cross section, drag, or wing loads. However, since there are limits on the control effectors, not all d_y^{des} are achievable. Therefore, d_y^{des} may need to be clipped or limited such that $u = \rho(d_y^{des})$ does not violate actuator limits.

Past control allocation research includes algorithms that minimize control deflections [11] or drag [17] and limit unachievable control law commands by preserving its direction [1, 18, 4]. However, it has been shown that preserving the direction of the command may unnecessarily degrade flying qualities [10].

This section poses the control allocation problem as a nonlinear constrained optimization problem. Simplifying assumptions are stated, and the control allocation problem is transformed into a standard linear program. An algorithm is designed to solve the constrained control allocation problem using a linear program solver as its basis.

3.3.1 Single-branch Control Allocation

The control allocation problem with no actuator limits, or unlimited control allocation problem, may be cast into the following optimization problem with a nonlinear objective and linear equality constraints that enforce the control law command

$$\min_u J = f(u) \text{ subject to } B_y u = d_y^{des}. \quad (3.4)$$

Analytical solutions exist to the problem in eq.(3.4) for certain forms of the objective. For example, a quadratic objective results in the common generalized right inverse

$$\begin{aligned} J &= \frac{1}{2} (u - u_{pref})^T W (u - u_{pref}) \\ u^c &= W^{-1} B_y^T (B_y W^{-1} B_y^T)^{-1} (d_y^{des} - B_y u_{pref}) + u_{pref} \end{aligned} \quad (3.5)$$

Limits on the actuators complicate the solution of the control allocation problem. Nonlinear inequality constraints are added to prohibit violation of actuator limits

$$\begin{aligned} \min_u J &= f(u) \\ \text{subject to } &\begin{cases} B_y u = d_y^{des} \\ \underline{u} \leq u \leq \bar{u} \end{cases} \end{aligned} \quad (3.6)$$

Rate and position limits are accounted for by defining \underline{u} and \bar{u} as the most restrictive actuator constraints

$$\begin{aligned} \bar{u} &= \min(u_u, \Delta T u_r) \\ \underline{u} &= \max(u_l, -\Delta T u_r) \end{aligned} \quad (3.7)$$

where u_u is the actuator upper position limit vector, u_l is the actuator lower position limit vector, u_r is the no-load actuator rate limit vector and ΔT is the digital flight control system update rate.

As stated, the problem in eq.(3.6) may be infeasible since there is no guarantee that the equality constraints can be satisfied in the presence of the inequality constraints. Additional constraints may be added to insure feasibility

$$\begin{aligned} \min_{u, \lambda} J &= f(u) - \lambda \\ \text{subject to } &\begin{cases} B_y u = \lambda d_y^{des} \\ 0 \leq \lambda \leq 1 \\ \underline{u} \leq u \leq \bar{u} \end{cases} \end{aligned} \quad (3.8)$$

assuming that $u = 0$ satisfies the inequality constraints. This assumption is not restrictive if increments from past values are used for all variables. Increments are natural for digital control system implementation.

The scalar λ allows the algorithm to relax the equality constraint if d_y^{des} is not achievable and therefore provides an indication whether d_y^{des} is achievable. If $\lambda = 1$ then d_y^{des} is achievable, otherwise it is not. In effect λ limits d_y^{des} , if necessary, by reducing its magnitude and

maintaining its direction. This optimization formulation is control law command feasibility, control deficiency and control sufficiency in a single step. Control law command feasibility is indicated by $\lambda = 1$ and infeasibility is indicated by $\lambda \neq 1$. Control sufficiency optimization is achieved through an appropriate choice of $f(u)$. Control deficiency is achieved by maximizing the magnitude of the control law command λ while maintaining direction. However, it has been shown that preserving the direction of the command may unnecessarily degrade performance and thus is not optimal [10]. A multi-branch formulation allows more flexibility and optimality during control deficiency.

3.3.2 Multi-branch Control Allocation

Redundant control effectors and actuator limits require essentially two parts for every control allocation algorithm: control sufficiency to provide solution uniqueness in the presence of control redundancy and control deficiency to prohibit violation of actuator limits. Sufficiency or deficiency is determined through a third part, control law command feasibility. Although the previous section shows that single-branch algorithms may be constructed, a multi-branch formulation allows more flexibility and optimality during control deficiency.

Control Law Command Feasibility and Control Deficiency

The control law command feasibility and deficiency functions are still achieved in a single step. The first step in the multi-branch control allocation algorithm is determining if the control law command is feasible. If it is feasible, control sufficiency provisions are made in a separate control allocation branch and if it is deficient, control deficient provisions are automatic. Control law command feasibility may be determined by solving the following nonlinear optimization problem

$$\begin{aligned} \min_u J &= \|B_y u - d_y^{des}\|_1 \\ \text{subject to } \underline{u} &\leq u \leq \bar{u} \end{aligned} \quad (3.9)$$

Note that the 1-norm is chosen to be amenable with linear program solvers. The feasibility optimization may be transformed into a standard linear program

$$\begin{aligned} \min_u J &= [0 \ \dots \ 0 \ 1 \ \dots \ 1] \begin{bmatrix} u \\ u_s \end{bmatrix} \\ \text{subject to } \begin{bmatrix} u_s \\ -u \\ u \\ -B_y u + u_s \\ B_y u + u_s \end{bmatrix} &\geq \begin{bmatrix} 0 \\ -\bar{u} \\ \underline{u} \\ -d_y^{des} \\ d_y^{des} \end{bmatrix} \end{aligned} \quad (3.10)$$

where u_s is a slack variable. If $J = 0$, the control law command is feasible otherwise it is infeasible. Linear programming is chosen due to the ubiquitous solvers commercially available.

The solution to the problem posed in eq.(3.10) may also be used during control deficiency. Since the objective of this optimization is to minimize the slack variables, u_s , the control deflection solution, u^* , provides an achieved d_y that is closest to d_y^{des} in the 1-norm sense. Weights may be added for greater flexibility in achieving optimality during control deficiency

$$\begin{aligned} \min_u \quad & J = W_d^T u_s \quad (3.11) \\ \text{subject to} \quad & \begin{bmatrix} u_s \\ -u \\ u \\ -B_y u + u_s \\ B_y u + u_s \end{bmatrix} \geq \begin{bmatrix} 0 \\ -\bar{u} \\ \underline{u} \\ -d_y^{des} \\ d_y^{des} \end{bmatrix} \\ & W_d^T \in \mathbb{R}^{n_y} \\ & u_s \in \mathbb{R}^{n_y} \end{aligned}$$

Summarizing, solution to eq.(3.11) with any linear program solver may be used to determine feasibility. If $J = 0$, the control law command is feasible and control sufficiency provisions must be made which is the subject of the next section. If $J \neq 0$, the control command is infeasible. Further, the solution from eq.(3.11) provides optimal control deficiency in the sense of minimizing the weighted 1-norm distance between $B_y u^*$ and d_y^{des} where u^* is the optimization solution.

Control Sufficiency

If the solution of eq.(3.11) results in $J = 0$, there is sufficient, and possibly excess, control power to achieve the control law command, d_y^{des} . The excess control power is used to optimize mission segment objectives such as minimum drag. The following linear program is formulated for control sufficiency

$$\begin{aligned} \min_u \quad & J = W_u u_s \quad (3.12) \\ \text{subject to} \quad & \begin{bmatrix} u_s \\ -u \\ u \\ -u + u_s \\ u + u_s \end{bmatrix} \geq \begin{bmatrix} 0 \\ -\bar{u} \\ \underline{u} \\ -u_{pref} \\ u_{pref} \end{bmatrix} \\ & B_y u = d_y^{des} \\ & W_u^T \in \mathbb{R}^m \\ & u_s \in \mathbb{R}^m \end{aligned}$$

where u_{pref} and W_u are chosen depending on the mission segment objective.

Six control allocation modes were implemented to address specific mission objectives. The minimum control deflection control allocation mode is designed to minimize deflections of all the control effectors which is a good approximation of multiple objectives such as minimum drag and minimum actuator power. The minimum drag mode is designed to reduce drag by adding a higher fidelity on-board model of drag due to control deflections. The minimum

wing loading mode is designed to reduce wing bending loads by minimizing the use of the all moving tips, the most outboard effectors. The minimum radar signature mode is designed to reduce radar signature by minimizing the use of spoiler slot deflectors which qualitatively give higher radar signatures than the other effectors. The minimum thrust vector mode was designed to emphasize the use of the aerodynamic effectors. The final mode is the null space injection mode which is described in the next section.

Null Space Injection Mode The eventual goal is to integrate the linear program control allocation with on-line adaptation to provide robustness to large errors and optimal performance [8]. A fundamental requirement for adaptive control is persistence of excitation and a well-conditioned regressor matrix [13]. Therefore, activity of all control effectors is necessary to accurately estimate the control effectiveness on-line. Furthermore, it has been experimentally observed, that columns of the regressor matrix should be of the same order of magnitude at each point in time, not just in the l_2 norm over the window. This is a noise effect, viz., small deflections yield low SNR, which is responsible for inaccurate estimates. Simulation analysis showed that the linear program control allocation typically results in most effectors following their preferences while using only a subset of the control effectors to achieve the control law command. This characteristic would make identification of control effectivenesses of each surface impossible since the deflections may be correlated and/or may not be of the same order of magnitude for all preferences (u_{pref}) and associated weights (W_u). For example, static preferences and weights ($u_{pref}=\text{constant}$, $W_u=\text{constant}$) result in highly correlated solutions and high variability in magnitude. Therefore, in this section alternative control preferences and weights are used to assist in estimating accurate control derivatives. The motivation for the injection control allocation mode is to maximize the condition number of a regressor matrix consisting of control deflections.

Actuator commands of uniform distribution are achieved with the following weighted pseudo-inverse control preference

$$u_{pref} = W^{-1} B_y^T (B_y W^{-1} B_y^T)^{-1} d_y^{des}. \quad (3.13)$$

Evidently, these commands will be highly correlated. Decorrelation is accomplished through random variations of the weighting matrix in eq.(3.13)

$$\begin{aligned} W &= \tilde{W} W_r \\ W_r &= \text{diag}(10^{rv_1}, 10^{rv_2}, \dots) \end{aligned} \quad (3.14)$$

where \tilde{W} is a nominal diagonal weighting matrix that scales each effector based upon deflection limits to equally distribute commands, and rv is a vector of uniformly distributed random variables between -1 and 1.

Most control derivative identification enhancement may be accomplished using the control preference in eq.(3.13) and random weighting in eq.(3.14). Although u_{pref} in eq.(3.13) with weight W in eq.(3.14) is completely decorrelated and equally distributed, it is just a preference. Unequally distributed actuator commands may still be prevalent due to the nature of extremals in linear programming. So stronger linear program solution enforcement

to u_{pref} will no doubt deter unequal distribution and correlation. This is accomplished using the following dynamic control weight in the linear program in eq.(3.12)

$$W_u = \text{diag}(\frac{|u0_1 - u0_{p1}|}{|u0_{p1}|}, \frac{|u0_2 - u0_{p2}|}{|u0_{p2}|}, \dots) \quad (3.15)$$

where $u0$ is the effector past value vector and $u0_p$ is the effector preference past value vector. Essentially, this dynamic weighting drives the effectors farthest from their preference hardest toward their preference.

Summary

The multi-branch, linear program-based control allocation method is summarized as follows. A B_y , u_l , u_u , u_r , W_d , W_u and u_{pref} is supplied by the MODEL module and a d_y^{des} is supplied by the FFA module. The linear program in eq.(3.11) is solved using these data (B_y , u_l , u_u , u_r , d_y^{des} , W_d) giving the optimal solution u^* . If $J(u^*) \neq 0$, then $u^c = u^*$ gives the closest moment $B_y u^c$ to d_y^{des} in the sense of the performance index in eq.(3.11) without violating the actuator limits. If $J = 0$, the linear program in eq.(3.12) is solved using these data (B_y , u_l , u_u , u_r , d_y^{des} , u_{pref} , W_u) giving u^* . Setting $u^c = u^*$ gives the desired moment $B_y u^* = d_y^{des}$ that achieves the mission segment objective in the sense of the performance index in eq.(3.12) without violating the actuator limits.

3.4 On-board Model

The purpose of the on-board model control law module is to compute all aircraft configuration and control law requirements data. For inner loop flight control, the most notable aircraft configuration data are the stability and control derivatives. The most notable control law requirements data are desired flying qualities parameters and feedback bandwidths. The aircraft configuration model caused the on-board model to be the control law module that required the most development effort, and it is the module that still needs the most refinement, especially at high speeds.

3.4.1 Requirements Model

The requirements model contains all functions and parameters that pertain to control law requirements. Data include nominal stability, nominal performance, robustness and optimization requirements.

Command Variables Requirements

A set of feedback command variables are defined such that acceptable levels of robustness to uncertainty and disturbance rejection are achieved. The following command variables were

chosen based on control law efforts for a similar class of fighter aircraft [25, 21]

$$\begin{aligned}
 y &= \begin{bmatrix} LCV \\ MCV \\ NCV \end{bmatrix} \\
 LCV &= (1 - f_{cv})LCV_{lo} + f_{cv}LCV_{hi} \\
 MCV &= (1 - f_{cv})MCV_{lo} + f_{cv}MCV_{hi} \\
 NCV &= (1 - f_{cv})NCV_{lo} + f_{cv}NCV_{hi} \\
 LCV_{hi} &= p \cos \alpha + r \sin \alpha \\
 MCV_{hi} &= K_{\alpha} \alpha + q \\
 NCV_{hi} &= K_{\beta} \beta - p \sin \alpha + r \cos \alpha \\
 LCV_{lo} &= p \\
 MCV_{lo} &= q \\
 NCV_{lo} &= r
 \end{aligned} \tag{3.16}$$

where f_{cv} is a blending function of dynamic pressure that blends the low and high speed commands as shown in Fig.(3.3).

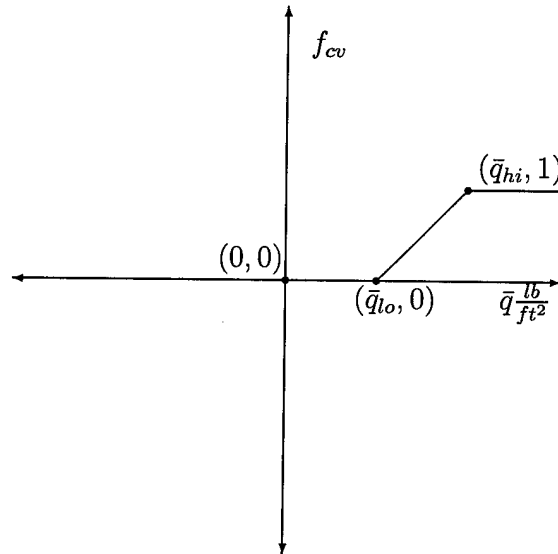


Figure 3.3: Command variable blending function

The parameter K_{α} is chosen to provide a natural blend of pitch and vertical acceleration since the longitudinal stick is used to control pitch rotation and vertical translation.

$$K_{\alpha} = \frac{\bar{q} S_{ref} C_{L_{\alpha}}^{ref}}{m V_{co}}$$

Table 3.1: Command variable requirements parameters

Parameter	Value
$C_{Y\beta}^{ref}$	$-1.0 \frac{1}{rad}$
\bar{q}_{lo}	$12 \frac{lb}{ft^2}$
\bar{q}_{hi}	$50 \frac{lb}{ft^2}$

$$C_{L\alpha}^{ref} = C_{L\alpha}|_{\alpha=0} \quad (3.17)$$

Similarly, the parameter K_β is chosen to provide a natural blend of yaw and side acceleration since the pedals are used to control yaw rotation and side translation.

$$K_\beta = \frac{\bar{q} S_{ref} C_{Y\beta}^{ref}}{m V_{co}} \quad (3.18)$$

Note that due to the tailless nature of the ICE aircraft, $C_{Y\beta}|_{\alpha=0}$ is very small as compared to similar aircraft with vertical tails such as the F-18 High Angle-of-attack Research Vehicle (HARV)

$$\begin{aligned} C_{Y\beta}|_{\alpha=0}^{ICE} &= -.046 \text{ rad}^{-1} \\ C_{Y\beta}|_{\alpha=0}^{HARV} &= -1.2 \text{ rad}^{-1} \end{aligned} \quad (3.19)$$

Use of $C_{Y\beta}^{ref} = C_{Y\beta}|_{\alpha=0}^{ICE}$ in eq.(3.18) resulted in poor sideslip regulation. This led to the most significant tailless aircraft specific dynamic inversion design change from past work [25]. The choice of K_β should reflect $C_{Y\beta}|_{\alpha=0}$ of a similar vehicle with a vertical tail otherwise, poor performance or even instability may result. The command variable requirements parameters are given in Table 3.1.

Command Shaping Requirements

The choice of command shaping parameters was based on similar aircraft such as the F-16 and F-18. The initial shaping parameters are given in Table 3.2 and will be tuned during the piloted simulation analysis effort. Note that variable superscripts refer to the corresponding control axis, and absence of a superscript implies use for all axes.

Feedback and Feedforward Augmentation Requirements

The nominal choice of augmentation parameters are given in Table 3.3. These parameter choices are based upon uncertainty bounds and flying qualities requirements for similar fighter aircraft [11, 25].

Table 3.2: Command shaping requirements parameters

Parameter	Nominal Value
ω_{fq}	$2.5 \frac{rad}{sec}$
x_1^{roll}	$0.0 lbs$
y_1^{roll}	$0.0 \frac{deg}{sec}$
x_2^{roll}	$1.0 lbs$
y_2^{roll}	$0.0 \frac{deg}{sec}$
x_3^{roll}	$4.0 lbs$
y_3^{roll}	$20.0 \frac{deg}{sec}$
x_4^{roll}	$8.0 lbs$
y_4^{roll}	$80.0 \frac{deg}{sec}$
x_5^{roll}	$16.57 lbs$
y_5^{roll}	$LCV_{max} \frac{deg}{sec}$
x_1^{pitch}	$0.0 lbs$
y_1^{pitch}	$0.0 \frac{deg}{sec}$
x_2^{pitch}	$1.75 lbs$
y_2^{pitch}	$0.0 \frac{deg}{sec}$
x_3^{pitch}	$4.0 lbs$
y_3^{pitch}	$5.0 \frac{deg}{sec}$
x_4^{pitch}	$15.0 lbs$
y_4^{pitch}	$40.0 \frac{deg}{sec}$
x_5^{pitch}	$30.25 lbs$
y_5^{pitch}	$MCV_{max} \frac{deg}{sec}$
x_1^{yaw}	$0.0 lbs$
y_1^{yaw}	$0.0 \frac{deg}{sec}$
x_2^{yaw}	$5.0 lbs$
y_2^{yaw}	$0.0 \frac{deg}{sec}$
x_3^{yaw}	$95.0 lbs$
y_3^{yaw}	$NCV_{max} \frac{deg}{sec}$
x_4^{yaw}	$95.0 lbs$
y_4^{yaw}	$NCV_{max} \frac{deg}{sec}$
x_5^{yaw}	$95.0 lbs$
y_5^{yaw}	$NCV_{max} \frac{deg}{sec}$
LCV_{max}	$\min\left(\frac{2}{3}\bar{q}, 200\right) \frac{deg}{sec}$
MCV_{max}	$100.0 \frac{deg}{sec}$
NCV_{max}	$30.0 \frac{deg}{sec}$

Table 3.3: Augmentation requirements parameters

Parameter	Nominal Value
ω_c	5 $\frac{rad}{sec}$
f_i	.25
f_c	.5

Table 3.4: Allocation requirements parameters

Parameter	Description	Nominal Value
ΔT	flight control system update rate	0.01 sec
W_d	control deficient weight	$\begin{bmatrix} 1 & 0 & 0 \\ 0 & 1 & 0 \\ 0 & 0 & 1 \end{bmatrix}$

Control Allocation Requirements

The nominal choice of control allocation requirements parameters are given in Table 3.4.

3.4.2 Configuration Model

The configuration model contains all functions and parameters that pertain to the aircraft configuration. The configuration model contains an airframe dynamical model, actuator model and mission segment objective models. The airframe dynamical model provides the stability and control derivatives to the augmentation and allocation modules. The actuator model provides actuator constraints to the allocation module. The mission segment objective models provide control preferences and weights for control sufficiency optimization.

The airframe model required the most development effort, and it still needs the most refinement, especially at high speeds. A tradeoff exists between airframe model fidelity and controller complexity. A high fidelity model will give good control law performance but will be complex requiring significant computational throughput and/or memory. On the other hand a low fidelity model will be simple, not require much computational throughput and/or memory, but control law performance may be poor. Highly robust controllers may be used to account for low model fidelity, but may be so complex that their computational throughput and memory requirements may negate the benefits of a simple model [3].

Dynamic inversion is chosen as the flight control law method for this study since it provides a nice compromise between controller complexity and robustness as indicated by past studies [22, 11, 25, 1, 21, 5]. The airframe model is developed to the lowest fidelity possible such that closed-loop stability and performance is adequate as determined by linear analytical robustness and flying qualities tools as well as nonlinear batch and piloted simulations. This lowest fidelity model approach is taken to determine the level of model fidelity required by the dynamic inversion synthesis method. The final on-board airframe model is nonlinear, but a scheduled linear model and a perfect model were developed for comparison purposes.

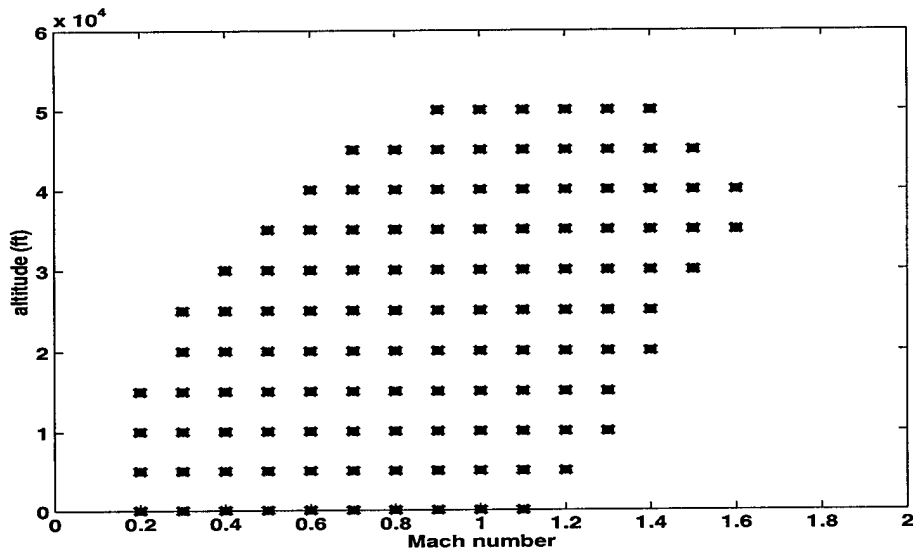


Figure 3.4: Flight Envelope Linear Model Grid

Scheduled Linear Airframe Model

A full-envelope airframe model consisting of linear interpolation between linear perturbational models was initially used to model the aircraft dynamics. Linear models were generated at the flight conditions indicated in the flight envelope in Fig.(3.4).

At each flight condition, the elevons and pitch flap were used to trim the aircraft moments in wings level flight at the following angles-of-attack

$$\alpha_{trim} = [-2 \ 0 \ 4 \ 8 \ 12 \ 16 \ 20 \ 24 \ 28]^T \text{ deg.} \quad (3.20)$$

Central difference numerical perturbations of the nonlinear aircraft simulation model in eq.(2.1) were used to generate 10 state linear models of the aircraft rigid body dynamics of the following form

$$\begin{aligned} \dot{x}_s &= A_s x_s + B_s u \\ x_s &\equiv [u \ \alpha \ q \ \theta \ h \ \beta \ p \ r \ \phi \ \psi]^T \\ u &\equiv [\delta_{e_l} \ \delta_{e_r} \ \delta_{pf} \ \delta_{amt_l} \ \delta_{amt_r} \ \delta_{ptv} \ \delta_{y_{tv}} \ \delta_{ssd_l} \ \delta_{ssd_r} \ \delta_{obl_{f_l}} \ \delta_{obl_{f_r}}]^T \end{aligned} \quad (3.21)$$

The 10 state linear models were reduced to 8 state linear models of the following form for control design

$$\begin{aligned} \dot{x}_m &= A_m^{LS} + B_m^{LS} u \\ x_m &\equiv [\alpha \ q \ \beta \ p \ r \ \phi \ \theta \ V]^T \end{aligned}$$

$$\begin{aligned}
A_m^{LS} &= \begin{bmatrix} A_{\alpha}^{LS} \\ A_{\dot{q}}^{LS} \\ A_{\beta}^{LS} \\ A_{\dot{p}}^{LS} \\ A_{\dot{r}}^{LS} \\ A_{\dot{\phi}}^{LS} \\ A_{\dot{\theta}}^{LS} \\ A_V^{LS} \end{bmatrix} \\
B_m^{LS} &= \begin{bmatrix} B_{\alpha, elev}^{LS} & B_{\alpha, elevr}^{LS} & B_{\alpha, pflap}^{LS} & B_{\alpha, aaml}^{LS} & B_{\alpha, amtr}^{LS} & B_{\alpha, ptv}^{LS} \\ B_{\dot{q}, elev}^{LS} & B_{\dot{q}, elevr}^{LS} & B_{\dot{q}, pflap}^{LS} & B_{\dot{q}, aaml}^{LS} & B_{\dot{q}, amtr}^{LS} & B_{\dot{q}, ptv}^{LS} \\ B_{\beta, elev}^{LS} & B_{\beta, elevr}^{LS} & B_{\beta, pflap}^{LS} & B_{\beta, aaml}^{LS} & B_{\beta, amtr}^{LS} & B_{\beta, ptv}^{LS} \\ B_{\dot{p}, elev}^{LS} & B_{\dot{p}, elevr}^{LS} & B_{\dot{p}, pflap}^{LS} & B_{\dot{p}, aaml}^{LS} & B_{\dot{p}, amtr}^{LS} & B_{\dot{p}, ptv}^{LS} \\ B_{\dot{r}, elev}^{LS} & B_{\dot{r}, elevr}^{LS} & B_{\dot{r}, pflap}^{LS} & B_{\dot{r}, aaml}^{LS} & B_{\dot{r}, amtr}^{LS} & B_{\dot{r}, ptv}^{LS} \\ B_{\dot{\phi}, elev}^{LS} & B_{\dot{\phi}, elevr}^{LS} & B_{\dot{\phi}, pflap}^{LS} & B_{\dot{\phi}, aaml}^{LS} & B_{\dot{\phi}, amtr}^{LS} & B_{\dot{\phi}, ptv}^{LS} \\ B_{\dot{\theta}, elev}^{LS} & B_{\dot{\theta}, elevr}^{LS} & B_{\dot{\theta}, pflap}^{LS} & B_{\dot{\theta}, aaml}^{LS} & B_{\dot{\theta}, amtr}^{LS} & B_{\dot{\theta}, ptv}^{LS} \\ B_{V, elev}^{LS} & B_{V, elevr}^{LS} & B_{V, pflap}^{LS} & B_{V, aaml}^{LS} & B_{V, amtr}^{LS} & B_{V, ptv}^{LS} \end{bmatrix} \dots \\
&\dots \begin{bmatrix} B_{\alpha, ytv}^{LS} & B_{\alpha, ssdl}^{LS} & B_{\alpha, ssdr}^{LS} & B_{\alpha, oblfl}^{LS} & B_{\alpha, oblfr}^{LS} \\ B_{\dot{q}, ytv}^{LS} & B_{\dot{q}, ssdl}^{LS} & B_{\dot{q}, ssdr}^{LS} & B_{\dot{q}, oblfl}^{LS} & B_{\dot{q}, oblfr}^{LS} \\ B_{\beta, ytv}^{LS} & B_{\beta, ssdl}^{LS} & B_{\beta, ssdr}^{LS} & B_{\beta, oblfl}^{LS} & B_{\beta, oblfr}^{LS} \\ B_{\dot{p}, ytv}^{LS} & B_{\dot{p}, ssdl}^{LS} & B_{\dot{p}, ssdr}^{LS} & B_{\dot{p}, oblfl}^{LS} & B_{\dot{p}, oblfr}^{LS} \\ B_{\dot{r}, ytv}^{LS} & B_{\dot{r}, ssdl}^{LS} & B_{\dot{r}, ssdr}^{LS} & B_{\dot{r}, oblfl}^{LS} & B_{\dot{r}, oblfr}^{LS} \\ B_{\dot{\phi}, ytv}^{LS} & B_{\dot{\phi}, ssdl}^{LS} & B_{\dot{\phi}, ssdr}^{LS} & B_{\dot{\phi}, oblfl}^{LS} & B_{\dot{\phi}, oblfr}^{LS} \\ B_{\dot{\theta}, ytv}^{LS} & B_{\dot{\theta}, ssdl}^{LS} & B_{\dot{\theta}, ssdr}^{LS} & B_{\dot{\theta}, oblfl}^{LS} & B_{\dot{\theta}, oblfr}^{LS} \\ B_{V, ytv}^{LS} & B_{V, ssdl}^{LS} & B_{V, ssdr}^{LS} & B_{V, oblfl}^{LS} & B_{V, oblfr}^{LS} \end{bmatrix} \\
A_{\alpha}^{LS} &= \begin{bmatrix} \frac{\partial F_{\alpha}}{\partial \alpha} \Big|_{eq} & \frac{\partial F_{\alpha}}{\partial q} \Big|_{eq} & \frac{\partial F_{\alpha}}{\partial \beta} \Big|_{eq} & \frac{\partial F_{\alpha}}{\partial p} \Big|_{eq} & \frac{\partial F_{\alpha}}{\partial r} \Big|_{eq} & 0 & 0 & 0 \end{bmatrix} x_m \\
A_{\dot{q}}^{LS} &= \begin{bmatrix} \frac{\partial F_{\dot{q}}}{\partial \alpha} \Big|_{eq} & \frac{\partial F_{\dot{q}}}{\partial q} \Big|_{eq} & \frac{\partial F_{\dot{q}}}{\partial \beta} \Big|_{eq} & \frac{\partial F_{\dot{q}}}{\partial p} \Big|_{eq} & \frac{\partial F_{\dot{q}}}{\partial r} \Big|_{eq} & 0 & 0 & 0 \end{bmatrix} x_m \\
A_{\beta}^{LS} &= \begin{bmatrix} \frac{\partial F_{\beta}}{\partial \alpha} \Big|_{eq} & \frac{\partial F_{\beta}}{\partial q} \Big|_{eq} & \frac{\partial F_{\beta}}{\partial \beta} \Big|_{eq} & \frac{\partial F_{\beta}}{\partial p} \Big|_{eq} & \frac{\partial F_{\beta}}{\partial r} \Big|_{eq} & 0 & 0 & 0 \end{bmatrix} x_m \\
A_{\dot{p}}^{LS} &= \begin{bmatrix} \frac{\partial F_{\dot{p}}}{\partial \alpha} \Big|_{eq} & \frac{\partial F_{\dot{p}}}{\partial q} \Big|_{eq} & \frac{\partial F_{\dot{p}}}{\partial \beta} \Big|_{eq} & \frac{\partial F_{\dot{p}}}{\partial p} \Big|_{eq} & \frac{\partial F_{\dot{p}}}{\partial r} \Big|_{eq} & 0 & 0 & 0 \end{bmatrix} x_m \\
A_{\dot{r}}^{LS} &= \begin{bmatrix} \frac{\partial F_{\dot{r}}}{\partial \alpha} \Big|_{eq} & \frac{\partial F_{\dot{r}}}{\partial q} \Big|_{eq} & \frac{\partial F_{\dot{r}}}{\partial \beta} \Big|_{eq} & \frac{\partial F_{\dot{r}}}{\partial p} \Big|_{eq} & \frac{\partial F_{\dot{r}}}{\partial r} \Big|_{eq} & 0 & 0 & 0 \end{bmatrix} x_m \\
A_{\dot{\phi}}^{LS} &= [0 \ 0 \ 0 \ 1 \ 0 \ 0 \ 0 \ 0] x_m \\
A_{\dot{\theta}}^{LS} &= [0 \ 1 \ 0 \ 0 \ 0 \ 0 \ 0 \ 0] x_m \\
A_V^{LS} &= [0 \ 0 \ 0 \ 0 \ 0 \ 0 \ 0 \ 0] x_m \\
B_{\alpha, elev}^{LS} &= \frac{\partial F_{\alpha}}{\partial \delta_{elev}} \Big|_{eq}
\end{aligned}$$

$$\begin{aligned}
B_{\dot{\alpha},elevr}^{LS} &= \left. \frac{\partial F_{\dot{\alpha}}}{\partial \delta_{elevr}} \right|_{eq} \\
B_{\dot{\alpha},pflap}^{LS} &= \left. \frac{\partial F_{\dot{\alpha}}}{\partial \delta_{pflap}} \right|_{eq} \\
B_{\dot{\alpha},amtl}^{LS} &= \left. \frac{\partial F_{\dot{\alpha}}}{\partial \delta_{amtl}} \right|_{eq} \\
B_{\dot{\alpha},amtr}^{LS} &= \left. \frac{\partial F_{\dot{\alpha}}}{\partial \delta_{amtr}} \right|_{eq} \\
B_{\dot{\alpha},ptv}^{LS} &= \left. \frac{\partial F_{\dot{\alpha}}}{\partial \delta_{ptv}} \right|_{eq} \\
B_{\dot{\alpha},ytv}^{LS} &= \left. \frac{\partial F_{\dot{\alpha}}}{\partial \delta_{ytv}} \right|_{eq} \\
B_{\dot{\alpha},ssdl}^{LS} &= \left. \frac{\partial F_{\dot{\alpha}}}{\partial \delta_{ssdl}} \right|_{eq} \\
B_{\dot{\alpha},ssdr}^{LS} &= \left. \frac{\partial F_{\dot{\alpha}}}{\partial \delta_{ssdr}} \right|_{eq} \\
B_{\dot{\alpha},oblfl}^{LS} &= \left. \frac{\partial F_{\dot{\alpha}}}{\partial \delta_{oblfl}} \right|_{eq} \\
B_{\dot{\alpha},oblfr}^{LS} &= \left. \frac{\partial F_{\dot{\alpha}}}{\partial \delta_{oblfr}} \right|_{eq} \\
B_{\dot{q},elevl}^{LS} &= \left. \frac{\partial F_{\dot{q}}}{\partial \delta_{elevl}} \right|_{eq} \\
B_{\dot{q},elevr}^{LS} &= \left. \frac{\partial F_{\dot{q}}}{\partial \delta_{elevr}} \right|_{eq} \\
B_{\dot{q},pflap}^{LS} &= \left. \frac{\partial F_{\dot{q}}}{\partial \delta_{pflap}} \right|_{eq} \\
B_{\dot{q},amtl}^{LS} &= \left. \frac{\partial F_{\dot{q}}}{\partial \delta_{amtl}} \right|_{eq} \\
B_{\dot{q},amtr}^{LS} &= \left. \frac{\partial F_{\dot{q}}}{\partial \delta_{amtr}} \right|_{eq} \\
B_{\dot{q},ptv}^{LS} &= \left. \frac{\partial F_{\dot{q}}}{\partial \delta_{ptv}} \right|_{eq} \\
B_{\dot{q},ytv}^{LS} &= \left. \frac{\partial F_{\dot{q}}}{\partial \delta_{ytv}} \right|_{eq}
\end{aligned}$$

$$\begin{aligned}
B_{\dot{q},ssdl}^{LS} &= \left. \frac{\partial F_{\dot{q}}}{\partial \delta_{ssdl}} \right|_{eq} \\
B_{\dot{q},ssdr}^{LS} &= \left. \frac{\partial F_{\dot{q}}}{\partial \delta_{ssdr}} \right|_{eq} \\
B_{\dot{q},oblfl}^{LS} &= \left. \frac{\partial F_{\dot{q}}}{\partial \delta_{oblfl}} \right|_{eq} \\
B_{\dot{q},oblfr}^{LS} &= \left. \frac{\partial F_{\dot{q}}}{\partial \delta_{oblfr}} \right|_{eq} \\
B_{\dot{\beta},elevl}^{LS} &= \left. \frac{\partial F_{\dot{\beta}}}{\partial \delta_{elevl}} \right|_{eq} \\
B_{\dot{\beta},elevr}^{LS} &= \left. \frac{\partial F_{\dot{\beta}}}{\partial \delta_{elevr}} \right|_{eq} \\
B_{\dot{\beta},pflap}^{LS} &= \left. \frac{\partial F_{\dot{\beta}}}{\partial \delta_{pflap}} \right|_{eq} \\
B_{\dot{\beta},amtl}^{LS} &= \left. \frac{\partial F_{\dot{\beta}}}{\partial \delta_{amtl}} \right|_{eq} \\
B_{\dot{\beta},amtr}^{LS} &= \left. \frac{\partial F_{\dot{\beta}}}{\partial \delta_{amtr}} \right|_{eq} \\
B_{\dot{\beta},ptv}^{LS} &= \left. \frac{\partial F_{\dot{\beta}}}{\partial \delta_{ptv}} \right|_{eq} \\
B_{\dot{\beta},ytv}^{LS} &= \left. \frac{\partial F_{\dot{\beta}}}{\partial \delta_{ytv}} \right|_{eq} \\
B_{\dot{\beta},ssdl}^{LS} &= \left. \frac{\partial F_{\dot{\beta}}}{\partial \delta_{ssdl}} \right|_{eq} \\
B_{\dot{\beta},ssdr}^{LS} &= \left. \frac{\partial F_{\dot{\beta}}}{\partial \delta_{ssdr}} \right|_{eq} \\
B_{\dot{\beta},oblfl}^{LS} &= \left. \frac{\partial F_{\dot{\beta}}}{\partial \delta_{oblfl}} \right|_{eq} \\
B_{\dot{\beta},oblfr}^{LS} &= \left. \frac{\partial F_{\dot{\beta}}}{\partial \delta_{oblfr}} \right|_{eq} \\
B_{\dot{p},elevl}^{LS} &= \left. \frac{\partial F_{\dot{p}}}{\partial \delta_{elevl}} \right|_{eq} \\
B_{\dot{p},elevr}^{LS} &= \left. \frac{\partial F_{\dot{p}}}{\partial \delta_{elevr}} \right|_{eq}
\end{aligned}$$

$$B_{\dot{p},pflap}^{LS} = \left. \frac{\partial F_{\dot{p}}}{\partial \delta_{pflap}} \right|_{eq}$$

$$B_{\dot{p},amtl}^{LS} = \left. \frac{\partial F_{\dot{p}}}{\partial \delta_{amtl}} \right|_{eq}$$

$$B_{\dot{p},amtr}^{LS} = \left. \frac{\partial F_{\dot{p}}}{\partial \delta_{amtr}} \right|_{eq}$$

$$B_{\dot{p},ptv}^{LS} = \left. \frac{\partial F_{\dot{p}}}{\partial \delta_{ptv}} \right|_{eq}$$

$$B_{\dot{p},ytl}^{LS} = \left. \frac{\partial F_{\dot{p}}}{\partial \delta_{ytl}} \right|_{eq}$$

$$B_{\dot{p},ssdl}^{LS} = \left. \frac{\partial F_{\dot{p}}}{\partial \delta_{ssdl}} \right|_{eq}$$

$$B_{\dot{p},ssdr}^{LS} = \left. \frac{\partial F_{\dot{p}}}{\partial \delta_{ssdr}} \right|_{eq}$$

$$B_{\dot{p},oblfl}^{LS} = \left. \frac{\partial F_{\dot{p}}}{\partial \delta_{oblfl}} \right|_{eq}$$

$$B_{\dot{p},oblfr}^{LS} = \left. \frac{\partial F_{\dot{p}}}{\partial \delta_{oblfr}} \right|_{eq}$$

$$B_{\dot{r},elevl}^{LS} = \left. \frac{\partial F_{\dot{r}}}{\partial \delta_{elevl}} \right|_{eq}$$

$$B_{\dot{r},elevr}^{LS} = \left. \frac{\partial F_{\dot{r}}}{\partial \delta_{elevr}} \right|_{eq}$$

$$B_{\dot{r},pflap}^{LS} = \left. \frac{\partial F_{\dot{r}}}{\partial \delta_{pflap}} \right|_{eq}$$

$$B_{\dot{r},amtl}^{LS} = \left. \frac{\partial F_{\dot{r}}}{\partial \delta_{amtl}} \right|_{eq}$$

$$B_{\dot{r},amtr}^{LS} = \left. \frac{\partial F_{\dot{r}}}{\partial \delta_{amtr}} \right|_{eq}$$

$$B_{\dot{r},ptv}^{LS} = \left. \frac{\partial F_{\dot{r}}}{\partial \delta_{ptv}} \right|_{eq}$$

$$B_{\dot{r},ytl}^{LS} = \left. \frac{\partial F_{\dot{r}}}{\partial \delta_{ytl}} \right|_{eq}$$

$$B_{\dot{r},ssdl}^{LS} = \left. \frac{\partial F_{\dot{r}}}{\partial \delta_{ssdl}} \right|_{eq}$$

$$\begin{aligned}
B_{\dot{r},ssdr}^{LS} &= \left. \frac{\partial F_{\dot{r}}}{\partial \delta_{ssdr}} \right|_{eq} \\
B_{\dot{r},oblfl}^{LS} &= \left. \frac{\partial F_{\dot{r}}}{\partial \delta_{oblfl}} \right|_{eq} \\
B_{\dot{r},oblfr}^{LS} &= \left. \frac{\partial F_{\dot{r}}}{\partial \delta_{oblfr}} \right|_{eq} \\
B_{\dot{\phi},elevl}^{LS} &= 0 \\
B_{\dot{\phi},elevr}^{LS} &= 0 \\
B_{\dot{\phi},pflap}^{LS} &= 0 \\
B_{\dot{\phi},amtl}^{LS} &= 0 \\
B_{\dot{\phi},amtr}^{LS} &= 0 \\
B_{\dot{\phi},ptv}^{LS} &= 0 \\
B_{\dot{\phi},ytv}^{LS} &= 0 \\
B_{\dot{\phi},ssdl}^{LS} &= 0 \\
B_{\dot{\phi},ssdr}^{LS} &= 0 \\
B_{\dot{\phi},oblfl}^{LS} &= 0 \\
B_{\dot{\phi},oblfr}^{LS} &= 0 \\
B_{\dot{\theta},elevl}^{LS} &= 0 \\
B_{\dot{\theta},elevr}^{LS} &= 0 \\
B_{\dot{\theta},pflap}^{LS} &= 0 \\
B_{\dot{\theta},amtl}^{LS} &= 0 \\
B_{\dot{\theta},amtr}^{LS} &= 0 \\
B_{\dot{\theta},ptv}^{LS} &= 0 \\
B_{\dot{\theta},ytv}^{LS} &= 0 \\
B_{\dot{\theta},ssdl}^{LS} &= 0 \\
B_{\dot{\theta},ssdr}^{LS} &= 0 \\
B_{\dot{\theta},oblfl}^{LS} &= 0 \\
B_{\dot{\theta},oblfr}^{LS} &= 0 \\
B_{\dot{V},elevl}^{LS} &= 0 \\
B_{\dot{V},elevr}^{LS} &= 0 \\
B_{\dot{V},pflap}^{LS} &= 0
\end{aligned}$$

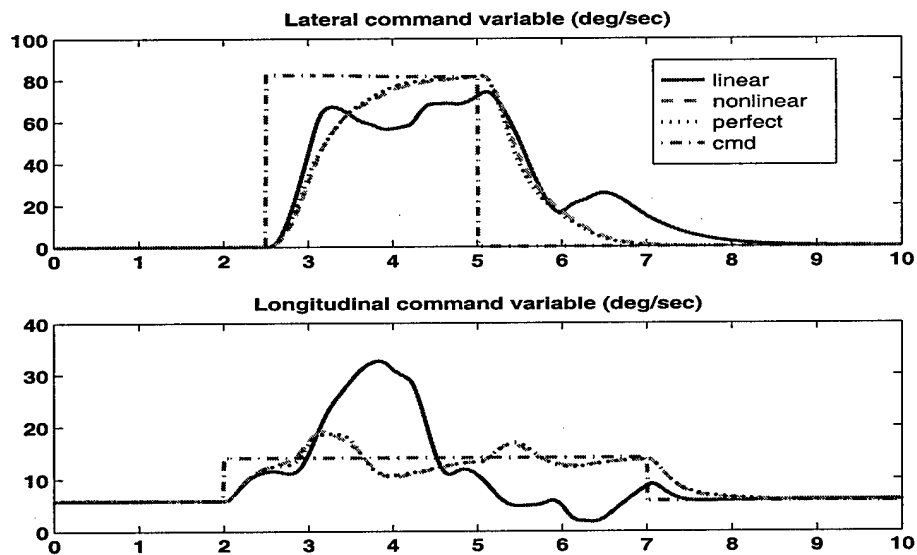


Figure 3.5: Mach 0.35, 5000 ft. Altitude, Min Vec CA Mode

$$\begin{aligned}
 B_{V,amtl}^{LS} &= 0 \\
 B_{V,amtr}^{LS} &= 0 \\
 B_{V,ptv}^{LS} &= 0 \\
 B_{V,ytv}^{LS} &= 0 \\
 B_{V,ssdl}^{LS} &= 0 \\
 B_{V,ssdr}^{LS} &= 0 \\
 B_{V,oblfl}^{LS} &= 0 \\
 B_{V,oblfr}^{LS} &= 0
 \end{aligned}$$

where $F_{\dot{\alpha}}, F_{\dot{q}}, F_{\dot{\beta}}, F_{\dot{p}}, F_{\dot{r}}$ are rows of F in eq.(2.1). The elements of the A_m^{LS} and B_m^{LS} matrices are stored in data tables as functions of Mach number, altitude, and angle-of-attack, and linear interpolation is used between data points.

As the simulation analysis proceeded, it became clear that higher fidelity models of some effects were necessary. The command variable and model error responses in Figs.(3.5)-(3.7) show a simulation example where the linear model is inadequate. The command variable tracking with the linear model is poor relative to the higher fidelity models due to the large model errors.

Nonlinear Airframe Model

A nonlinear on-board model was designed to improve control law performance by including nonlinear state dependencies such as inertial coupling and off-trim effects such as maneuver-

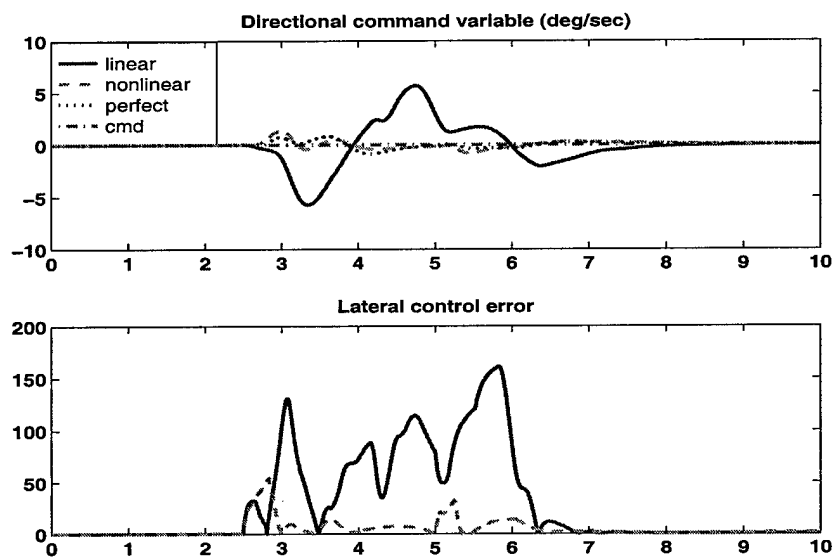


Figure 3.6: Mach 0.35, 5000 ft. Altitude, Min Vec CA Mode

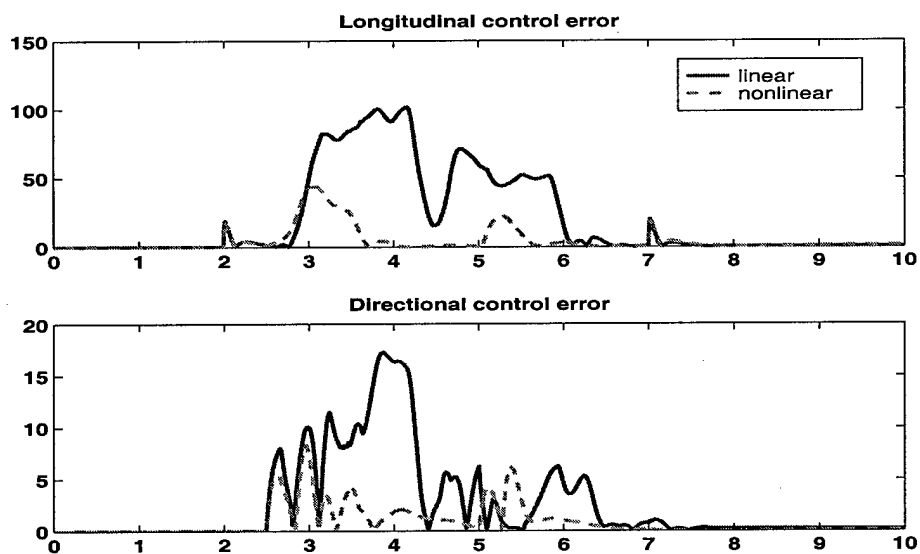


Figure 3.7: Mach 0.35, 5000 ft. Altitude, Min Vec CA Mode

ing thrust. Refinements to the scheduled linear model of the previous section were made to generate the nonlinear model. Least squares polynomial data fits were used to generate some of the nonlinear aerodynamic and propulsive forces and moments. The nonlinear on-board model has the following form

$$\begin{aligned} \dot{x}_m &= A_m^{NL} + B_m^{NL} u \\ A_m^{NL} &= \begin{bmatrix} A_{\dot{\alpha}}^{NL} \\ A_{\dot{q}}^{NL} \\ A_{\dot{\beta}}^{NL} \\ A_{\dot{p}}^{NL} \\ A_{\dot{r}}^{NL} \\ A_{\dot{\phi}}^{NL} \\ A_{\dot{\theta}}^{NL} \\ A_{\dot{V}}^{NL} \end{bmatrix} \\ B_m^{LS} &= \begin{bmatrix} B_{\alpha, \text{elev}}^{NL} & B_{\alpha, \text{elevr}}^{NL} & B_{\alpha, \text{pflap}}^{NL} & B_{\alpha, \text{amtl}}^{NL} & B_{\alpha, \text{amtr}}^{NL} & B_{\alpha, \text{ptv}}^{NL} \\ B_{q, \text{elev}}^{NL} & B_{q, \text{elevr}}^{NL} & B_{q, \text{pflap}}^{NL} & B_{q, \text{amtl}}^{NL} & B_{q, \text{amtr}}^{NL} & B_{q, \text{ptv}}^{NL} \\ B_{\beta, \text{elev}}^{NL} & B_{\beta, \text{elevr}}^{NL} & B_{\beta, \text{pflap}}^{NL} & B_{\beta, \text{amtl}}^{NL} & B_{\beta, \text{amtr}}^{NL} & B_{\beta, \text{ptv}}^{NL} \\ B_{p, \text{elev}}^{NL} & B_{p, \text{elevr}}^{NL} & B_{p, \text{pflap}}^{NL} & B_{p, \text{amtl}}^{NL} & B_{p, \text{amtr}}^{NL} & B_{p, \text{ptv}}^{NL} \\ B_{r, \text{elev}}^{NL} & B_{r, \text{elevr}}^{NL} & B_{r, \text{pflap}}^{NL} & B_{r, \text{amtl}}^{NL} & B_{r, \text{amtr}}^{NL} & B_{r, \text{ptv}}^{NL} \\ B_{\phi, \text{elev}}^{NL} & B_{\phi, \text{elevr}}^{NL} & B_{\phi, \text{pflap}}^{NL} & B_{\phi, \text{amtl}}^{NL} & B_{\phi, \text{amtr}}^{NL} & B_{\phi, \text{ptv}}^{NL} \\ B_{\theta, \text{elev}}^{NL} & B_{\theta, \text{elevr}}^{NL} & B_{\theta, \text{pflap}}^{NL} & B_{\theta, \text{amtl}}^{NL} & B_{\theta, \text{amtr}}^{NL} & B_{\theta, \text{ptv}}^{NL} \\ B_{V, \text{elev}}^{NL} & B_{V, \text{elevr}}^{NL} & B_{V, \text{pflap}}^{NL} & B_{V, \text{amtl}}^{NL} & B_{V, \text{amtr}}^{NL} & B_{V, \text{ptv}}^{NL} \end{bmatrix} \dots \\ &\dots \begin{bmatrix} B_{\alpha, \text{ytlv}}^{NL} & B_{\alpha, \text{ssdl}}^{NL} & B_{\alpha, \text{ssdr}}^{NL} & B_{\alpha, \text{oblfl}}^{NL} & B_{\alpha, \text{oblfr}}^{NL} \\ B_{q, \text{ytlv}}^{NL} & B_{q, \text{ssdl}}^{NL} & B_{q, \text{ssdr}}^{NL} & B_{q, \text{oblfl}}^{NL} & B_{q, \text{oblfr}}^{NL} \\ B_{\beta, \text{ytlv}}^{NL} & B_{\beta, \text{ssdl}}^{NL} & B_{\beta, \text{ssdr}}^{NL} & B_{\beta, \text{oblfl}}^{NL} & B_{\beta, \text{oblfr}}^{NL} \\ B_{p, \text{ytlv}}^{NL} & B_{p, \text{ssdl}}^{NL} & B_{p, \text{ssdr}}^{NL} & B_{p, \text{oblfl}}^{NL} & B_{p, \text{oblfr}}^{NL} \\ B_{r, \text{ytlv}}^{NL} & B_{r, \text{ssdl}}^{NL} & B_{r, \text{ssdr}}^{NL} & B_{r, \text{oblfl}}^{NL} & B_{r, \text{oblfr}}^{NL} \\ B_{\phi, \text{ytlv}}^{NL} & B_{\phi, \text{ssdl}}^{NL} & B_{\phi, \text{ssdr}}^{NL} & B_{\phi, \text{oblfl}}^{NL} & B_{\phi, \text{oblfr}}^{NL} \\ B_{\theta, \text{ytlv}}^{NL} & B_{\theta, \text{ssdl}}^{NL} & B_{\theta, \text{ssdr}}^{NL} & B_{\theta, \text{oblfl}}^{NL} & B_{\theta, \text{oblfr}}^{NL} \\ B_{V, \text{ytlv}}^{NL} & B_{V, \text{ssdl}}^{NL} & B_{V, \text{ssdr}}^{NL} & B_{V, \text{oblfl}}^{NL} & B_{V, \text{oblfr}}^{NL} \end{bmatrix} \\ A_{\alpha}^{NL} &= \frac{u\dot{w} - w\dot{u}}{u^2 + w^2} \\ A_{\dot{q}}^{NL} &= \frac{I_{zz} - I_{xx}}{I_{yy}} rp + \frac{I_{xz}}{I_{yy}} (r^2 - p^2) q \\ &\quad + \frac{1}{I_{yy}} (\bar{q} S_{ref} \bar{c} C_m - T d_{TWL} + D_e d_{DWL} \cos \alpha - D_e d_{DFS} \sin \alpha) \\ A_{\beta}^{NL} &= \frac{\dot{v}(u^2 + w^2) - v(u\dot{u} + w\dot{w})}{V^2 \sqrt{u^2 + w^2}} \\ A_p^{NL} &= \left(\frac{(I_{yy} - I_{zz}) I_{zz} - I_{xz}^2}{I_{xx} I_{zz} - I_{xz}^2} r + \frac{(I_{xx} - I_{yy} + I_{zz}) I_{xz}}{I_{xx} I_{zz} - I_{xz}^2} p \right) q \end{aligned}$$

$$\begin{aligned}
& + \frac{I_{zz}}{I_{xx}I_{zz} - I_{xz}^2} (\bar{q}S_{ref}bC_l) + \frac{I_{xz}}{I_{xx}I_{zz} - I_{xz}^2} (\bar{q}S_{ref}bC_n) \\
A_r^{NL} &= \left(\frac{(I_{xx} - I_{yy})I_{xx} + I_{xz}^2}{I_{xx}I_{zz} - I_{xz}^2} p + \frac{(I_{yy} - I_{zz} - I_{xx})I_{xz}}{I_{xx}I_{zz} - I_{xz}^2} r \right) q \\
& + \frac{I_{xz}}{I_{xx}I_{zz} - I_{xz}^2} (\bar{q}S_{ref}bC_l) + \frac{I_{xx}}{I_{xx}I_{zz} - I_{xz}^2} (\bar{q}S_{ref}bC_n) \\
A_\phi^{NL} &= A_\phi^{LS} \\
A_\theta^{NL} &= A_\theta^{LS} \\
A_V^{NL} &= A_V^{LS} \\
B_{\alpha, elev}^{NL} &= B_{\alpha, elev}^{LS} \\
B_{\alpha, elevr}^{NL} &= B_{\alpha, elevr}^{LS} \\
B_{\alpha, pflap}^{NL} &= B_{\alpha, pflap}^{LS} \\
B_{\alpha, aaml}^{NL} &= B_{\alpha, aaml}^{LS} \\
B_{\alpha, amtr}^{NL} &= B_{\alpha, amtr}^{LS} \\
B_{\alpha, ptv}^{NL} &= -\frac{uT}{m(u^2 + w^2)} \\
B_{\alpha, ytv}^{NL} &= B_{\alpha, ytv}^{LS} \\
B_{\alpha, ssdl}^{NL} &= B_{\alpha, ssdl}^{LS} \\
B_{\alpha, ssdr}^{NL} &= B_{\alpha, ssdr}^{LS} \\
B_{\alpha, oblfl}^{NL} &= B_{\alpha, oblfl}^{LS} \\
B_{\alpha, oblfr}^{NL} &= B_{\alpha, oblfr}^{LS} \\
B_{\dot{q}, elev}^{NL} &= \frac{1}{I_{yy}} \bar{q}S_{ref} \bar{c} C_{m_{elev}} \\
B_{\dot{q}, elevr}^{NL} &= \frac{1}{I_{yy}} \bar{q}S_{ref} \bar{c} C_{m_{elevr}} \\
B_{\dot{q}, pflap}^{NL} &= \frac{1}{I_{yy}} \bar{q}S_{ref} \bar{c} C_{m_{pflap}} \\
B_{\dot{q}, aaml}^{NL} &= \frac{1}{I_{yy}} \bar{q}S_{ref} \bar{c} C_{m_{aaml}} \\
B_{\dot{q}, amtr}^{NL} &= \frac{1}{I_{yy}} \bar{q}S_{ref} \bar{c} C_{m_{amtr}} \\
B_{\dot{q}, ptv}^{NL} &= -\frac{1}{I_{yy}} T d_{TFS} \\
B_{\dot{q}, ytv}^{NL} &= B_{\dot{q}, ytv}^{LS} \\
B_{\dot{q}, ssdl}^{NL} &= \frac{1}{I_{yy}} \bar{q}S_{ref} \bar{c} C_{m_{ssdl}}
\end{aligned}$$

$$\begin{aligned}
B_{\dot{q},ssdr}^{NL} &= \frac{1}{I_{yy}} \bar{q} S_{ref} \bar{c} C_{m_{ssd}} \\
B_{\dot{q},oblfl}^{NL} &= B_{\dot{q},oblfl}^{LS} \\
B_{\dot{q},oblfr}^{NL} &= B_{\dot{q},oblfr}^{LS} \\
B_{\dot{\beta},elevl}^{NL} &= B_{\dot{\beta},elevl}^{LS} \\
B_{\dot{\beta},elevr}^{NL} &= B_{\dot{\beta},elevr}^{LS} \\
B_{\dot{\beta},pflap}^{NL} &= B_{\dot{\beta},pflap}^{LS} \\
B_{\dot{\beta},amtl}^{NL} &= B_{\dot{\beta},amtl}^{LS} \\
B_{\dot{\beta},amtr}^{NL} &= B_{\dot{\beta},amtr}^{LS} \\
B_{\dot{\beta},ptv}^{NL} &= \frac{wvT}{mV^2 \sqrt{u^2 + w^2}} \\
B_{\dot{\beta},ytl}^{NL} &= \frac{(u^2 + w^2) T}{mV^2 \sqrt{u^2 + w^2}} \\
B_{\dot{\beta},ssdl}^{NL} &= B_{\dot{\beta},ssdl}^{LS} \\
B_{\dot{\beta},ssdr}^{NL} &= B_{\dot{\beta},ssdr}^{LS} \\
B_{\dot{\beta},oblfl}^{NL} &= B_{\dot{\beta},oblfl}^{LS} \\
B_{\dot{\beta},oblfr}^{NL} &= B_{\dot{\beta},oblfr}^{LS} \\
B_{\dot{p},elevl}^{NL} &= \bar{q} S_{ref} b \left(-\frac{I_{zz}}{I_{xx}I_{zz} - I_{xz}^2} C_{l_{elev}} - \frac{I_{xz}}{I_{xx}I_{zz} - I_{xz}^2} C_{n_{elev}} \right) \\
B_{\dot{p},elevr}^{NL} &= \bar{q} S_{ref} b \left(\frac{I_{zz}}{I_{xx}I_{zz} - I_{xz}^2} C_{l_{elev}} + \frac{I_{xz}}{I_{xx}I_{zz} - I_{xz}^2} C_{n_{elev}} \right) \\
B_{\dot{p},pflap}^{NL} &= B_{\dot{p},pflap}^{LS} \\
B_{\dot{p},amtl}^{NL} &= \bar{q} S_{ref} b \left(\frac{I_{zz}}{I_{xx}I_{zz} - I_{xz}^2} C_{l_{amt}} + \frac{I_{xz}}{I_{xx}I_{zz} - I_{xz}^2} C_{n_{amt}} \right) \\
B_{\dot{p},amtr}^{NL} &= \bar{q} S_{ref} b \left(-\frac{I_{zz}}{I_{xx}I_{zz} - I_{xz}^2} C_{l_{amt}} - \frac{I_{xz}}{I_{xx}I_{zz} - I_{xz}^2} C_{n_{amt}} \right) \\
B_{\dot{p},ptv}^{NL} &= 0 \\
B_{\dot{p},ytl}^{NL} &= \frac{I_{zz}}{I_{xx}I_{zz} - I_{xz}^2} T d_{TWL} - \frac{I_{xz}}{I_{xx}I_{zz} - I_{xz}^2} T d_{TFS} \\
B_{\dot{p},ssdl}^{NL} &= \bar{q} S_{ref} b \left(-\frac{I_{zz}}{I_{xx}I_{zz} - I_{xz}^2} C_{l_{ssd}} - \frac{I_{xz}}{I_{xx}I_{zz} - I_{xz}^2} C_{n_{ssd}} \right) \\
B_{\dot{p},ssdr}^{NL} &= \bar{q} S_{ref} b \left(\frac{I_{zz}}{I_{xx}I_{zz} - I_{xz}^2} C_{l_{ssd}} + \frac{I_{xz}}{I_{xx}I_{zz} - I_{xz}^2} C_{n_{ssd}} \right) \\
B_{\dot{p},oblfl}^{NL} &= -\frac{I_{zz}}{I_{xx}I_{zz} - I_{xz}^2} \bar{q} S_{ref} b C_{l_{oblfl}}
\end{aligned}$$

$$\begin{aligned}
B_{\dot{p},oblfr}^{NL} &= \frac{I_{zz}}{I_{xx}I_{zz} - I_{xz}^2} \bar{q} S_{ref} b C_{l_{oblfr}} \\
B_{\dot{r},elevl}^{NL} &= B_{\dot{r},elevl}^{LS} \\
B_{\dot{r},elevr}^{NL} &= B_{\dot{r},elevr}^{LS} \\
B_{\dot{r},pflap}^{NL} &= B_{\dot{r},pflap}^{LS} \\
B_{\dot{r},amtl}^{NL} &= \bar{q} S_{ref} b \left(\frac{I_{xx}}{I_{xx}I_{zz} - I_{xz}^2} C_{n_{amt}} + \frac{I_{xz}}{I_{xx}I_{zz} - I_{xz}^2} C_{l_{amt}} \right) \\
B_{\dot{r},amtr}^{NL} &= \bar{q} S_{ref} b \left(-\frac{I_{xx}}{I_{xx}I_{zz} - I_{xz}^2} C_{n_{amt}} - \frac{I_{xz}}{I_{xx}I_{zz} - I_{xz}^2} C_{l_{amt}} \right) \\
B_{\dot{r},ptv}^{NL} &= 0 \\
B_{\dot{r},yvu}^{NL} &= \frac{I_{xz}}{I_{xx}I_{zz} - I_{xz}^2} T d_{TWL} - \frac{I_{xx}}{I_{xx}I_{zz} - I_{xz}^2} T d_{TFS} \\
B_{\dot{r},ssdl}^{NL} &= \bar{q} S_{ref} b \left(-\frac{I_{xx}}{I_{xx}I_{zz} - I_{xz}^2} C_{n_{ssd}} - \frac{I_{xz}}{I_{xx}I_{zz} - I_{xz}^2} C_{l_{ssd}} \right) \\
B_{\dot{r},ssdr}^{NL} &= \bar{q} S_{ref} b \left(\frac{I_{xx}}{I_{xx}I_{zz} - I_{xz}^2} C_{n_{ssd}} + \frac{I_{xz}}{I_{xx}I_{zz} - I_{xz}^2} C_{l_{ssd}} \right) \\
B_{\dot{r},oblfl}^{NL} &= -\frac{I_{xx}}{I_{xx}I_{zz} - I_{xz}^2} \bar{q} S_{ref} b C_{n_{oblfr}} \\
B_{\dot{r},oblfr}^{NL} &= \frac{I_{xx}}{I_{xx}I_{zz} - I_{xz}^2} \bar{q} S_{ref} b C_{n_{oblfr}} \\
B_{\dot{\phi},elevl}^{NL} &= B_{\dot{\phi},elevl}^{LS} \\
B_{\dot{\phi},elevr}^{NL} &= B_{\dot{\phi},elevr}^{LS} \\
B_{\dot{\phi},pflap}^{NL} &= B_{\dot{\phi},pflap}^{LS} \\
B_{\dot{\phi},amtl}^{NL} &= B_{\dot{\phi},amtl}^{LS} \\
B_{\dot{\phi},amtr}^{NL} &= B_{\dot{\phi},amtr}^{LS} \\
B_{\dot{\phi},ptv}^{NL} &= B_{\dot{\phi},ptv}^{LS} \\
B_{\dot{\phi},yvu}^{NL} &= B_{\dot{\phi},yvu}^{LS} \\
B_{\dot{\phi},ssdl}^{NL} &= B_{\dot{\phi},ssdl}^{LS} \\
B_{\dot{\phi},ssdr}^{NL} &= B_{\dot{\phi},ssdr}^{LS} \\
B_{\dot{\phi},oblfl}^{NL} &= B_{\dot{\phi},oblfl}^{LS} \\
B_{\dot{\phi},oblfr}^{NL} &= B_{\dot{\phi},oblfr}^{LS} \\
B_{\dot{\theta},elevl}^{NL} &= B_{\dot{\theta},elevl}^{LS} \\
B_{\dot{\theta},elevr}^{NL} &= B_{\dot{\theta},elevr}^{LS} \\
B_{\dot{\theta},pflap}^{NL} &= B_{\dot{\theta},pflap}^{LS}
\end{aligned}$$

$$\begin{aligned}
B_{\dot{\theta},amtl}^{NL} &= B_{\dot{\theta},amtl}^{LS} \\
B_{\dot{\theta},amtr}^{NL} &= B_{\dot{\theta},amtr}^{LS} \\
B_{\dot{\theta},ptv}^{NL} &= B_{\dot{\theta},ptv}^{LS} \\
B_{\dot{\theta},ytl}^{NL} &= B_{\dot{\theta},ytl}^{LS} \\
B_{\dot{\theta},ssdl}^{NL} &= B_{\dot{\theta},ssdl}^{LS} \\
B_{\dot{\theta},ssdr}^{NL} &= B_{\dot{\theta},ssdr}^{LS} \\
B_{\dot{\theta},oblfl}^{NL} &= B_{\dot{\theta},oblfl}^{LS} \\
B_{\dot{\theta},oblfr}^{NL} &= B_{\dot{\theta},oblfr}^{LS} \\
B_{\dot{V},elevl}^{NL} &= B_{\dot{V},elevl}^{LS} \\
B_{\dot{V},elevr}^{NL} &= B_{\dot{V},elevr}^{LS} \\
B_{\dot{V},pflap}^{NL} &= B_{\dot{V},pflap}^{LS} \\
B_{\dot{V},amtl}^{NL} &= B_{\dot{V},amtl}^{LS} \\
B_{\dot{V},amtr}^{NL} &= B_{\dot{V},amtr}^{LS} \\
B_{\dot{V},ptv}^{NL} &= B_{\dot{V},ptv}^{LS} \\
B_{\dot{V},ytl}^{NL} &= B_{\dot{V},ytl}^{LS} \\
B_{\dot{V},ssdl}^{NL} &= B_{\dot{V},ssdl}^{LS} \\
B_{\dot{V},ssdr}^{NL} &= B_{\dot{V},ssdr}^{LS} \\
B_{\dot{V},oblfl}^{NL} &= B_{\dot{V},oblfl}^{LS} \\
B_{\dot{V},oblfr}^{NL} &= B_{\dot{V},oblfr}^{LS} \\
u &= \frac{V}{\sqrt{(1 + \tan^2 \alpha)(1 + \tan^2 \beta)}} \\
v &= \frac{V \tan \beta}{\sqrt{1 + \tan^2 \beta}} \\
w &= u \tan \alpha \\
\dot{u} &= rv - qw + \frac{\bar{q} S_{ref} C_x + T - D_e \cos \alpha - W \sin \theta}{m} \\
\dot{v} &= pw - ru + \frac{\bar{q} S_{ref} C_y + W \cos \theta \sin \phi}{m} \\
\dot{w} &= qu - pv + \frac{\bar{q} S_{ref} C_z + D_e \sin \alpha + W \cos \theta \cos \phi}{m}
\end{aligned} \tag{3.22}$$

The aerodynamic and propulsive parameters from eq.(3.22) that are modeled using piecewise least squares polynomials of the data are contained in Table 3.5. Note that the fit structure in Table 3.5 is notional. So for example, although the coefficient c_0 appears for many parameters, it is not the same for each parameter.

Table 3.5: Nonlinear model data fits

Symbol	Description	Fit Structure
T	Thrust	$c_0 + c_1 M + c_2 M^2 + c_3 M^3 + h(c_4 + c_5 M + c_6 M^2 + c_7 M^3)$
D_e	Engine ram drag	$c_0 + c_1 M + c_2 M^2 + h(c_3 + c_4 M + c_5 M^2)$
C_x	X body axis force coefficient	$c_0 + c_1 \alpha + c_2 \alpha^2 + \beta^2(c_3 + c_4 \alpha + c_5 \alpha^2 + c_6 \alpha^3)$
C_y	Y body axis force coefficient	$\beta(c_0 + c_1 \alpha + c_2 \alpha^2 + c_3 \alpha^3 + c_4 \alpha^4) + \frac{b}{2V}(c_5 p + c_6 r)$
C_z	Z body axis force coefficient	$c_0 + c_1 \alpha + c_2 \alpha^2 + c_3 \alpha^3 + \beta^2(c_4 + c_5 \alpha + c_6 \alpha^2 + c_7 \alpha^3) + c_8 \frac{q\bar{c}}{2V}$
C_l	Roll moment coefficient	$\beta(c_0 + c_1 \alpha + c_2 \alpha^2 + c_3 \alpha^3 + c_4 \alpha^4 + c_5 \alpha^5) + \frac{b}{2V}((c_0 + c_1 \alpha + c_2 \alpha^2 + c_3 \alpha^3 + c_4 \alpha^4)p + (c_0 + c_1 \alpha + c_2 \alpha^2 + c_3 \alpha^3 + c_4 \alpha^4)r)$
C_m	Pitch moment coefficient	$(c_0(\alpha) + c_1(\alpha)\alpha + c_2(\alpha)\alpha^2 + c_3(\alpha)\alpha^3) + (c_0 + c_1 \alpha + c_2 \alpha^2 + c_3 \alpha^3 + c_4 \alpha^4 + c_5 M + c_6 M \alpha) \frac{q\bar{c}}{2V}$
C_n	Yaw moment coefficient	$c_0 + c_1 \alpha + c_2 \alpha^2 + c_3 \alpha^3 + \beta^2(c_4 + c_5 \alpha + c_6 \alpha^2 + c_7 \alpha^3) + \frac{b}{2V}((c_0 + c_1 \alpha + c_2 \alpha^2 + c_3 \alpha^3 + c_4 \alpha^4)p + (c_0 + c_1 \alpha + c_2 \alpha^2 + c_3 \alpha^3 + c_4 \alpha^4)r)$
$C_{l_{elev}}$	Roll moment due to elevon	$c_0 + c_1 \alpha + c_2 \alpha^2 + c_3 \alpha^3$
$C_{l_{amt}}$	Roll moment due to all moving tip	$c_0 + c_1 \alpha + c_2 \alpha^2 + c_3 \alpha^3$
$C_{l_{ssd}}$	Roll moment due to spoiler slot deflector	$c_0 + c_1 \alpha + c_2 \alpha^2 + c_3 \alpha^3$
$C_{l_{oblif}}$	Roll moment due to outboard leading edge flap	$c_0 + c_1 \alpha + c_2 \alpha^2 + c_3 \alpha^3$
$C_{m_{elev}}$	Pitch moment due to elevon	$c_0 + c_1 \alpha + c_2 \alpha^2 + c_3 \alpha^3$
$C_{m_{pflap}}$	Pitch moment due to pitch flap	$c_0 + c_1 \alpha + c_2 \alpha^2 + c_3 \alpha^3$
$C_{m_{amt}}$	Pitch moment due to all moving tip	$c_0(\alpha) + c_1(\alpha)\alpha + c_2(\alpha)\alpha^2 + c_3(\alpha)\alpha^3$
$C_{m_{ssd}}$	Pitch moment due to spoiler slot deflector	$c_0 + c_1 \alpha + c_2 \alpha^2 + c_3 \alpha^3$
$C_{n_{amt}}$	Yaw moment due to all moving tip	$c_0 + c_1 \alpha + c_2 \alpha^2 + c_3 \alpha^3$
$C_{n_{ssd}}$	Yaw moment due to spoiler slot deflector	$c_0 + c_1 \alpha + c_2 \alpha^2 + c_3 \alpha^3$
$C_{n_{oblif}}$	Yaw moment due to outboard leading edge flap	$c_0 + c_1 \alpha + c_2 \alpha^2 + c_3 \alpha^3$

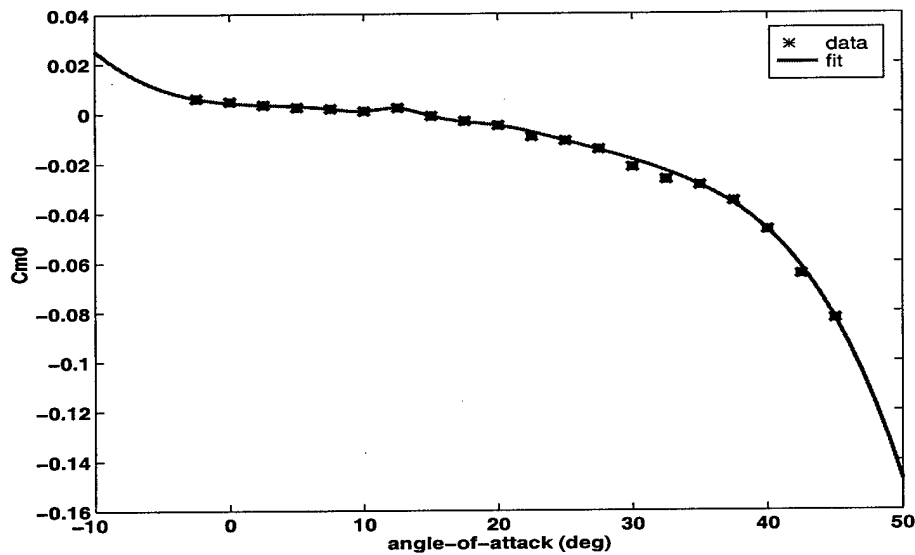


Figure 3.8: Static pitching moment spline fit

Although not explicitly annotated, the propulsion parameter (T , D_e) coefficients are functions of power lever angle. Recall that the simulation aerodynamic model has a low speed ($\text{Mach} \leq 0.5$) and a high speed part ($\text{Mach} \geq 0.6$) and are blended together at intermediate speeds ($0.5 < \text{Mach} < 0.6$). The aerodynamic parameter coefficients in Table 3.5 are also functions of these Mach partitions.

The dynamic inversion controller was particularly sensitive to the low speed aerodynamic static pitching moment, so high fidelity cubic splines were used as a model. A polynomial representation of the static pitching moment cubic spline is given from Table 3.5 as

$$C_{m_0} = c_0(\alpha) + c_1(\alpha)\alpha + c_2(\alpha)\alpha^2 + c_3(\alpha)\alpha^3 \quad (3.23)$$

The final spline fit is shown in Fig.(3.8).

Perfect Airframe Model

Besides a linear and nonlinear on-board aircraft model, a “perfect” on-board model mode was implemented for comparison purposes. This “perfect” on-board model is truly only nearly perfect since it has the following affine form

$$\dot{x}_m = A_m^{PERF} + B_m^{PERF}u$$

$$A_m^{PERF} = \begin{bmatrix} a_{\dot{\alpha}} \\ a_{\dot{q}} \\ A_{\dot{\beta}}^{NL} \\ a_{\dot{p}} \\ a_{\dot{r}} \\ A_{\dot{\phi}}^{NL} \\ A_{\dot{\theta}}^{NL} \\ A_{\dot{v}}^{NL} \end{bmatrix} \quad (3.24)$$

where $a_{\dot{\alpha}}, a_{\dot{q}}, a_{\dot{p}}, a_{\dot{r}}$ are elements of a in eq.(2.2) and B_m^{PERF} is identical to B_m^{NL} in eq.(3.22) except that the true thrust T and ram drag D_e data are used. Of course this mode is not intended to be a viable alternative for implementation, but it does provide a useful mode for comparison.

Actuator model

The on-board actuator model consists of actuator position and no-load rate limits. The hinge moment effect for all surfaces were neglected since the simulation model also did not include these effects. Actuator dynamics are neglected since the control allocation approach is inherently static. Control effector rate and position limits are derived from the simulation model data in Table 2.1 and are given by the following

$$\begin{aligned} u_u &= [30 \ 30 \ 30 \ 60 \ 60 \ 10 \ 10 \ 10 \ 10 \ 40 \ 40]^T \\ u_l &= [-30 \ -30 \ -30 \ 0 \ 0 \ -10 \ -10 \ 0 \ 0 \ 0 \ 0]^T \\ u_r &= [150 \ 150 \ 50 \ 150 \ 150 \ 60 \ 60 \ 150 \ 150 \ 40 \ 40]^T \end{aligned} \quad (3.25)$$

Note that for the on-board model, the spoiler slot deflector (elements 8,9) upper limits are artificially reduced from the actual actuator data in Table 2.1. This was done to limit the spoiler slot deflector and elevon interactions.

Mission Segment Objective Model

The following models are used by the control allocation algorithm to optimize specific mission segment objectives such as minimum drag or wing loads. Recall that a mission segment objective is completely specified by a control preference (u_{pref}) and corresponding weight (W_u) from eq.(3.12).

Minimum Control Deflection The minimum control deflection control allocation mode is implemented by the following choice of parameters

$$\begin{aligned} u_{pref} &= [0 \ 0 \ 0 \ 0 \ 0 \ 0 \ 0 \ 0 \ 0 \ 0 \ 0]^T \\ W_u &= [1 \ 1 \ 1 \ 1 \ 1 \ 1 \ 1 \ 1 \ 1 \ 1 \ 1] \end{aligned} \quad (3.26)$$

which equally emphasizes all effectors toward zero deflections.

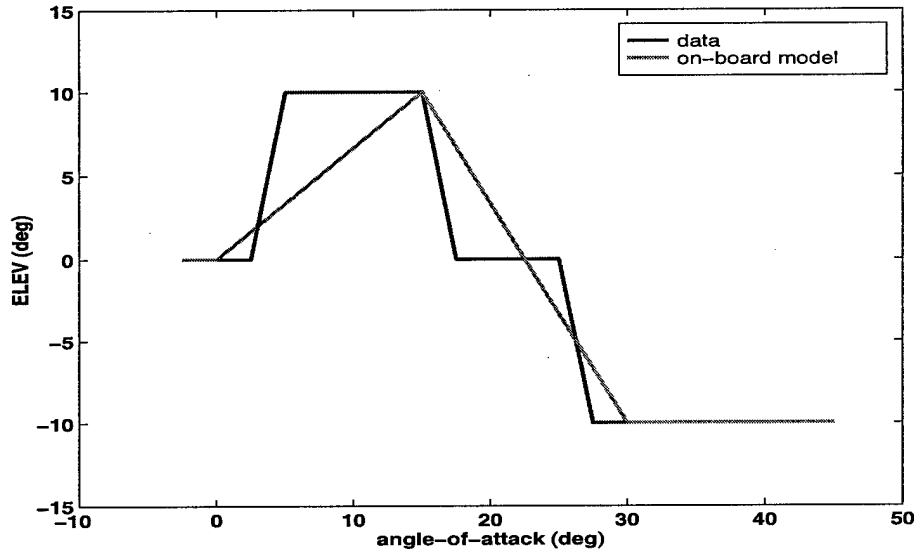


Figure 3.9: Elevon minimum drag deflection

Minimum Drag At low subsonic speeds, $\text{Mach} \leq 0.5$, the minimum drag control allocation mode uses an on-board drag model to compute u_{pref} . Due to time limitations, no on-board drag model was developed above Mach 0.5. So for $\text{Mach} > 0.5$, the minimum drag control allocation mode is exactly the same as the minimum deflection mode.

The low speed on-board drag model was generated from the control surface axial force wind tunnel data. The minimal axial force deflections for the elevons, pitch flaps, and outboard leading edge flaps are given in Figs.(3.9, 3.10, 3.11) respectively. The minimum drag deflection data is questionable since large constant deflections result in the minimum axial forces which seems counter intuitive. Although the wind tunnel data looks suspect, the minimum drag control allocation mode may be demonstrated using this data. As better data is collected, the on-board model may also be revised.

The minimum drag control allocation mode is implemented by the following choice of parameters for $\text{Mach} \leq 0.5$

$$\begin{aligned} u_{pref} &= [f_{el}(\alpha) \ f_{el}(\alpha) \ f_{pf}(\alpha) \ 0 \ 0 \ 0 \ 0 \ 0 \ 0 \ f_{obl}(\alpha) \ f_{obl}(\alpha)]^T \\ W_u &= [10.0 \ 10.0 \ 10.0 \ 0.1 \ 0.1 \ 0.01 \ 0.01 \ 100.0 \ 100.0 \ 1.0 \ 1.0] \end{aligned} \quad (3.27)$$

where $f_{el}(\alpha)$, $f_{pf}(\alpha)$, $f_{obl}(\alpha)$ are the on-board drag due to control deflection models indicated in Figs.(3.9, 3.10, 3.11). The minimum drag control allocation mode is implemented by the following choice of parameters for $\text{Mach} > 0.5$

$$\begin{aligned} u_{pref} &= [0 \ 0 \ 0 \ 0 \ 0 \ 0 \ 0 \ 0 \ 0 \ 0 \ 0]^T \\ W_u &= [1 \ 1 \ 1 \ 1 \ 1 \ 1 \ 1 \ 1 \ 1 \ 1 \ 1] \end{aligned} \quad (3.28)$$

which are identical to the minimum control deflection values.

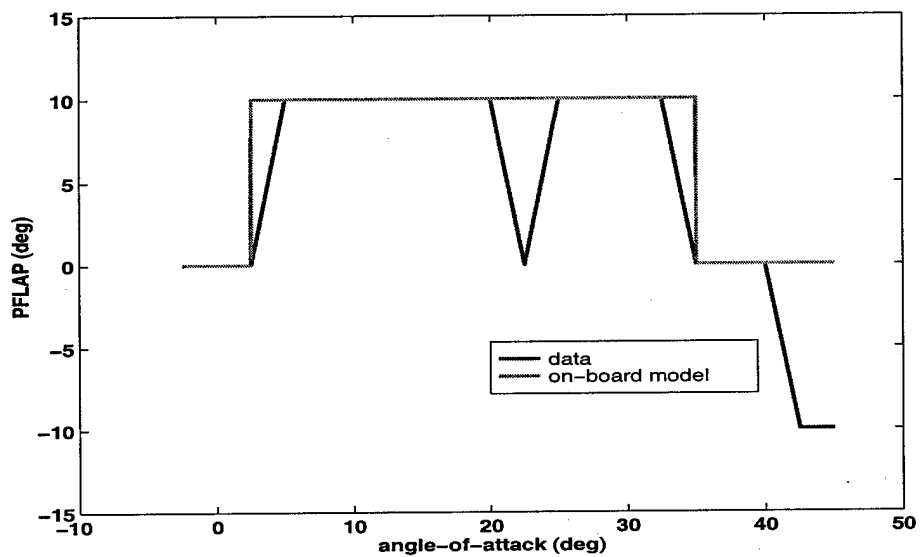


Figure 3.10: Pitch flap minimum drag deflection

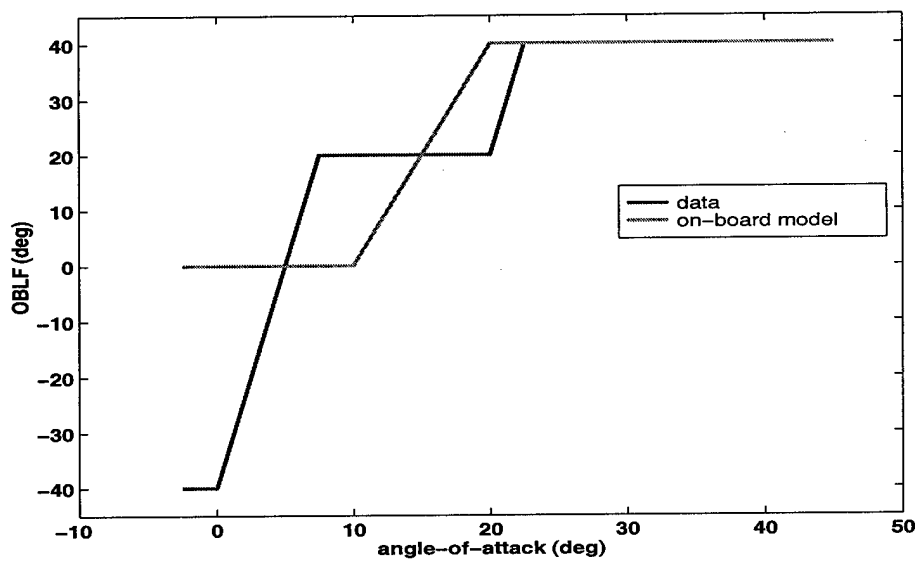


Figure 3.11: Outboard leading edge flap minimum drag deflection

Minimum Wing Loading The minimum wing load model is simplistic. Higher weights are chosen for outboard control effectors since they qualitatively give higher wing root bending moments than inboard surfaces. The minimum wing loading control allocation mode is implemented by the following choice of parameters

$$\begin{aligned} u_{pref} &= [0 \ 0 \ 0 \ 0 \ 0 \ 0 \ 0 \ 0 \ 0 \ 0 \ 0 \ 0]^T \\ W_u &= [1.0 \ 1.0 \ 0.1 \ 1000. \ 1000. \ 0.01 \ 0.01 \ 1.0 \ 1.0 \ 10.0 \ 10.0] \end{aligned} \quad (3.29)$$

which emphasize the all moving tips toward a zero deflection.

Minimum Signature The minimum radar signature model is also simplistic. Higher weights are chosen for spoiler slot-deflectors and all-moving tips since they qualitatively give higher radar signatures than the other effectors. The minimum signature control allocation mode is implemented by the following choice of parameters

$$\begin{aligned} u_{pref} &= [0 \ 0 \ 0 \ 0 \ 0 \ 0 \ 0 \ 0 \ 0 \ 0 \ 0]^T \\ W_u &= [1.0 \ 1.0 \ 1.0 \ 10. \ 10. \ 0.01 \ 0.01 \ 100.0 \ 100.0 \ 1.0 \ 1.0] \end{aligned} \quad (3.30)$$

Null Space Injection The only parameter that is required for the null space injection mode is the nominal weight \tilde{W} in eq.(3.14) chosen to equally distribute commands. The elements of \tilde{W} were nominally chosen as the inverse of the absolute value of the corresponding effector deflection limit. These were tuned to the following values based on simulation responses to achieve equally distributed commands.

$$\tilde{W} = \text{diag} \left(\frac{1}{30}, \frac{1}{30}, \frac{1}{30}, \frac{1}{120}, \frac{1}{120}, \frac{1}{15}, \frac{1}{15}, \frac{1}{120}, \frac{1}{120}, \frac{1}{80}, \frac{1}{80} \right) \quad (3.31)$$

Minimum Thrust Vectoring The minimum thrust vectoring control allocation mode is implemented by the following choice of parameters

$$\begin{aligned} u_{pref} &= [0 \ 0 \ 0 \ 0 \ 0 \ 0 \ 0 \ 0 \ 0 \ 0 \ 0]^T \\ W_u &= [1.0 \ 1.0 \ 1.0 \ 1.0 \ 1.0 \ 1000.0 \ 1000.0 \ 1.0 \ 1.0 \ 1.0 \ 1.0] \end{aligned} \quad (3.32)$$

which emphasize the thrust vector nozzle toward zero deflection.

Constants and Measurements

Required constants for the configuration model are contained in Table 3.6, and required measured variables are contained in Table 3.7.

Table 3.6: Nonlinear model constants

Symbol	Description	Value
$C_{L_\alpha} _{\alpha=0}$	lift coefficient due to angle of attack at zero angle of attack	$2.42 \frac{1}{rad}$
V_{co}	crossover velocity	$400 \frac{ft}{sec}$
I_{xx}	x -axis moment of inertia	$35,479 slug - ft^2$
I_{yy}	y -axis moment of inertia	$78,451 slug - ft^2$
I_{zz}	z -axis moment of inertia	$110,627 slug - ft^2$
I_{xz}	xz -axes product of inertia	$-525 slug - ft^2$
S_{ref}	wing planform area	$808.6 ft^2$
\bar{c}	wing mean aerodynamic chord	$28.75 ft$
b	wing span	$37.5 ft$
m	aircraft mass	$1017.9 slug$
W	aircraft gross weight	$32,750 lb$
d_{TWL}	waterline distance between center of gravity and thrust application point	$0.5025 ft$
d_{TFS}	fuselage station distance between center of gravity and thrust application point	$18.76 ft$
d_{DWL}	waterline distance between center of gravity and ram drag application point	$-0.3308 ft$
d_{DFS}	fuselage station distance between center of gravity and ram drag application point	$-12.66 ft$

Table 3.7: Nonlinear model required measurements

Symbol	Description	Units
p	roll rate	$\frac{deg}{sec}$
q	pitch rate	$\frac{deg}{sec}$
r	yaw rate	$\frac{deg}{sec}$
α	angle of attack	deg
β	angle of slip	deg
V	total velocity	$\frac{ft}{sec}$
\bar{q}	dynamic pressure	$\frac{lb}{ft^2}$
ϕ	roll attitude angle	deg
θ	pitch attitude angle	deg

Summary

The on-board model contains configuration and requirements data. Configuration data includes aerodynamic, propulsion and actuator models. Requirements data includes command variable definitions and desired command variable bandwidths. The configuration data has the following known modeling errors compared to the simulation model: neglected actuator dynamics, aerodynamic and propulsive approximations, control effector interaction effects neglected, velocity changes neglected.

3.5 Model Error Compensation

The on-board model in Section 3.4 will contain errors from many possible sources. The robustness of the control law accounts for some level of model error. Adaptation may be used to account for higher levels of model error due to failures, damage or highly nonlinear phenomena [7, 12, 19]. Indirect and direct adaptation methods have already been successfully demonstrated on flight test aircraft [2, 5]. Future plans include integration of on-line system identification [13] and adaptive neural networks [28] to provide adaptive model error compensation.

Chapter 4

Flight Control Law Analysis

Analysis of the flight control law in Chapter 3 is contained in this chapter. Eigenvalue analysis is used to analyze the nominal stability, flying qualities criteria are used for nominal performance analysis and structured singular values and batch simulations are used to analyze robust stability and performance. Real time simulation analysis has begun to assess pilot in the loop performance, and results will be reported in a future document.

Eigenvalue and batch simulation analyses are presented at four representative flight conditions. The first flight condition is Mach 0.35 and 5,000 ft. altitude and represents a low dynamic pressure powered approach condition. The second flight condition is Mach 0.60 and 15,000 ft. altitude and represents a center of the envelope, air combat maneuvering condition. The third flight condition is Mach 0.90 and 1,000 ft. altitude and represents a low altitude high subsonic ingress condition. The final flight condition is Mach 1.20 and 22,500 ft. altitude and represents a supersonic cruise condition. Table 4.1 lists the properties of these four analysis flight conditions.

Structured singular value and flying qualities analyses are presented for a subset of the flight conditions in Fig.(3.4). These analysis flight conditions provide a complete dynamic pressure variation of the subsonic flight envelope and are given in Table 4.2.

Table 4.1: Eigenvalue and batch simulation analyses flight conditions

Description	Notation	Mach	Altitude (ft)	Angle of attack (deg)	Dynamic pressure ($\frac{lb}{ft^2}$)
Low \bar{q} , powered approach	m35h5	0.35	5,000	8.01	151
Envelope center, air combat	m6h15	0.60	15,000	3.70	306
High subsonic, ingress	m9h1	0.90	1,000	0.904	1157
Supersonic, cruise	m12h225	1.20	22,500	1.48	882

Table 4.2: Structured singular value and flying qualities analyses flight conditions

Mach	Altitude (ft)	Angle of attack (deg)	Dynamic pressure ($\frac{lb}{ft^2}$)
0.35	15,000	10.8	102
0.75	40,000	7.09	154
0.45	10,000	6.16	206
0.85	35,000	4.24	252
0.75	25,000	3.54	309
0.50	1,000	3.90	357
0.65	10,000	2.61	430
0.85	20,000	2.18	492
0.65	1,000	1.86	604
0.75	5,000	1.58	694
0.75	1,000	1.37	804
0.85	5,000	1.20	891

4.1 Nominal Stability

Nominal stability of the closed loop flight control system is guaranteed from the dynamic inversion flight control theory if the chosen command variable dynamics are stabilizing and the aircraft is minimum phase (stable zero dynamics), see Section 2.2. The stability of the command variable and zero dynamics is determined by eigenvalue analysis and confirmed by simulations.

The nominal closed loop command variable dynamics are linear by design and given by

$$\begin{bmatrix} \dot{y} \\ \dot{x}_i \end{bmatrix} = \begin{bmatrix} -\omega_c & 0 & 0 & \omega_c & 0 & 0 \\ 0 & -\omega_c & 0 & 0 & \omega_c & 0 \\ 0 & 0 & -\omega_c & 0 & 0 & \omega_c \\ -\omega_c f_i & 0 & 0 & 0 & 0 & 0 \\ 0 & -\omega_c f_i & 0 & 0 & 0 & 0 \\ 0 & 0 & -\omega_c f_i & 0 & 0 & 0 \end{bmatrix} \begin{bmatrix} y \\ x_i \end{bmatrix} + \begin{bmatrix} \omega_c f_c & 0 & 0 \\ 0 & \omega_c f_c & 0 \\ 0 & 0 & \omega_c f_c \\ \omega_c f_i & 0 & 0 \\ 0 & \omega_c f_i & 0 \\ 0 & 0 & \omega_c f_i \end{bmatrix} y^{cmd} \quad (4.1)$$

The nominal stability of the command variables is completely specified by the eigenvalues of the following system matrix

$$A_{CV} \equiv \begin{bmatrix} -\omega_c & 0 & 0 & \omega_c & 0 & 0 \\ 0 & -\omega_c & 0 & 0 & \omega_c & 0 \\ 0 & 0 & -\omega_c & 0 & 0 & \omega_c \\ -\omega_c f_i & 0 & 0 & 0 & 0 & 0 \\ 0 & -\omega_c f_i & 0 & 0 & 0 & 0 \\ 0 & 0 & -\omega_c f_i & 0 & 0 & 0 \end{bmatrix} = \begin{bmatrix} -5 & 0 & 0 & 5 & 0 & 0 \\ 0 & -5 & 0 & 0 & 5 & 0 \\ 0 & 0 & -5 & 0 & 0 & 5 \\ -5\frac{1}{4} & 0 & 0 & 0 & 0 & 0 \\ 0 & -5\frac{1}{4} & 0 & 0 & 0 & 0 \\ 0 & 0 & -5\frac{1}{4} & 0 & 0 & 0 \end{bmatrix} \quad (4.2)$$

$$\text{eig}(A_{cv}) = -2.5, -2.5, -2.5, -2.5, -2.5, -2.5$$

which proves nominal asymptotic stability of the command variables since all eigenvalues have negative real parts.

The stability analysis of the zero dynamics is more complicated due to nonlinearities. The assessment of nominal stability is made by analyzing the following linear approximation

to the complementary dynamics in eq.(2.8)

$$\begin{aligned}\dot{z} &= A_{zz}z + B_z\tilde{u}(z) \\ \tilde{u}(z) &= -W^{-1}B_y^T (B_yW^{-1}B_y^T)^{-1} A_{yz}z\end{aligned}\quad (4.3)$$

which assumes the following linear form for the control allocator

$$u = -W^{-1}B_y^T (B_yW^{-1}B_y^T)^{-1} d_y^{des} \quad (4.4)$$

The asymptotic stability of the system in eq.(4.3) is determined by the eigenvalues of the following system matrix

$$A_{ZD} = A_{zz} - B_zW^{-1}B_y^T (B_yW^{-1}B_y^T)^{-1} A_{yz} \quad (4.5)$$

The linear control allocation weight in eqs.(4.3, 4.4, 4.5) is chosen to best reflect simulation responses of the linear programming control allocation method in Section (3.3). Simulation responses have shown that the linear programming control allocation method attempts to put as many control effectors on their preferences as possible thus only using a few to achieve the control law moment command automatically canceling the residual moment effect of those effectors on their preference. Recall that most control allocation modes in Section (3.3) have zero preferences. Thus, the linear control allocation function in eq.(4.4) is a good approximation to the linear program control allocator if very large weights corresponding to those effectors that follow zero are chosen. Weights are chosen to approximate the linear program control allocation at the corresponding flight condition based on simulation time histories of the control deflections. For example, the linear program primarily uses the elevons and all moving tips for small inputs at Mach=0.35 and 5000 ft. altitude. Therefore, all diagonal elements of the inverse weight matrix at this flight condition are chosen zero except those corresponding to the elevons (elements 1 and 2) and all moving tips (elements 4 and 5). Similar weights are constructed based on simulation responses for the other flight conditions as well. Two other weights were generated for illustrative comparison purposes. One weight was constructed to mimic a control allocator that only uses spoiler slot deflectors for yaw control. The final weight was an identity matrix which corresponds to using all surfaces. The four weights used for analysis are given by the following

$$\begin{aligned}W_{m35h5}^{-1} &= \text{diag}([1 \ 1 \ 0 \ 1 \ 1 \ 0 \ 0 \ 0 \ 0 \ 0 \ 0 \ 0]) \\ W_{m6h15}^{-1} &= \text{diag}([1 \ 1 \ 1 \ 0 \ 0 \ 1 \ 1 \ 0 \ 0 \ 0 \ 0]) \\ W_{m9h1}^{-1} &= \text{diag}([1 \ 1 \ 0 \ 0 \ 0 \ 1 \ 1 \ 0 \ 0 \ 0 \ 0]) \\ W_{m12h225}^{-1} &= \text{diag}([1 \ 1 \ 0 \ 0 \ 0 \ 0 \ 1 \ 0 \ 0 \ 0 \ 0]) \\ W_{ssd}^{-1} &= \text{diag}([1 \ 1 \ 1 \ 0 \ 0 \ 1 \ 0 \ 1 \ 1 \ 0 \ 0]) \\ W_{ident}^{-1} &= \text{diag}([1 \ 1 \ 1 \ 1 \ 1 \ 1 \ 1 \ 1 \ 1 \ 1 \ 1])\end{aligned}\quad (4.6)$$

Table 4.3 shows the eigenvalues of the zero dynamics system matrix in eq.(4.5) at each analysis flight condition in Table 4.1 for each weight in eq.(4.6). Note that the diagonal

Table 4.3: Subroutine Functionality

Flight Condition	Mach=0.35 Alt=5000 ft.	Mach=0.60 Alt=15000 ft.	Mach=0.90 Alt=1000 ft.	Mach=1.20 Alt=22500 ft.
W_{m35h5}	-1.47, -0.321	-2.21, -0.580	-7.46, -2.72	-5.24, -2.86
W_{m6h15}	-1.47, -0.320	-2.22, -0.563	-7.48, -2.18	-5.33, -1.67
W_{m9h1}	-1.47, -0.320	-2.22, -0.563	-7.48, -2.18	-5.33, -1.67
$W_{m12h225}$	-1.47, -0.320	-2.22, -0.563	-7.48, -2.18	-5.34, -1.67
W_{ssd}	-1.47, 0.551	-2.22, -0.526	-7.48, -2.24	-5.33, -1.70
W_{ident}	-1.47, -0.326	-2.21, -0.555	-7.46, -2.19	-5.25, -1.67

elements of Table 4.3 correspond to the linear approximation of the nominal allocation mode for the particular flight condition.

It is seen that the stability of the zero dynamics is relatively insensitive to the choice of weights at all flight conditions except the low dynamic pressure condition. Although W_{m35h5} gives nominally stable zero dynamics at Mach 0.35 and 5000 ft. altitude, W_{ssd} destabilizes the zero dynamics. Small roll stick pulse command simulation responses in Figs.(4.1,4.2) confirm the eigenvalue stability analysis of the zero dynamics at this flight condition. It is seen that the aircraft departs when using only spoiler slot deflectors. Note that SSD refers to the control allocation that primarily uses the spoiler slot deflectors for yaw control, and AMT refers to the control allocation that primarily uses the all moving tips for yaw control.

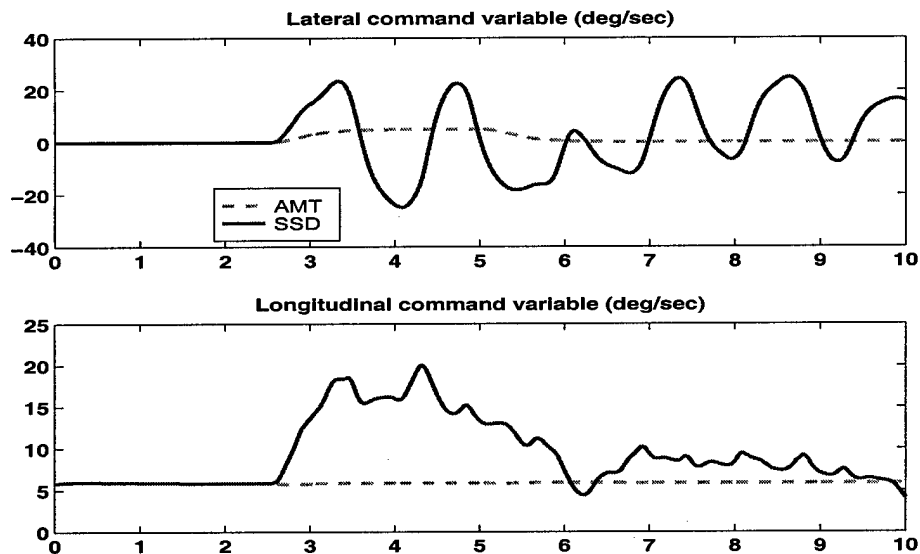


Figure 4.1: Mach 0.35, 5000 ft. Altitude, Zero Dynamics Stability

This analysis shows that the linear program control allocation method may reduce stability margins or even destabilize the zero dynamics when it does not use all of the effectors. This possibly explains the lightly damped behavior in the simulation responses for some control allocation modes at Mach 0.35 and 5000 ft. altitude in Section (4.4).

4.2 Flying qualities

The MATLAB flying qualities toolbox [14] was used to initially analyze the flying qualities of the flight control system at the flight conditions in Table 4.2. The longitudinal flying qualities were analyzed using the bandwidth criterion and the control anticipation parameter (CAP) from a low order equivalent system (LOES). It is seen in Fig.(4.3) that Level 1 CAP is achieved and borderline Level 1, Level 2 bandwidth is achieved. The lateral/directional flying qualities were analyzed using LOES parameters and the roll pilot induced oscillation (PIO) criterion. It is seen in Figs.(4.4,4.5) that Level 1 flying qualities are achieved and PIO tendencies do not exist.

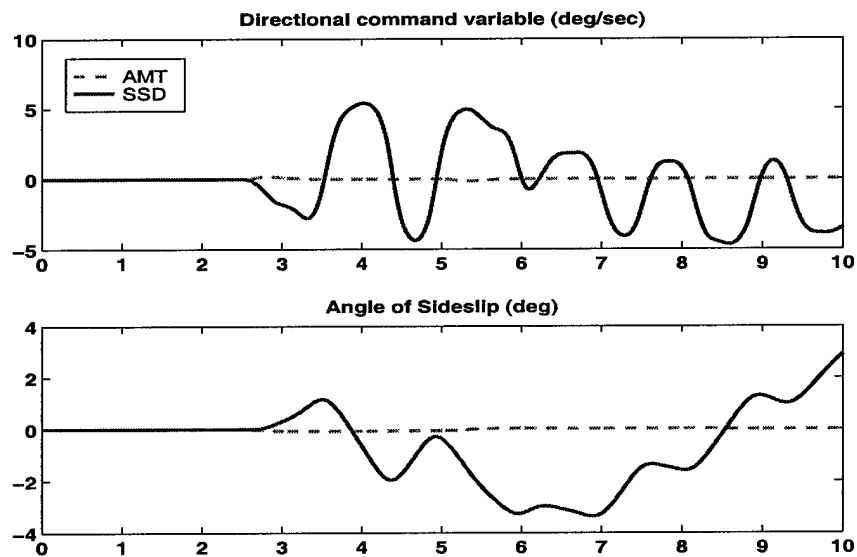


Figure 4.2: Mach 0.35, 5000 ft. Altitude, Zero Dynamics Stability

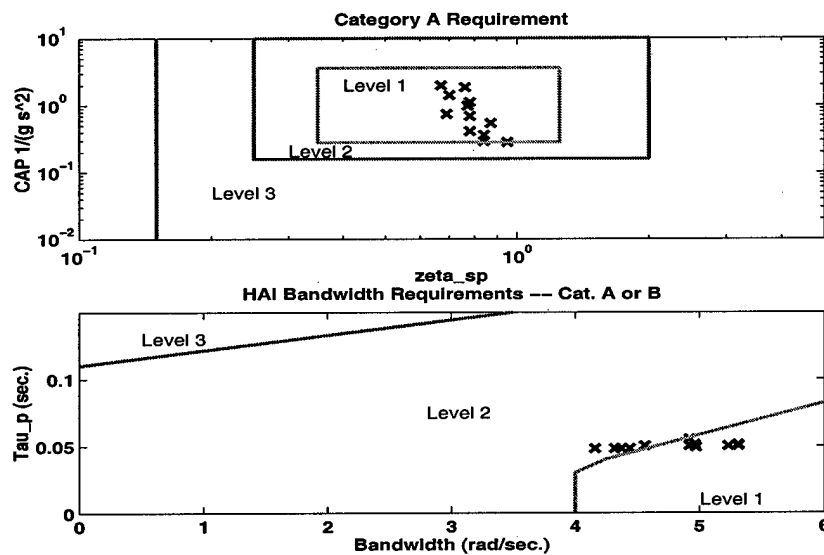


Figure 4.3: Longitudinal Flying Qualities Criteria

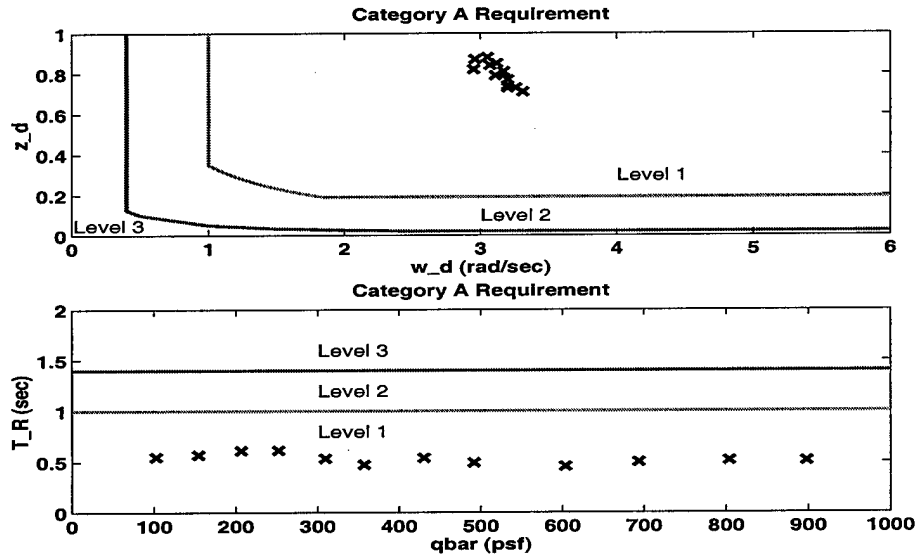


Figure 4.4: Lateral/Directional Flying Qualities Criteria

More details of this analysis, as well as a comparison with a linear parameter varying control law, appear in [9].

4.3 Robustness

Structured singular values were used to assess robust stability and performance of the flight control system at the flight conditions in Table 4.2. Separate longitudinal and lateral/directional analyses were performed. Note that identity weights were used for the linear control allocator approximation in eq.(4.4) for this analysis. Figure (4.6) shows the structured singular value analysis model for the lateral/directional axes. There are three uncertainty blocks. The first uncertainty block is unstructured with 2 inputs and 2 outputs. Command response performance is captured in this block with the following roll and yaw error weight

$$W_e = \frac{1}{.01s^2 + 0.14s + 1} \quad (4.7)$$

which is a low pass filter to emphasize low frequency tracking. The second uncertainty block is unstructured with 2 inputs and 2 outputs. Controller bandwidth constraints are captured in this block with the following roll and yaw input uncertainty weight

$$W_i = \frac{10s + 1}{s + 100} \quad (4.8)$$

which is a high pass filter with a gain crossover frequency of $10 \frac{rad}{sec}$ to emphasize high frequency attenuation. The third uncertainty block is a structured uncertainty block with 2 inputs

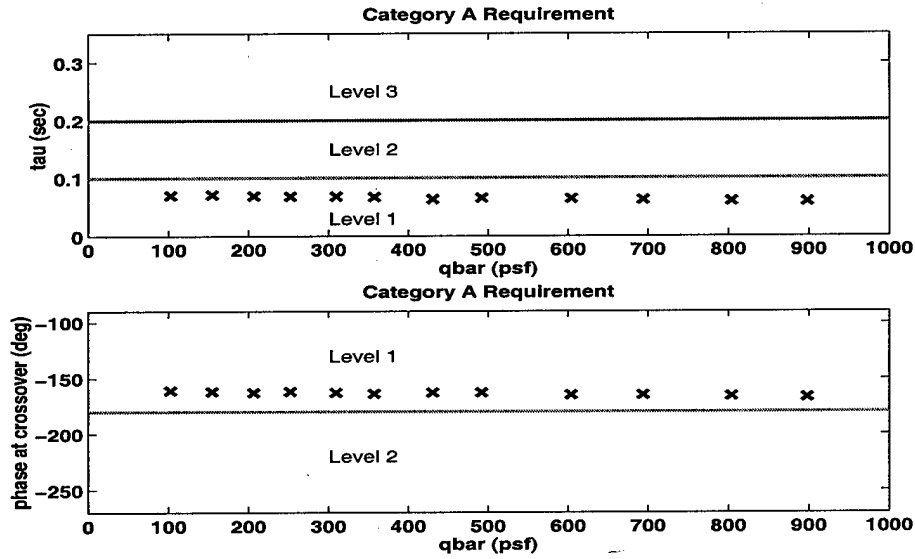


Figure 4.5: Lateral/Directional Flying Qualities Criteria

and 2 outputs. Stability derivative parameter uncertainty of $0.2N_\beta$ and $0.5L_\beta$ is captured in this block. The lateral/directional structured singular values for robust stability and robust performance are shown in Fig.(4.7). Since the maximum structured singular value for robust stability is approximately 1.4 for all flight conditions, robust stability is guaranteed at all flight conditions for $\frac{1}{1.4}\Delta_{lat/dir}$ where $\Delta_{lat/dir}$ represents the uncertainty in Fig.(4.6). Similarly since the maximum structured singular value for robust performance is approximately 1.9 for all flight conditions, robust performance is guaranteed at all flight conditions for $\frac{1}{1.9}\Delta_{lat/dir}$.

Figure (4.8) shows the structured singular value analysis model for the longitudinal axis. There are three uncertainty blocks. The first uncertainty block is unstructured with 1 input and 1 output. Command response performance is captured in this block with the error weight in eq.(4.7). The second uncertainty block is unstructured with 1 input and 1 output. Controller bandwidth constraints are captured in this block with the input uncertainty weight in eq(4.8). The third uncertainty block is a structured uncertainty block with 2 inputs and 2 outputs. Stability derivative parameter uncertainty of $0.1Z_\alpha$ and $1.0M_\alpha$ is captured in this block. The longitudinal structured singular values for robust stability and robust performance are shown in Fig.(4.9). Since the maximum structured singular value for robust stability is approximately 0.9 for all flight conditions, robust stability is guaranteed at all flight conditions for $\frac{1}{0.9}\Delta_{long}$ where Δ_{long} represents the uncertainty in Fig.(4.8). Similarly since the maximum structured singular value for robust performance is approximately 1.2 for all flight conditions, robust performance is guaranteed at all flight conditions for $\frac{1}{1.2}\Delta_{long}$. More details of this analysis, as well as a comparison with a linear parameter varying control law, appear in [9].

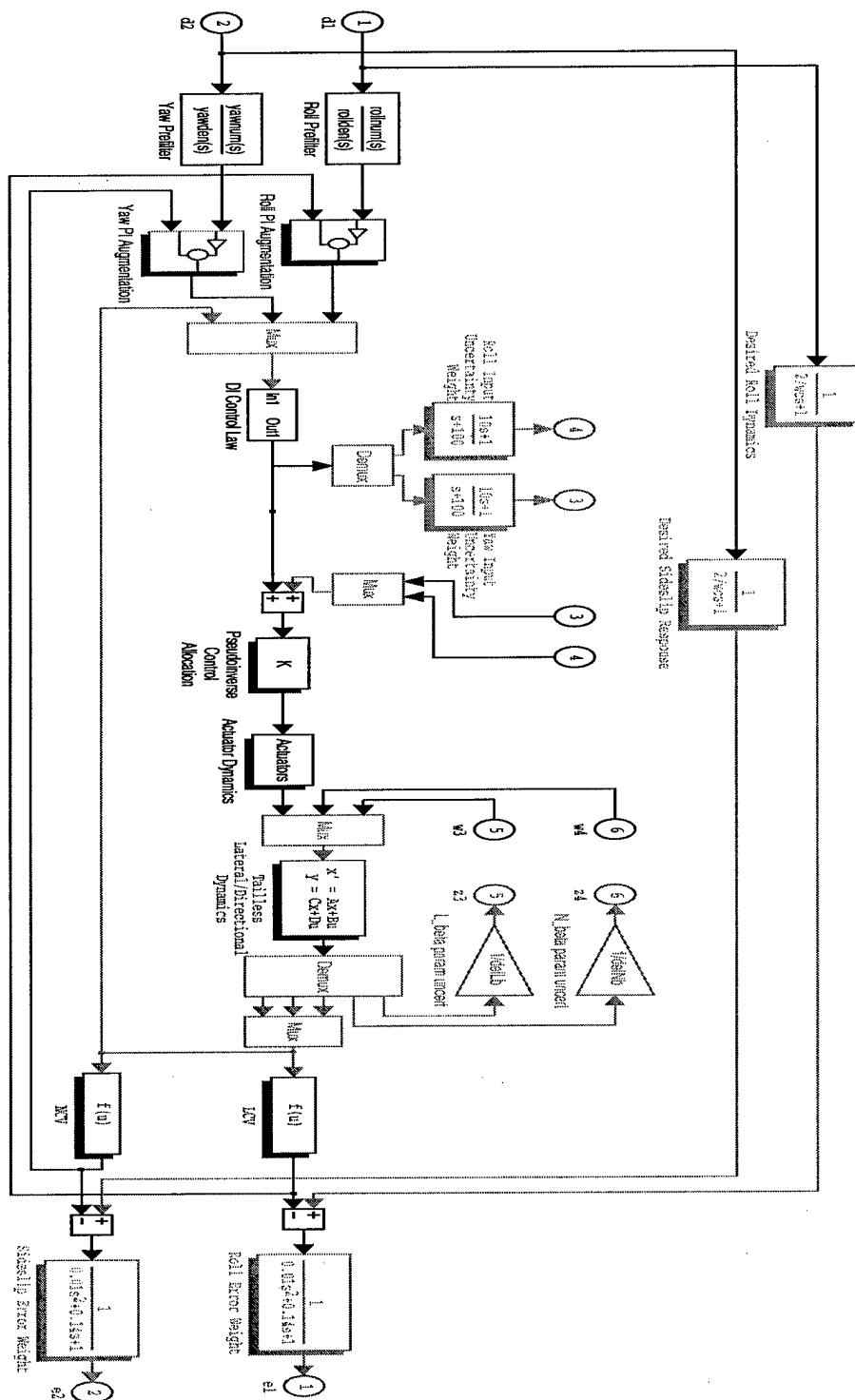


Figure 4.6: Lateral/Directional Axes Robustness Block Diagram

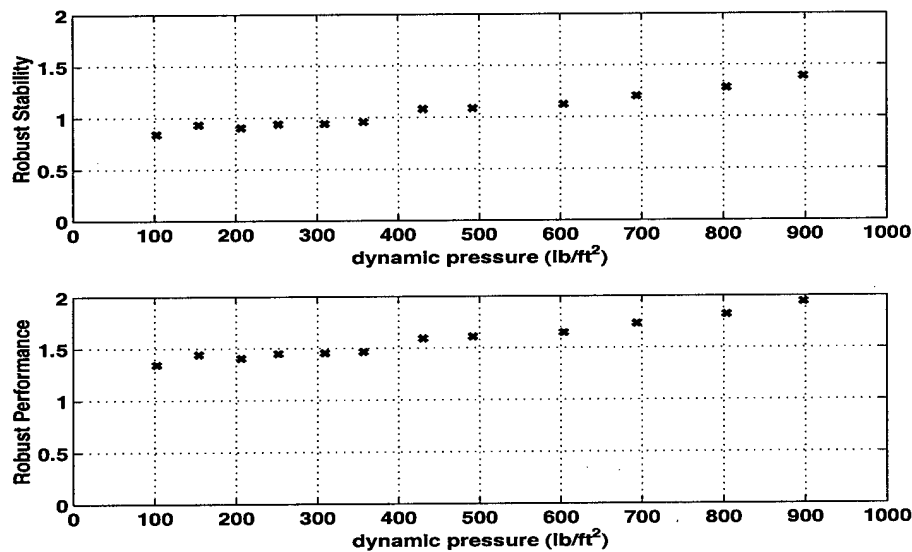


Figure 4.7: Lateral/Directional Axes Structured Singular Values

4.4 Batch simulation

The non-real time batch simulation analysis was done using the GENESIS simulation environment to assess robust stability and performance at the flight conditions in Table 4.1. There are two parts to the batch simulation analysis: control allocation mode verification analysis and final control law analysis. The objectives of the control allocation mode verification analysis were to verify that each mode minimized the corresponding objective, identify any problems associated with each mode and choose nominal control allocation modes for each flight condition. The objective of the final control law analysis was to evaluate the entire control law with the nominal control allocation mode choice at each flight condition.

The presentation of simulation time histories is consistent throughout this document. The inner loop command variable responses are plotted with the corresponding reference commands (CMD). Left and right control surface deflections (DEF) are plotted with the corresponding actuator command (CMD) and control allocation optimal preference (PREF). Symmetric and asymmetric deflections are also plotted to show contributions of control pairs to each axis. Control law command errors are plotted which indicate when there is insufficient control power to achieve the control law command. Errors in the on-board models of the aerodynamics and actuators are indicated for each axis. Aerodynamic, specifically control derivative, model errors are indicated by differences between model and truth acceleration responses. Actuator model errors, specifically due to neglecting actuator bandwidth limitations, are indicated by differences between control law commands (CMD) and achieved accelerations due to control deflections (OUT).

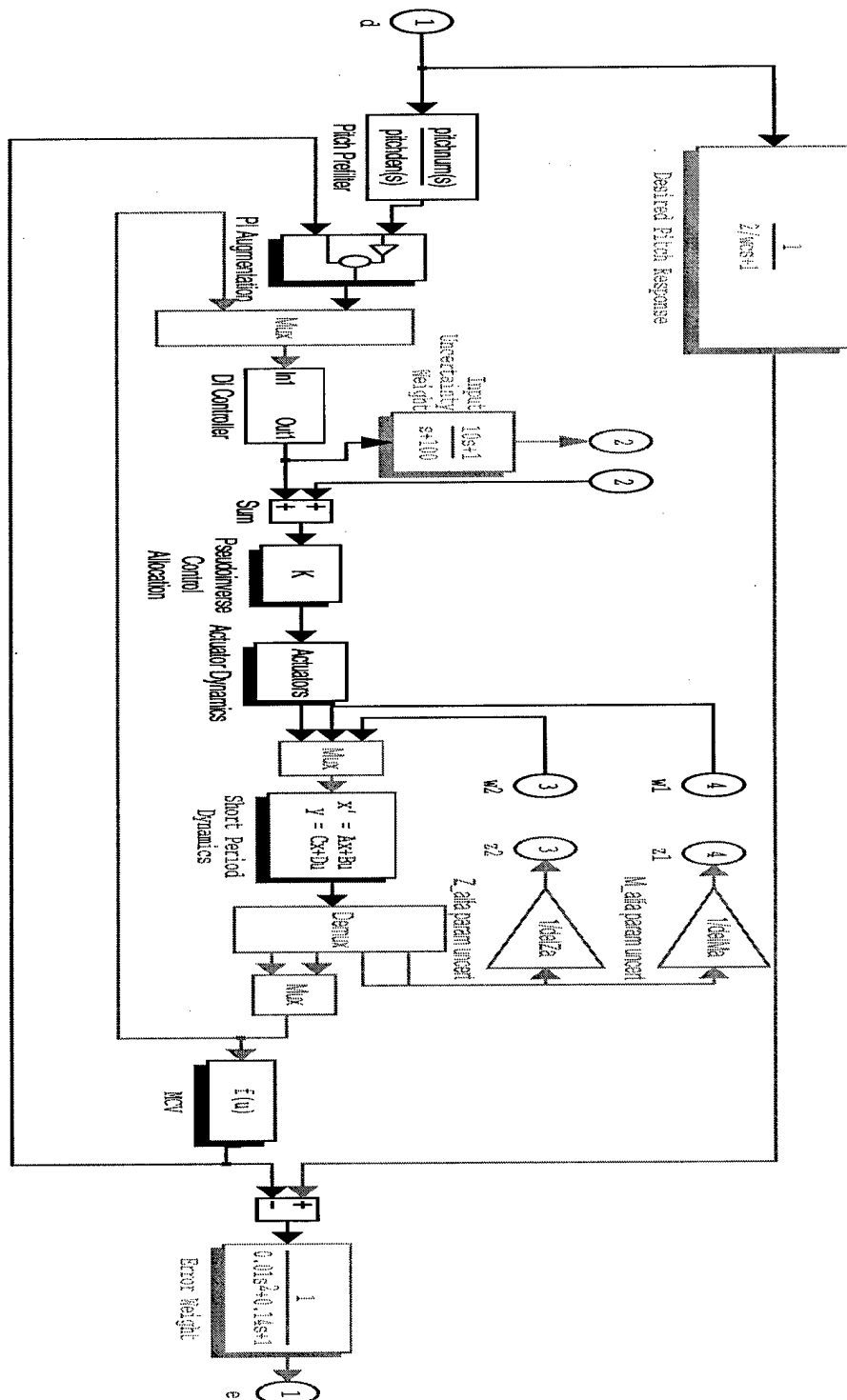


Figure 4.8: Longitudinal Axis Robustness Block Diagram

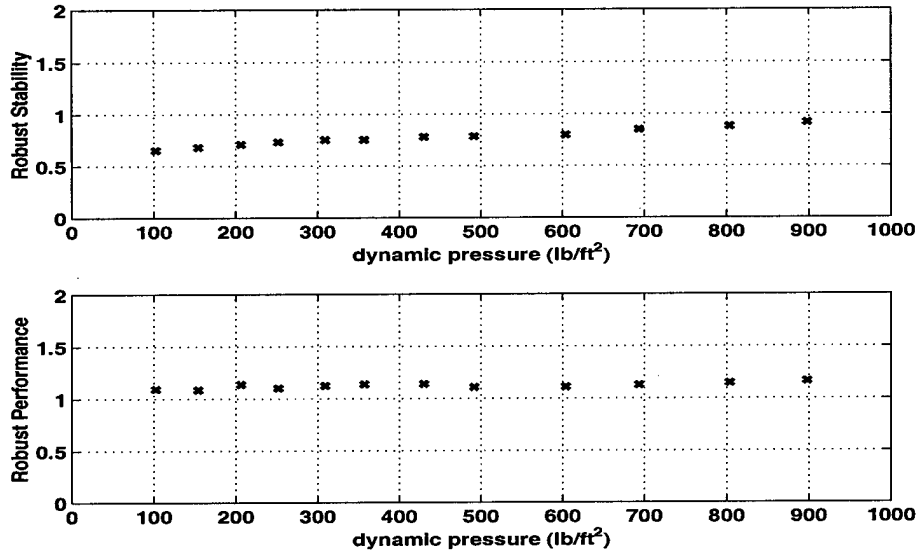


Figure 4.9: Longitudinal Axis Structured Singular Values

4.4.1 Control Allocation Mode Verification Analysis

The control allocation mode verification analysis was done for a single loaded roll maneuver at a single flight condition for all control allocation modes. The low dynamic pressure flight condition at Mach 0.35 and 5000 ft. altitude was chosen for this analysis since the zero dynamics at this flight condition were the least stable and were most sensitive to control allocation modes as indicated in Sec. 4.1.

Performance of the control allocation modes is evaluated by metrics that correspond to the intended objective of each mode. The following control allocation metrics were used for evaluation

$$\begin{aligned}
 J_{def} &= \sum_{k=0}^{\frac{t_f+\Delta T}{\Delta T}} |\delta(k)|_1 \Delta T \\
 J_{drag} &= \sum_{k=0}^{\frac{t_f+\Delta T}{\Delta T}} C_D(k) \Delta T \\
 J_{load} &= \sum_{k=0}^{\frac{t_f+\Delta T}{\Delta T}} \Delta T \left(\begin{bmatrix} \delta_{amtl}(k) \\ \delta_{amtr}(k) \\ \delta_{oblfl}(k) \\ \delta_{oblfr}(k) \end{bmatrix}^T \begin{bmatrix} 100 & 0 & 0 & 0 \\ 0 & 100 & 0 & 0 \\ 0 & 0 & 10 & 0 \\ 0 & 0 & 0 & 10 \end{bmatrix} \begin{bmatrix} \delta_{amtl}(k) \\ \delta_{amtr}(k) \\ \delta_{oblfl}(k) \\ \delta_{oblfr}(k) \end{bmatrix} \right)^{\frac{1}{2}} \\
 J_{sig} &= \sum_{k=0}^{\frac{t_f+\Delta T}{\Delta T}} \Delta T \left(\begin{bmatrix} \delta_{amtl}(k) \\ \delta_{amtr}(k) \\ \delta_{ssdl}(k) \\ \delta_{ssdr}(k) \end{bmatrix}^T \begin{bmatrix} 10 & 0 & 0 & 0 \\ 0 & 10 & 0 & 0 \\ 0 & 0 & 100 & 0 \\ 0 & 0 & 0 & 100 \end{bmatrix} \begin{bmatrix} \delta_{amtl}(k) \\ \delta_{amtr}(k) \\ \delta_{ssdl}(k) \\ \delta_{ssdr}(k) \end{bmatrix} \right)^{\frac{1}{2}}
 \end{aligned}$$

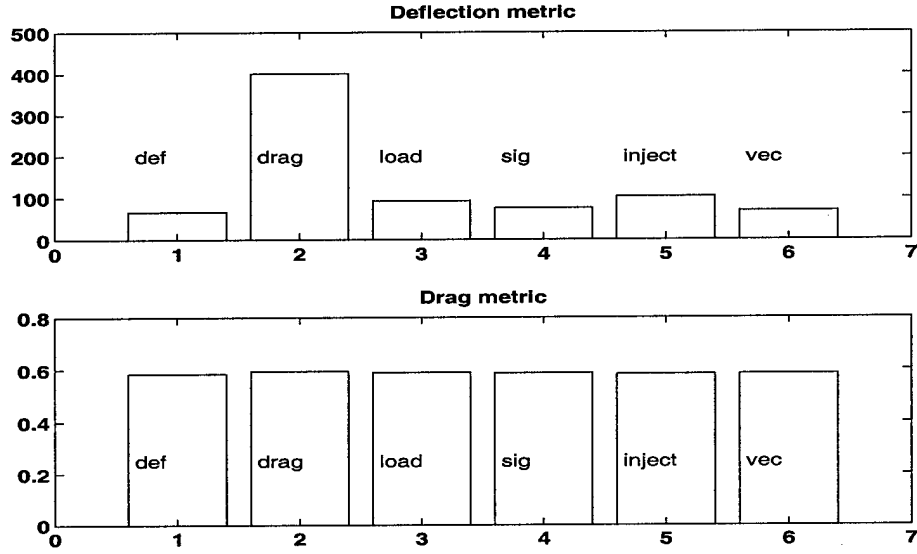


Figure 4.10: Control Allocation Mode Metrics

$$J_{inject} = \sum_{k=0}^{\frac{t_f + \Delta T}{\Delta T}} \frac{1}{\text{cond}(H(k))}$$

$$J_{vec} = \sum_{k=0}^{\frac{t_f + \Delta T}{\Delta T}} \Delta T \left(\begin{bmatrix} \delta_{ptv}(k) \\ \delta_{ytv}(k) \end{bmatrix}^T \begin{bmatrix} \delta_{ptv}(k) \\ \delta_{ytv}(k) \end{bmatrix} \right)^{\frac{1}{2}} \quad (4.9)$$

where ΔT is the simulation time step, t_f is the simulation run time, $\delta(k)$ is the vector of control deflections at the k^{th} simulation time step, and $C_D(k)$ is the coefficient of drag. The regressor matrix $H(k)$ consists of symmetric left and right control pairs and pitch thrust vectoring for the longitudinal axis analysis. It consists of asymmetric left and right control pairs and yaw thrust vectoring for the lateral/directional axes analysis. The $H(k)$ matrix has data from the previous 0.8 sec or $80\Delta T$, and each column is scaled by the maximum absolute value of the column.

The functionality of the control allocation modes is verified by the bar charts in Figs.(4.10)-(4.12). Each figure corresponds to an evaluation metric in eq.(4.9), and each bar in the figures corresponds to a control allocation mode. For example, the second bar in the first figure is the minimum drag control allocation mode performance measured by the minimum deflection metric J_{def} .

It is seen that all control allocation modes minimize the corresponding objective except minimum drag mode. All of the modes give approximately the same drag. This is due to the fact that drag due to control deflections is a very small part of total drag. Therefore, any drag benefits from minimum drag control allocation does not seem to be worth the added complexity of modeling control effector drag in the control law. It is interesting to note that the null space injection mode increases the deflection metric by only 56% while minimum drag

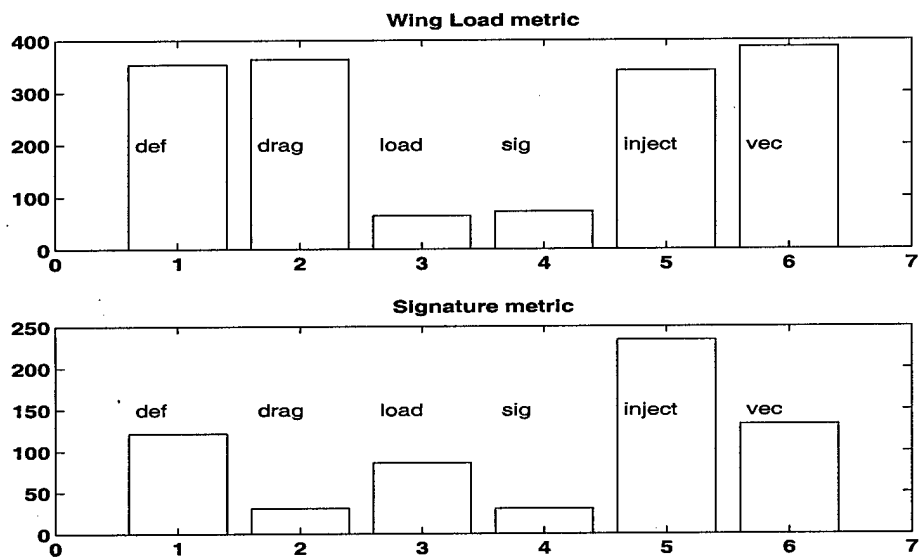


Figure 4.11: Control Allocation Mode Metrics

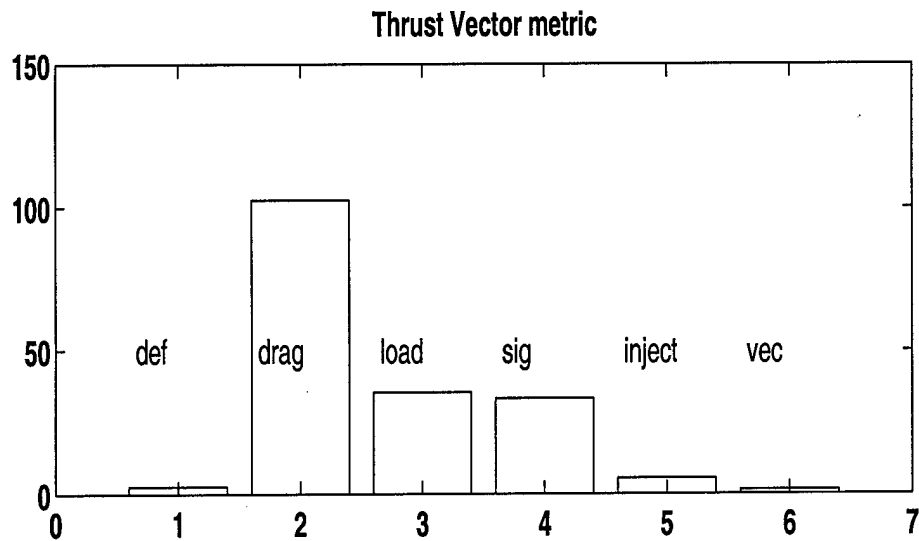


Figure 4.12: Control Allocation Mode Metrics

mode increases the deflection metric by 503%. This shows that extremely large deflections do not always increase drag. The minimum wing load, minimum signature and minimum vector modes resist motion of specific surfaces which result in very poor performance of modes that use those surfaces. The minimum deflection mode does well for each metric as it is not the worst performing mode for any metric. Another interesting note is that the injection mode performs similarly to the minimum deflection mode except for minimizing signature.

The purpose of the injection mode is to enhance on-board system identification for control law reconfiguration capability. Although no on-line system identification was included in the flight control system of the present study, it could easily be integrated into the modular control law architecture to enhance the fidelity of the parameters from the on-board model. It has been shown that the condition number of a matrix containing scaled control deflections is a good indicator of system identification performance [29]. Low condition numbers may result in good parameter estimates, while high condition numbers will certainly result in poor estimates. It has also been shown [29] that condition numbers less than 250 will typically give good estimates. The inverse of the condition numbers of a matrix containing scaled control deflections are plotted in Figs.(4.13)-(4.18). Note that larger numbers indicate better conditioned matrices since condition number inverses are plotted. The straight line in all the plots correspond to a condition number of 250. It is seen that all the control modes result in good condition numbers only during maneuvering except the injection mode which results in good condition numbers all the time.

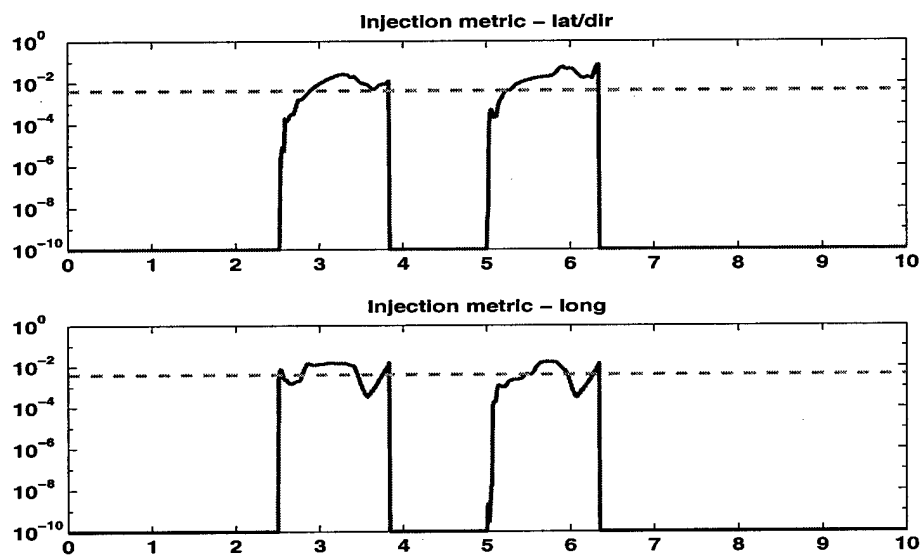


Figure 4.13: Mach 0.35, 5000 ft. Altitude, Min Def CA Mode

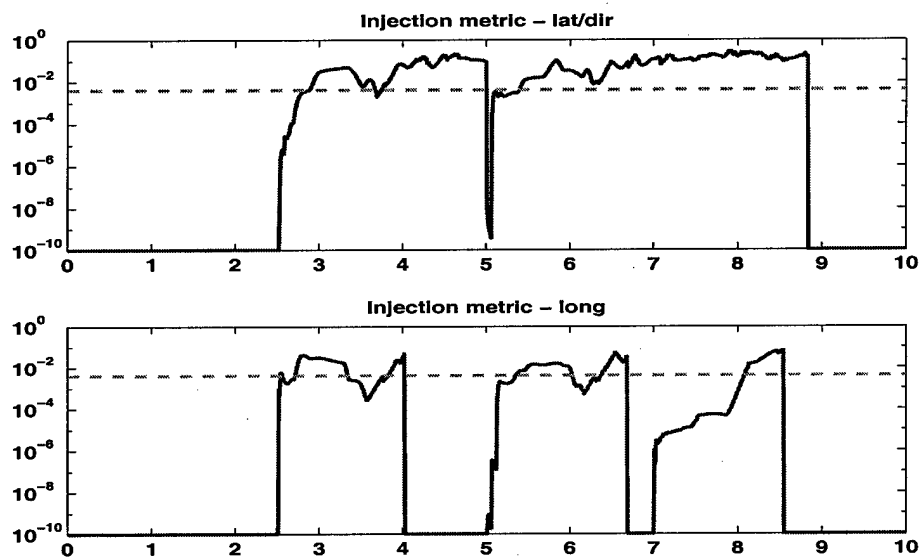


Figure 4.14: Mach 0.35, 5000 ft. Altitude, Min Drag CA Mode

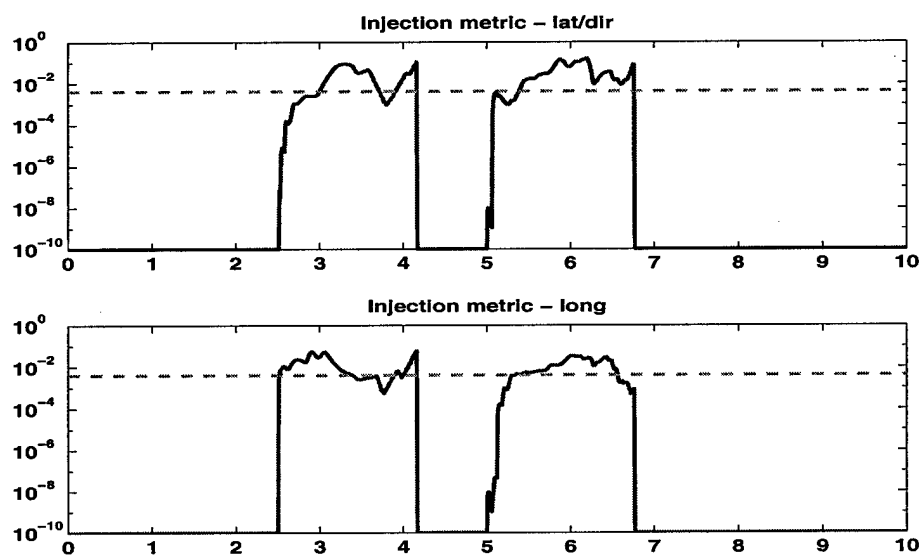


Figure 4.15: Mach 0.35, 5000 ft. Altitude, Min Load CA Mode

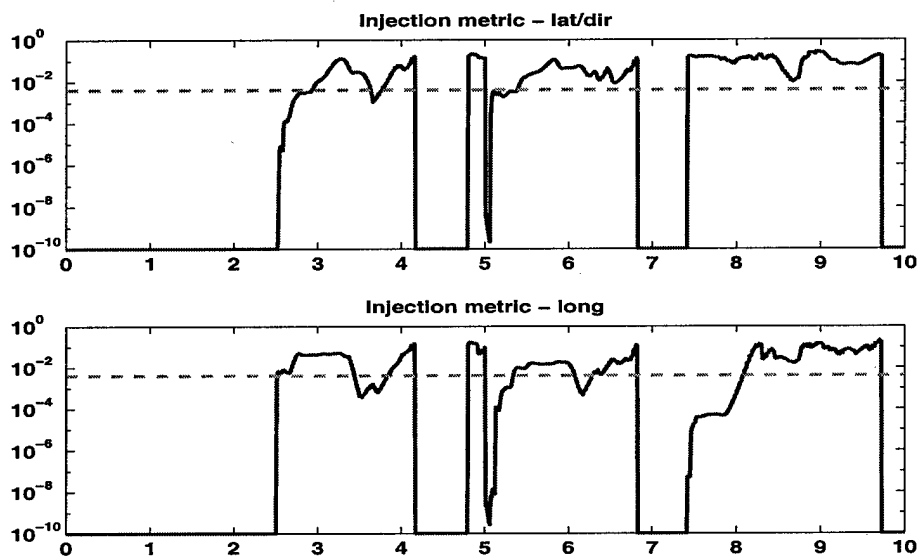


Figure 4.16: Mach 0.35, 5000 ft. Altitude, Min Signature CA Mode

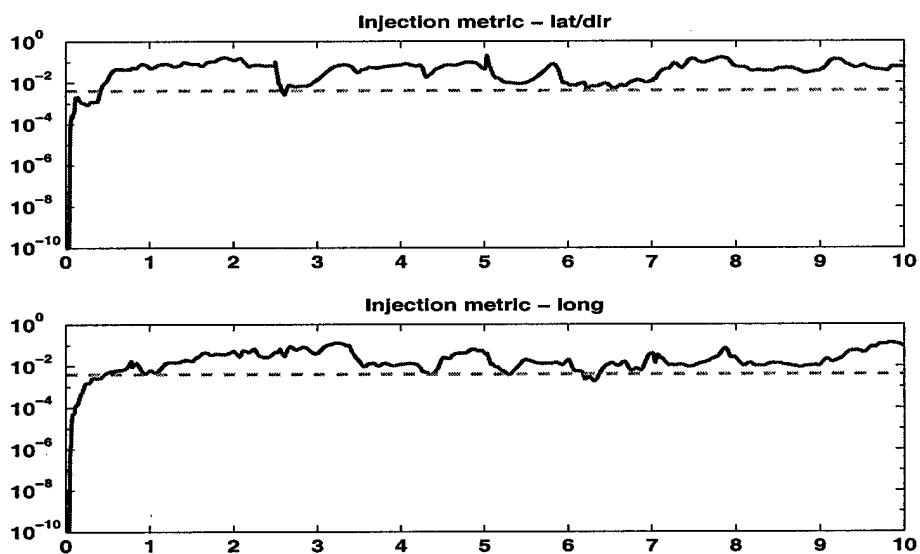


Figure 4.17: Mach 0.35, 5000 ft. Altitude, Injection CA Mode

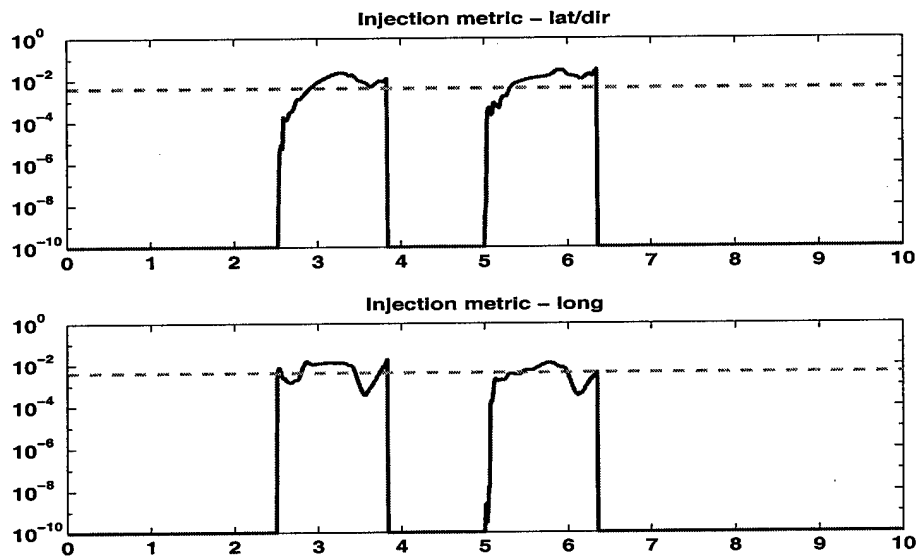


Figure 4.18: Mach 0.35, 5000 ft. Altitude, Min Vec CA Mode

The plots in Figs.(4.19)-(4.84) are batch simulation time histories of a loaded roll maneuver at the low dynamic pressure condition for the 5 control allocation modes.

Minimum deflection mode

The minimum deflection control allocation mode time histories are contained in Figs.(4.19)-(4.29). Note that there is only slight coupling between command variable axes, and angle of slip regulation is very good. Elevons and all moving tips are the most active control effectors with all other surfaces only deviating from their preferences at the onset of stick commands when insufficient control power exists to achieve the control law acceleration commands. Note the slight directional oscillations prevalent in the yaw thrust vector and directional command variable responses. This is due to the lower bandwidth actuator of the thrust vector nozzle compared to the aerodynamic effectors. There is almost no on-board actuator model errors and only slight aerodynamic model errors.

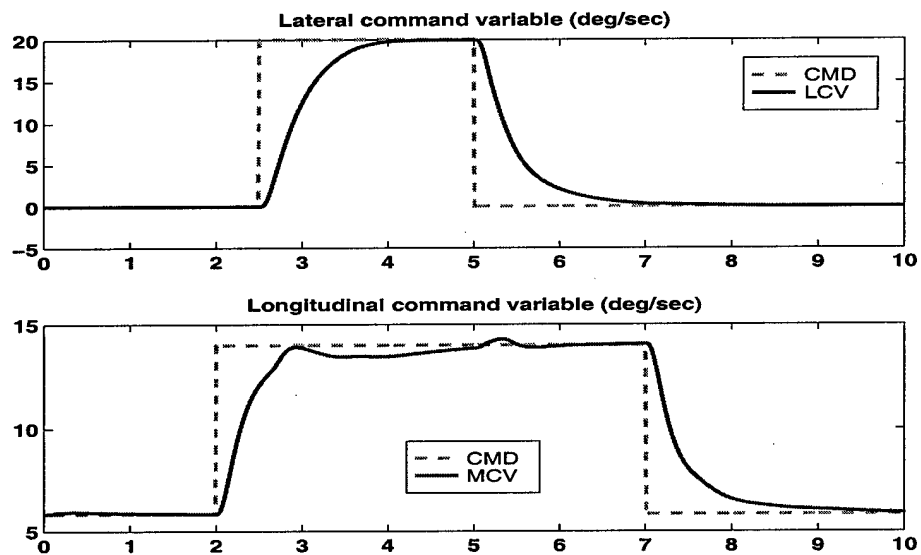


Figure 4.19: Mach 0.35, 5000 ft. Altitude, Min Def CA Mode

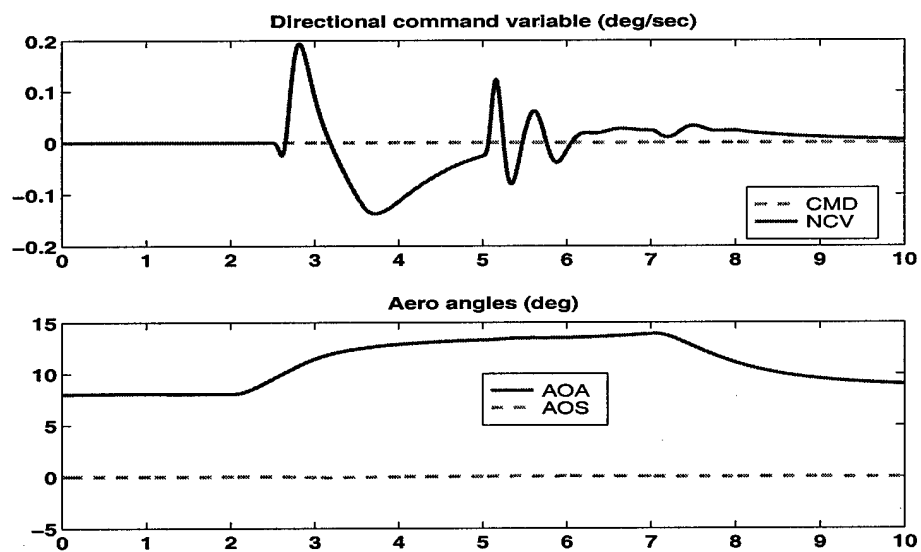


Figure 4.20: Mach 0.35, 5000 ft. Altitude, Min Def CA Mode

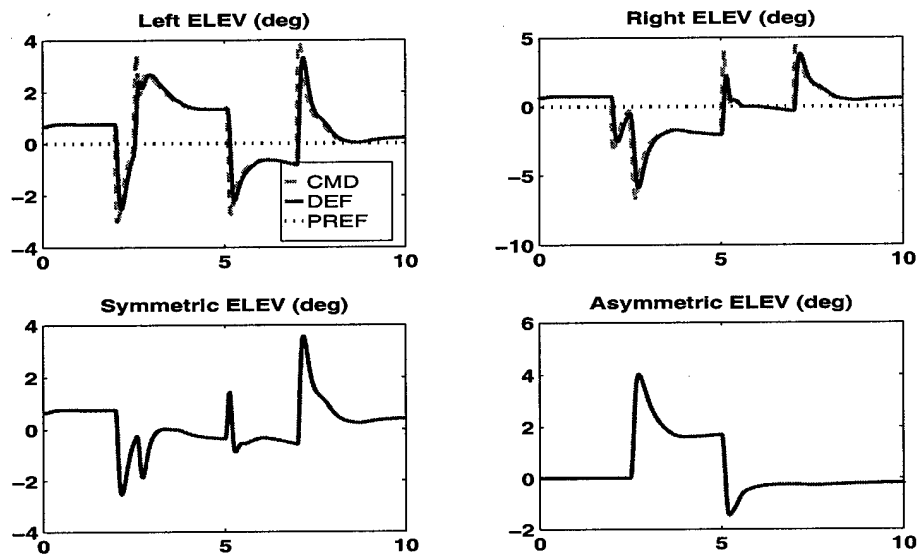


Figure 4.21: Mach 0.35, 5000 ft. Altitude, Min Def CA Mode

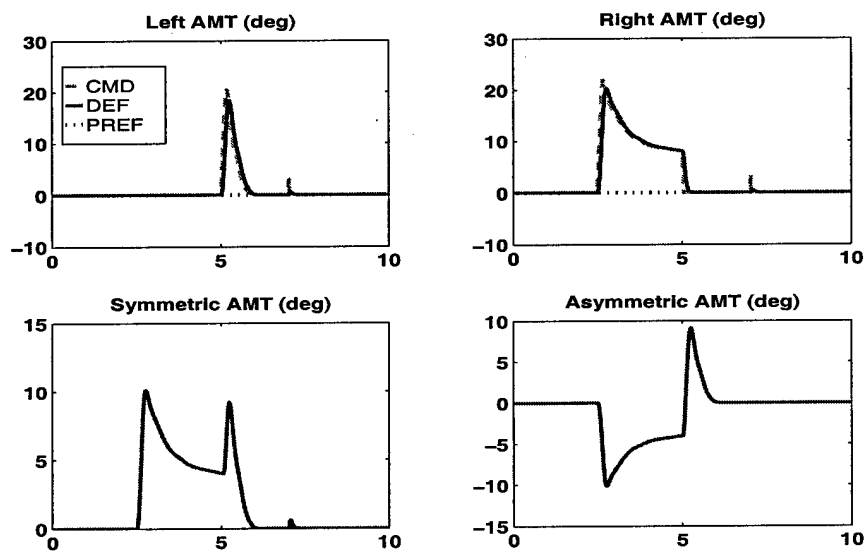


Figure 4.22: Mach 0.35, 5000 ft. Altitude, Min Def CA Mode

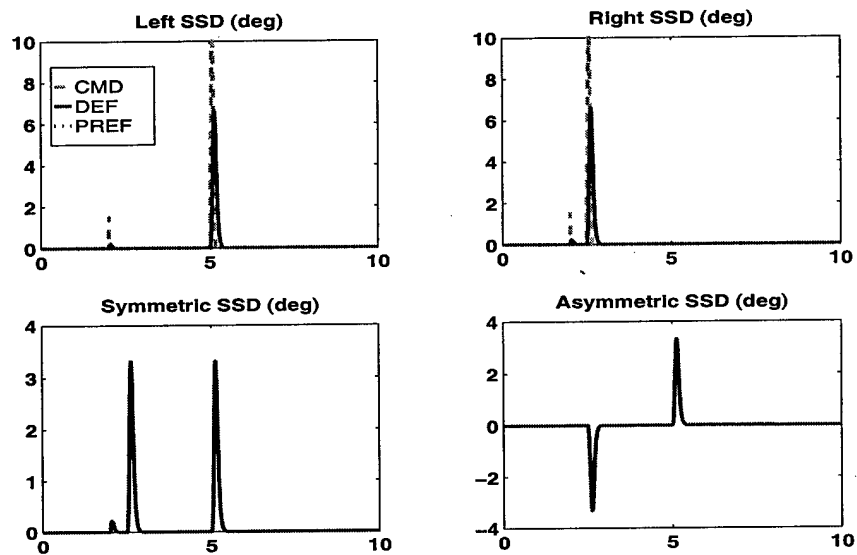


Figure 4.23: Mach 0.35, 5000 ft. Altitude, Min Def CA Mode

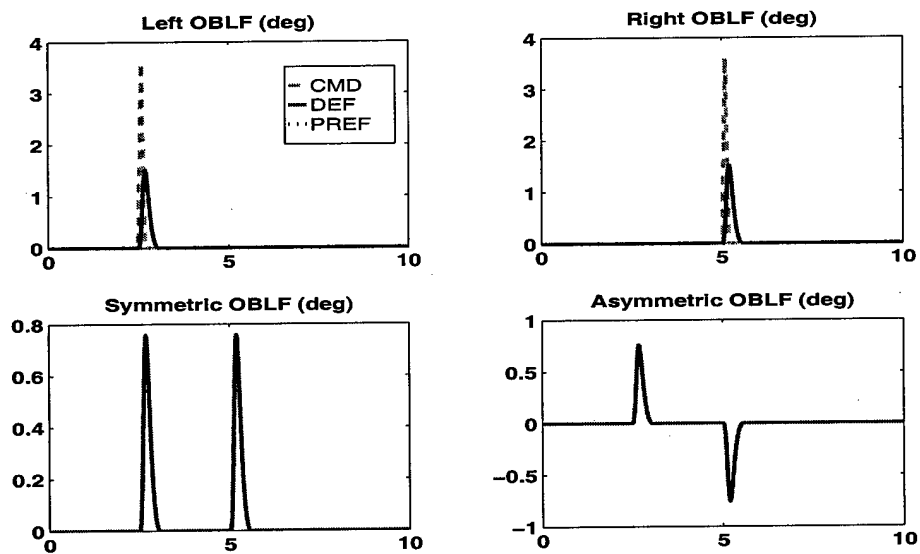


Figure 4.24: Mach 0.35, 5000 ft. Altitude, Min Def CA Mode

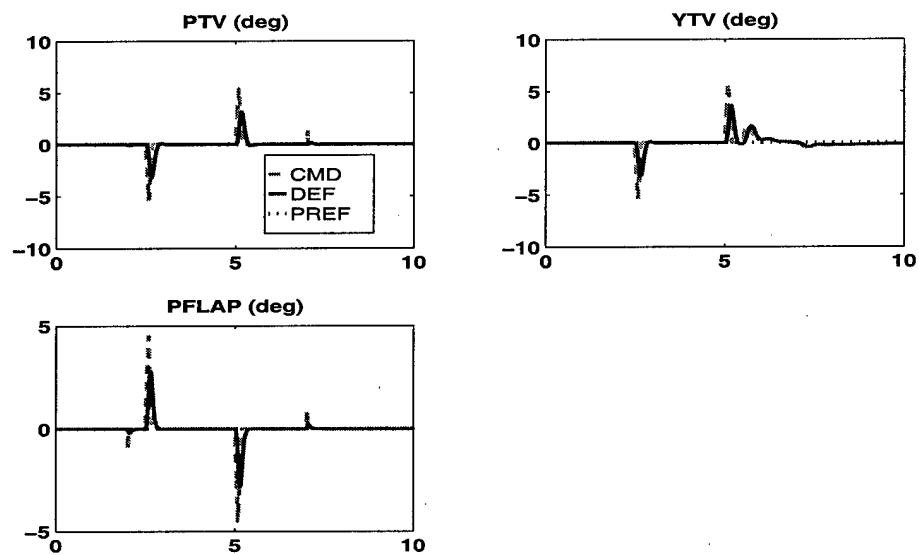


Figure 4.25: Mach 0.35, 5000 ft. Altitude, Min Def CA Mode

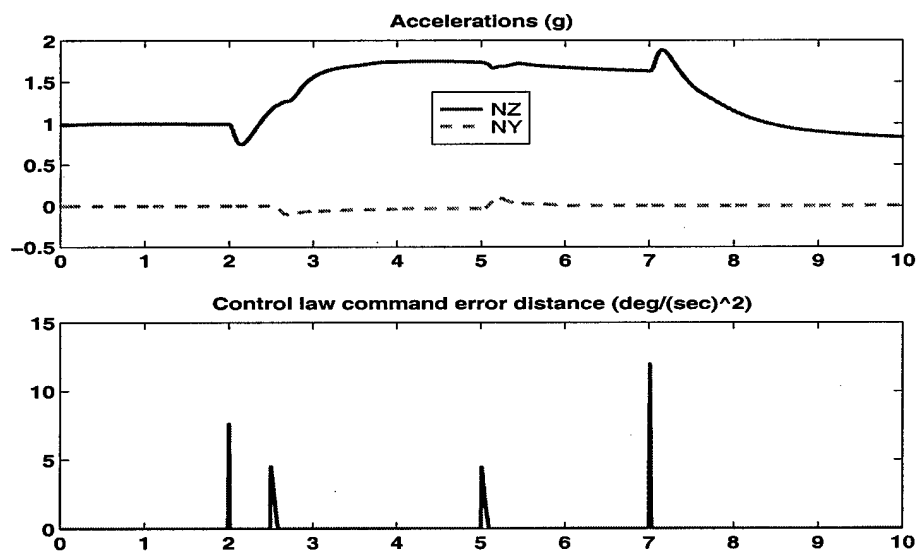


Figure 4.26: Mach 0.35, 5000 ft. Altitude, Min Def CA Mode

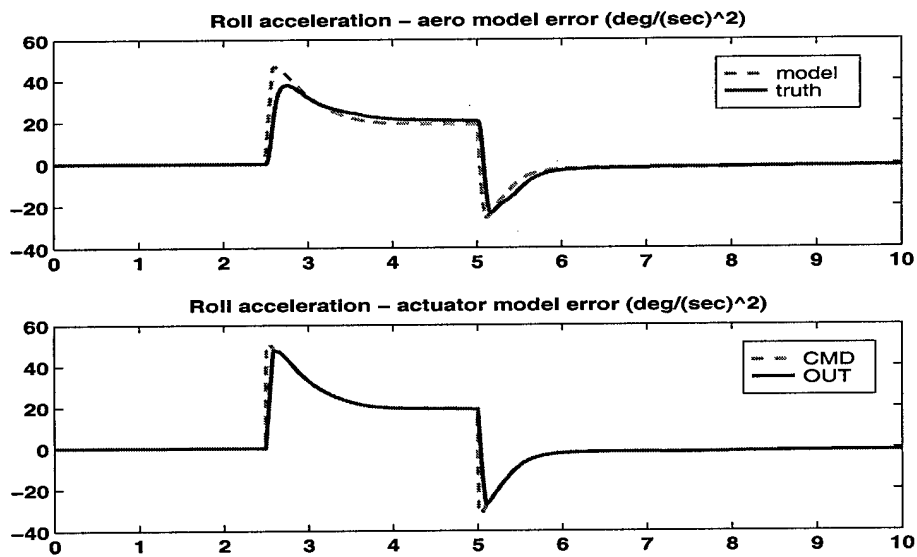


Figure 4.27: Mach 0.35, 5000 ft. Altitude, Min Def CA Mode

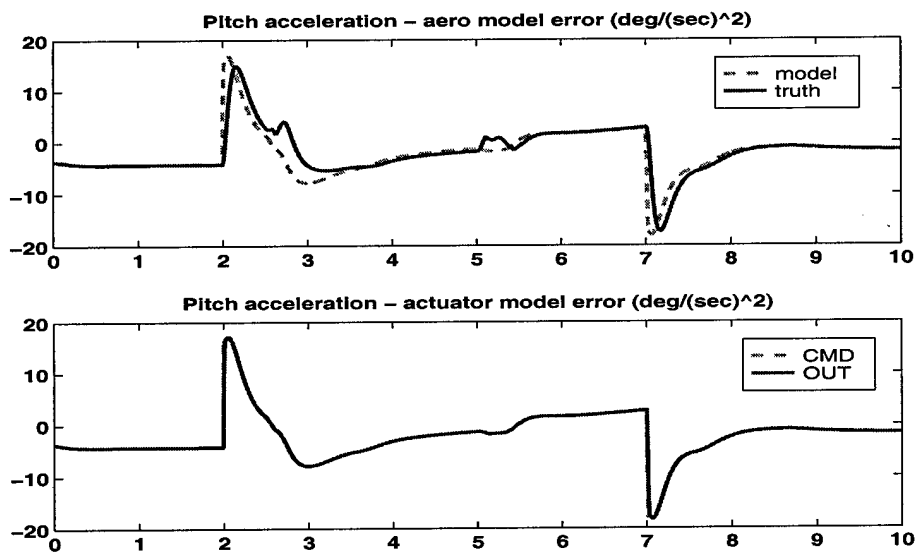


Figure 4.28: Mach 0.35, 5000 ft. Altitude, Min Def CA Mode

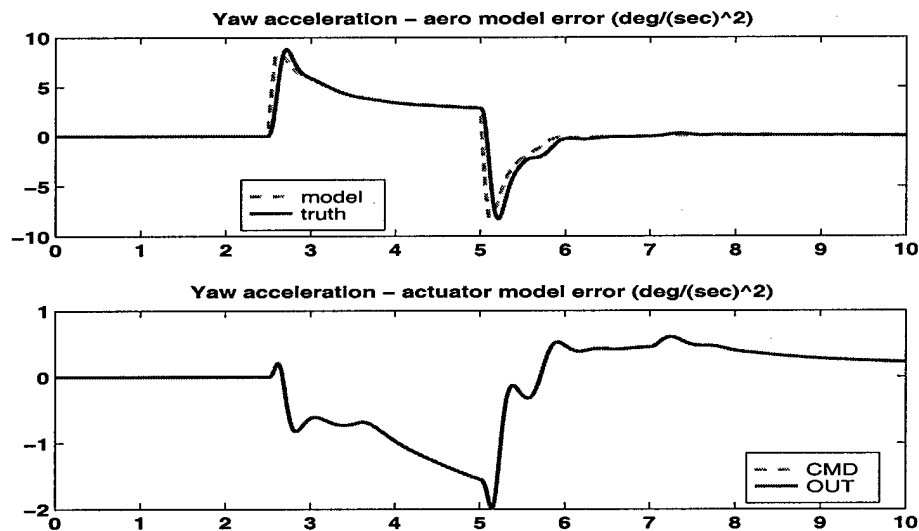


Figure 4.29: Mach 0.35, 5000 ft. Altitude, Min Def CA Mode

Minimum drag mode

The minimum drag control allocation mode time histories are contained in Figs.(4.30)-(4.40). Note that there is more coupling between command variable axes, and angle of slip regulation is good. Elevons and yaw thrust vectoring are the control effectors that deviate from their preferences the most with all other surfaces only deviating from their preferences at the onset of stick commands when insufficient control power exists to achieve the control law acceleration commands. The leading edge flaps do not deviate from their preference, but note the preference is non-zero. More directional oscillations are prevalent in the yaw thrust vector, directional command variable and side acceleration responses. This again is due to the lower bandwidth actuator of the thrust vector nozzle compared to the aerodynamic effectors. There is almost no on-board actuator model errors and only slight aerodynamic model errors in the lateral and directional axes. There is significantly more longitudinal aerodynamic errors due to the unmodeled interactions between the leading edge flaps and elevons which leads to the command variable coupling.

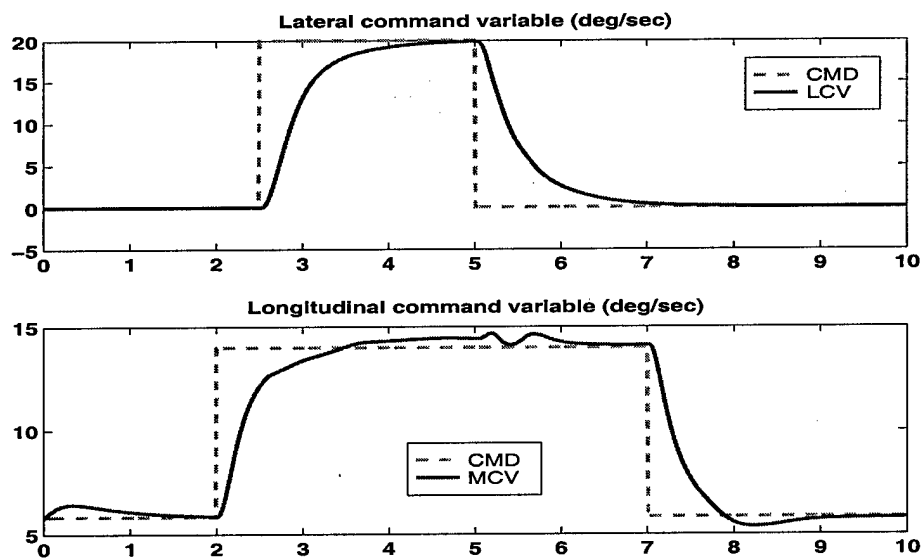


Figure 4.30: Mach 0.35, 5000 ft. Altitude, Min Drag CA Mode

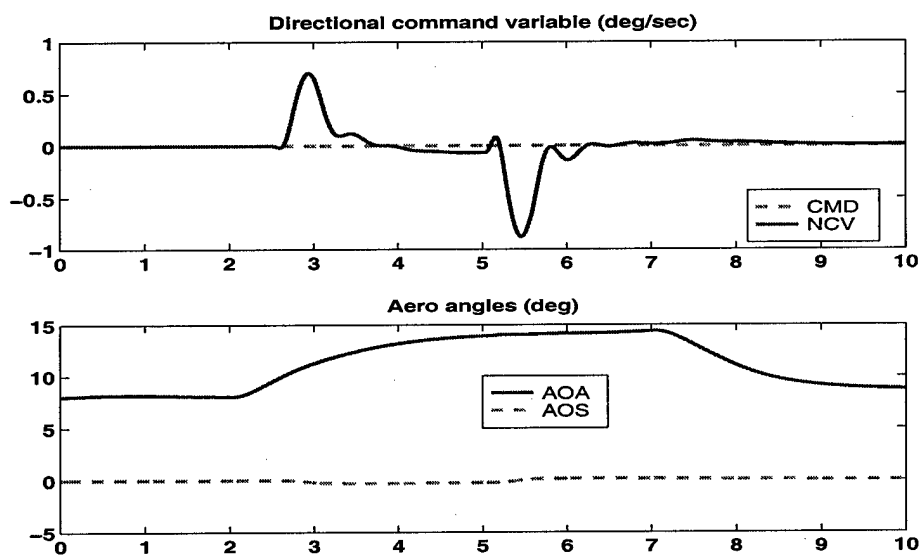


Figure 4.31: Mach 0.35, 5000 ft. Altitude, Min Drag CA Mode

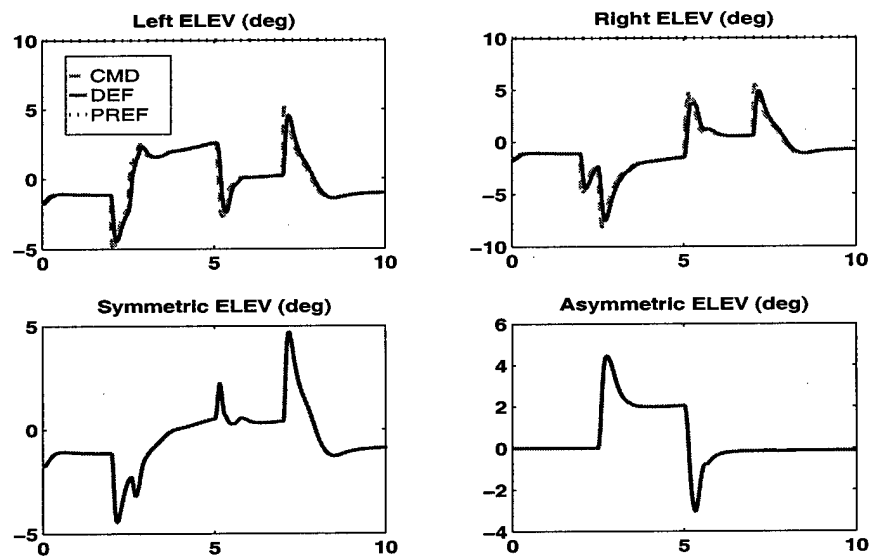


Figure 4.32: Mach 0.35, 5000 ft. Altitude, Min Drag CA Mode

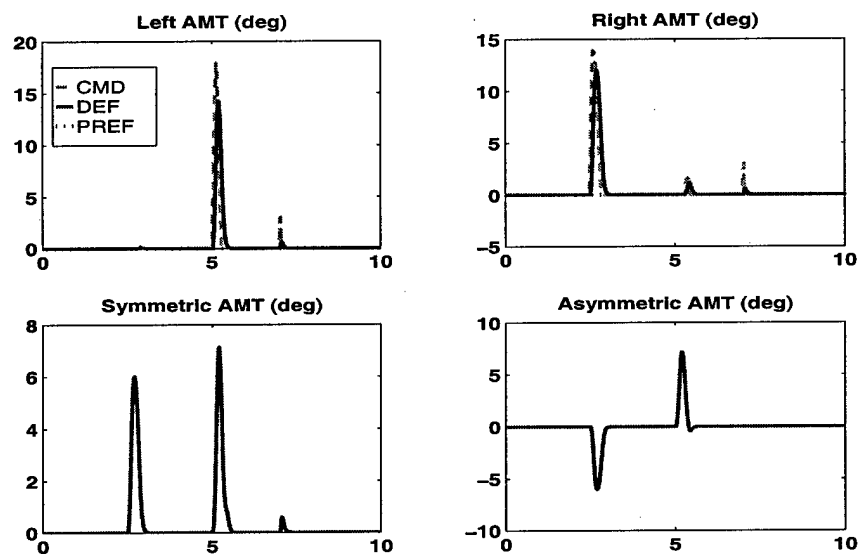


Figure 4.33: Mach 0.35, 5000 ft. Altitude, Min Drag CA Mode

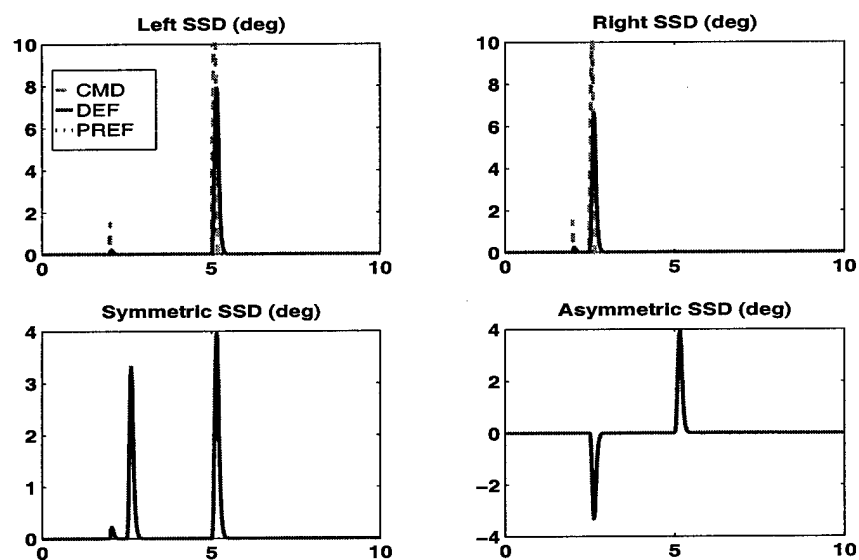


Figure 4.34: Mach 0.35, 5000 ft. Altitude, Min Drag CA Mode

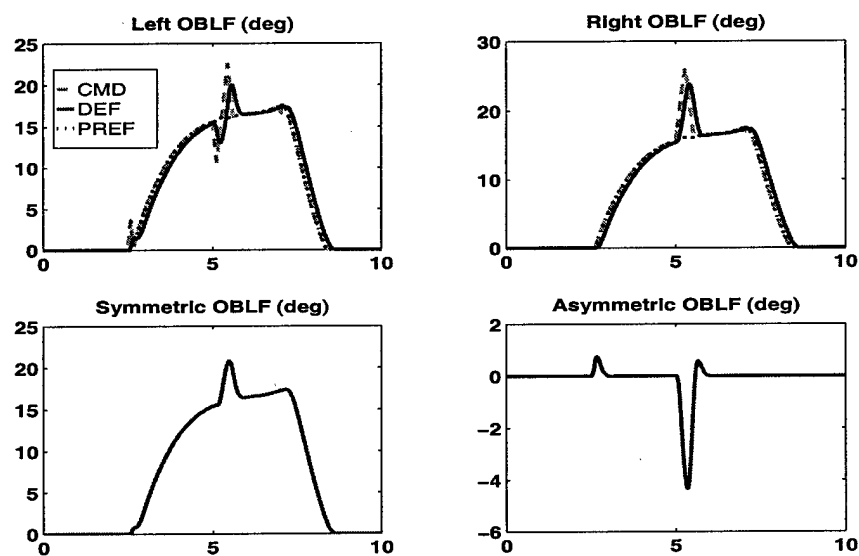


Figure 4.35: Mach 0.35, 5000 ft. Altitude, Min Drag CA Mode

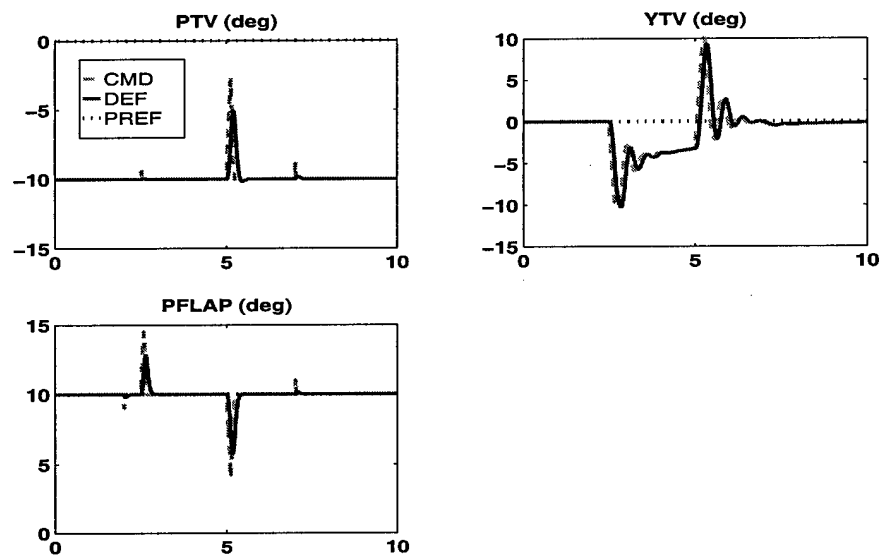


Figure 4.36: Mach 0.35, 5000 ft. Altitude, Min Drag CA Mode

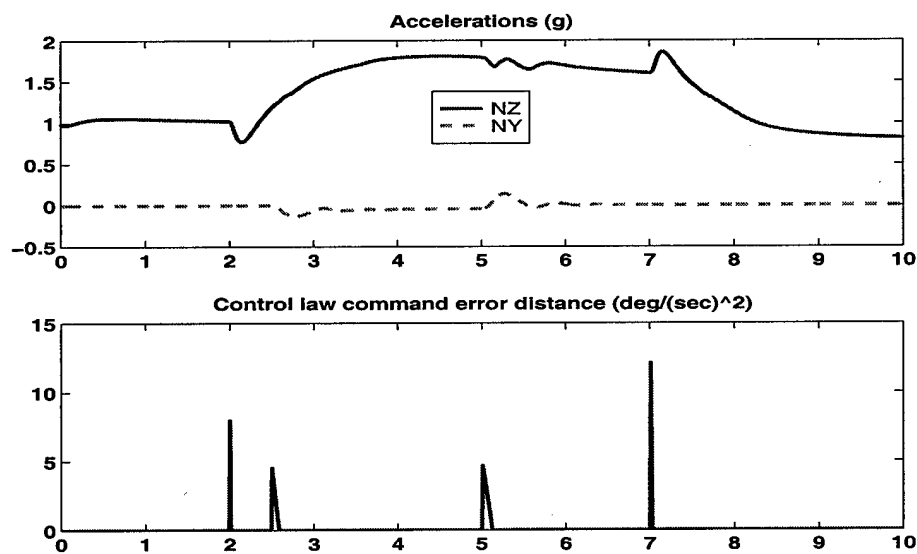


Figure 4.37: Mach 0.35, 5000 ft. Altitude, Min Drag CA Mode

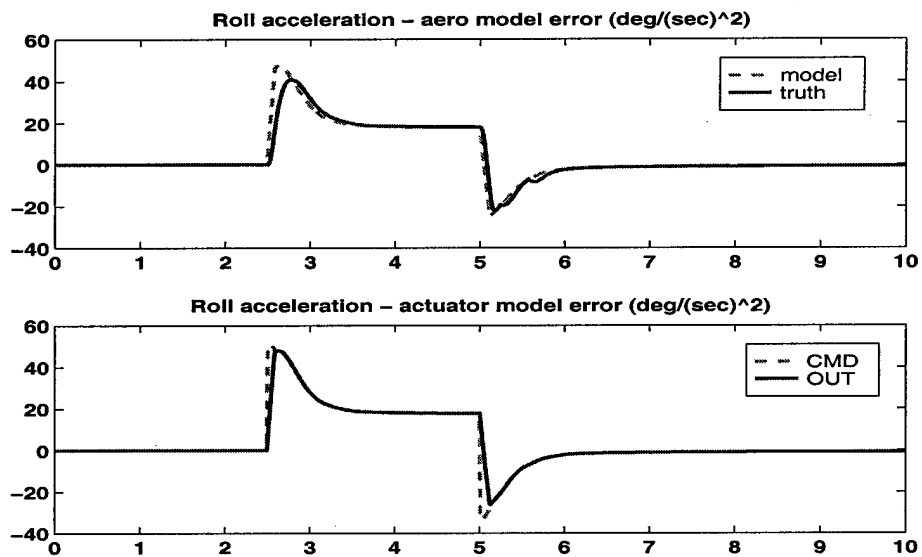


Figure 4.38: Mach 0.35, 5000 ft. Altitude, Min Drag CA Mode

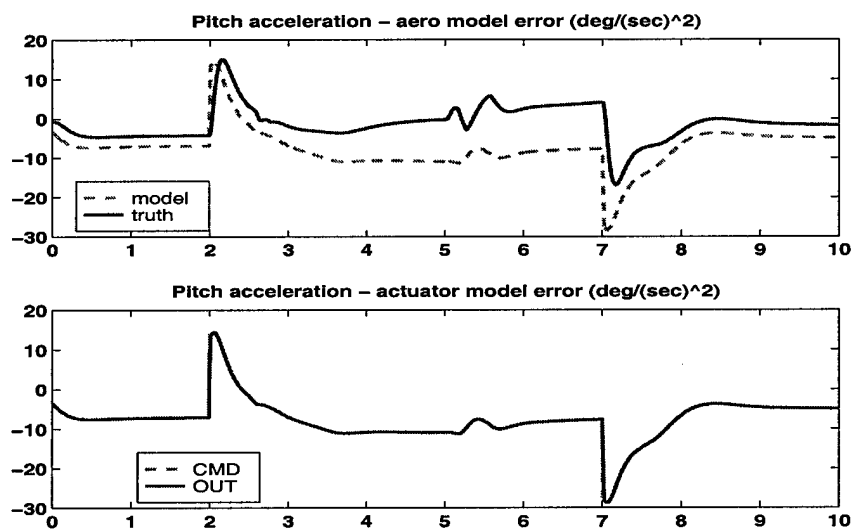


Figure 4.39: Mach 0.35, 5000 ft. Altitude, Min Drag CA Mode

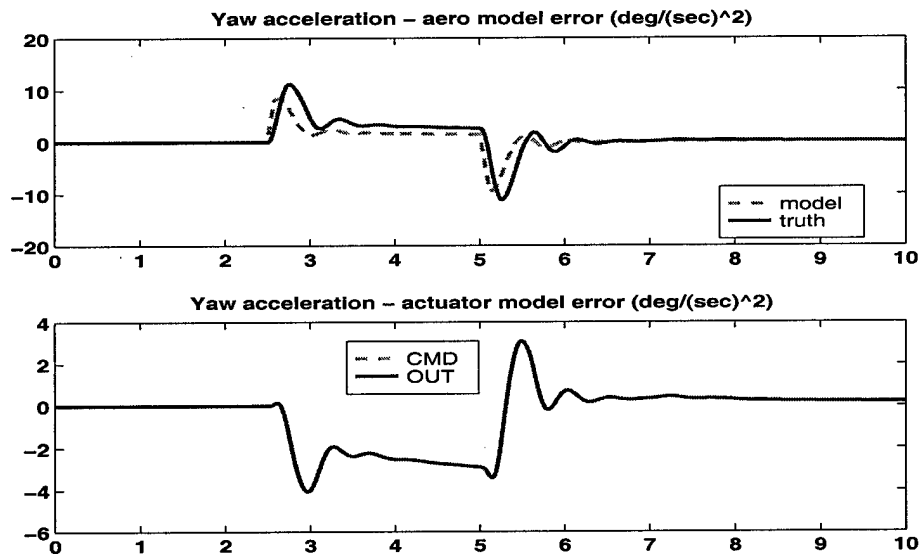


Figure 4.40: Mach 0.35, 5000 ft. Altitude, Min Drag CA Mode

Minimum wing load mode

The minimum wing load control allocation mode time histories are contained in Figs.(4.41)-(4.51). Note that there is much more coupling between command variable axes, and angle of slip regulation is good. The spoiler slot deflectors and pitch flaps deviate from their preferences more in this mode to make up for stronger preference adherence of the all moving tips and leading edge flaps. All moving tips and leading edge flaps only deviate from their preferences at the onset of stick commands when insufficient control power exists to achieve the control law acceleration commands since these surfaces produce large wing loads. Even more directional oscillations prevalent in the yaw thrust vector, directional command variable and side acceleration responses exist. This is due to the lower bandwidth actuator of the thrust vector nozzle compared to the aerodynamic effectors. There is almost no on-board actuator model errors and only slight aerodynamic model errors in the longitudinal and directional axes. More lateral aerodynamic errors are prevalent due to unmodeled spoiler slot deflector and elevon interactions.

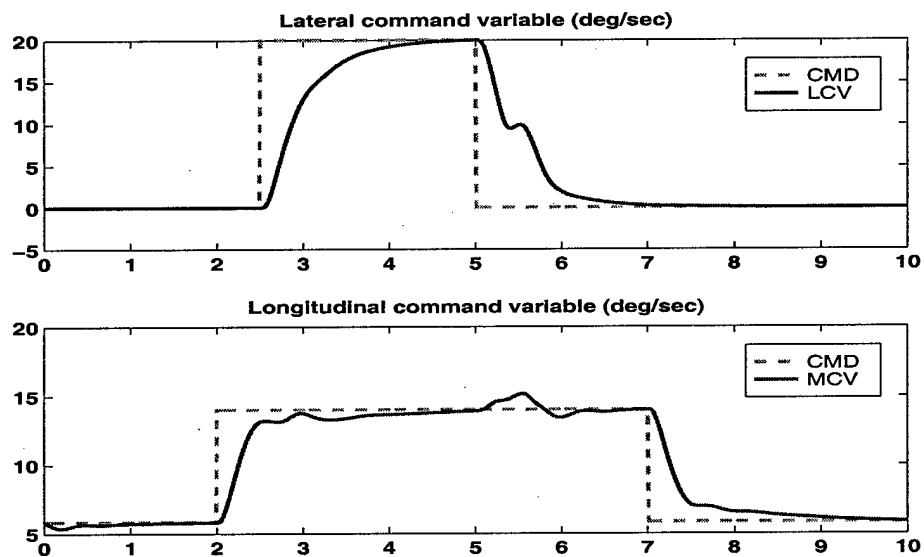


Figure 4.41: Mach 0.35, 5000 ft. Altitude, Min Load CA Mode

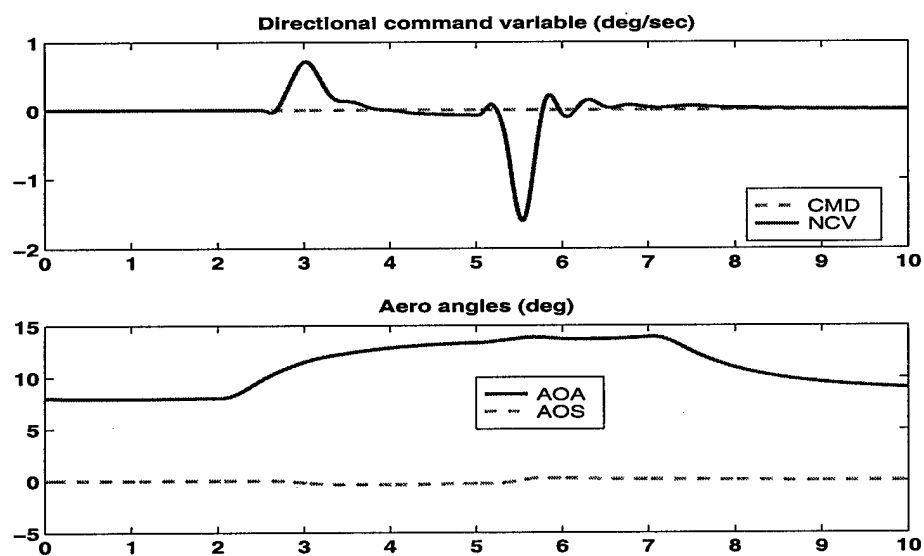


Figure 4.42: Mach 0.35, 5000 ft. Altitude, Min Load CA Mode

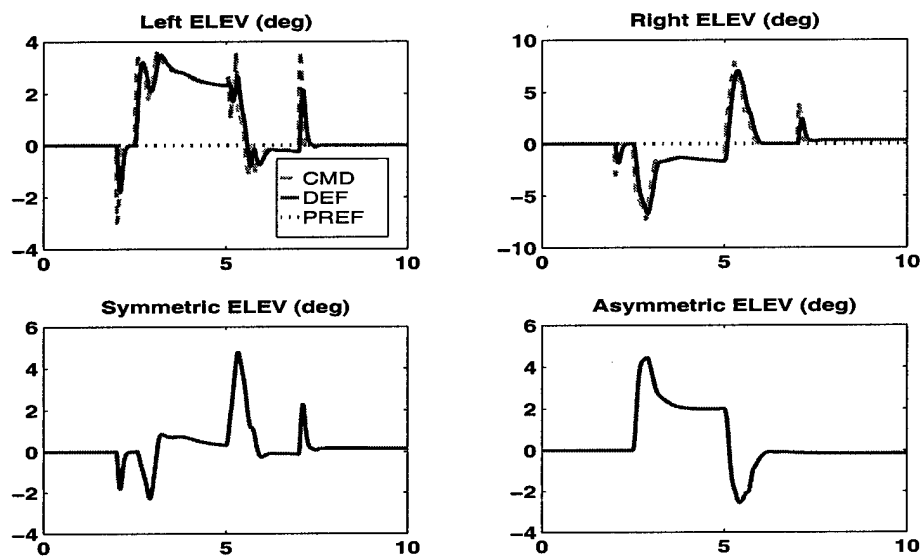


Figure 4.43: Mach 0.35, 5000 ft. Altitude, Min Load CA Mode

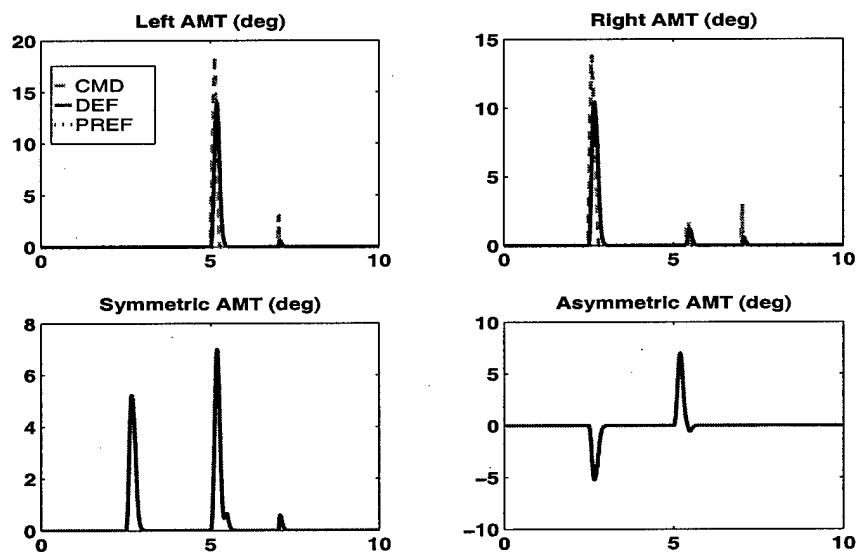


Figure 4.44: Mach 0.35, 5000 ft. Altitude, Min Load CA Mode

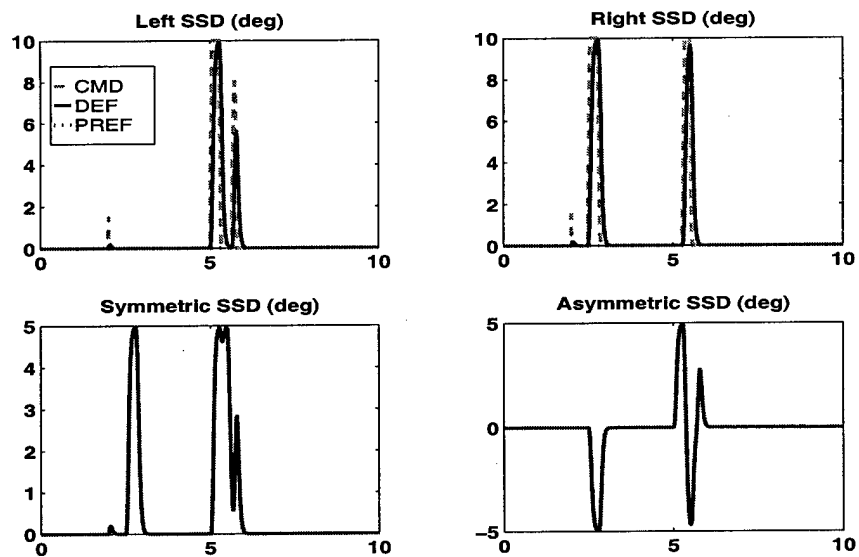


Figure 4.45: Mach 0.35, 5000 ft. Altitude, Min Load CA Mode

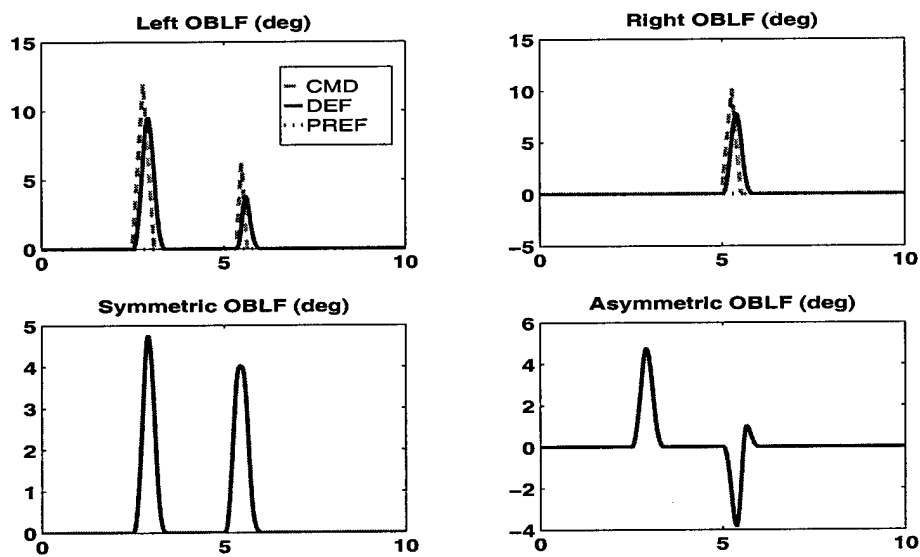


Figure 4.46: Mach 0.35, 5000 ft. Altitude, Min Load CA Mode

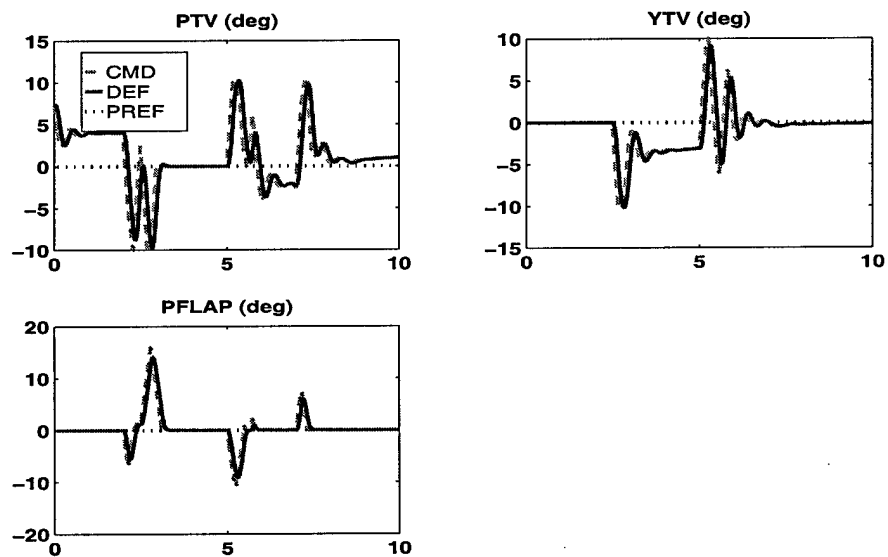


Figure 4.47: Mach 0.35, 5000 ft. Altitude, Min Load CA Mode

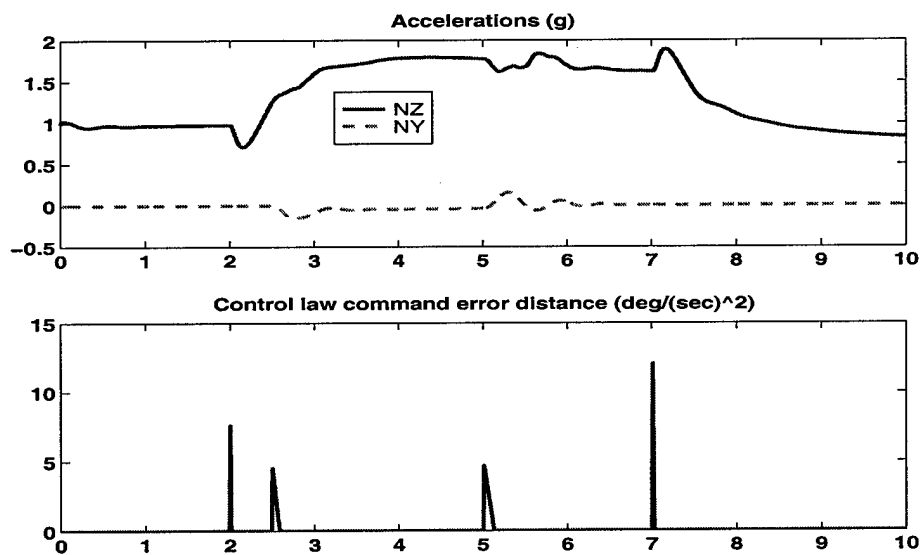


Figure 4.48: Mach 0.35, 5000 ft. Altitude, Min Load CA Mode

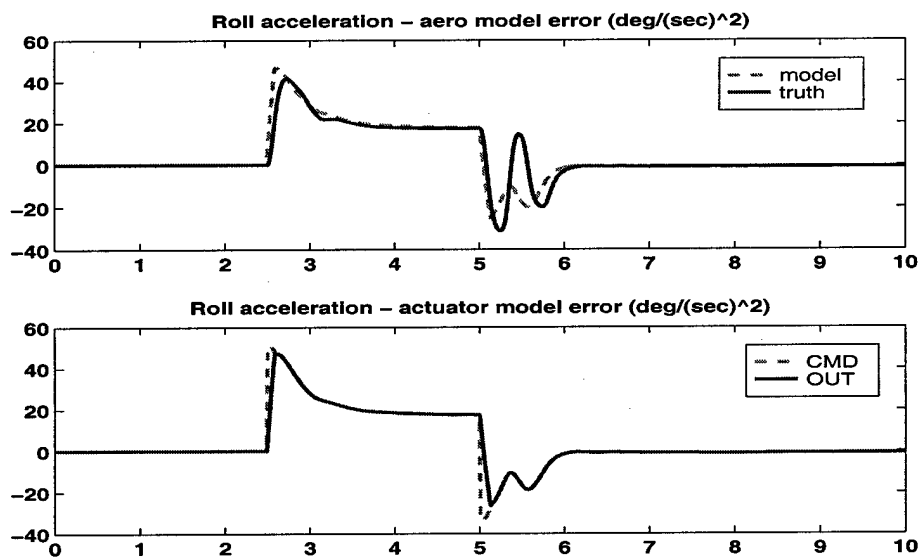


Figure 4.49: Mach 0.35, 5000 ft. Altitude, Min Load CA Mode

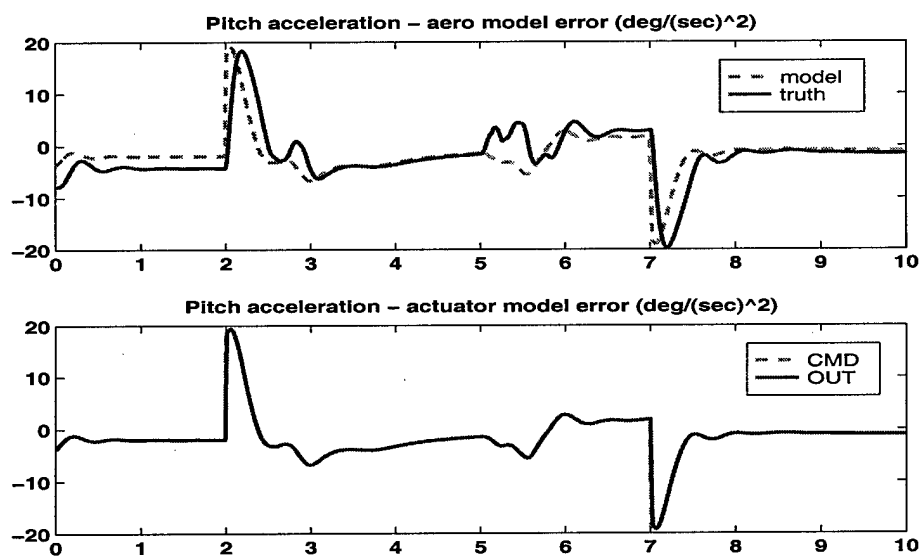


Figure 4.50: Mach 0.35, 5000 ft. Altitude, Min Load CA Mode

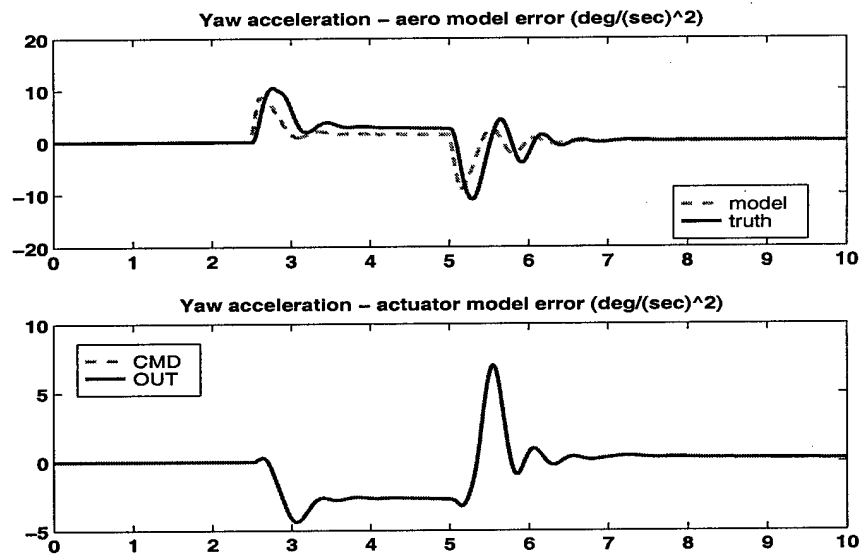


Figure 4.51: Mach 0.35, 5000 ft. Altitude, Min Load CA Mode

Minimum radar signature mode

The minimum radar signature control allocation mode time histories are contained in Figs.(4.52)-(4.62). Note that there is only slight coupling between command variable axes, and angle of slip regulation is very good. Elevons and thrust vectoring are the most active control effectors with all other surfaces only deviating from their preferences at the onset of stick commands when insufficient control power exists to achieve the control law acceleration commands. The spoiler slot deflectors and all moving tips follow their preferences closely since these effectors increase radar signature more than other effectors. There are still slight directional oscillations prevalent in the yaw thrust vector, directional command variable and side acceleration responses. This is due to the lower bandwidth actuator of the thrust vector nozzle compared to the aerodynamic effectors. There is almost no on-board actuator model errors and only slight aerodynamic model errors.

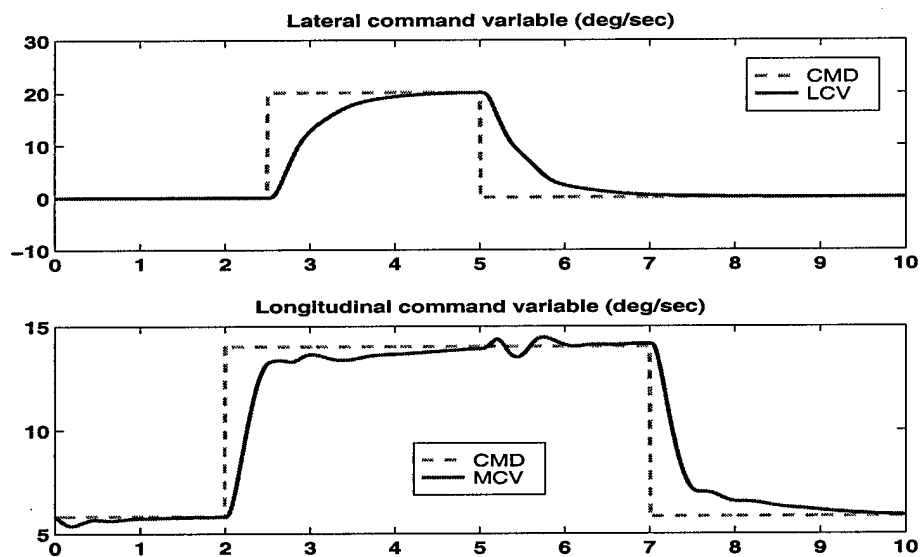


Figure 4.52: Mach 0.35, 5000 ft. Altitude, Min Signature CA Mode

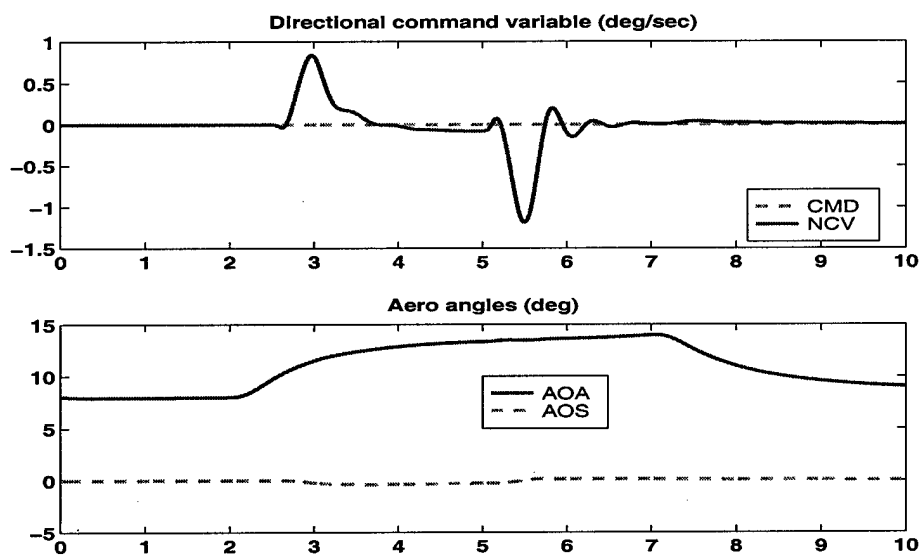


Figure 4.53: Mach 0.35, 5000 ft. Altitude, Min Signature CA Mode

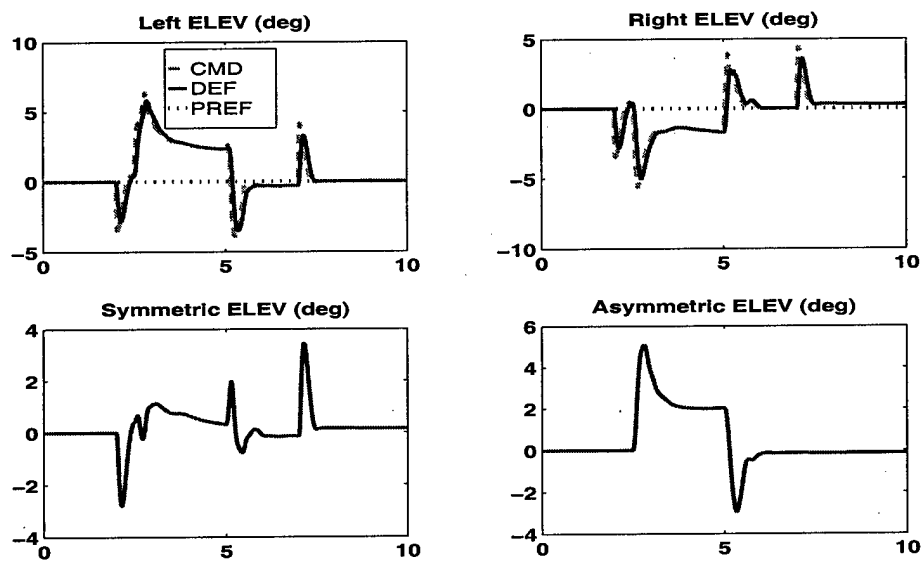


Figure 4.54: Mach 0.35, 5000 ft. Altitude, Min Signature CA Mode

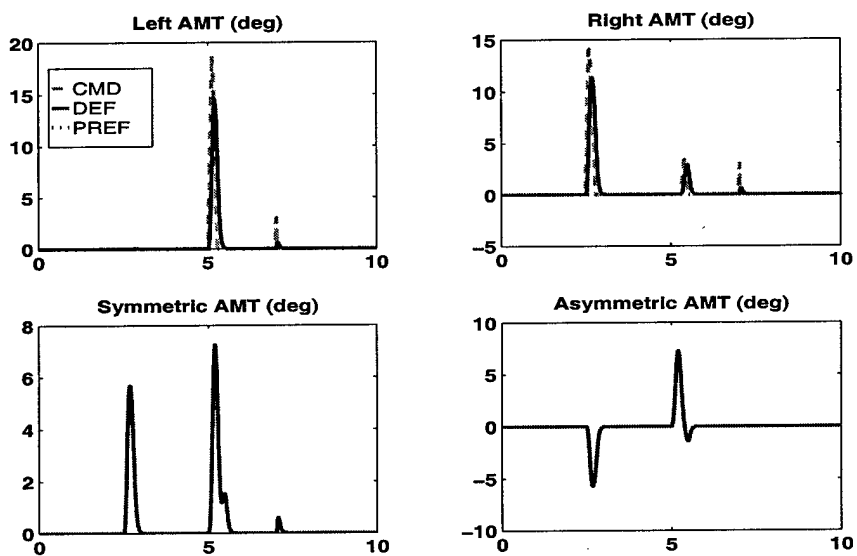


Figure 4.55: Mach 0.35, 5000 ft. Altitude, Min Signature CA Mode

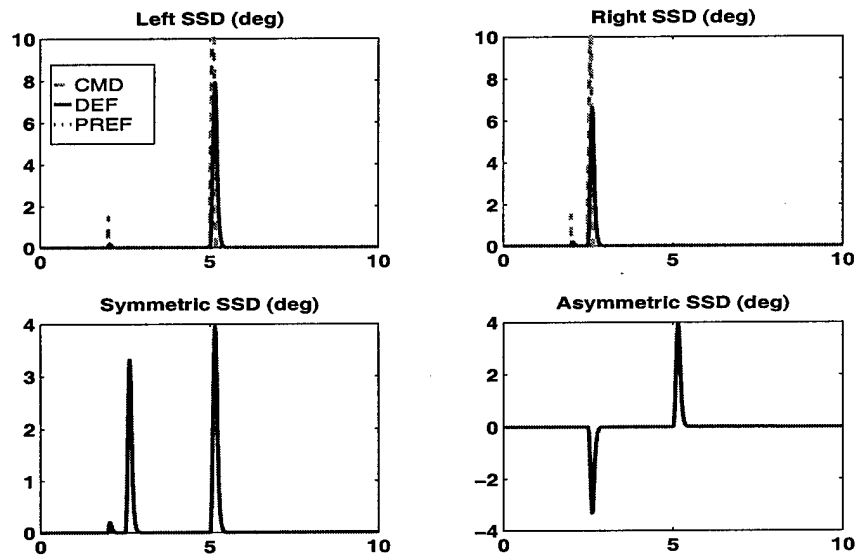


Figure 4.56: Mach 0.35, 5000 ft. Altitude, Min Signature CA Mode

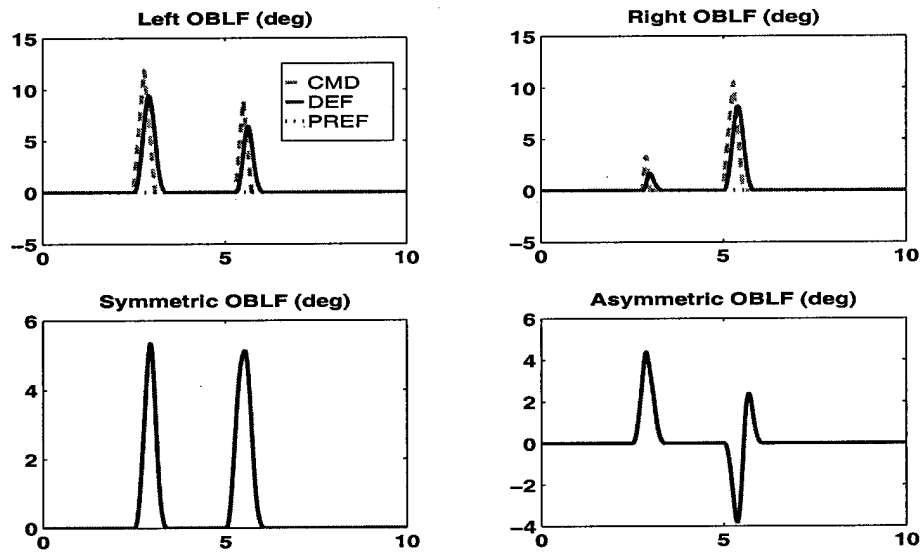


Figure 4.57: Mach 0.35, 5000 ft. Altitude, Min Signature CA Mode

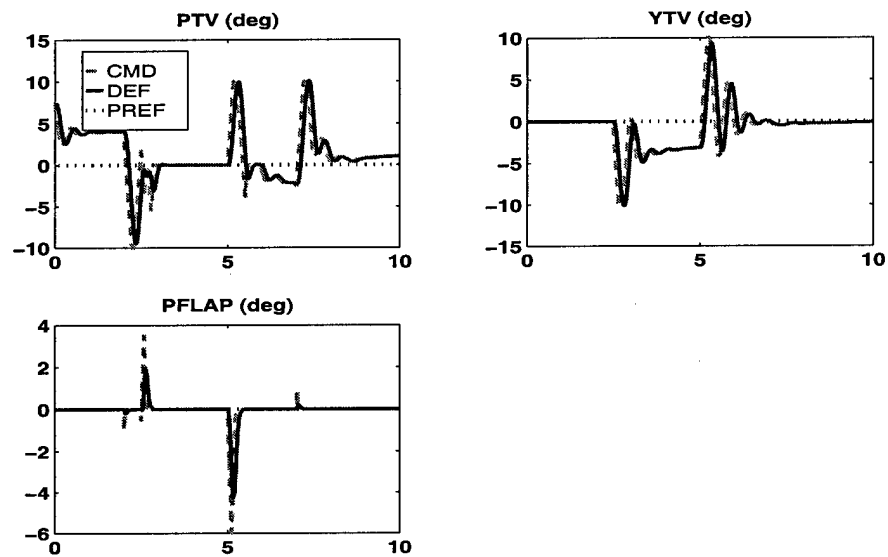


Figure 4.58: Mach 0.35, 5000 ft. Altitude, Min Signature CA Mode

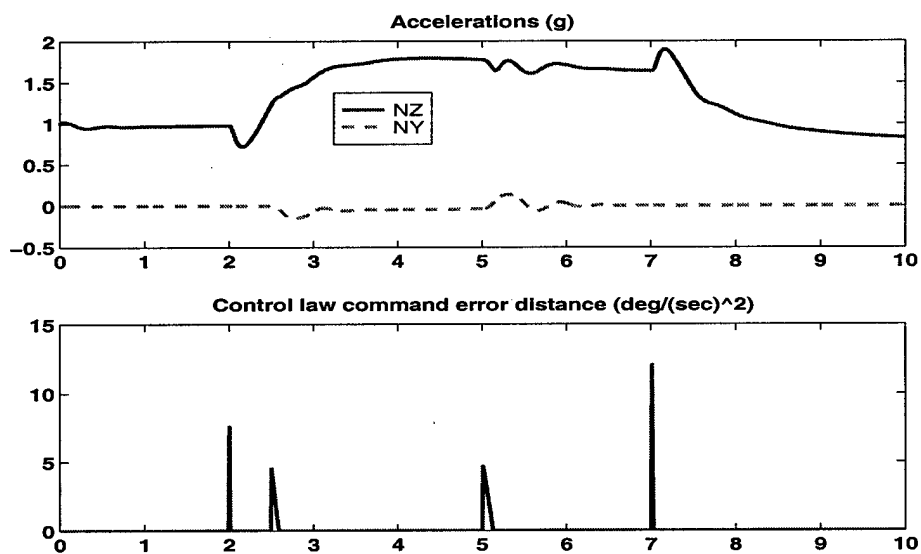


Figure 4.59: Mach 0.35, 5000 ft. Altitude, Min Signature CA Mode

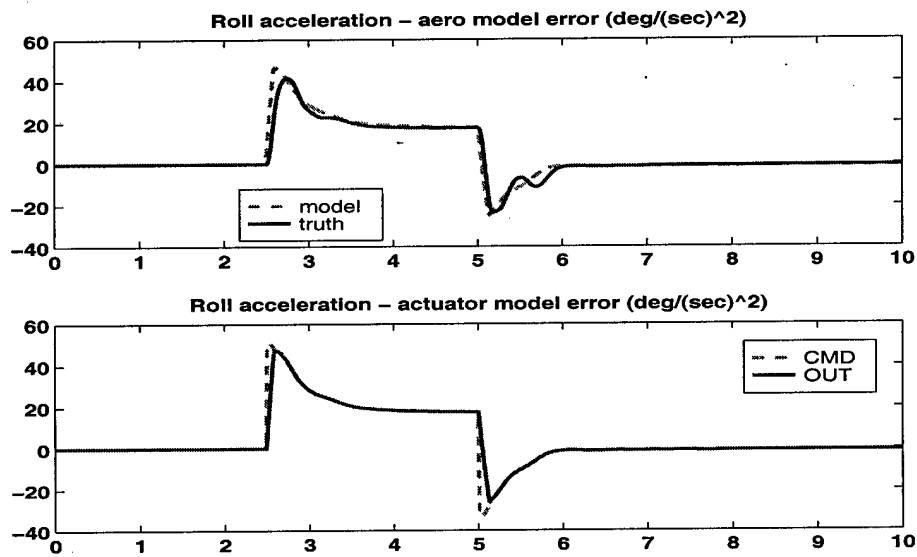


Figure 4.60: Mach 0.35, 5000 ft. Altitude, Min Signature CA Mode

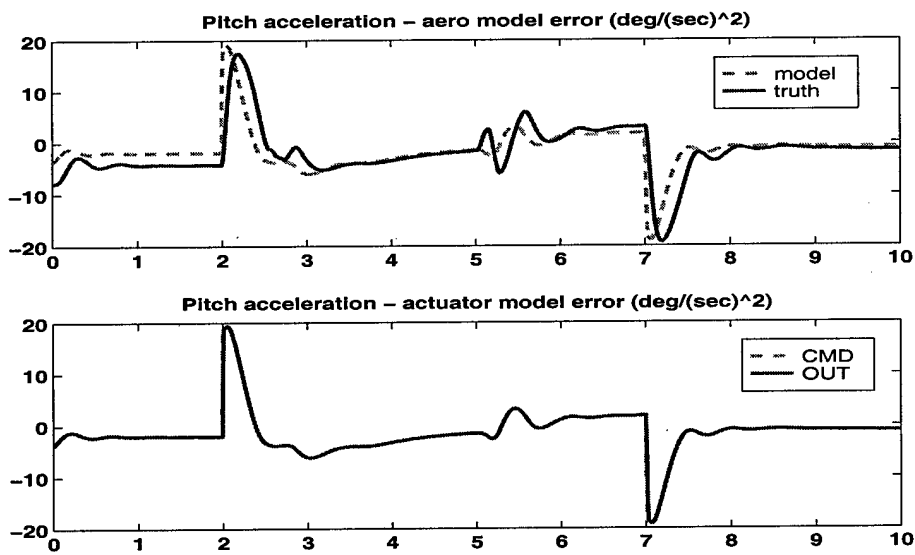


Figure 4.61: Mach 0.35, 5000 ft. Altitude, Min Signature CA Mode

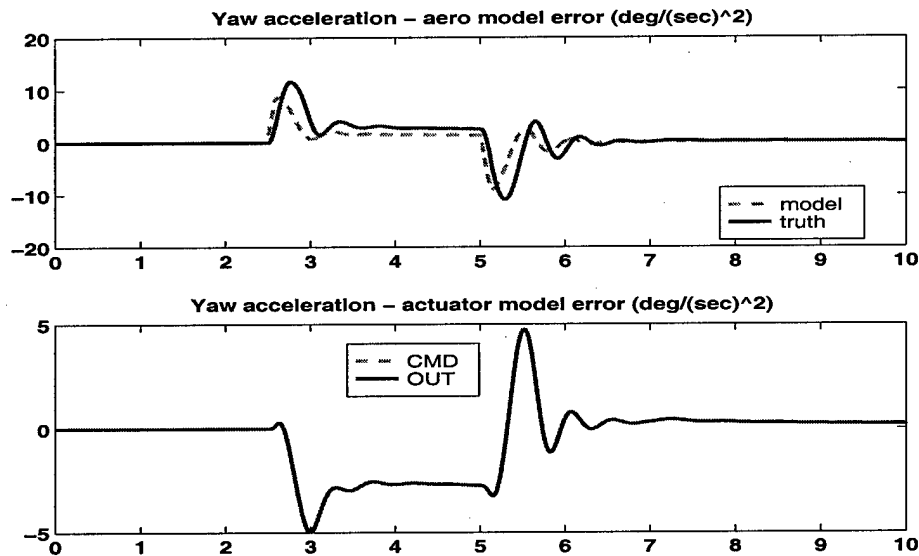


Figure 4.62: Mach 0.35, 5000 ft. Altitude, Min Signature CA Mode

Injection mode

The injection control allocation mode time histories are contained in Figs.(4.63)-(4.73). Note that there is almost no coupling between command variable axes, and angle of slip regulation is very good. All surfaces are active and follow their preferences very closely since the preferences were generated with knowledge of the control law command. There are no directional oscillations. There is almost no on-board actuator model errors and only slight aerodynamic model errors.

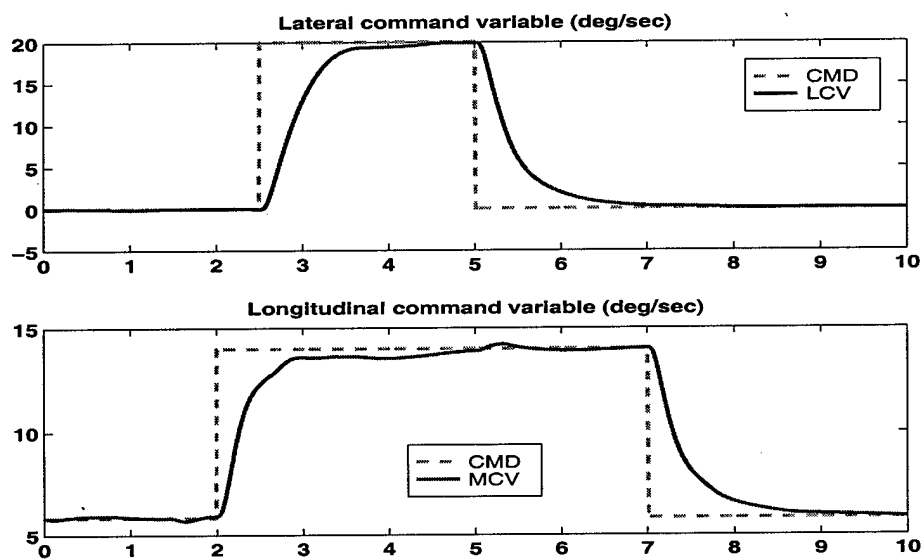


Figure 4.63: Mach 0.35, 5000 ft. Altitude, Injection CA Mode

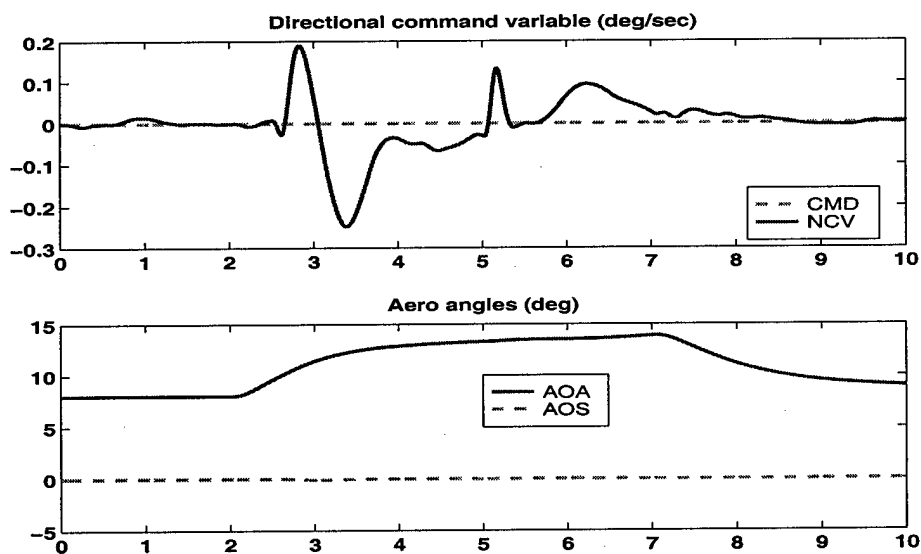


Figure 4.64: Mach 0.35, 5000 ft. Altitude, Injection CA Mode

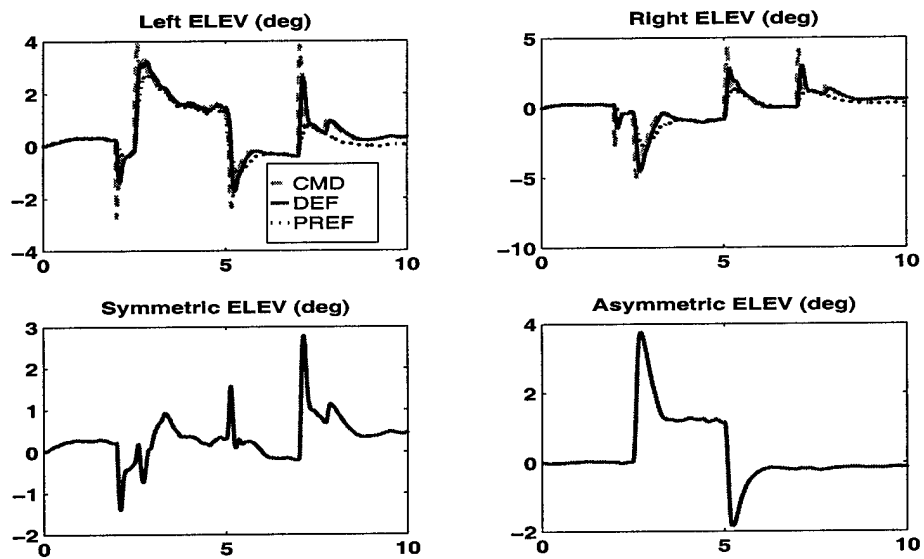


Figure 4.65: Mach 0.35, 5000 ft. Altitude, Injection CA Mode

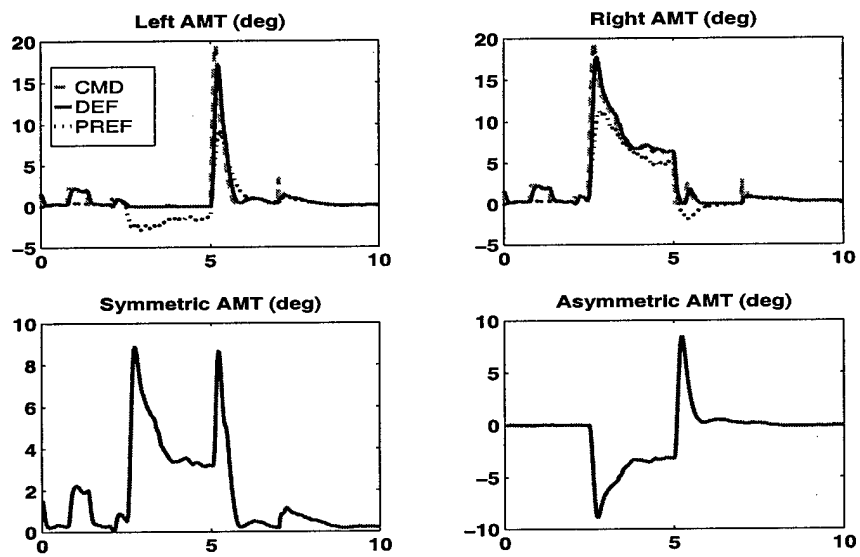


Figure 4.66: Mach 0.35, 5000 ft. Altitude, Injection CA Mode

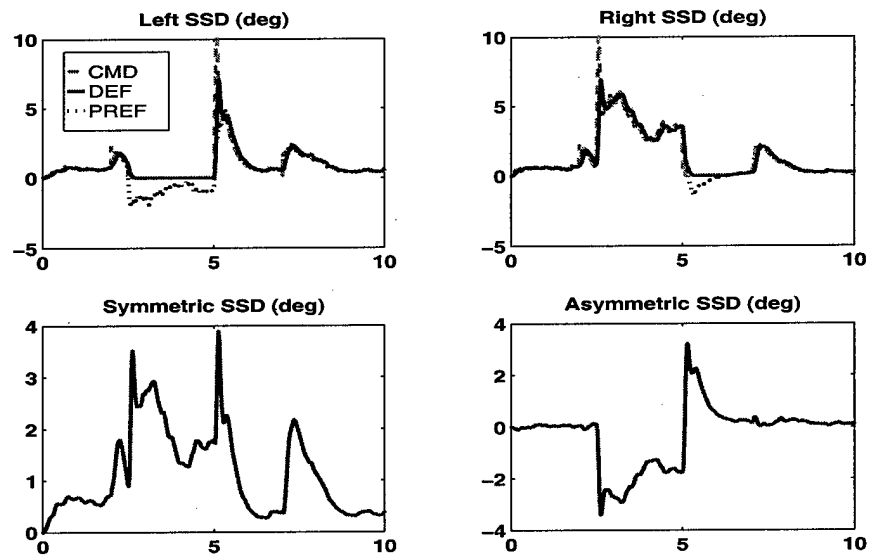


Figure 4.67: Mach 0.35, 5000 ft. Altitude, Injection CA Mode

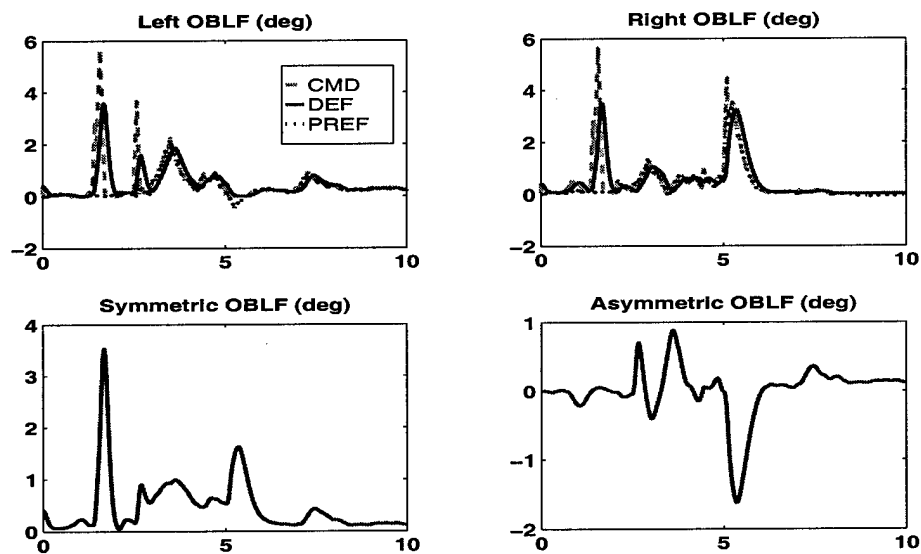


Figure 4.68: Mach 0.35, 5000 ft. Altitude, Injection CA Mode

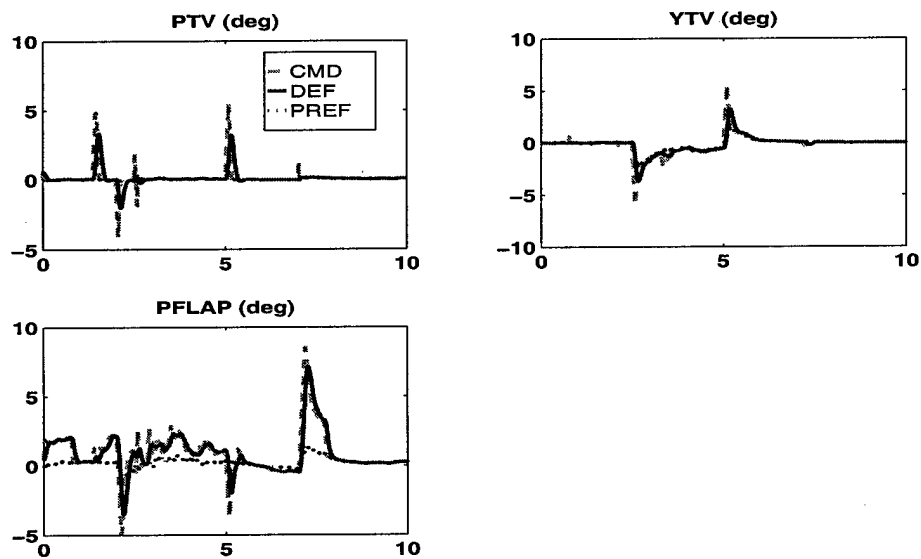


Figure 4.69: Mach 0.35, 5000 ft. Altitude, Injection CA Mode

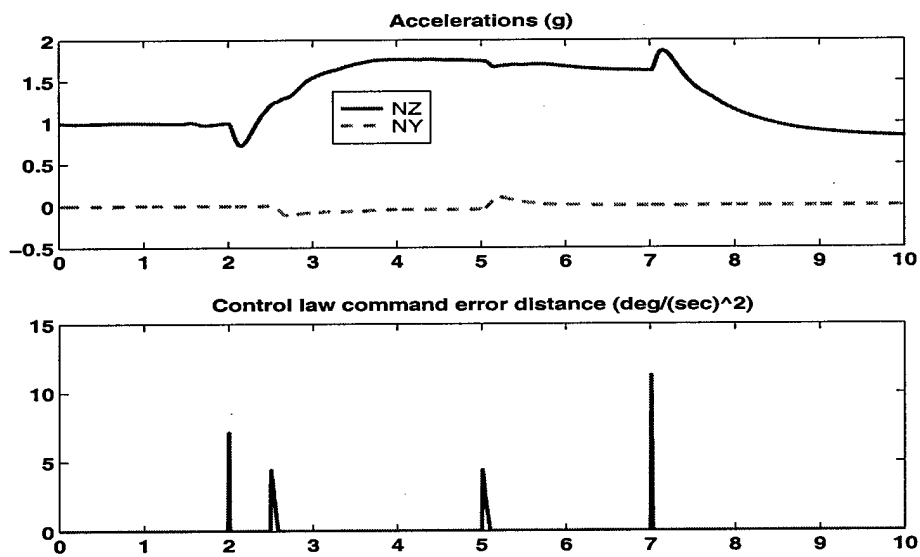


Figure 4.70: Mach 0.35, 5000 ft. Altitude, Injection CA Mode

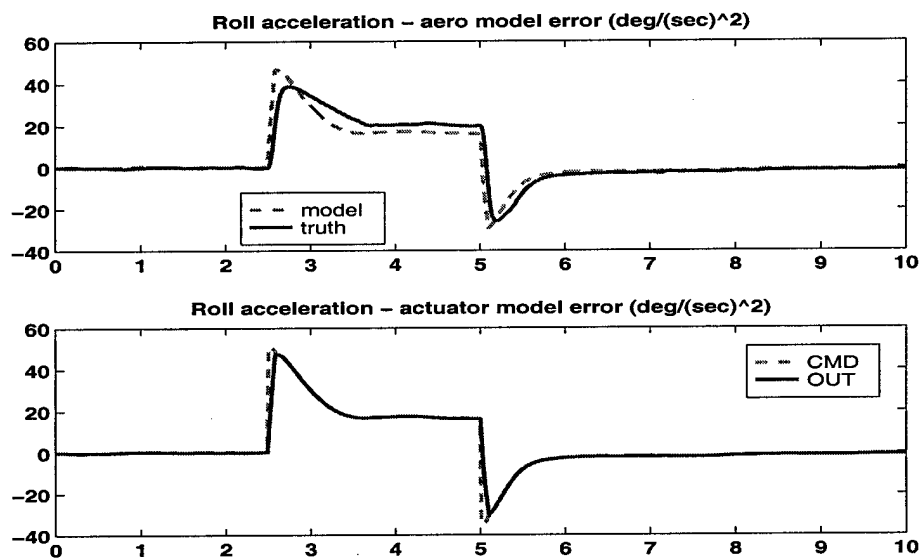


Figure 4.71: Mach 0.35, 5000 ft. Altitude, Injection CA Mode

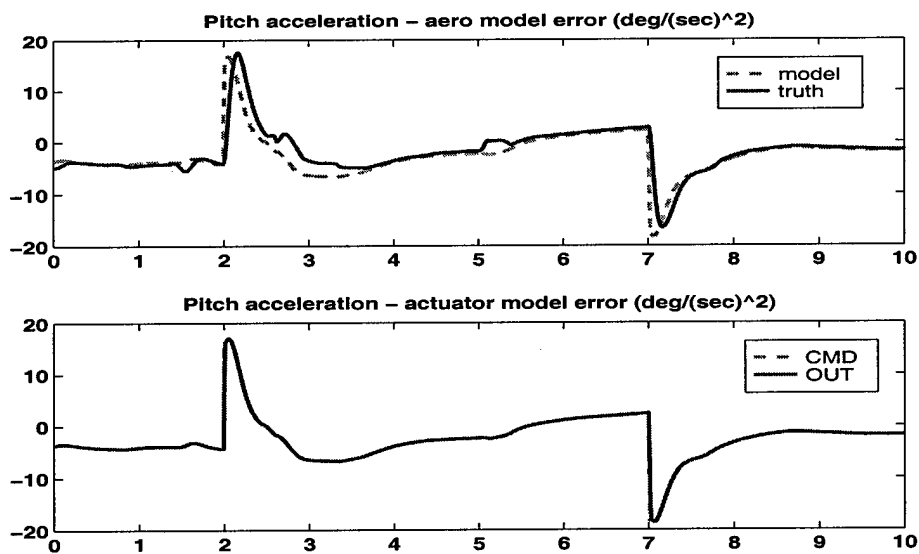


Figure 4.72: Mach 0.35, 5000 ft. Altitude, Injection CA Mode

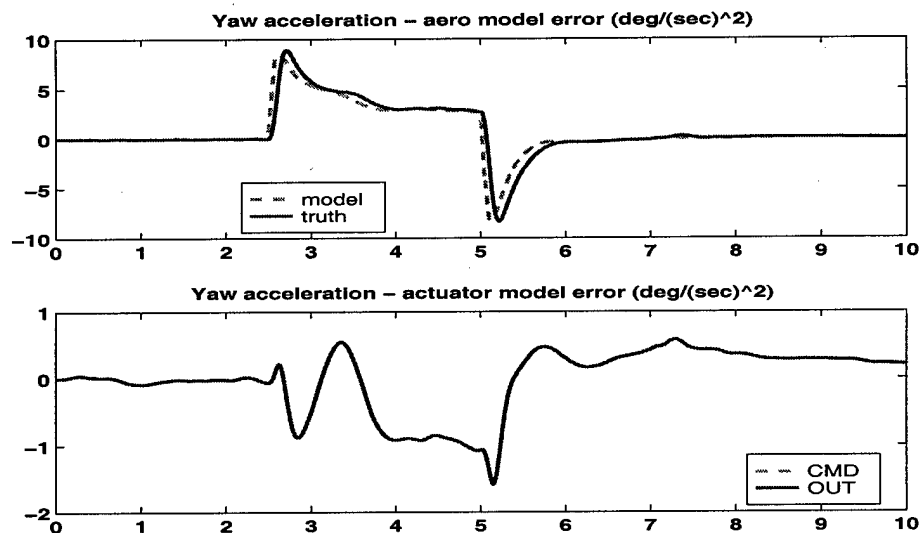


Figure 4.73: Mach 0.35, 5000 ft. Altitude, Injection CA Mode

Minimum thrust vector mode

The minimum thrust vector control allocation mode time histories are contained in Figs.(4.74)-(4.84). This mode was a late addition to the control law attempting to alleviate the directional oscillations prevalent in the other modes. Note that there is only slight coupling between command variable axes, and angle of slip regulation is very good. Thrust vectoring only deviates from the preferences at the onset of stick commands when insufficient control power exists to achieve the control law acceleration commands. There are no directional oscillations which led to the nominal choice of this mode at the low dynamic pressure flight condition. There is almost no on-board actuator model errors and only slight aerodynamic model errors.

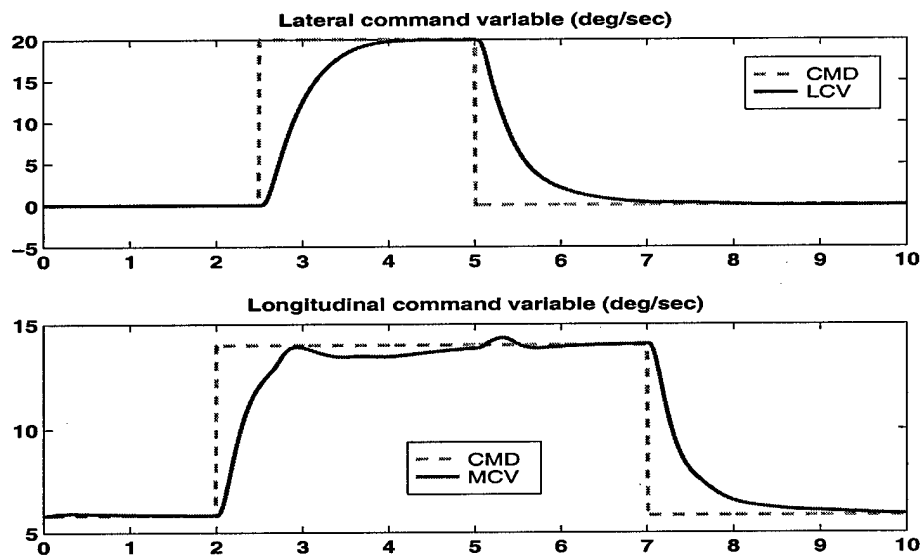


Figure 4.74: Mach 0.35, 5000 ft. Altitude, Min Vec CA Mode

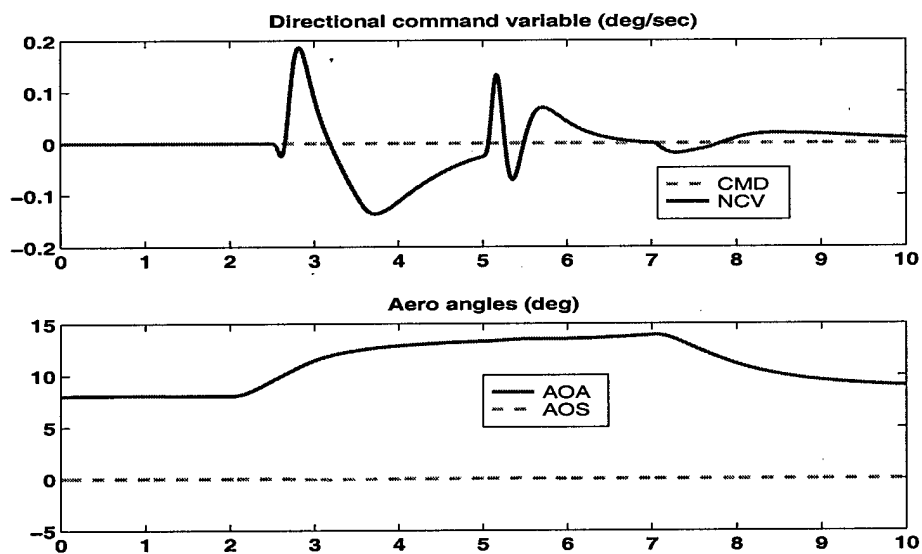


Figure 4.75: Mach 0.35, 5000 ft. Altitude, Min Vec CA Mode

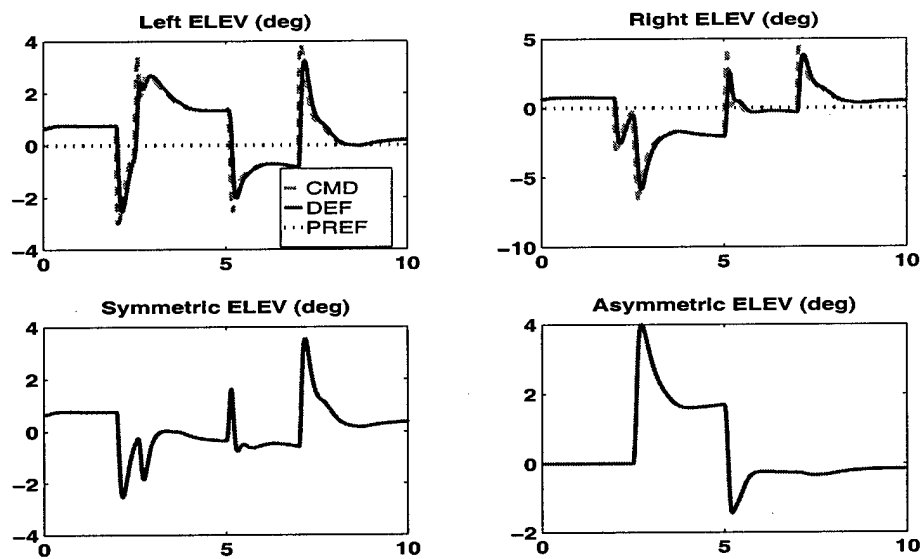


Figure 4.76: Mach 0.35, 5000 ft. Altitude, Min Vec CA Mode

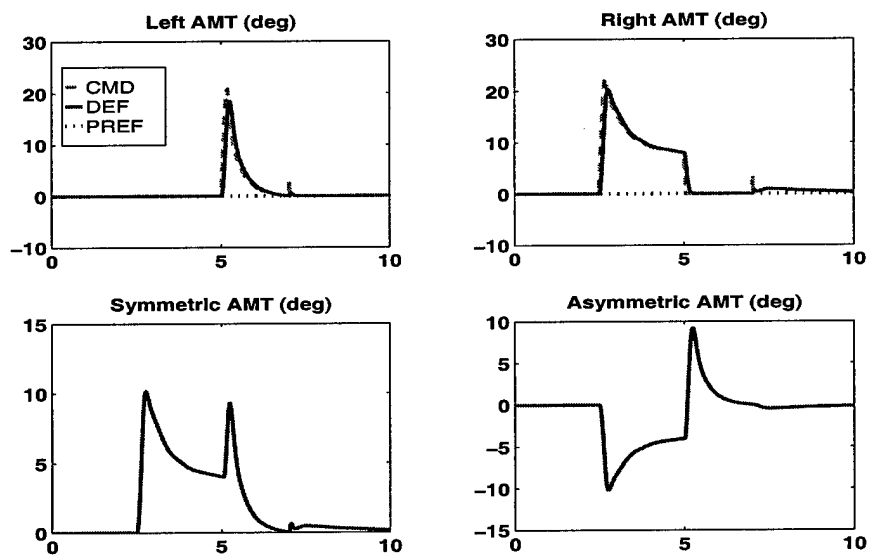


Figure 4.77: Mach 0.35, 5000 ft. Altitude, Min Vec CA Mode

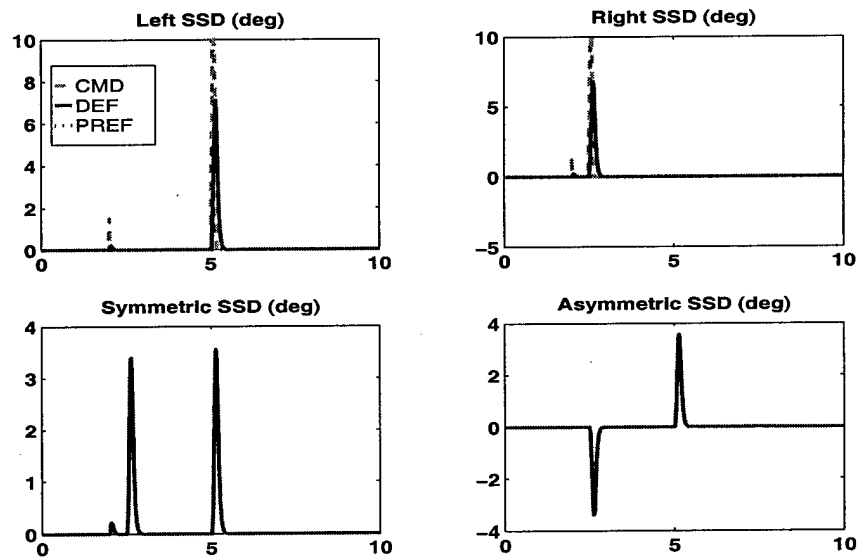


Figure 4.78: Mach 0.35, 5000 ft. Altitude, Min Vec CA Mode

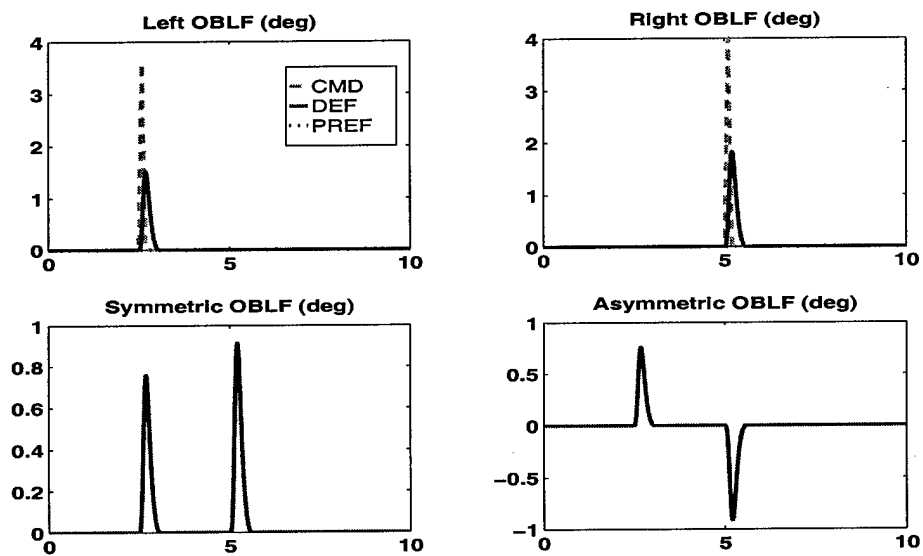


Figure 4.79: Mach 0.35, 5000 ft. Altitude, Min Vec CA Mode

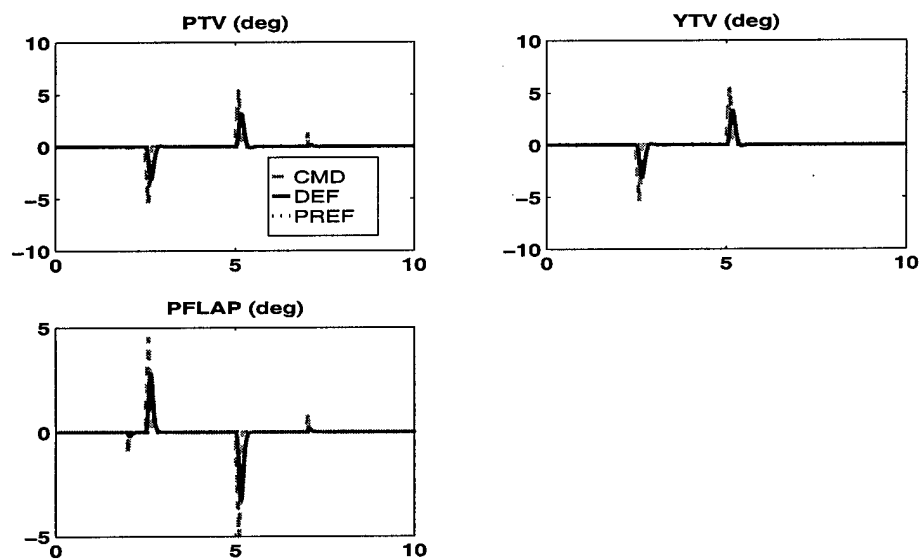


Figure 4.80: Mach 0.35, 5000 ft. Altitude, Min Vec CA Mode

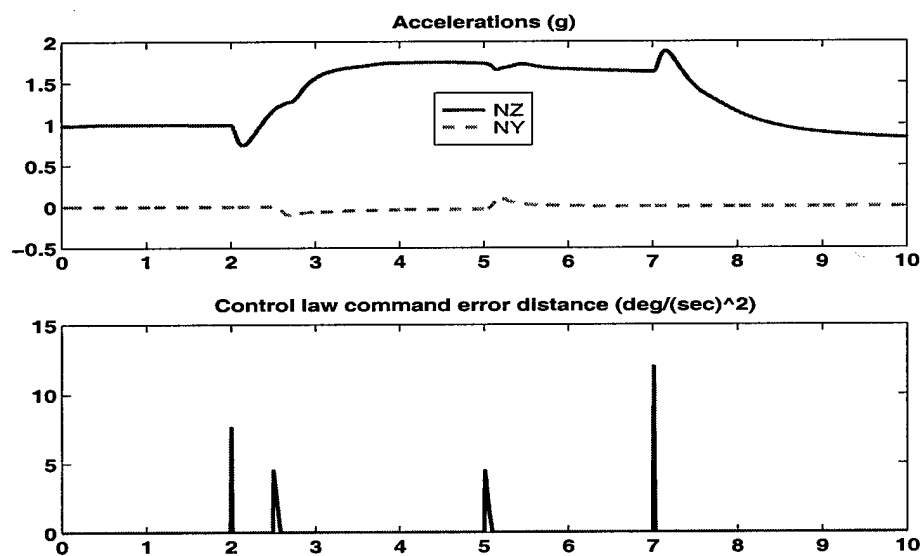


Figure 4.81: Mach 0.35, 5000 ft. Altitude, Min Vec CA Mode

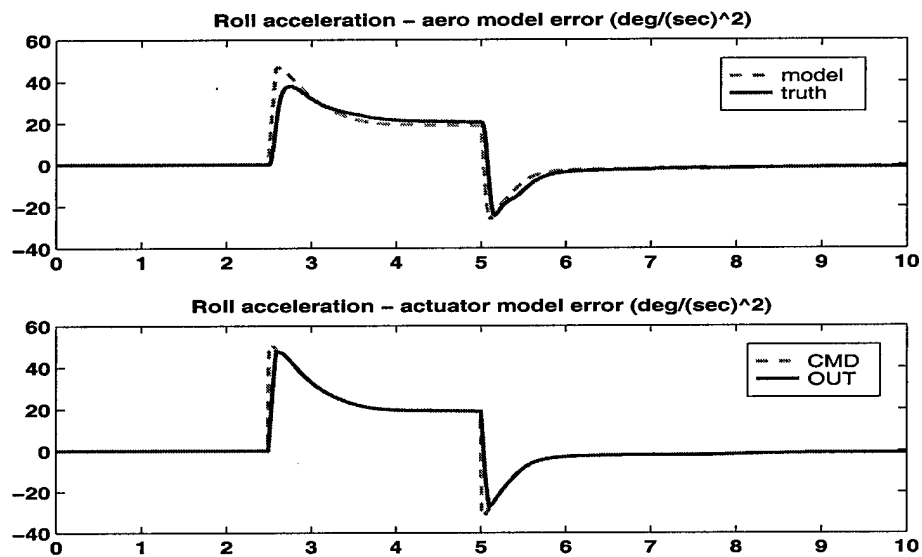


Figure 4.82: Mach 0.35, 5000 ft. Altitude, Min Vec CA Mode

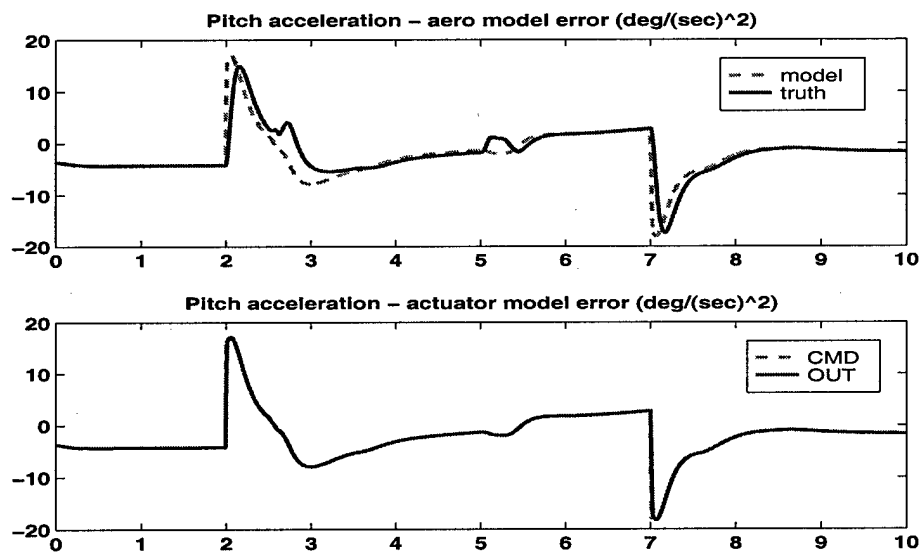


Figure 4.83: Mach 0.35, 5000 ft. Altitude, Min Vec CA Mode

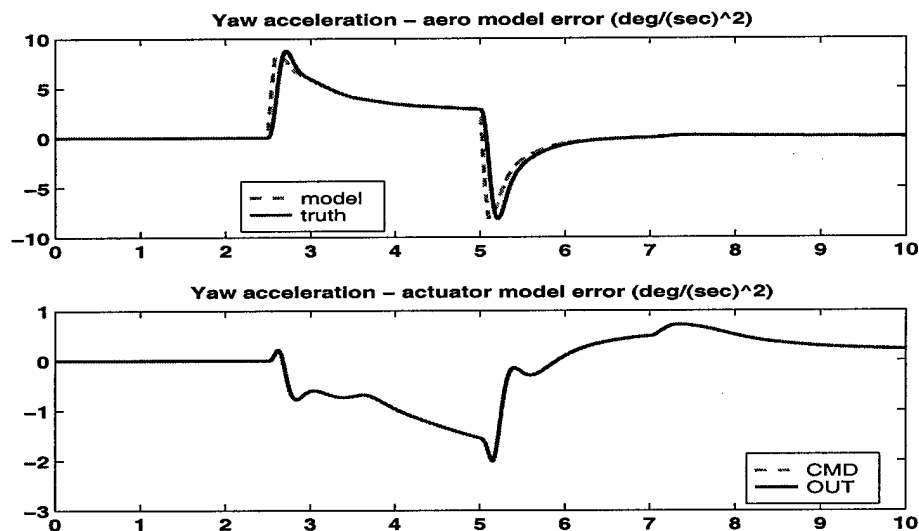


Figure 4.84: Mach 0.35, 5000 ft. Altitude, Min Vec CA Mode

Summary

The various control allocation modes minimize their corresponding objectives. The linear program control allocation deviates the minimum number of control effectors from their preferences to achieve the control law command. The injection mode results in almost no residual aircraft motion and decoupled command variable response. Directional oscillations occur for those modes that use thrust vectoring as the primary yaw control effector. This is attributed to the fact that the thrust vectoring nozzle has the lowest bandwidth actuator of all the actuators. The low bandwidth vector actuator reduces the stability margins at this flight condition. Further recall that the zero dynamics were least stable and most sensitive to control allocation at this flight condition. The nominal mode for this flight condition was chosen to be minimum vectoring due to these factors. Command variable response coupling was prevalent, in those modes that led to large leading edge flap and spoiler slot deflector deflections, due to unmodeled interactions of these surfaces with the elevons.

4.4.2 Final control law analysis

This section contains batch simulation responses of loaded roll and full stick roll maneuvers with the control laws in the final configuration at each of the four analysis flight conditions.

Low dynamic pressure flight condition, Mach 0.35 5,000 ft. altitude

This section contains simulation responses at the low dynamic pressure flight condition. The control allocation mode at this condition minimizes thrust vectoring.

The responses in Figs.(4.85)-(4.95) are for the loaded roll maneuver. These responses are identical to the responses in Figs.(4.74)-(4.84). There is only slight coupling between command variable axes, and angle of slip regulation is very good. Thrust vectoring only deviates from the preferences at the onset of stick commands when insufficient control power exists to achieve the control law acceleration commands. There is almost no on-board actuator model errors and only slight aerodynamic model errors.

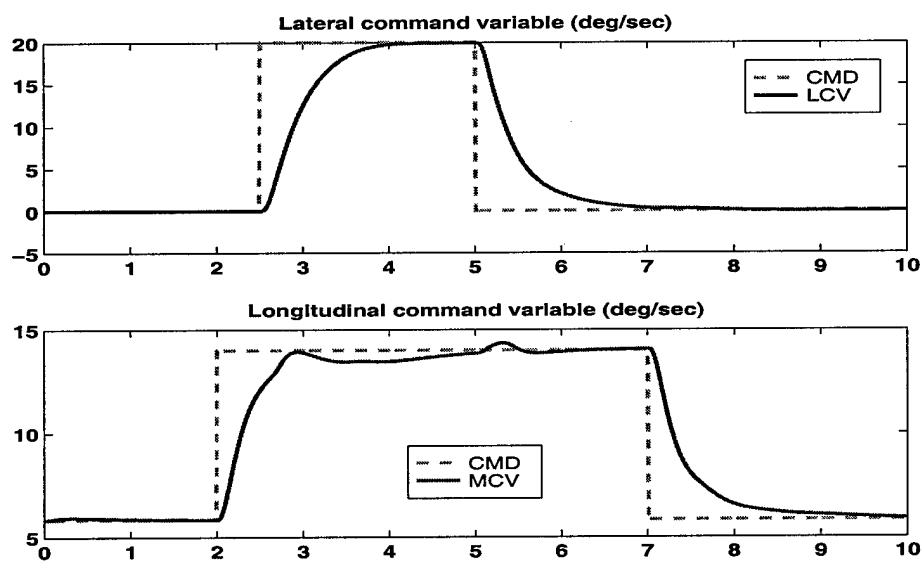


Figure 4.85: Mach 0.35, 5,000 ft. Altitude, Min Thrust Vector CA Mode, Loaded Roll

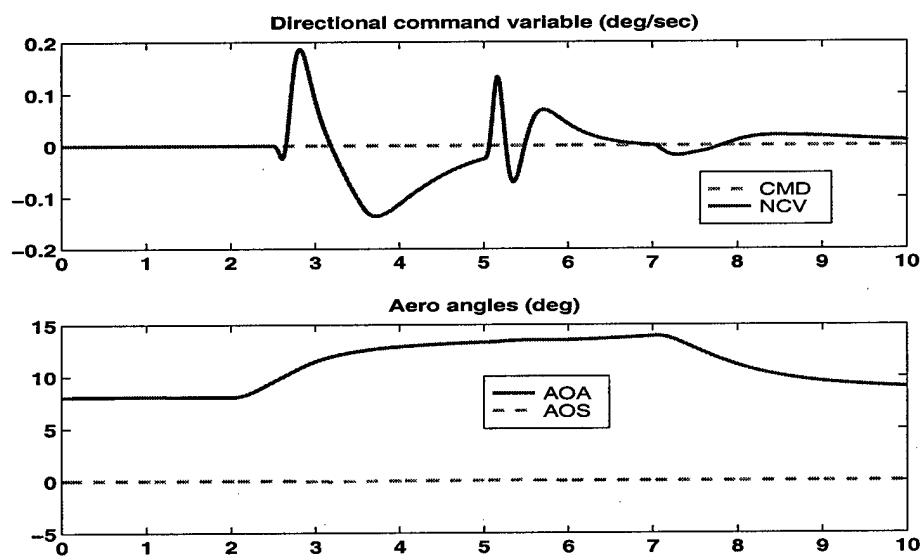


Figure 4.86: Mach 0.35, 5,000 ft. Altitude, Min Thrust Vector CA Mode, Loaded Roll

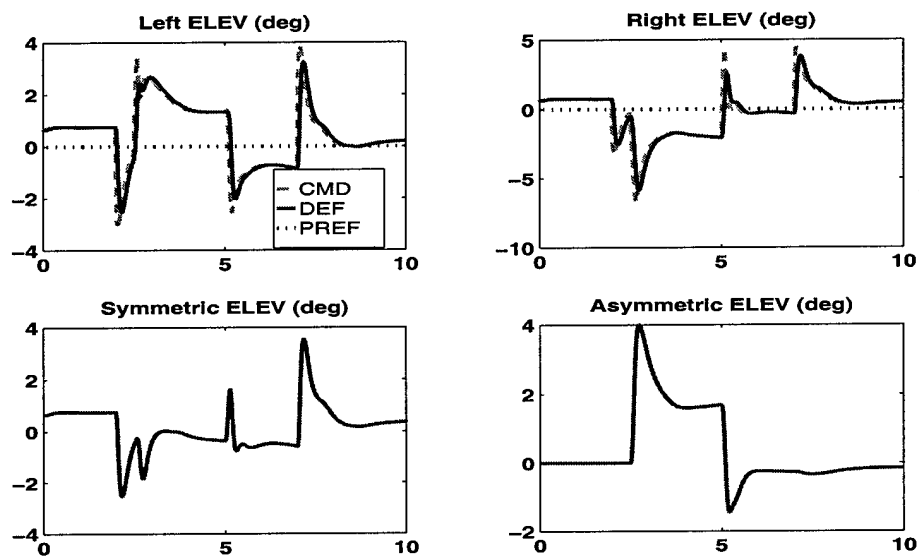


Figure 4.87: Mach 0.35, 5,000 ft. Altitude, Min Thrust Vector CA Mode, Loaded Roll

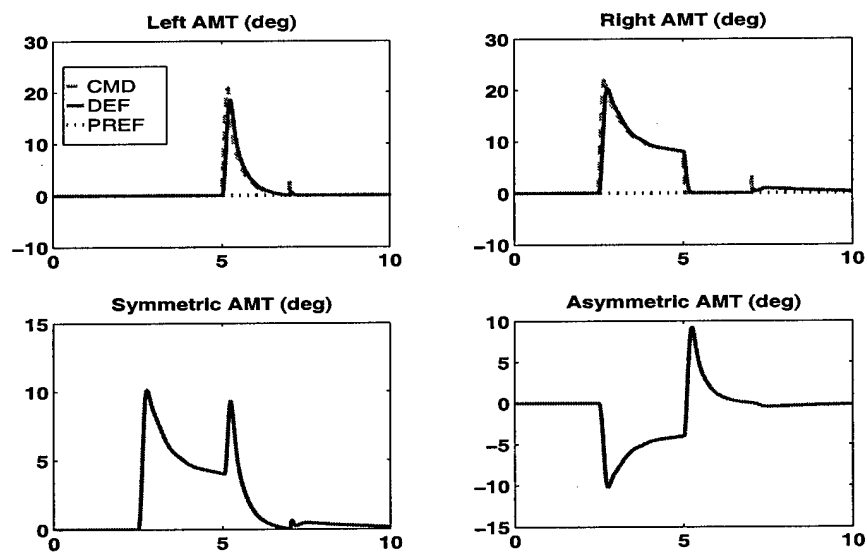


Figure 4.88: Mach 0.35, 5,000 ft. Altitude, Min Thrust Vector CA Mode, Loaded Roll

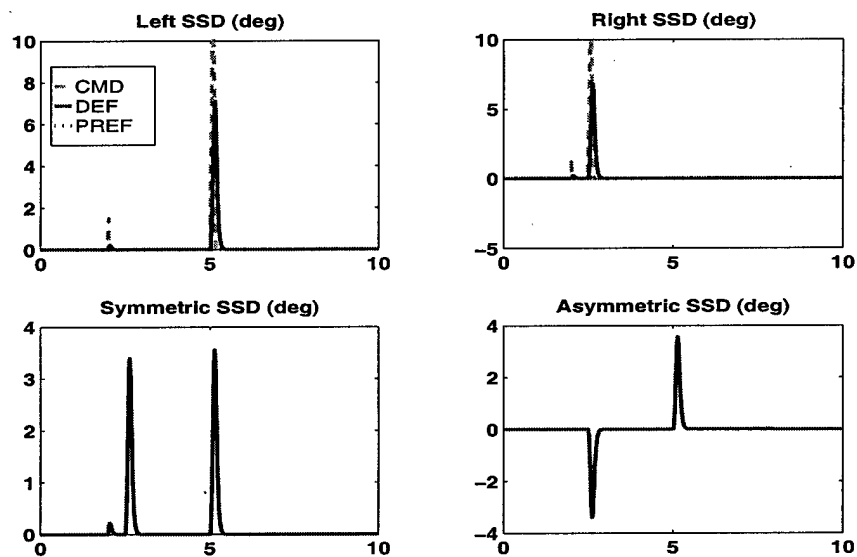


Figure 4.89: Mach 0.35, 5,000 ft. Altitude, Min Thrust Vector CA Mode, Loaded Roll

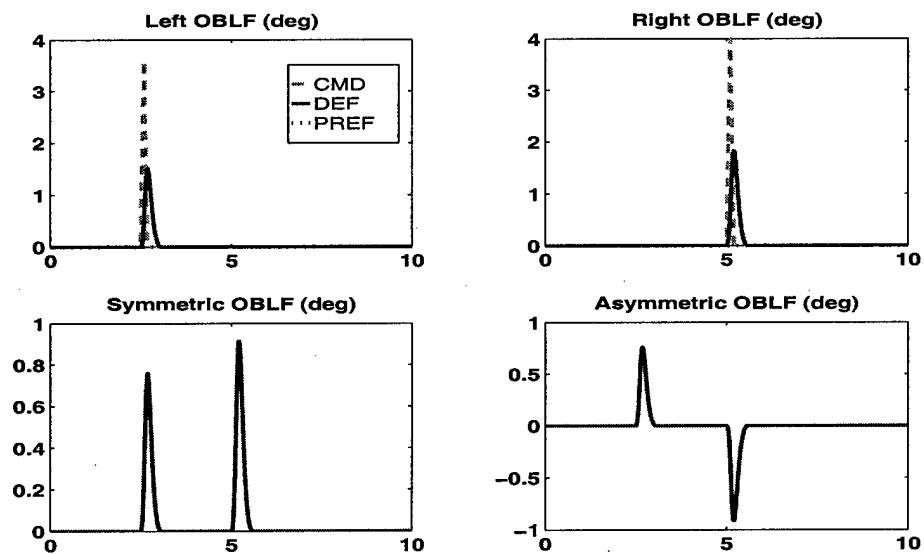


Figure 4.90: Mach 0.35, 5,000 ft. Altitude, Min Thrust Vector CA Mode, Loaded Roll

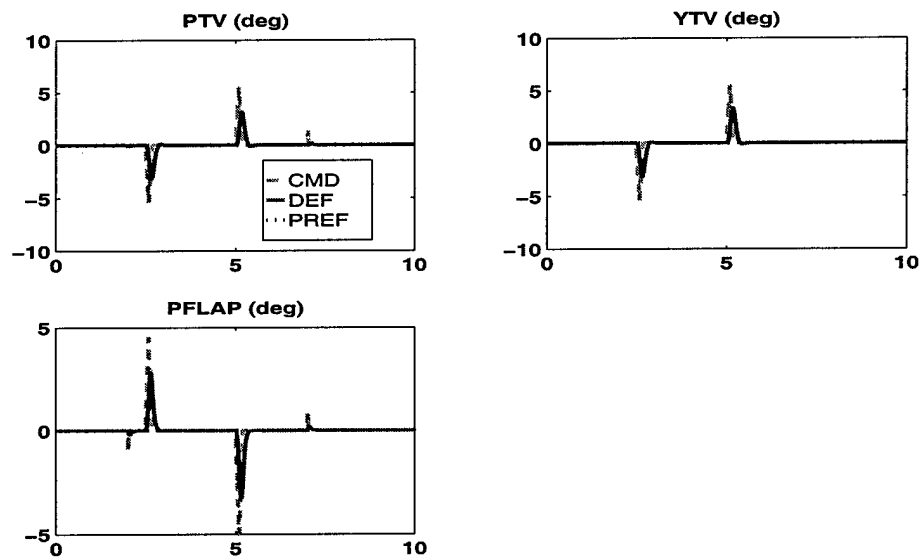


Figure 4.91: Mach 0.35, 5,000 ft. Altitude, Min Thrust Vector CA Mode, Loaded Roll

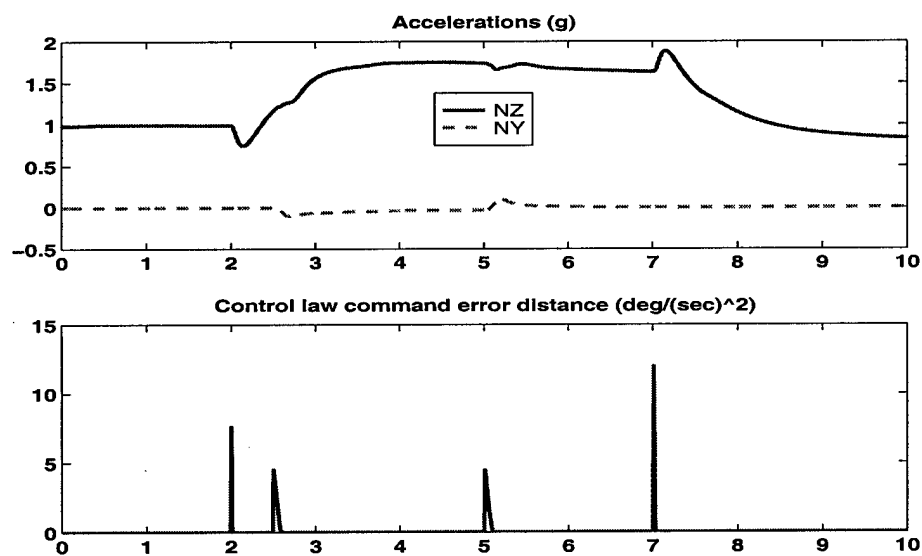


Figure 4.92: Mach 0.35, 5,000 ft. Altitude, Min Thrust Vector CA Mode, Loaded Roll

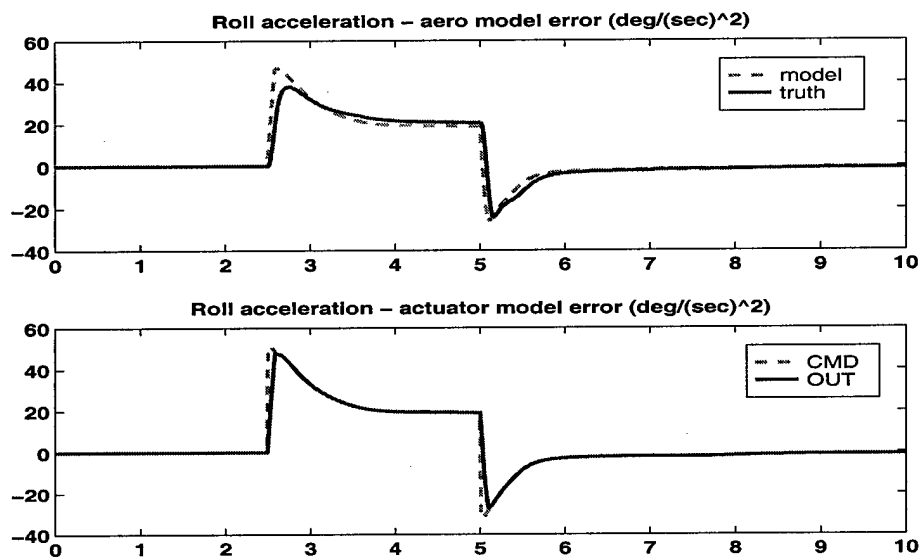


Figure 4.93: Mach 0.35, 5,000 ft. Altitude, Min Thrust Vector CA Mode, Loaded Roll

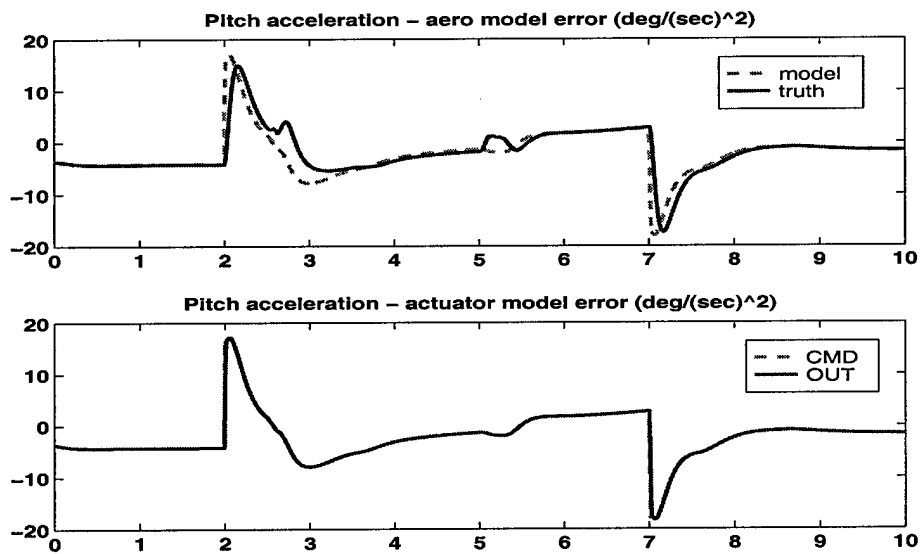


Figure 4.94: Mach 0.35, 5,000 ft. Altitude, Min Thrust Vector CA Mode, Loaded Roll

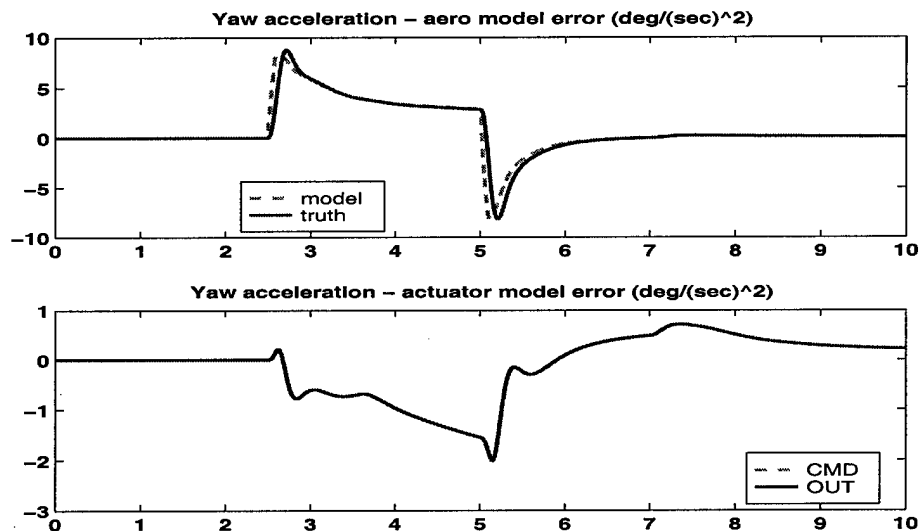


Figure 4.95: Mach 0.35, 5,000 ft. Altitude, Min Thrust Vector CA Mode, Loaded Roll

The responses in Figs.(4.96)-(4.106) are for the full stick roll maneuver. The lateral command variable tracks the command well and slight directional coupling exists. Angle of slip regulation is very good. Longitudinal coupling caused by aerodynamic model errors degrades longitudinal command variable regulation. The aerodynamic model errors are due to unmodeled spoiler slot deflector and leading edge flap interactions with the elevons. Thrust vector deflections only deviate from their preferences at the onset of stick commands when insufficient control power exists to achieve the control law acceleration commands. There are roll acceleration errors due to unmodeled actuator dynamics.

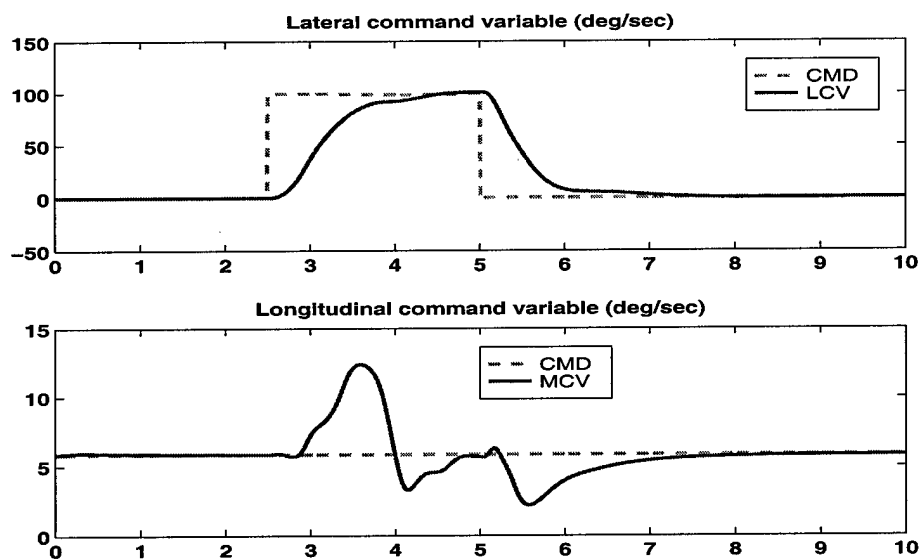


Figure 4.96: Mach 0.35, 5,000 ft. Altitude, Min Thrust Vector CA Mode, Full Stick Roll

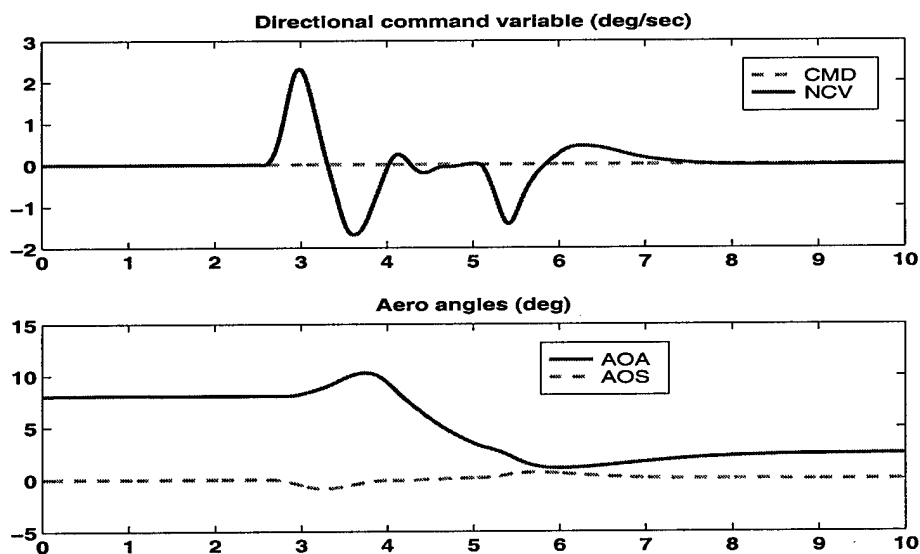


Figure 4.97: Mach 0.35, 5,000 ft. Altitude, Min Thrust Vector CA Mode, Full Stick Roll

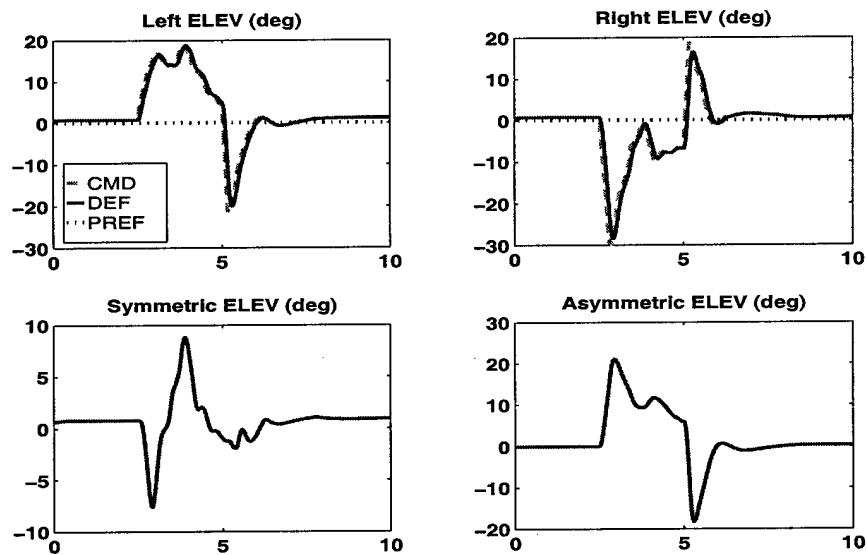


Figure 4.98: Mach 0.35, 5,000 ft. Altitude, Min Thrust Vector CA Mode, Full Stick Roll

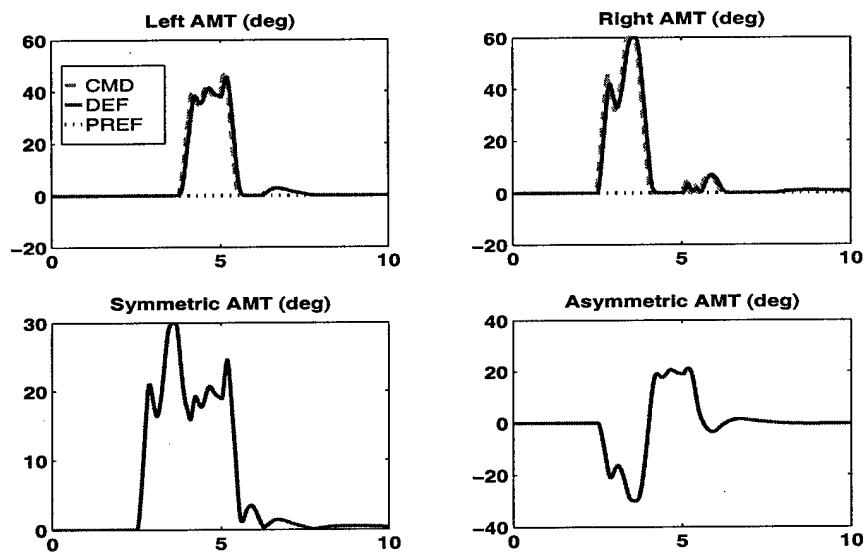


Figure 4.99: Mach 0.35, 5,000 ft. Altitude, Min Thrust Vector CA Mode, Full Stick Roll

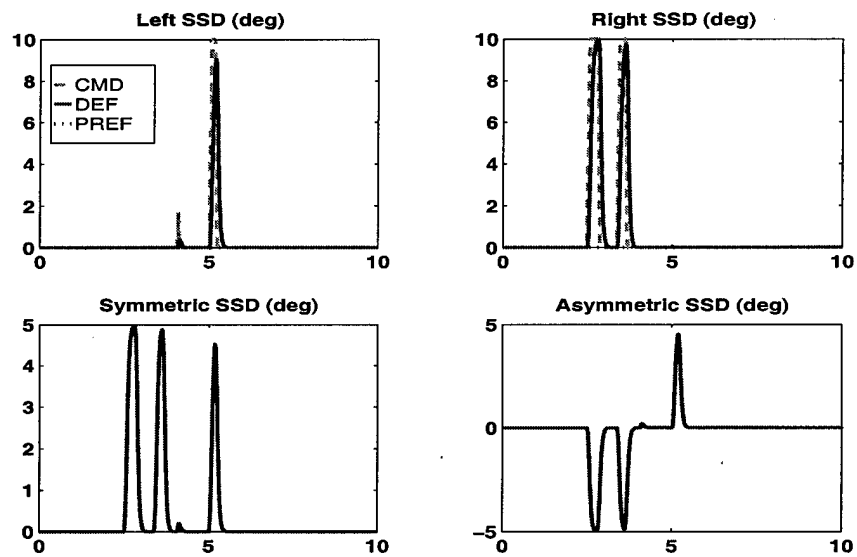


Figure 4.100: Mach 0.35, 5,000 ft. Altitude, Min Thrust Vector CA Mode, Full Stick Roll

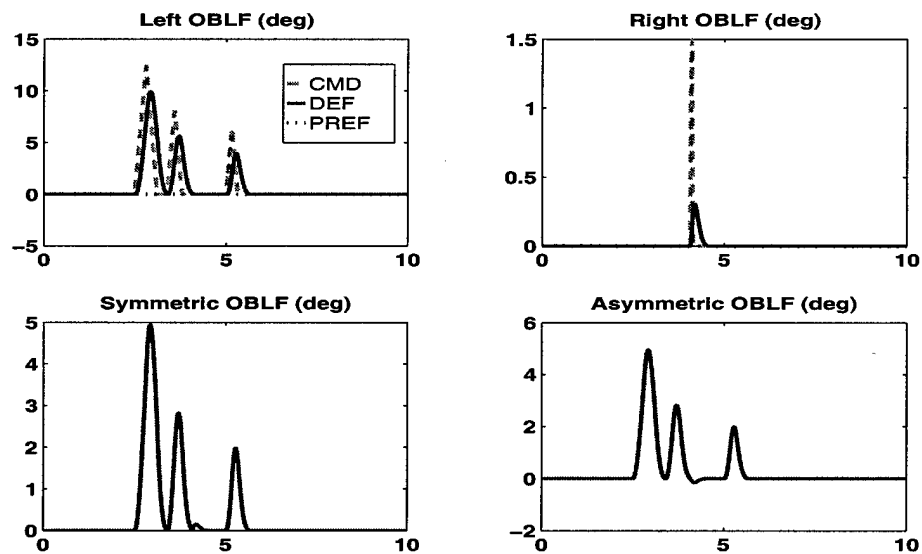


Figure 4.101: Mach 0.35, 5,000 ft. Altitude, Min Thrust Vector CA Mode, Full Stick Roll

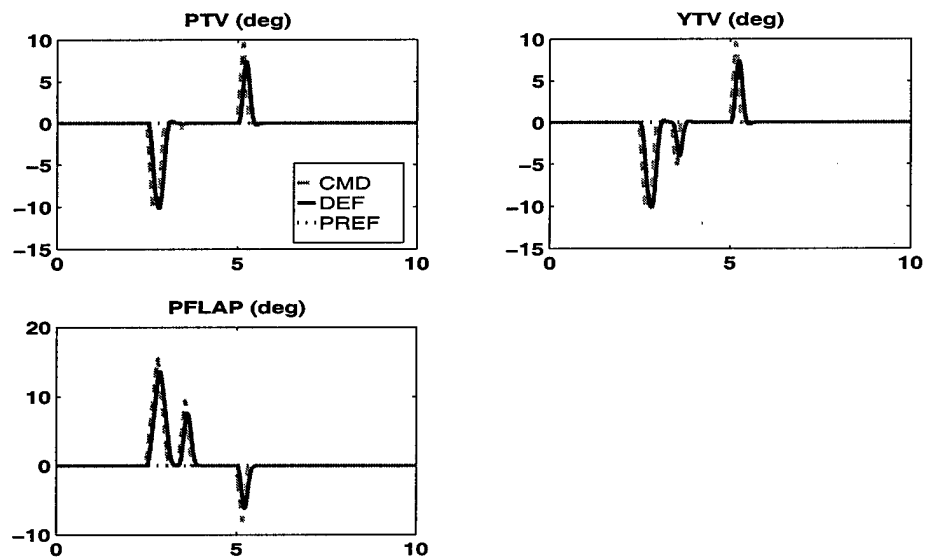


Figure 4.102: Mach 0.35, 5,000 ft. Altitude, Min Thrust Vector CA Mode, Full Stick Roll

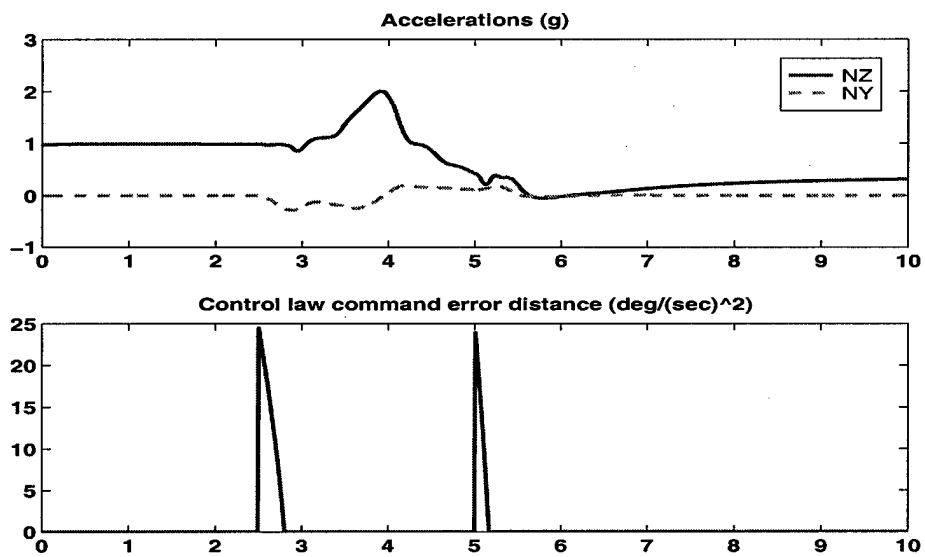


Figure 4.103: Mach 0.35, 5,000 ft. Altitude, Min Thrust Vector CA Mode, Full Stick Roll

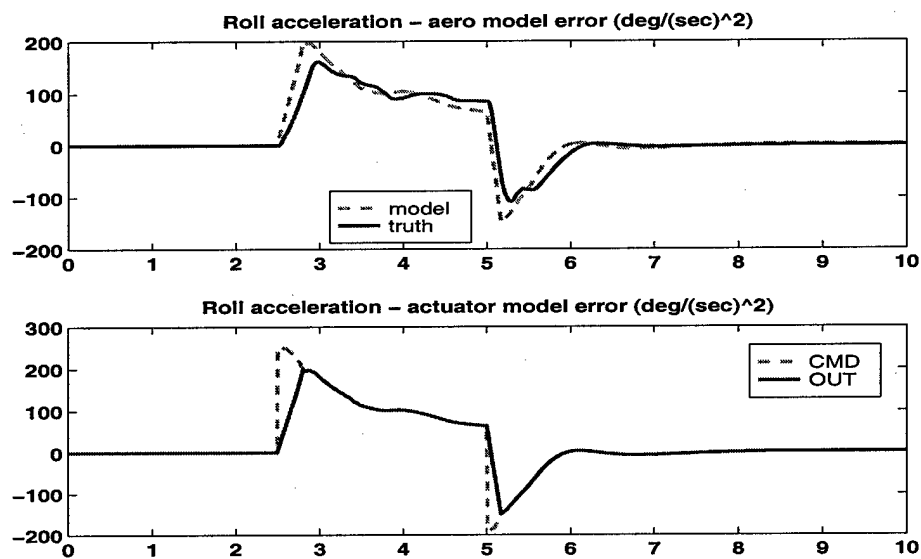


Figure 4.104: Mach 0.35, 5,000 ft. Altitude, Min Thrust Vector CA Mode, Full Stick Roll

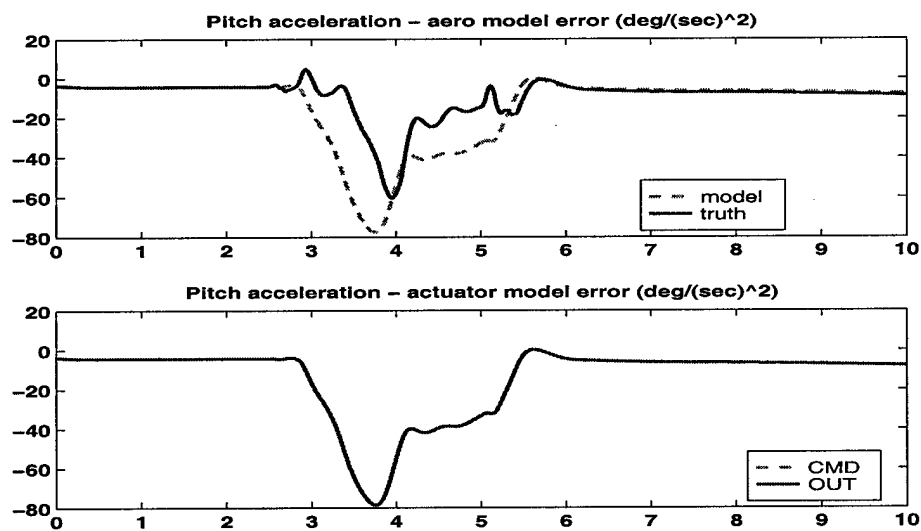


Figure 4.105: Mach 0.35, 5,000 ft. Altitude, Min Thrust Vector CA Mode, Full Stick Roll

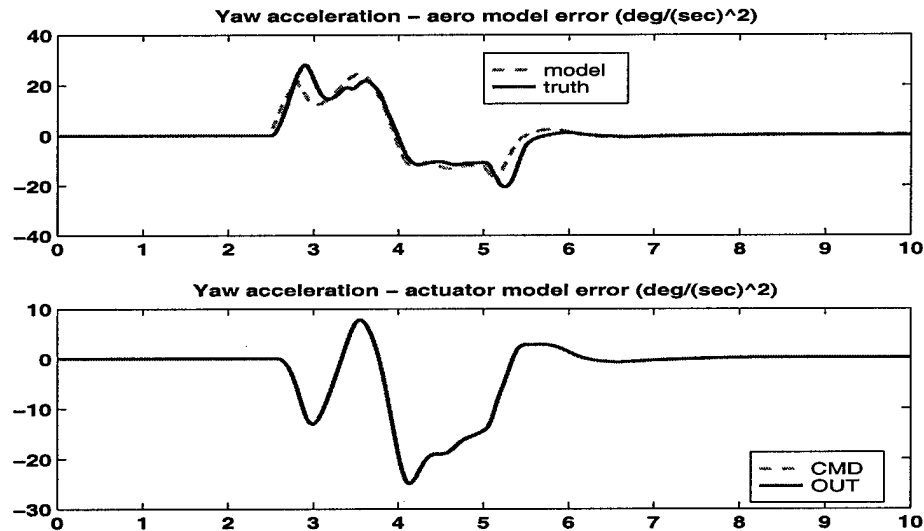


Figure 4.106: Mach 0.35, 5,000 ft. Altitude, Min Thrust Vector CA Mode, Full Stick Roll

Subsonic ingress flight condition, Mach 0.90 1,000 ft. altitude

This section contains simulation responses at the subsonic ingress flight condition. The control allocation mode at this condition minimizes radar signature.

The responses in Figs.(4.107)-(4.117) are for the loaded roll maneuver. There is only slight coupling between command variable axes, and angle of slip regulation is very good. The all moving tips, spoiler slot deflectors, leading edge flaps and pitch flap are not used for this maneuver since there is plenty of control power, and use of these effectors increases radar signature. There is no on-board actuator model errors and only slight aerodynamic model errors.

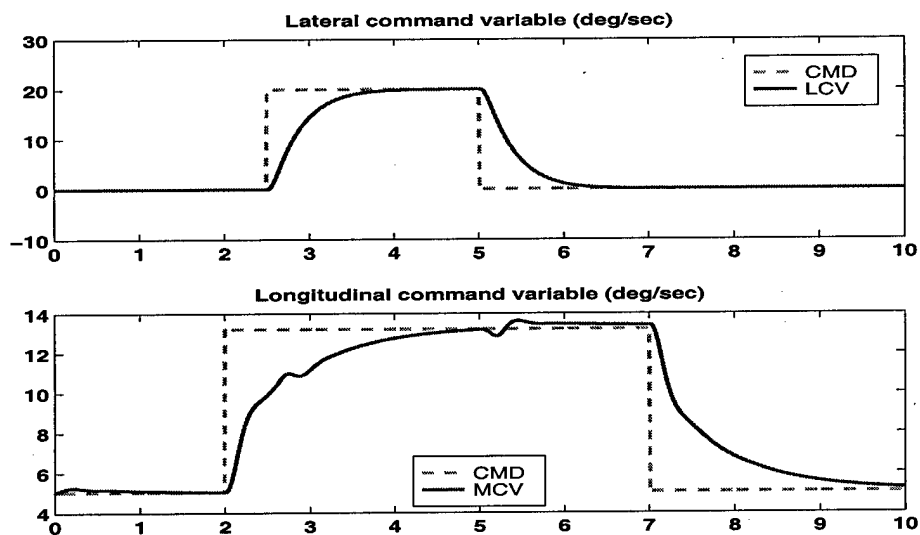


Figure 4.107: Mach 0.90, 1000 ft. Altitude, Min Signature CA Mode, Loaded Roll

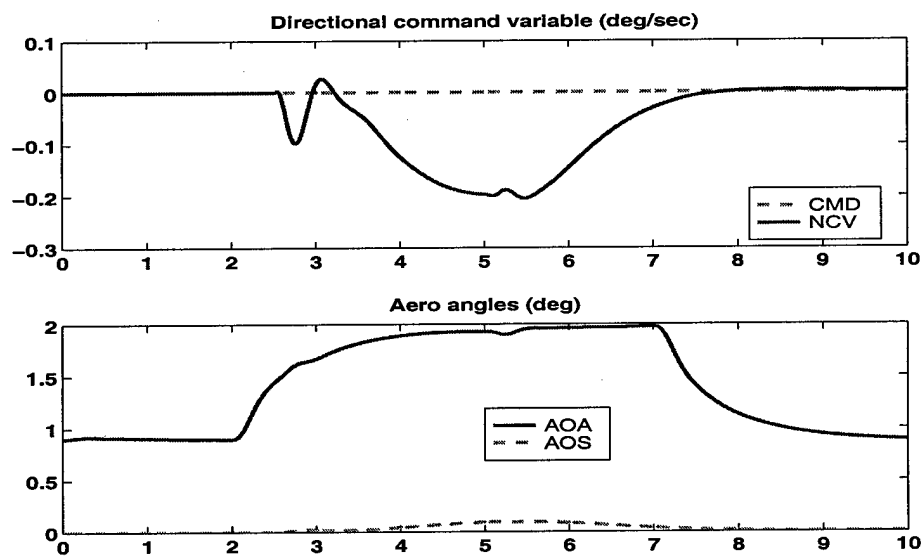


Figure 4.108: Mach 0.90, 1000 ft. Altitude, Min Signature CA Mode, Loaded Roll

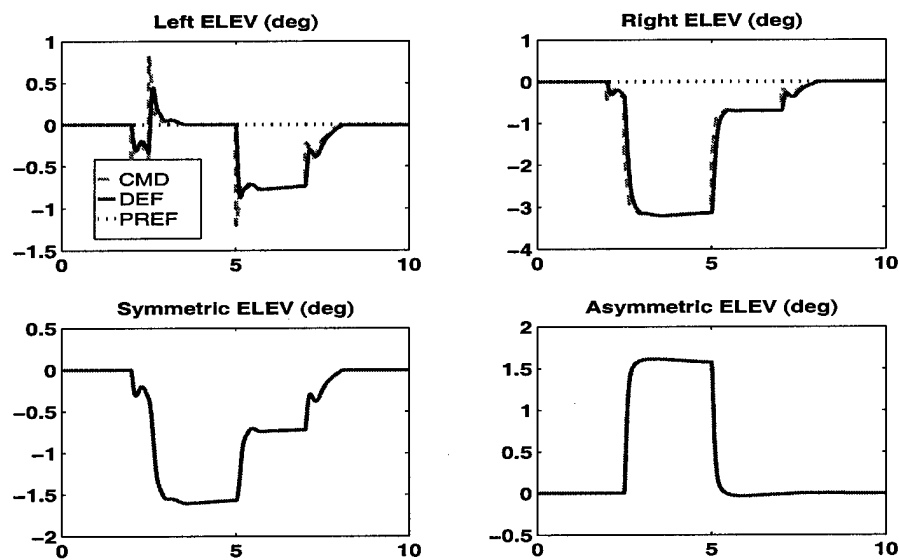


Figure 4.109: Mach 0.90, 1000 ft. Altitude, Min Signature CA Mode, Loaded Roll

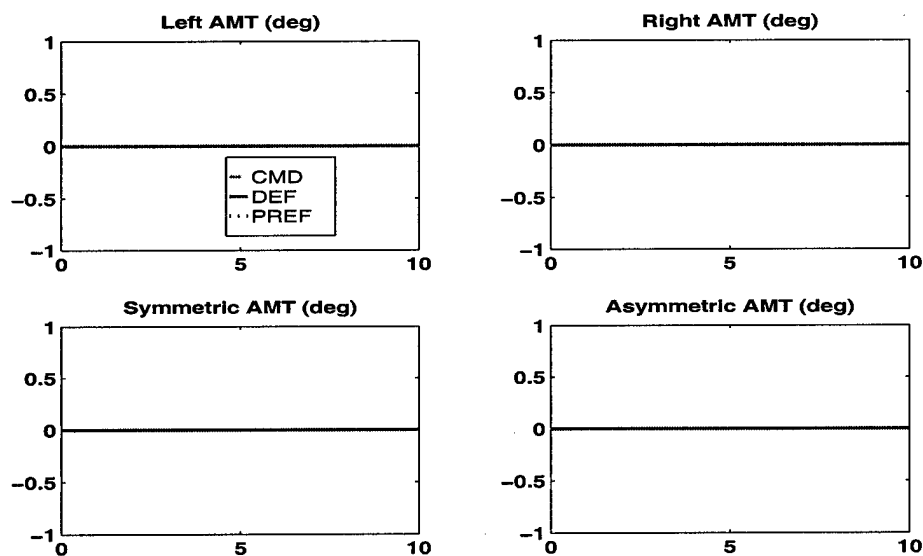


Figure 4.110: Mach 0.90, 1000 ft. Altitude, Min Signature CA Mode, Loaded Roll

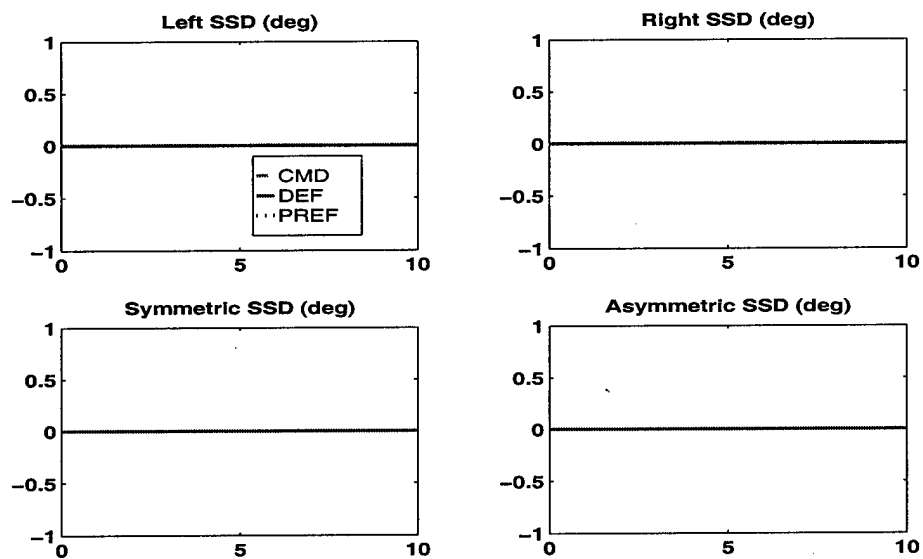


Figure 4.111: Mach 0.90, 1000 ft. Altitude, Min Signature CA Mode, Loaded Roll

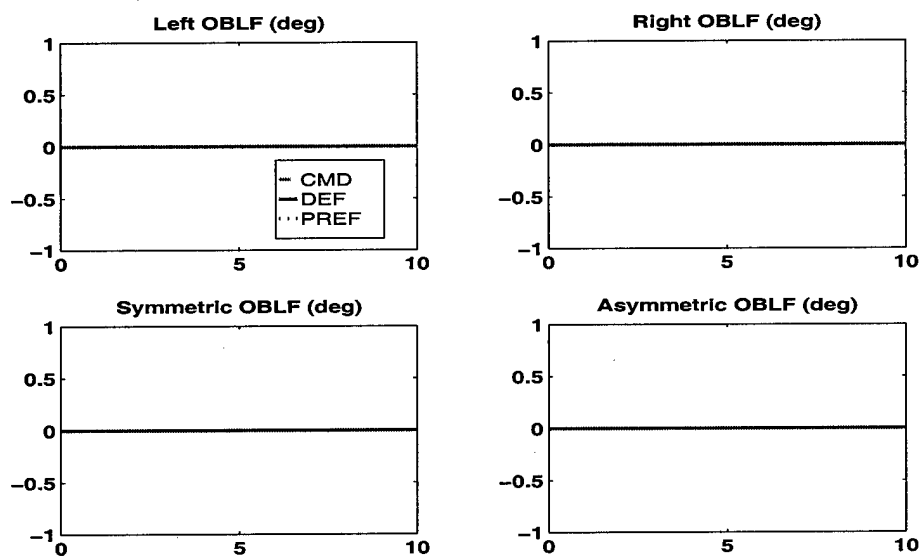


Figure 4.112: Mach 0.90, 1000 ft. Altitude, Min Signature CA Mode, Loaded Roll

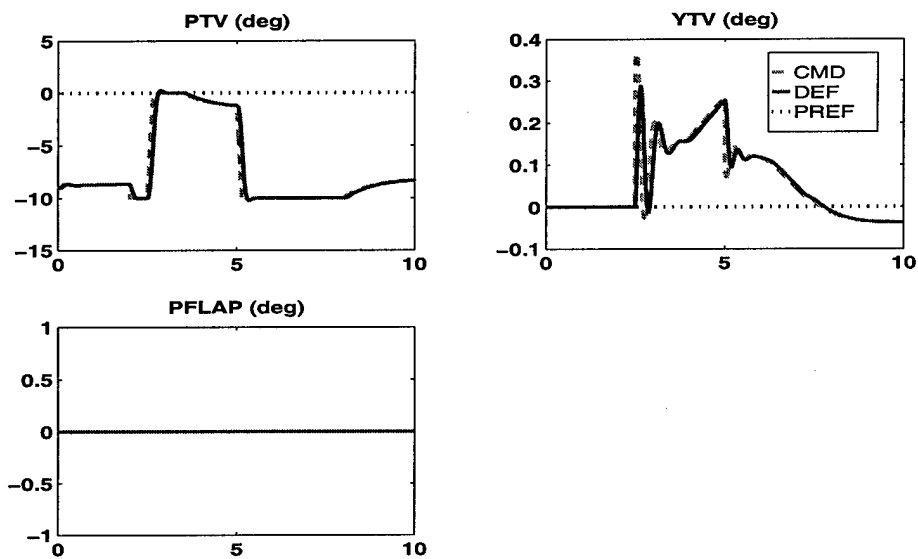


Figure 4.113: Mach 0.90, 1000 ft. Altitude, Min Signature CA Mode, Loaded Roll

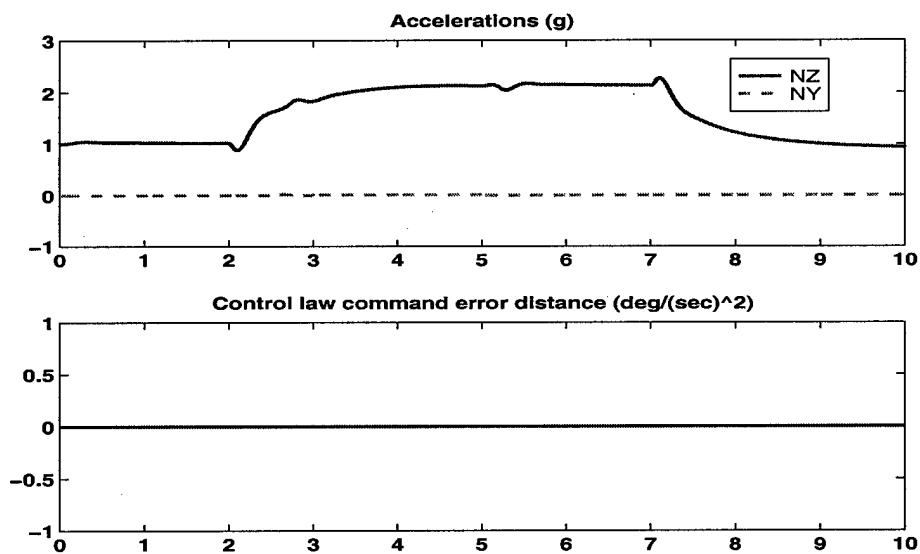


Figure 4.114: Mach 0.90, 1000 ft. Altitude, Min Signature CA Mode, Loaded Roll

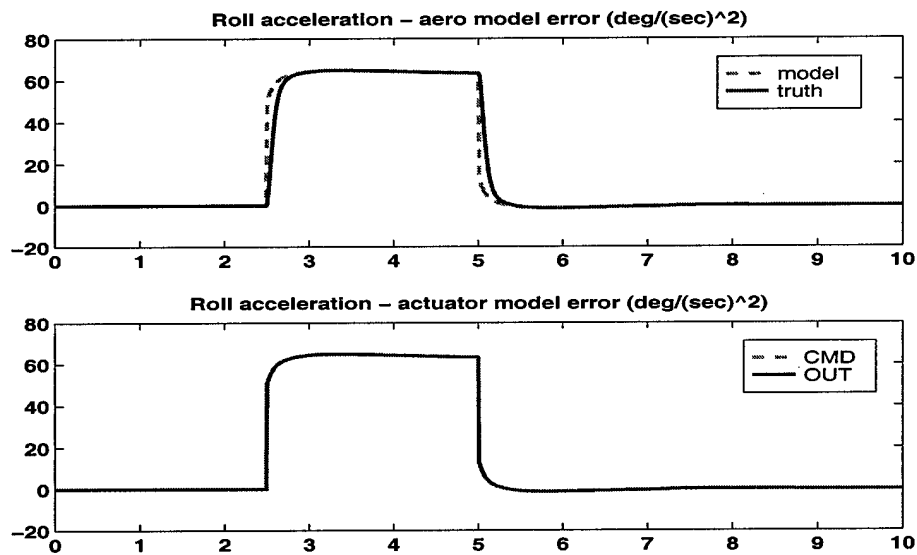


Figure 4.115: Mach 0.90, 1000 ft. Altitude, Min Signature CA Mode, Loaded Roll

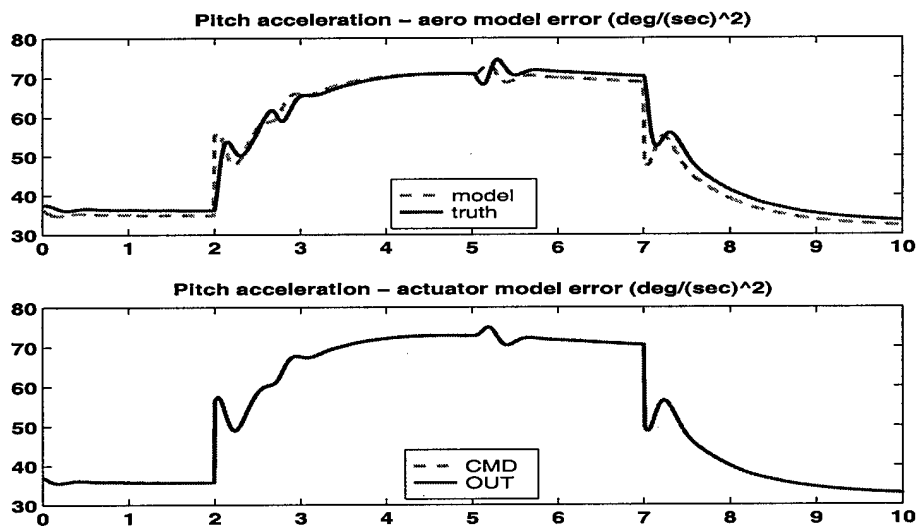


Figure 4.116: Mach 0.90, 1000 ft. Altitude, Min Signature CA Mode, Loaded Roll

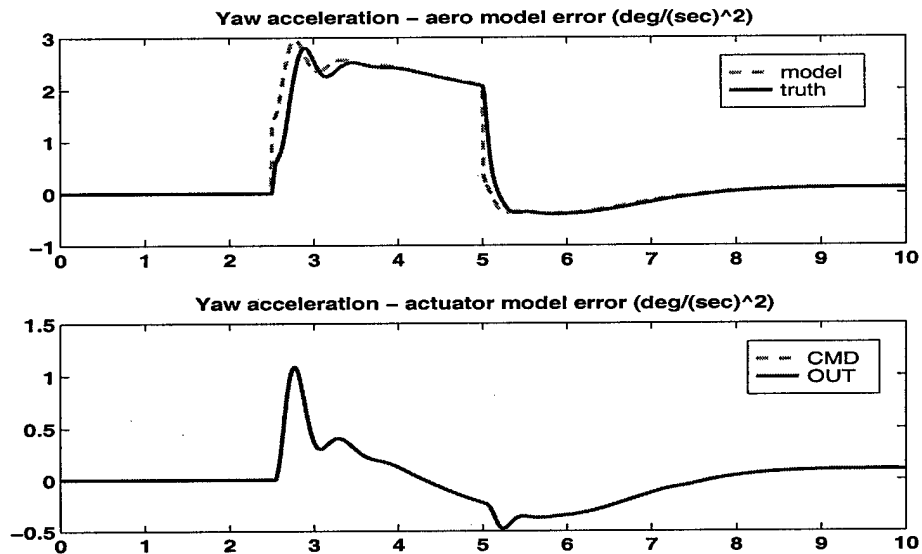


Figure 4.117: Mach 0.90, 1000 ft. Altitude, Min Signature CA Mode, Loaded Roll

The responses in Figs.(4.118)-(4.128) are for the full stick roll maneuver. The lateral command variable tracks the command well, and angle of slip regulation is good. Longitudinal and directional coupling caused by aerodynamic model errors degrades command variable regulation. The aerodynamic model errors are due to low model fidelity of the control derivatives at high speeds. Recall that the on-board high speed control derivative model is constructed from linear interpolated linear models. The large elevon deflections violate the small angle assumptions of the on-board linear models. A higher fidelity high speed control derivative model would alleviate the aerodynamic model errors. Spoiler slot defectors and all moving tips only deviate from their preferences at the onset of stick commands when insufficient control power exists to achieve the control law acceleration commands since these effectors increase radar signature. There are almost no roll acceleration errors due to unmodeled actuator dynamics.

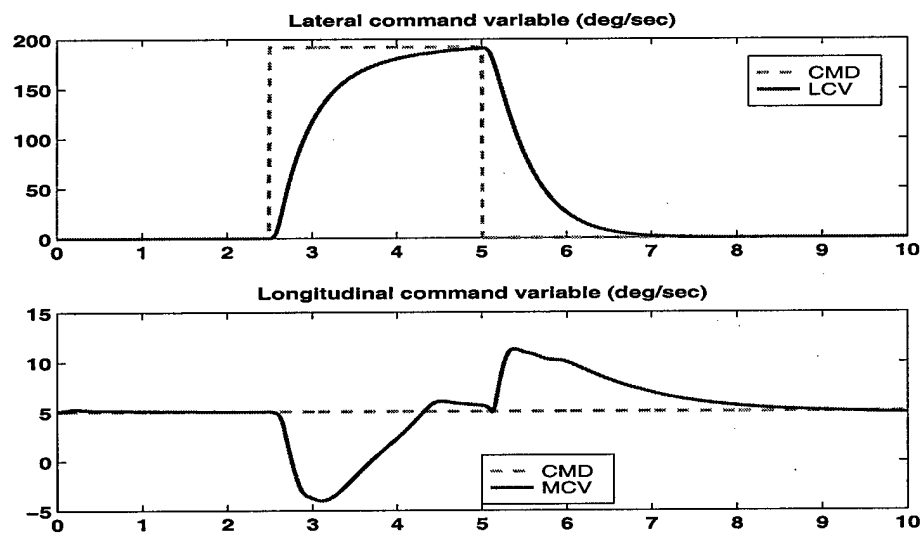


Figure 4.118: Mach 0.90, 1000 ft. Altitude, Min Signature CA Mode, Full Stick Roll

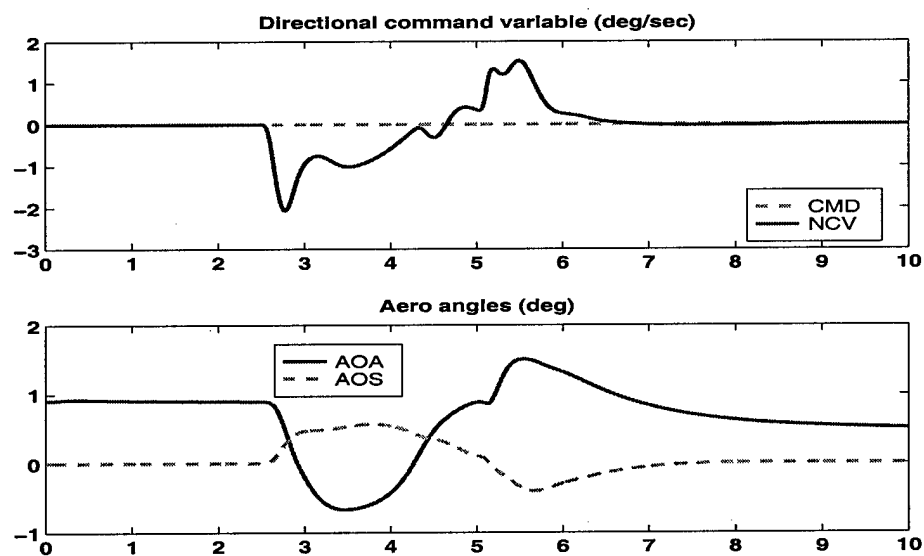


Figure 4.119: Mach 0.90, 1000 ft. Altitude, Min Signature CA Mode, Full Stick Roll

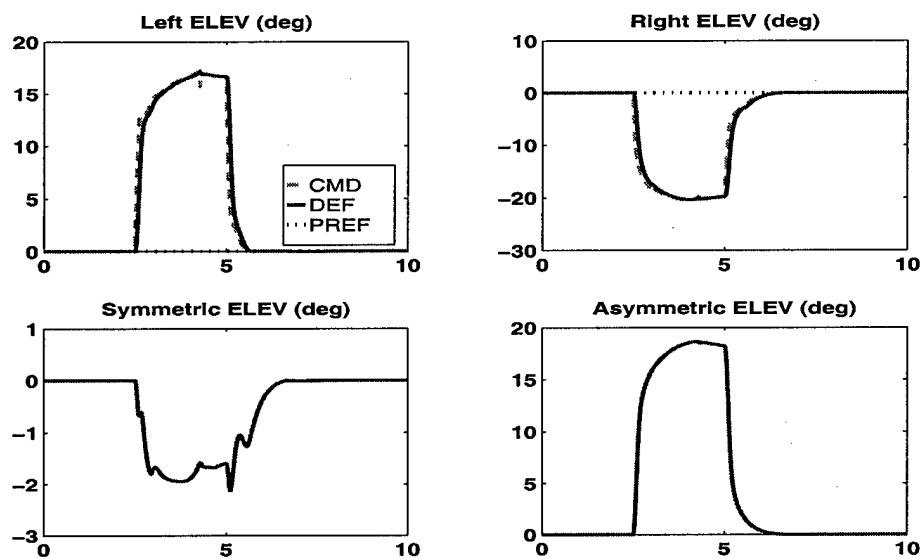


Figure 4.120: Mach 0.90, 1000 ft. Altitude, Min Signature CA Mode, Full Stick Roll

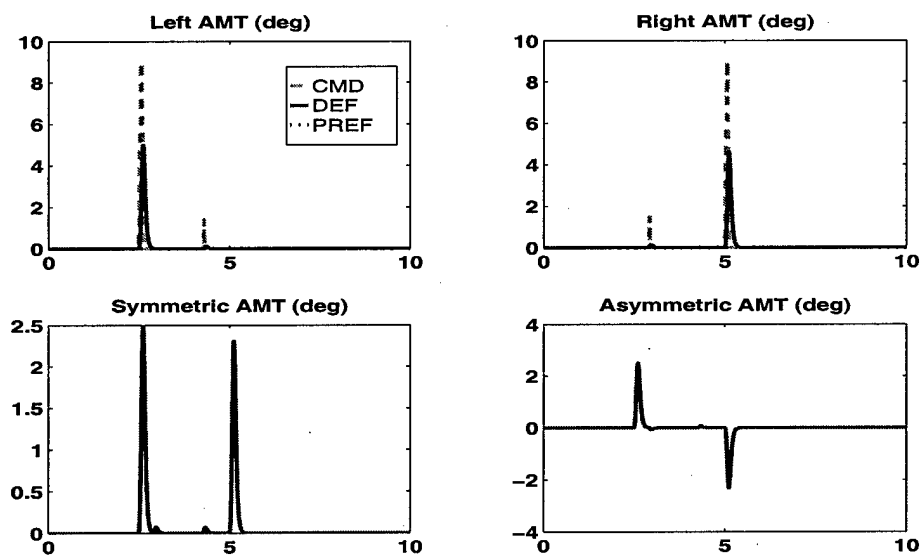


Figure 4.121: Mach 0.90, 1000 ft. Altitude, Min Signature CA Mode, Full Stick Roll

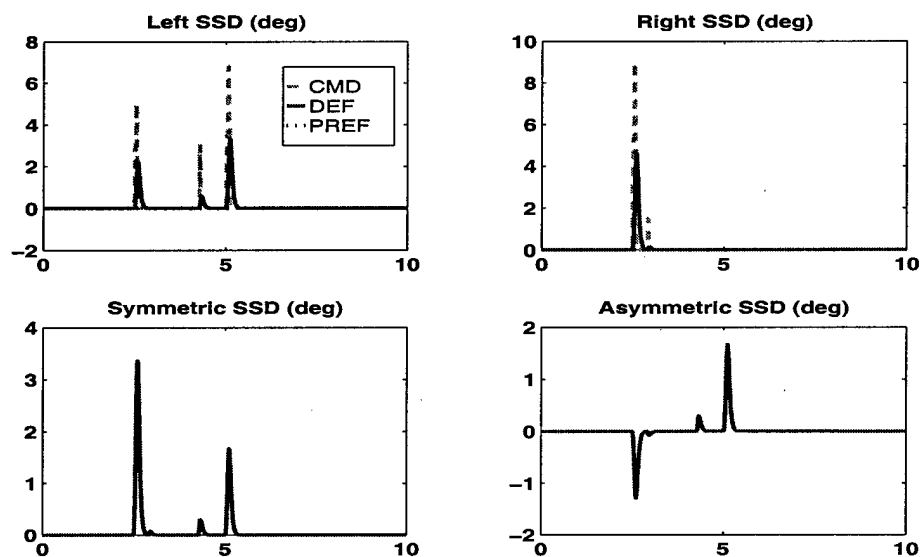


Figure 4.122: Mach 0.90, 1000 ft. Altitude, Min Signature CA Mode, Full Stick Roll

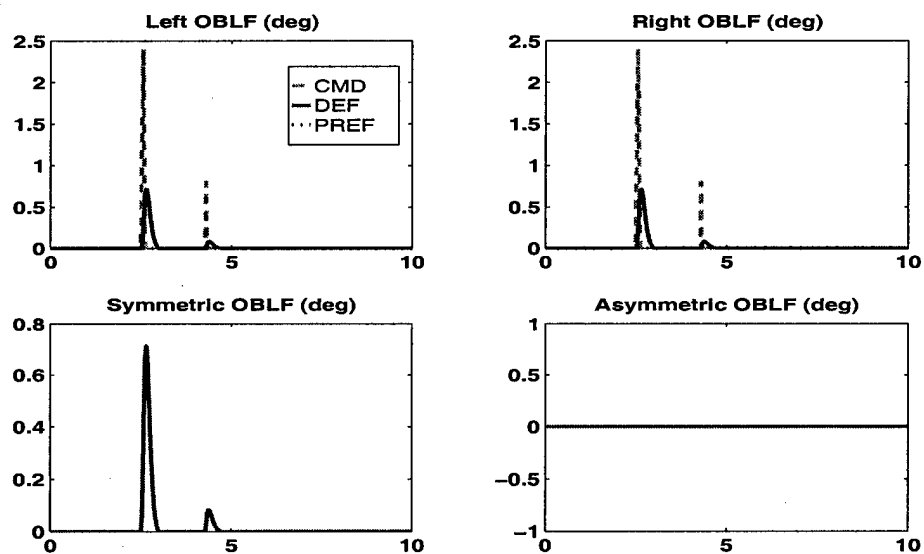


Figure 4.123: Mach 0.90, 1000 ft. Altitude, Min Signature CA Mode, Full Stick Roll

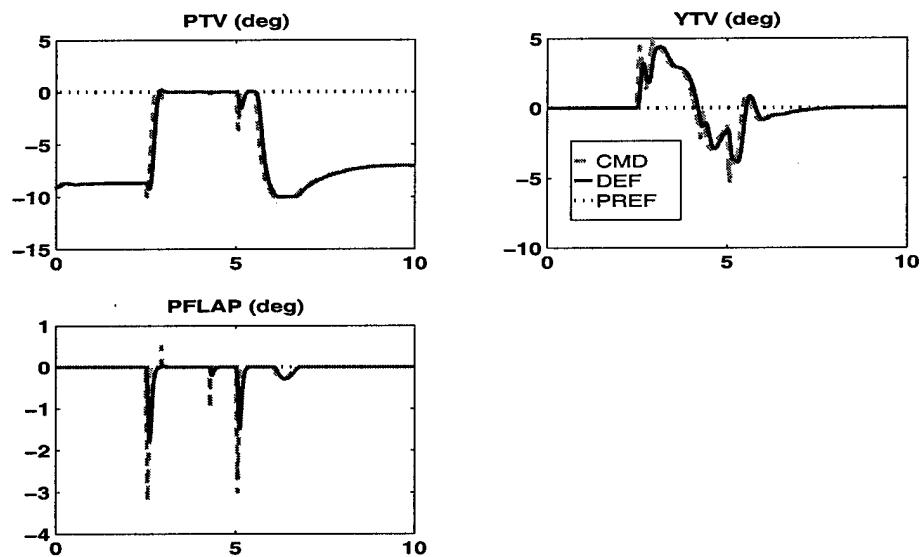


Figure 4.124: Mach 0.90, 1000 ft. Altitude, Min Signature CA Mode, Full Stick Roll

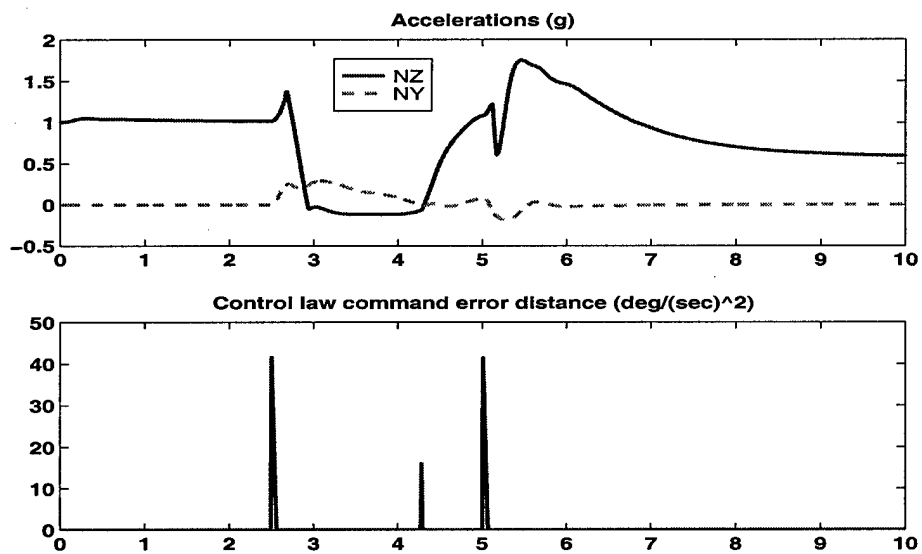


Figure 4.125: Mach 0.90, 1000 ft. Altitude, Min Signature CA Mode, Full Stick Roll

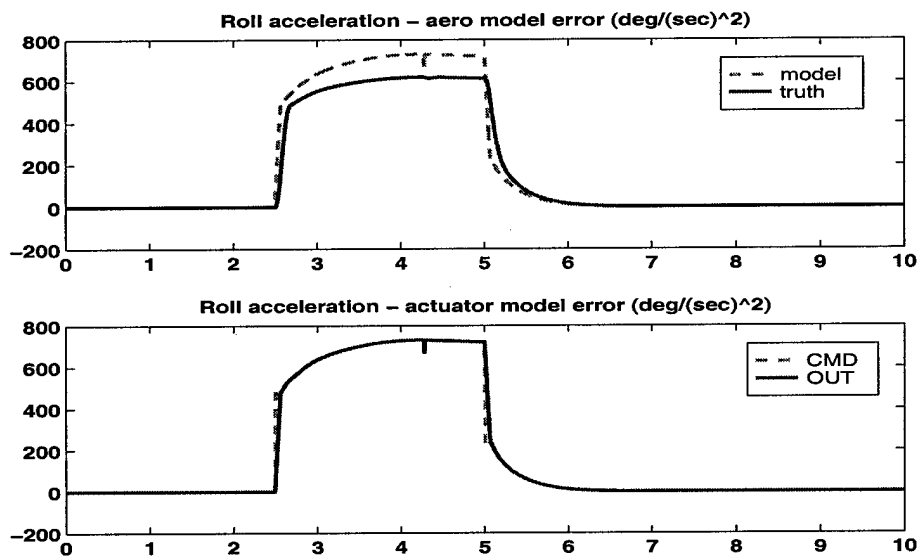


Figure 4.126: Mach 0.90, 1000 ft. Altitude, Min Signature CA Mode, Full Stick Roll

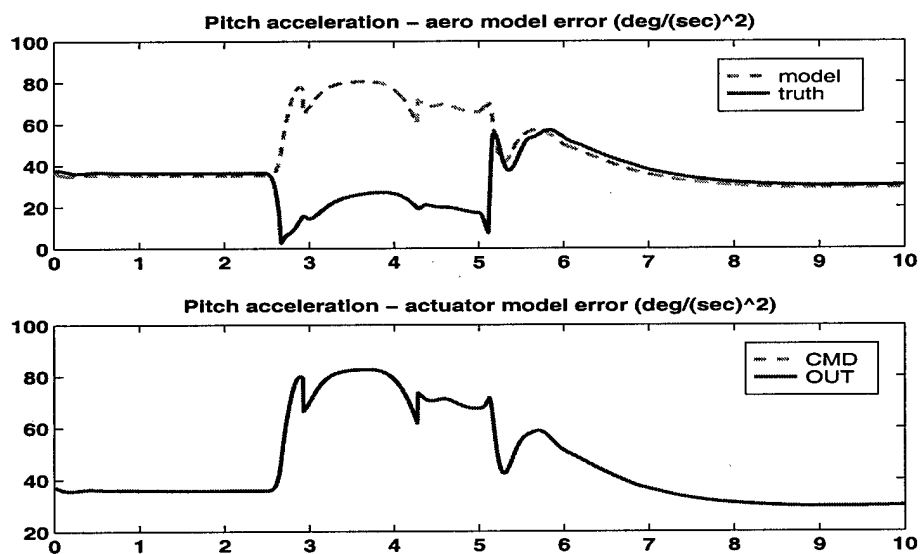


Figure 4.127: Mach 0.90, 1000 ft. Altitude, Min Signature CA Mode, Full Stick Roll

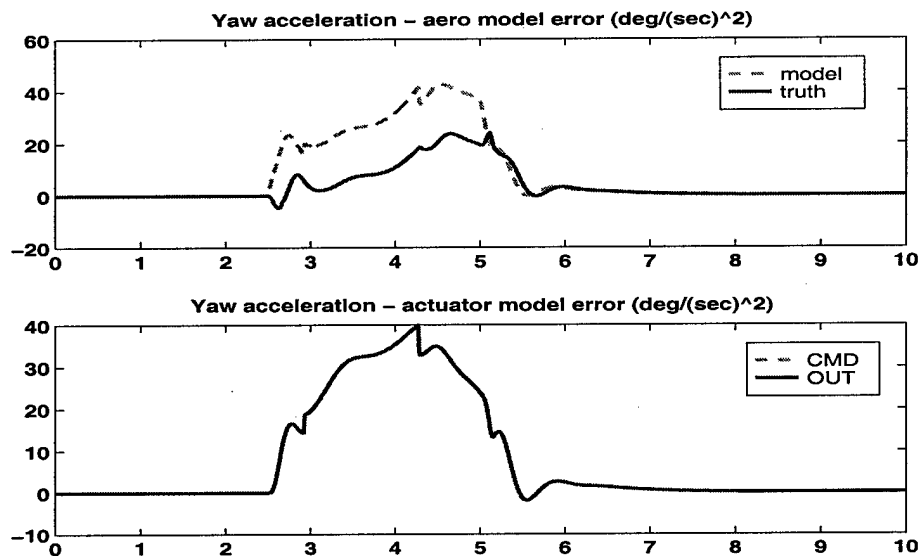


Figure 4.128: Mach 0.90, 1000 ft. Altitude, Min Signature CA Mode, Full Stick Roll

Supersonic cruise flight condition, Mach 1.20 22,500 ft. altitude

This section contains simulation responses at the supersonic cruise flight condition. The control allocation mode at this condition minimizes drag which is modeled the same as minimum deflection at this flight condition.

The responses in Figs.(4.129)-(4.139) are for the loaded roll maneuver. There is only slight coupling between command variable axes, and angle of slip regulation is very good. The elevons and yaw thrust vectoring are the primary control effectors used for this maneuver. The all moving tips, spoiler slot deflectors, pitch thrust vectoring and pitch flap are only used at the onset of stick commands where there is insufficient control power to achieve the control law command. The leading edge flaps are not used for this maneuver. There is no on-board actuator model errors and only slight aerodynamic model errors due to low fidelity on-board control derivative models at high speeds.

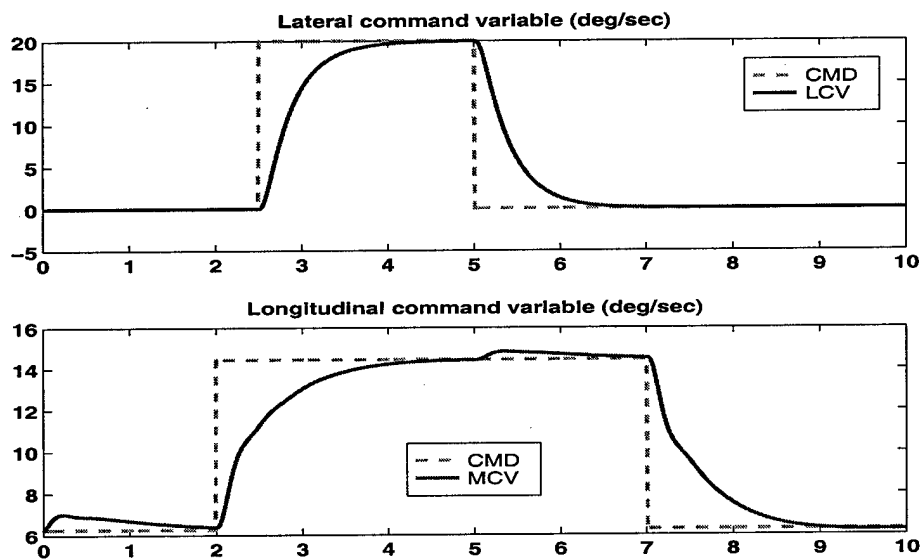


Figure 4.129: Mach 1.2, 22,500 ft. Altitude, Min Drag CA Mode, Loaded Roll

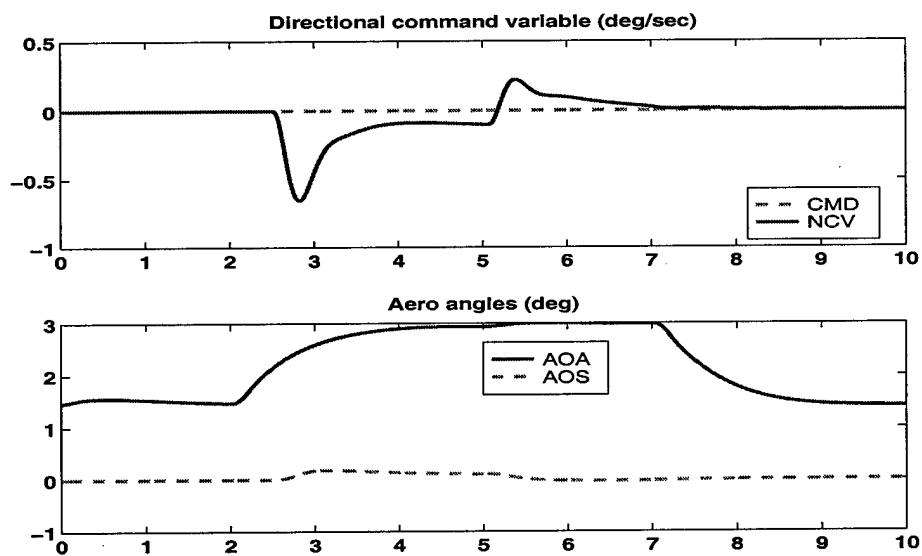


Figure 4.130: Mach 1.2, 22,500 ft. Altitude, Min Drag CA Mode, Loaded Roll

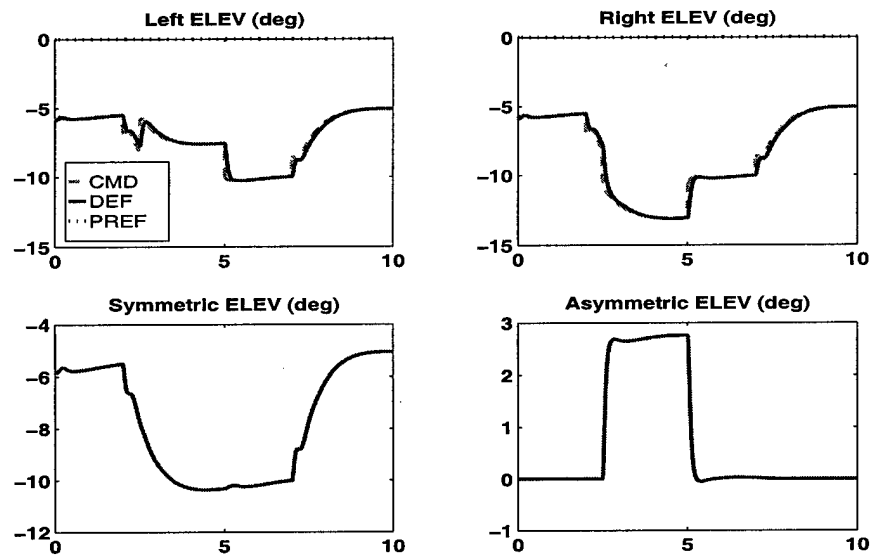


Figure 4.131: Mach 1.2, 22,500 ft. Altitude, Min Drag CA Mode, Loaded Roll

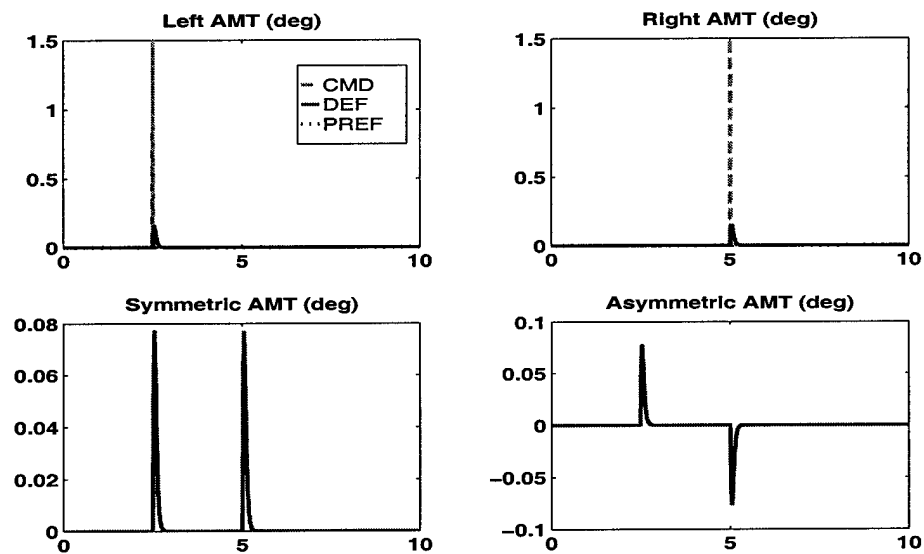


Figure 4.132: Mach 1.2, 22,500 ft. Altitude, Min Drag CA Mode, Loaded Roll

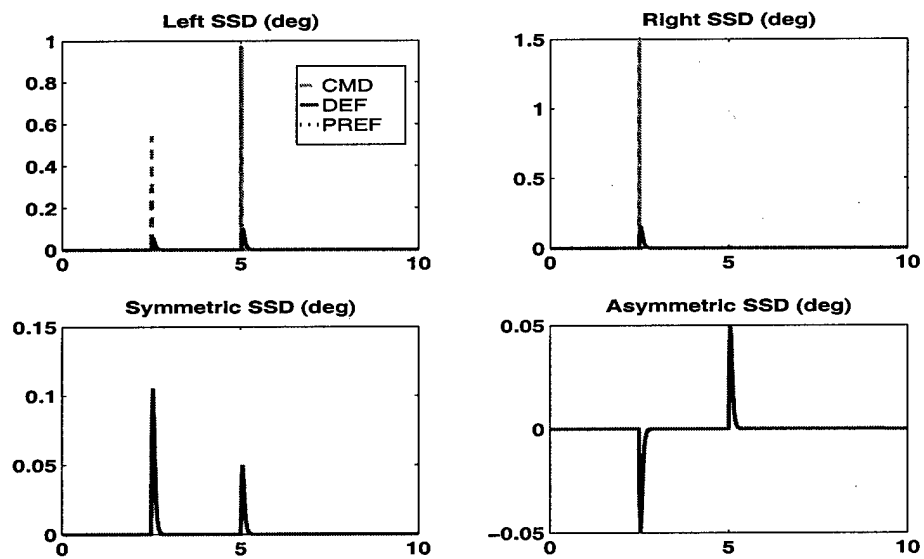


Figure 4.133: Mach 1.2, 22,500 ft. Altitude, Min Drag CA Mode, Loaded Roll

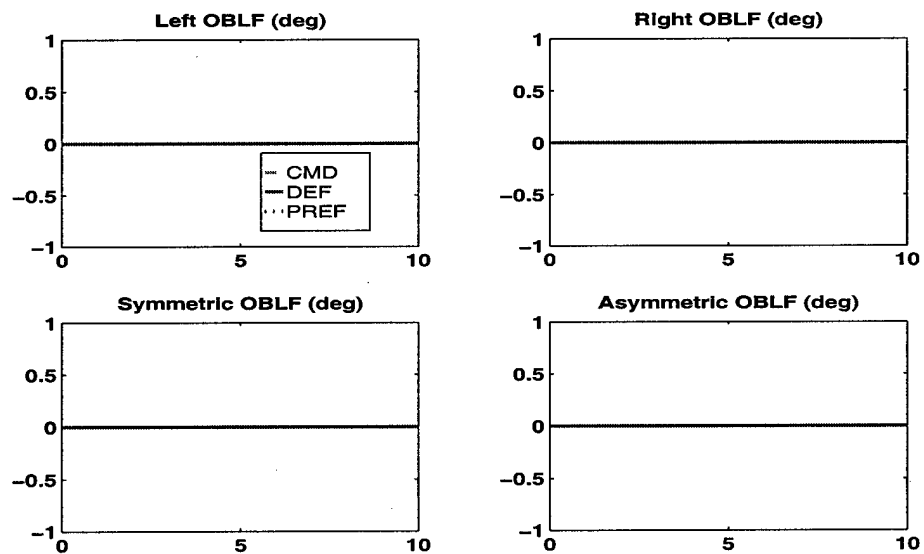


Figure 4.134: Mach 1.2, 22,500 ft. Altitude, Min Drag CA Mode, Loaded Roll

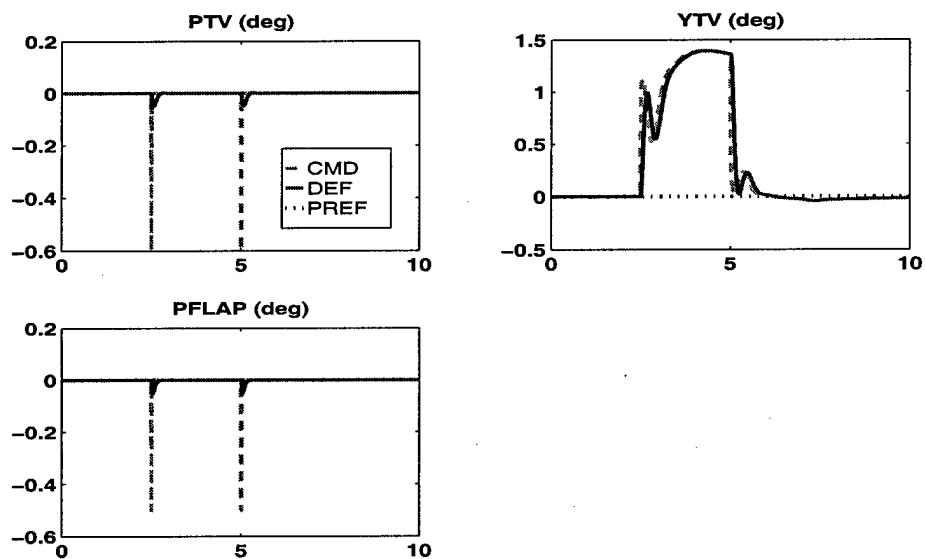


Figure 4.135: Mach 1.2, 22,500 ft. Altitude, Min Drag CA Mode, Loaded Roll

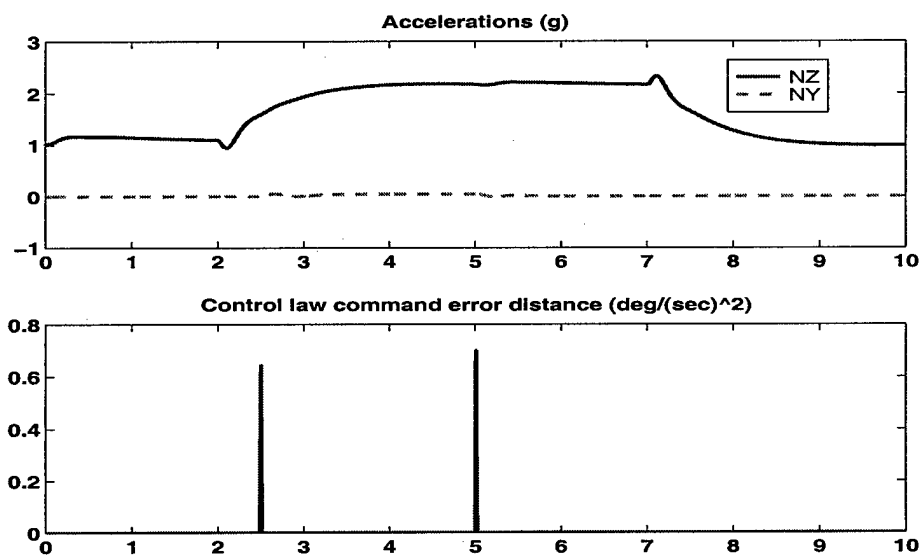


Figure 4.136: Mach 1.2, 22,500 ft. Altitude, Min Drag CA Mode, Loaded Roll

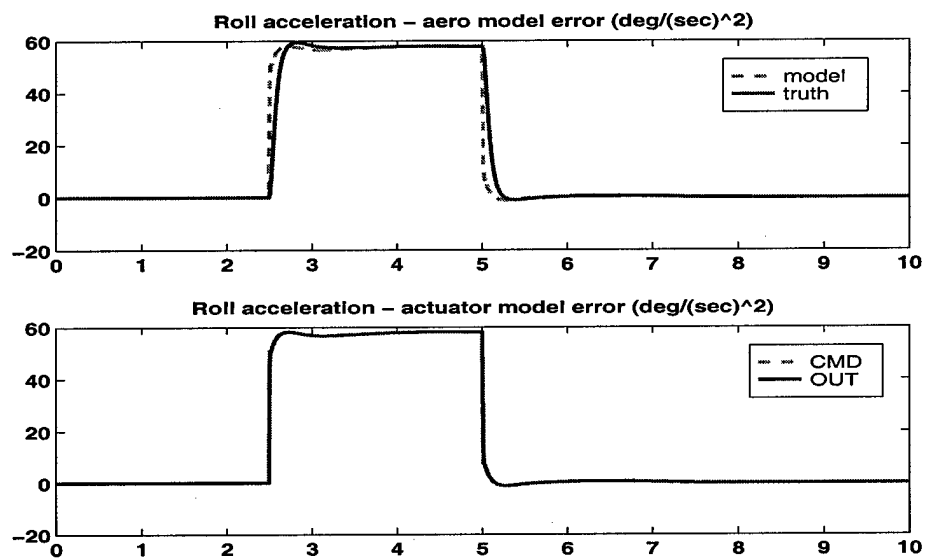


Figure 4.137: Mach 1.2, 22,500 ft. Altitude, Min Drag CA Mode, Loaded Roll

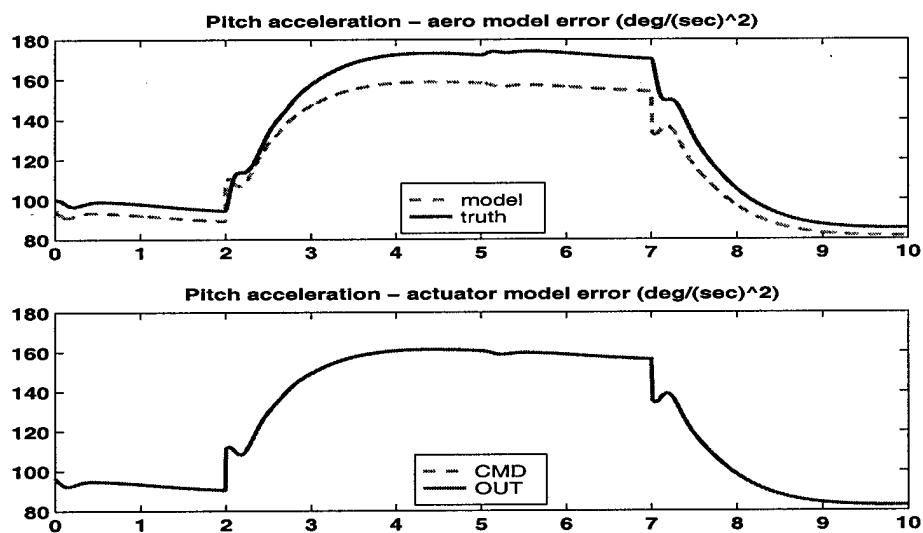


Figure 4.138: Mach 1.2, 22,500 ft. Altitude, Min Drag CA Mode, Loaded Roll

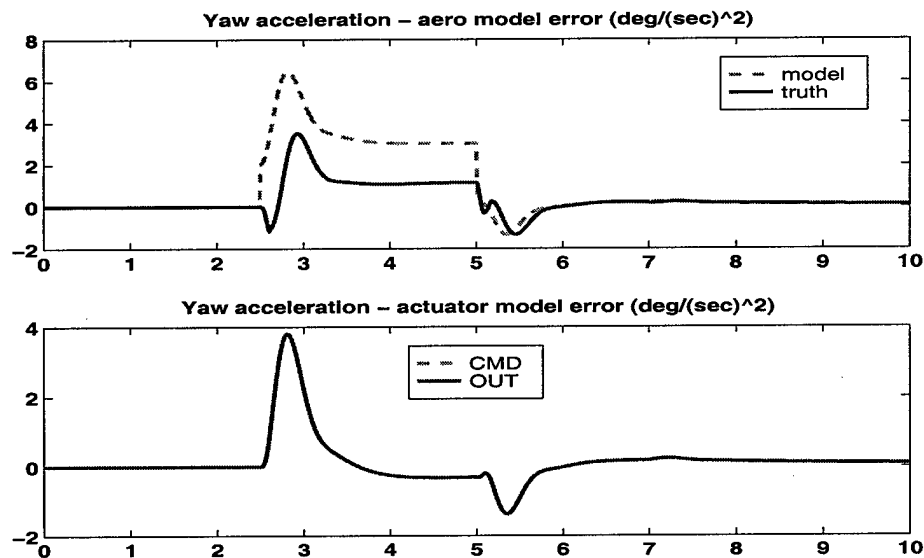


Figure 4.139: Mach 1.2, 22,500 ft. Altitude, Min Drag CA Mode, Loaded Roll

The responses in Figs.(4.140)-(4.150) are for the full stick roll maneuver. The lateral command variable tracks the command well ,and angle of slip regulation is degraded. Longitudinal and directional coupling caused by aerodynamic model errors degrades command variable regulation. The aerodynamic model errors are due to low model fidelity of the control derivatives at high speeds. There are almost no roll acceleration errors due to unmodeled actuator dynamics.

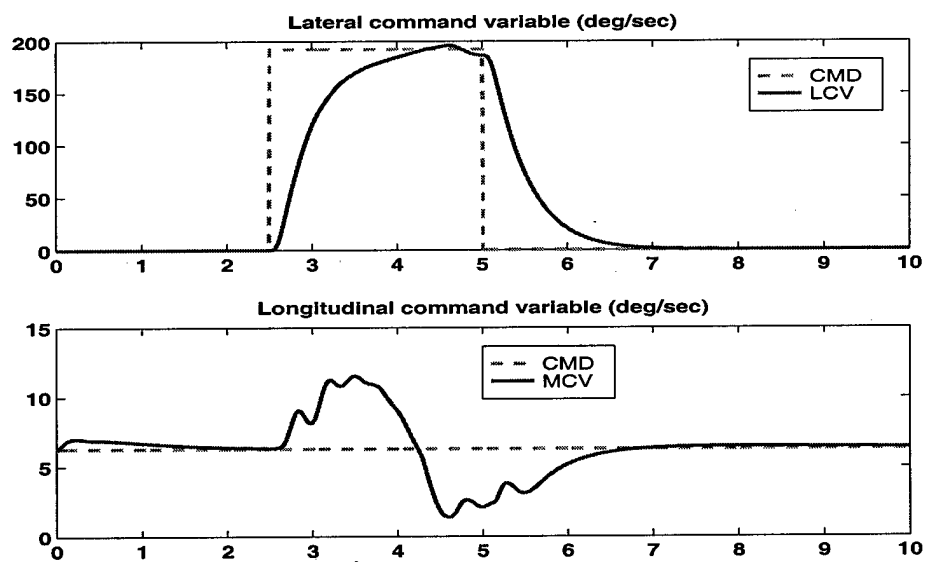


Figure 4.140: Mach 1.2, 22,500 ft. Altitude, Min Drag CA Mode, Full Stick Roll

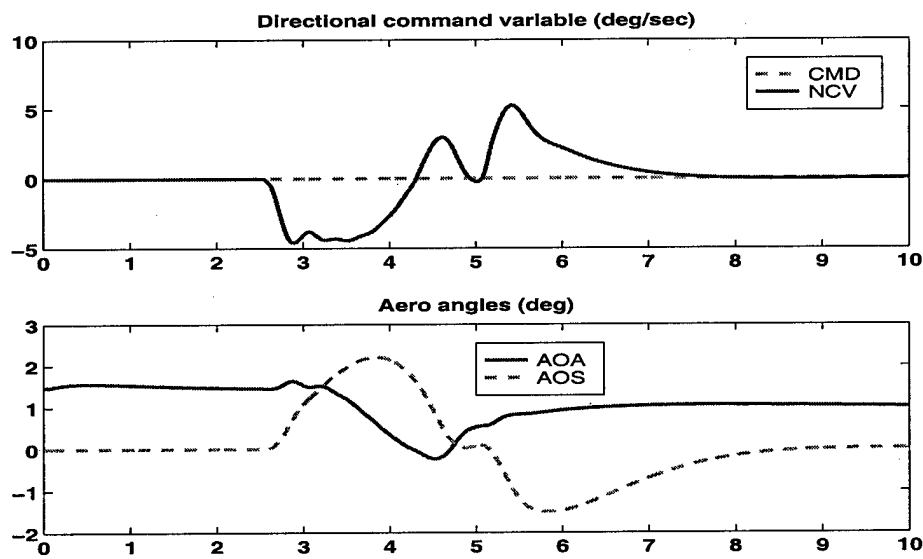


Figure 4.141: Mach 1.2, 22,500 ft. Altitude, Min Drag CA Mode, Full Stick Roll

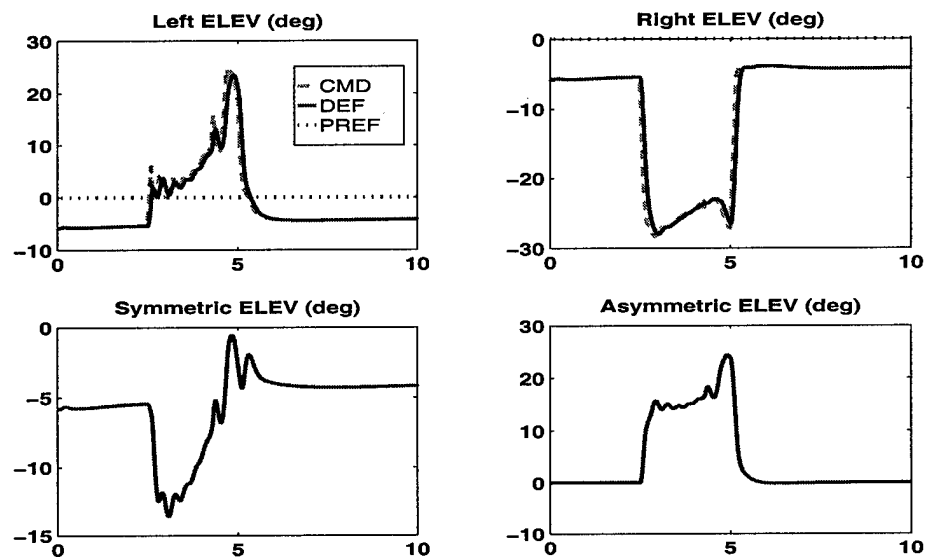


Figure 4.142: Mach 1.2, 22,500 ft. Altitude, Min Drag CA Mode, Full Stick Roll

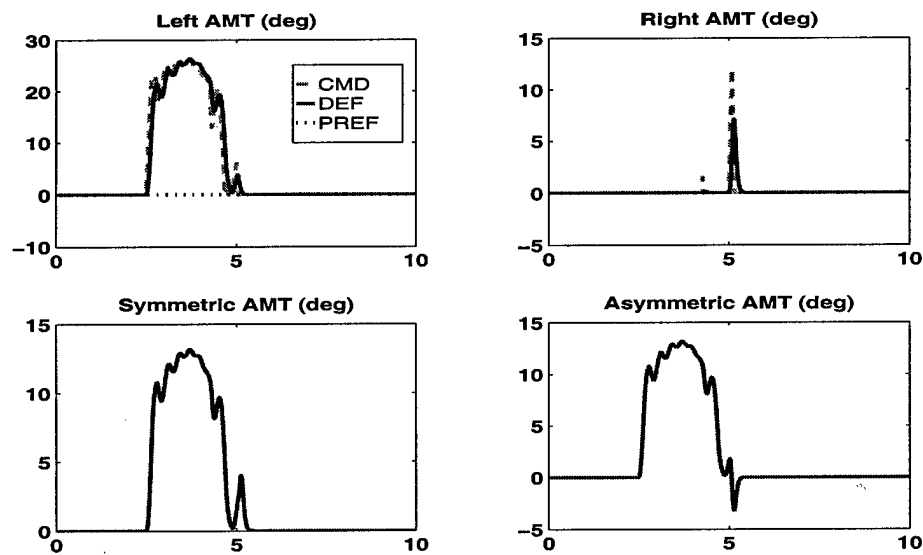


Figure 4.143: Mach 1.2, 22,500 ft. Altitude, Min Drag CA Mode, Full Stick Roll

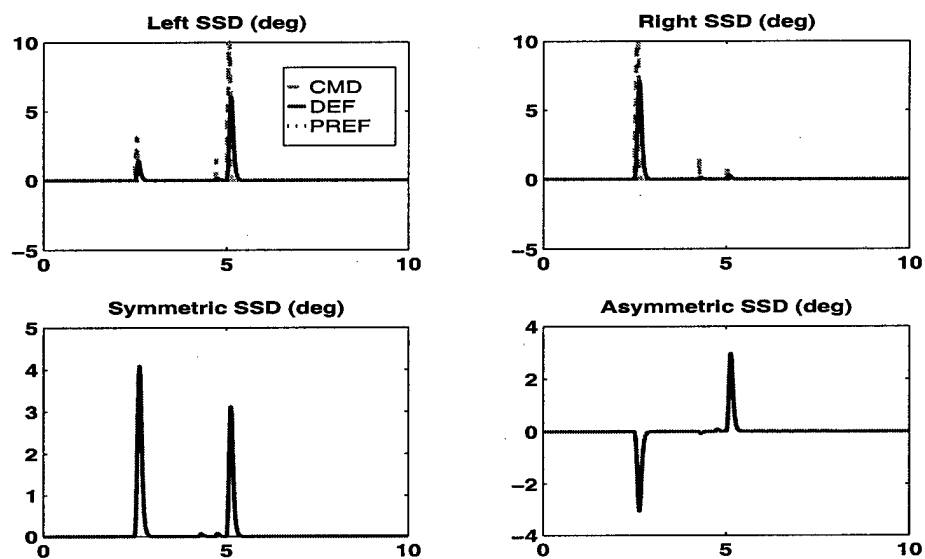


Figure 4.144: Mach 1.2, 22,500 ft. Altitude, Min Drag CA Mode, Full Stick Roll

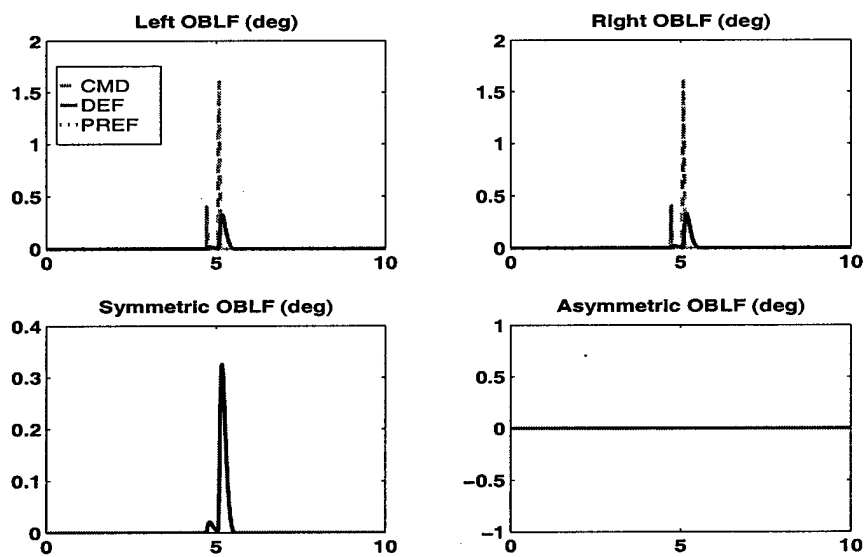


Figure 4.145: Mach 1.2, 22,500 ft. Altitude, Min Drag CA Mode, Full Stick Roll

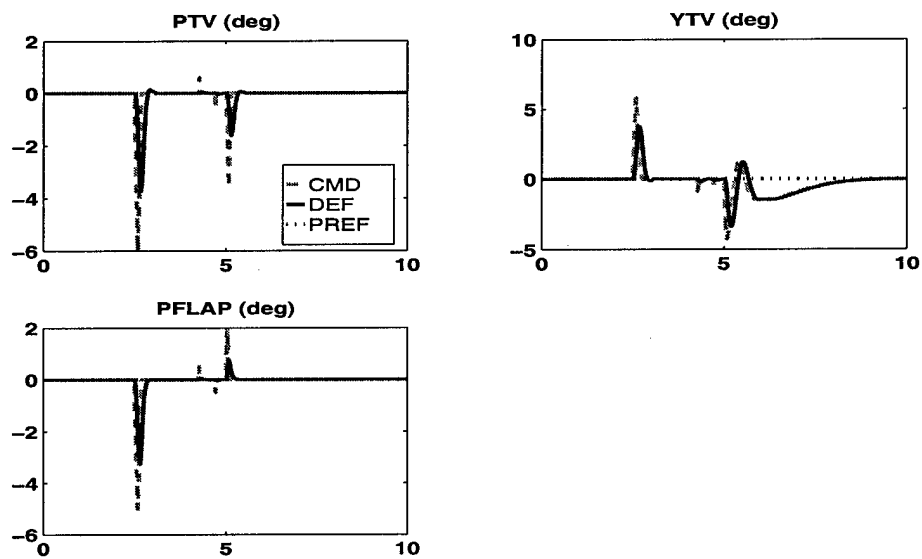


Figure 4.146: Mach 1.2, 22,500 ft. Altitude, Min Drag CA Mode, Full Stick Roll

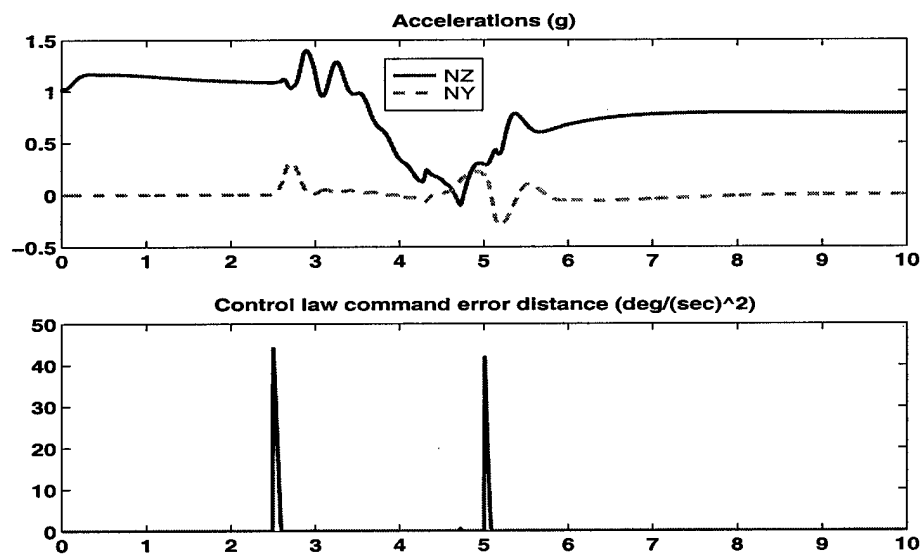


Figure 4.147: Mach 1.2, 22,500 ft. Altitude, Min Drag CA Mode, Full Stick Roll

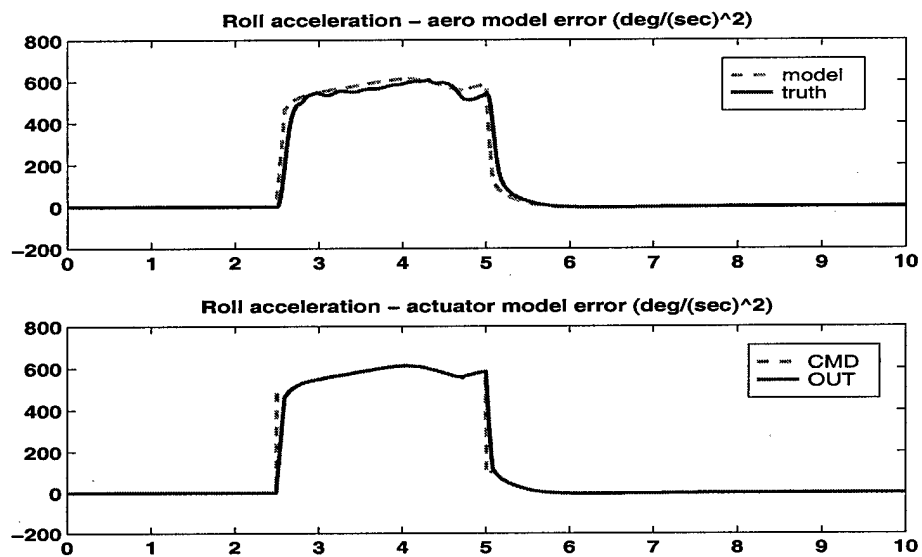


Figure 4.148: Mach 1.2, 22,500 ft. Altitude, Min Drag CA Mode, Full Stick Roll

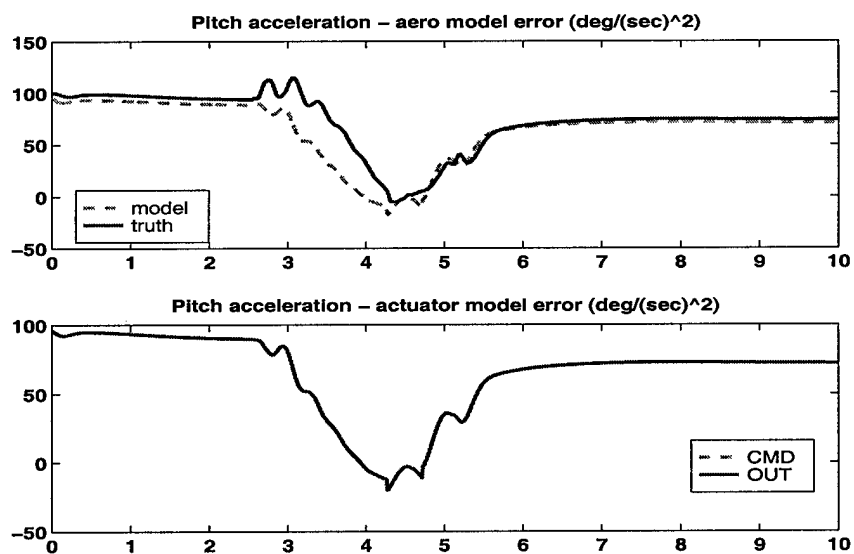


Figure 4.149: Mach 1.2, 22,500 ft. Altitude, Min Drag CA Mode, Full Stick Roll

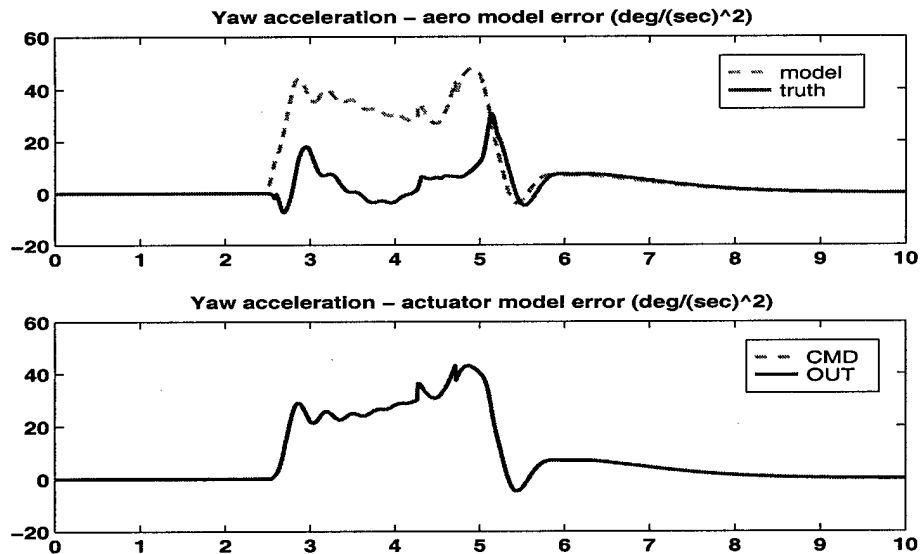


Figure 4.150: Mach 1.2, 22,500 ft. Altitude, Min Drag CA Mode, Full Stick Roll

Envelope center flight condition, Mach 0.60 15,000 ft. altitude

This section contains simulation responses at the envelope center flight condition. The control allocation mode at this condition minimizes wing loads.

The responses in Figs.(4.151)-(4.161) are for the loaded roll maneuver. There is only slight coupling between command variable axes, and angle of slip regulation is very good. The elevons and yaw thrust vectoring are the primary control effectors used for this maneuver. The all moving tips, leading edge flaps and spoiler slot deflectors are only used at the onset of stick commands where there is insufficient control power to achieve the control law command since these effectors cause high wing loads. There are no on-board actuator model errors and only slight aerodynamic model errors.

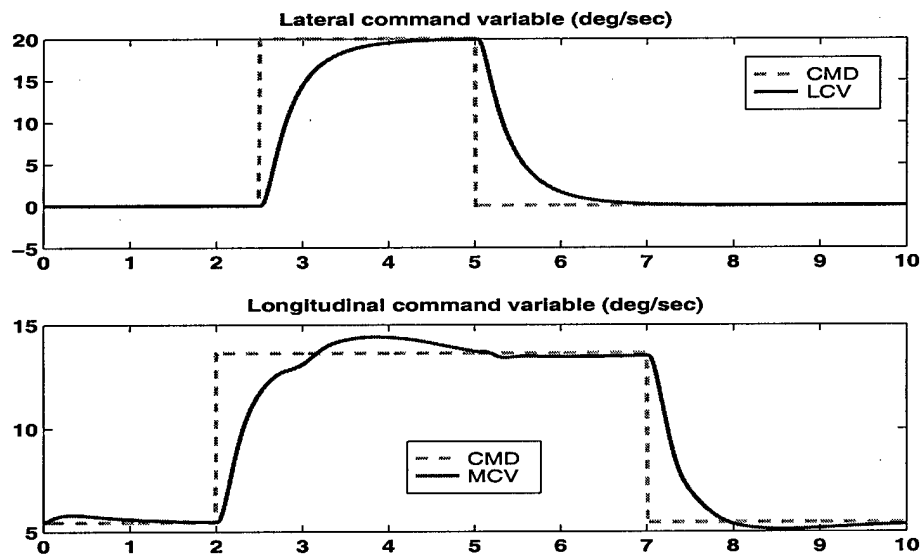


Figure 4.151: Mach 0.6, 15,000 ft. Altitude, Min Load CA Mode, Loaded Roll

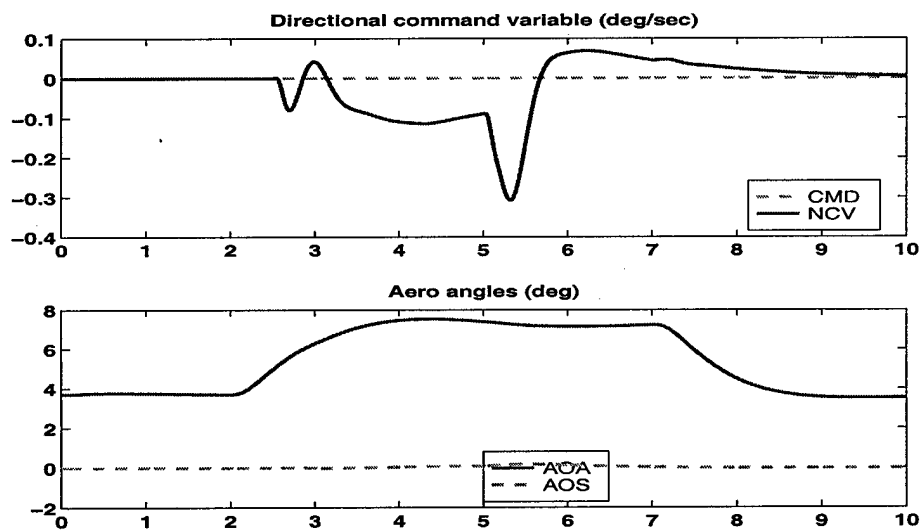


Figure 4.152: Mach 0.6, 15,000 ft. Altitude, Min Load CA Mode, Loaded Roll

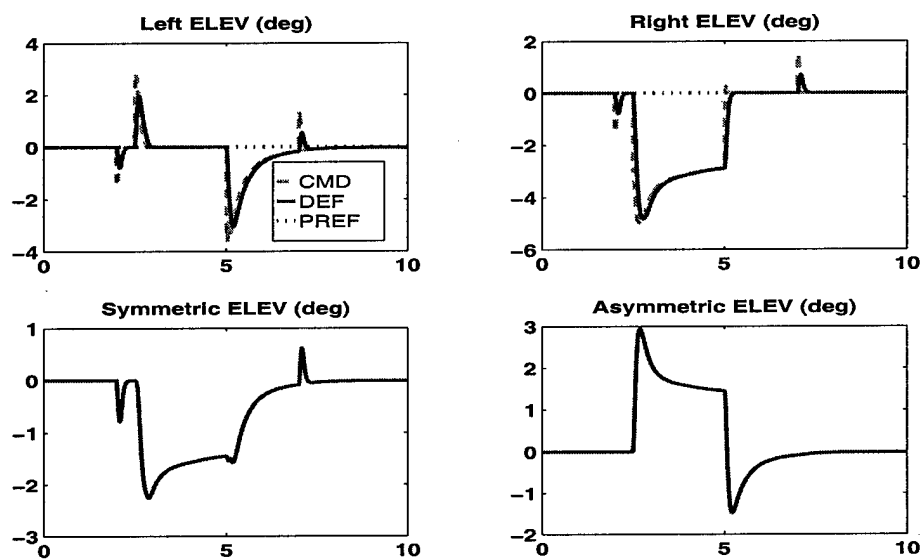


Figure 4.153: Mach 0.6, 15,000 ft. Altitude, Min Load CA Mode, Loaded Roll

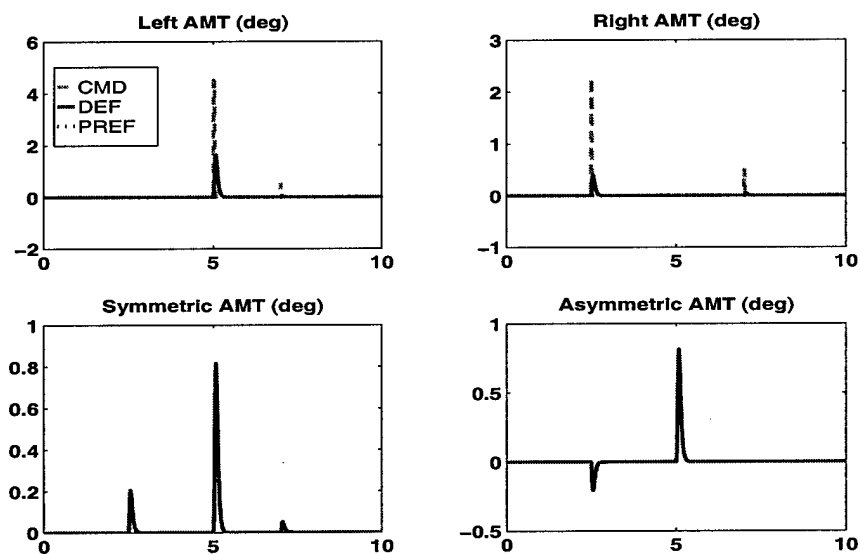


Figure 4.154: Mach 0.6, 15,000 ft. Altitude, Min Load CA Mode, Loaded Roll

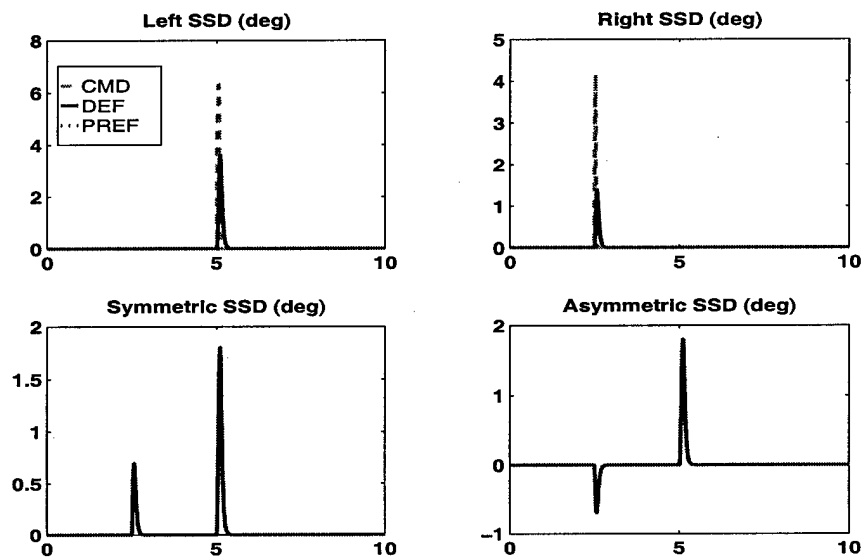


Figure 4.155: Mach 0.6, 15,000 ft. Altitude, Min Load CA Mode, Loaded Roll

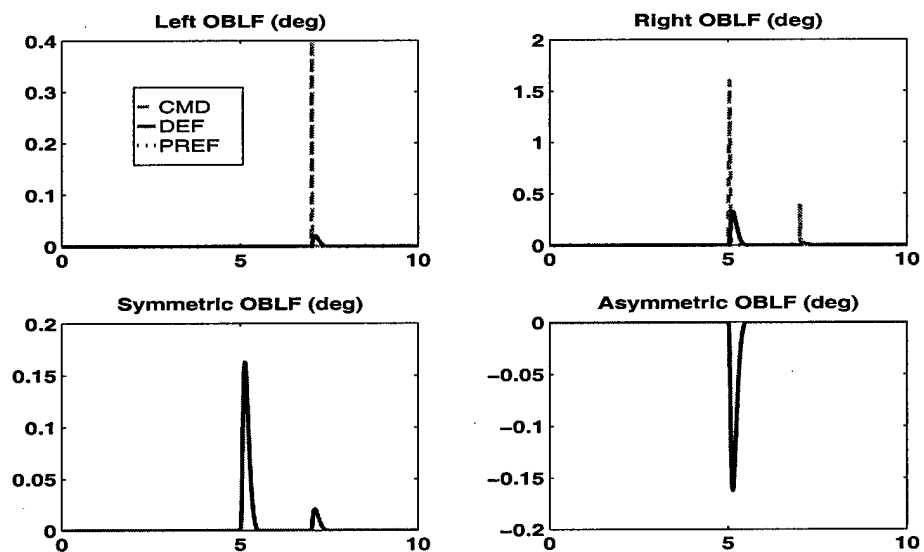


Figure 4.156: Mach 0.6, 15,000 ft. Altitude, Min Load CA Mode, Loaded Roll

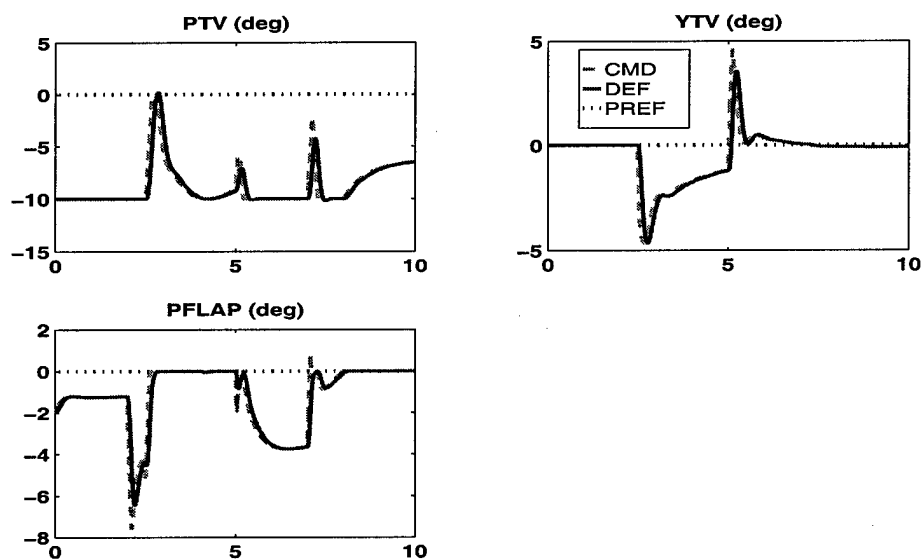


Figure 4.157: Mach 0.6, 15,000 ft. Altitude, Min Load CA Mode, Loaded Roll

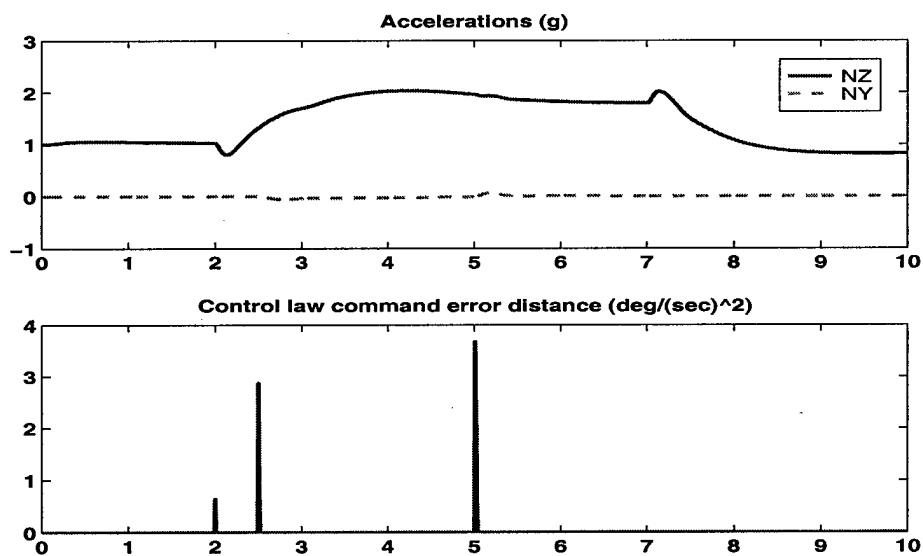


Figure 4.158: Mach 0.6, 15,000 ft. Altitude, Min Load CA Mode, Loaded Roll

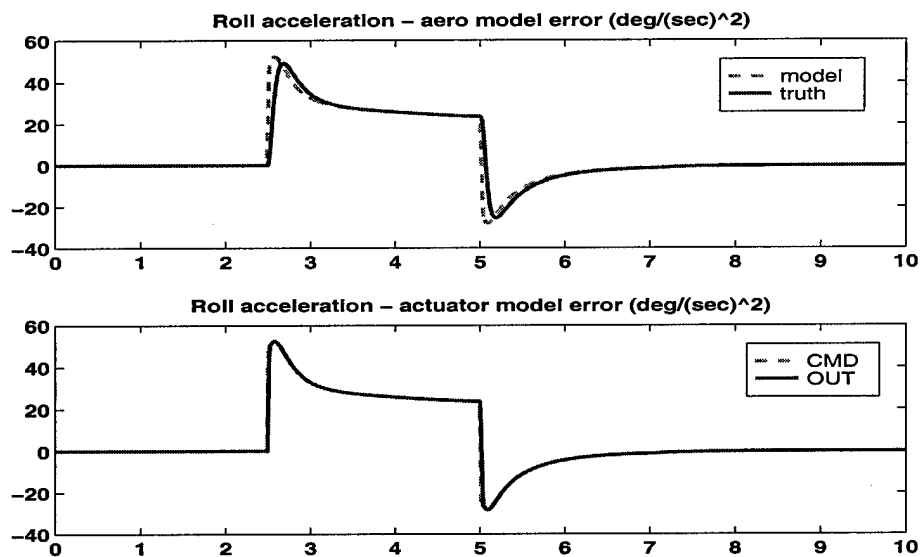


Figure 4.159: Mach 0.6, 15,000 ft. Altitude, Min Load CA Mode, Loaded Roll

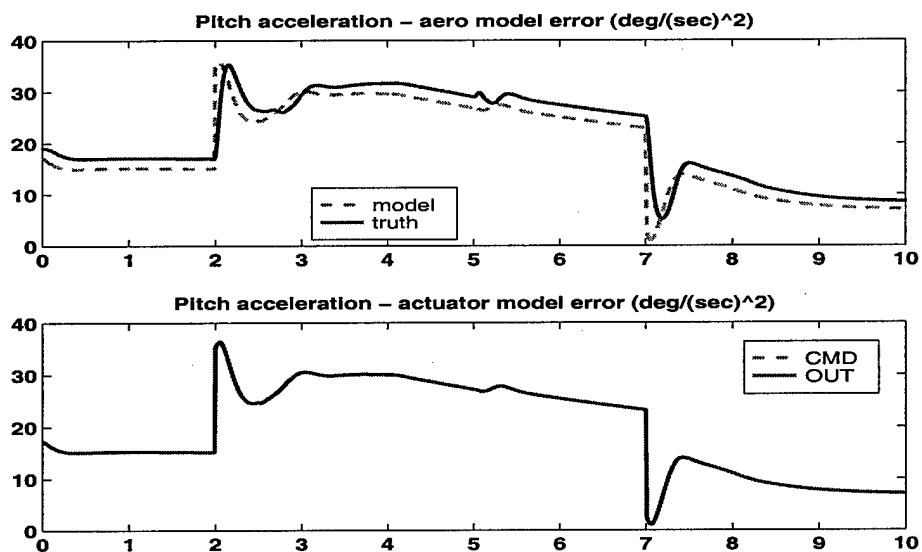


Figure 4.160: Mach 0.6, 15,000 ft. Altitude, Min Load CA Mode, Loaded Roll

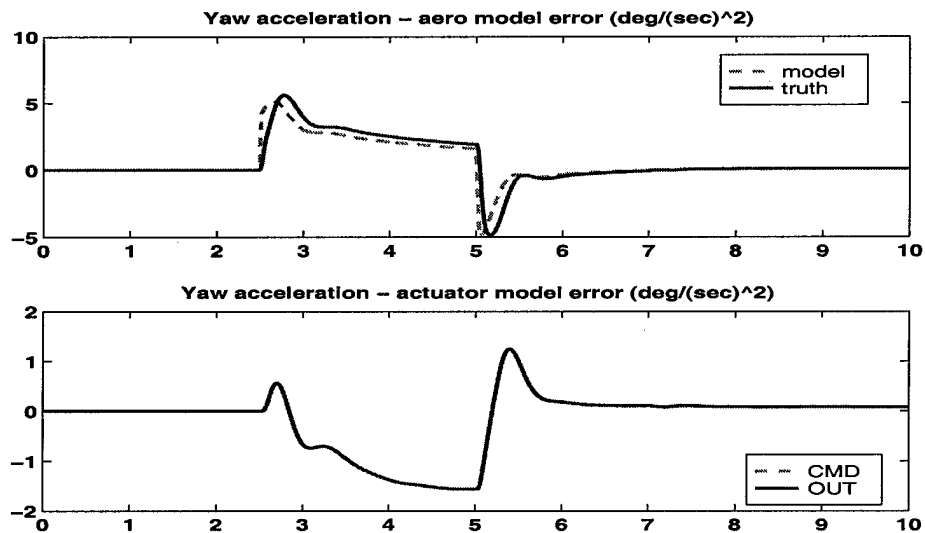


Figure 4.161: Mach 0.6, 15,000 ft. Altitude, Min Load CA Mode, Loaded Roll

The responses in Figs.(4.162)-(4.172) are for the full stick roll maneuver. The lateral command variable tracks the command well, and angle of slip regulation is degraded. Longitudinal and directional coupling caused by aerodynamic model errors degrades command variable regulation. The aerodynamic model errors are due to unmodeled spoiler slot deflector and leading edge flap interactions with the elevons. There are roll acceleration errors due to unmodeled actuator dynamics.

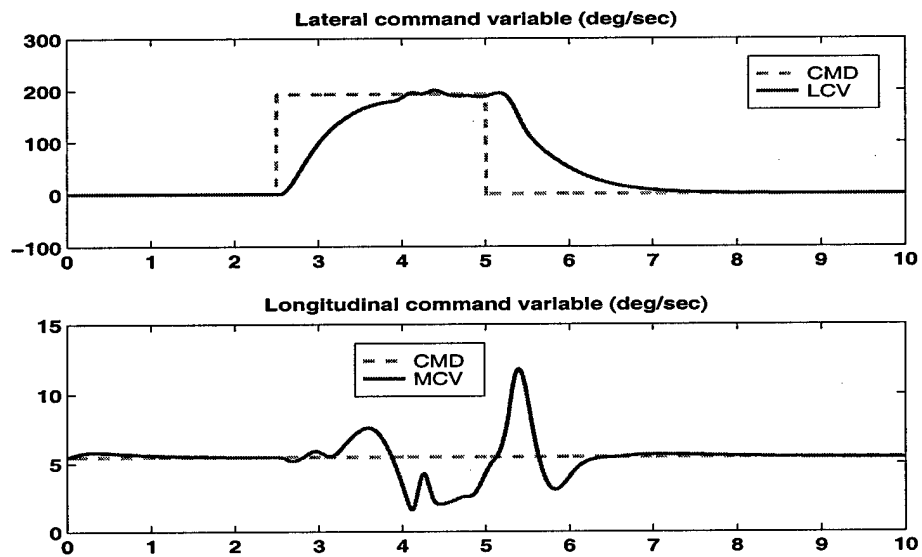


Figure 4.162: Mach 0.6, 15,000 ft. Altitude, Min Load CA Mode, Full Stick Roll

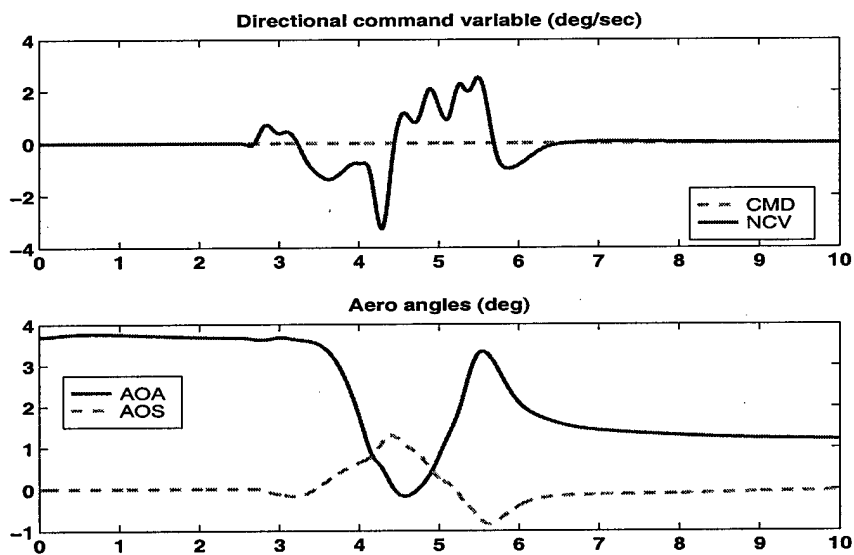


Figure 4.163: Mach 0.6, 15,000 ft. Altitude, Min Load CA Mode, Full Stick Roll

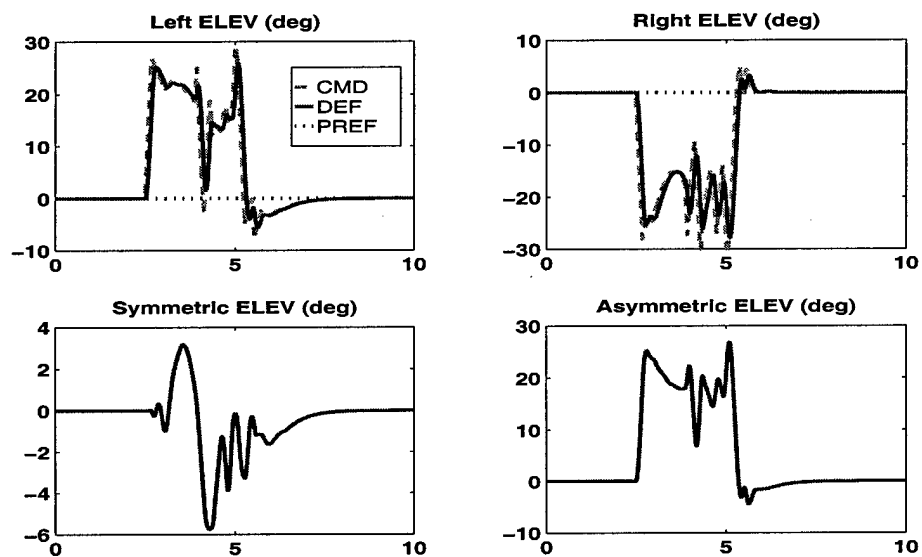


Figure 4.164: Mach 0.6, 15,000 ft. Altitude, Min Load CA Mode, Full Stick Roll

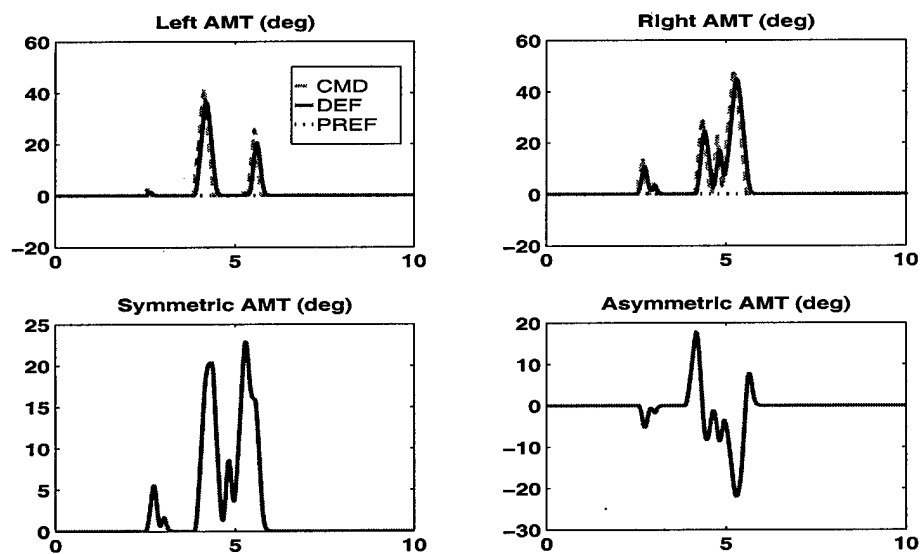


Figure 4.165: Mach 0.6, 15,000 ft. Altitude, Min Load CA Mode, Full Stick Roll

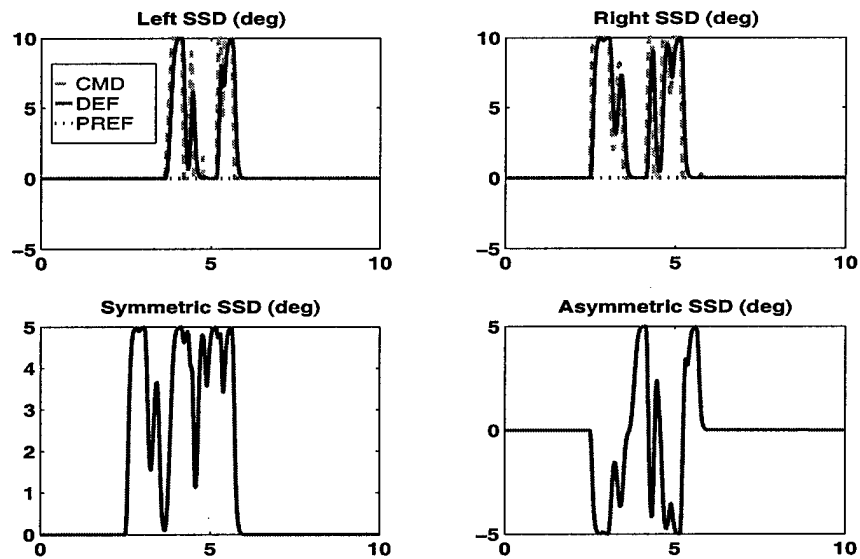


Figure 4.166: Mach 0.6, 15,000 ft. Altitude, Min Load CA Mode, Full Stick Roll

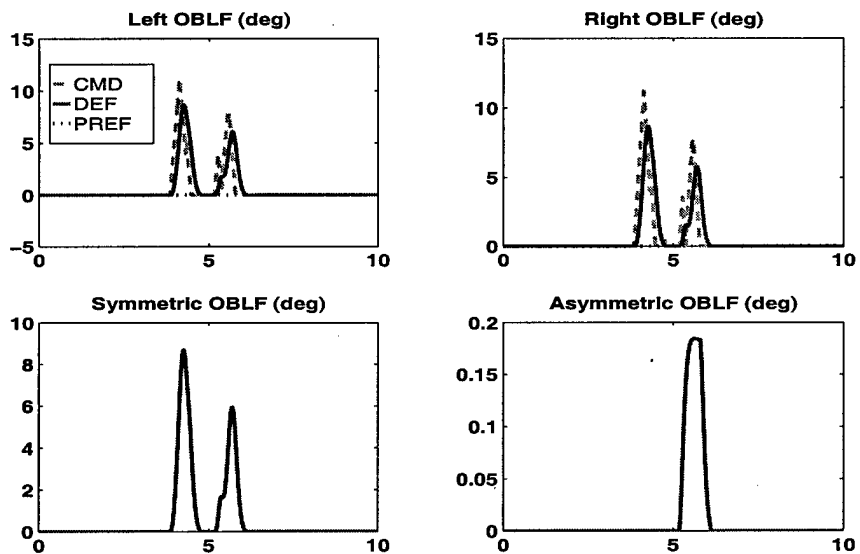


Figure 4.167: Mach 0.6, 15,000 ft. Altitude, Min Load CA Mode, Full Stick Roll

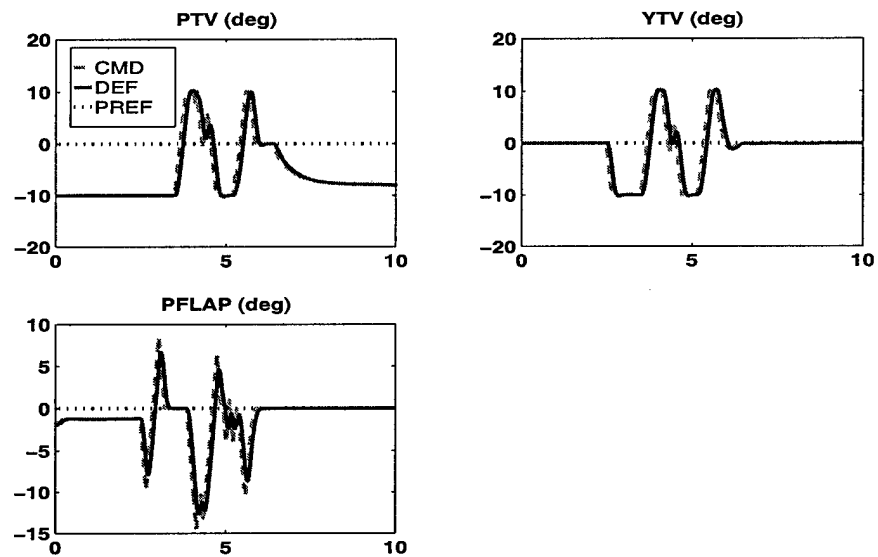


Figure 4.168: Mach 0.6, 15,000 ft. Altitude, Min Load CA Mode, Full Stick Roll

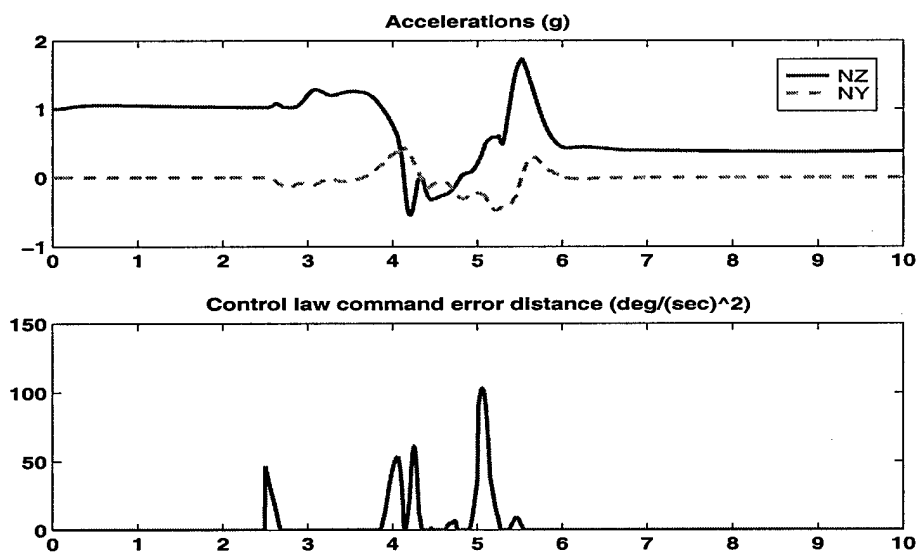


Figure 4.169: Mach 0.6, 15,000 ft. Altitude, Min Load CA Mode, Full Stick Roll

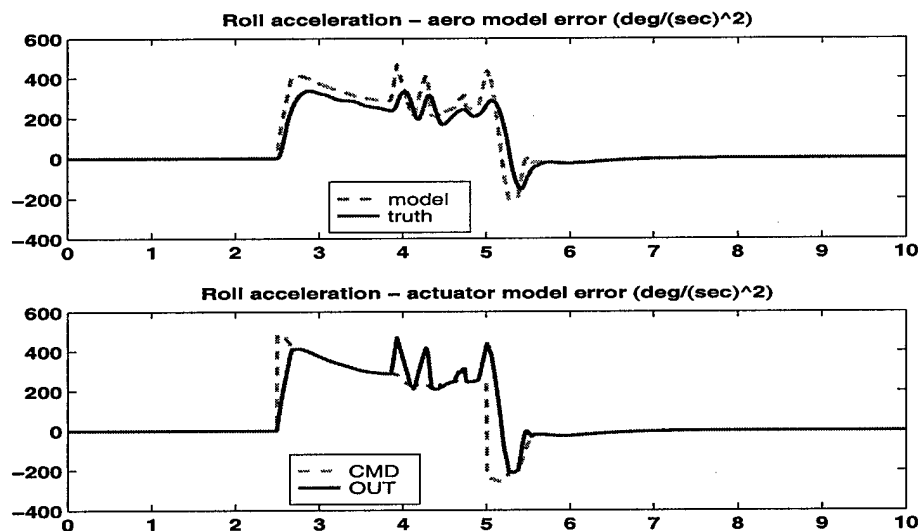


Figure 4.170: Mach 0.6, 15,000 ft. Altitude, Min Load CA Mode, Full Stick Roll

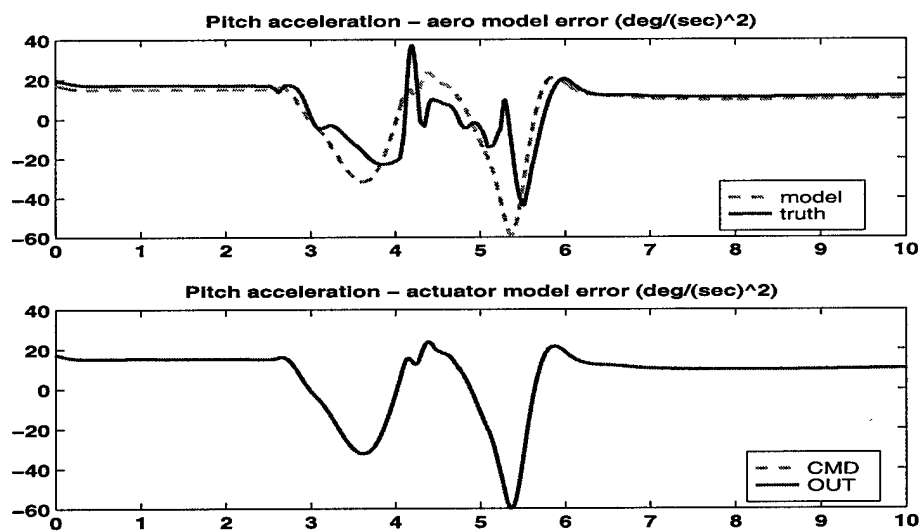


Figure 4.171: Mach 0.6, 15,000 ft. Altitude, Min Load CA Mode, Full Stick Roll

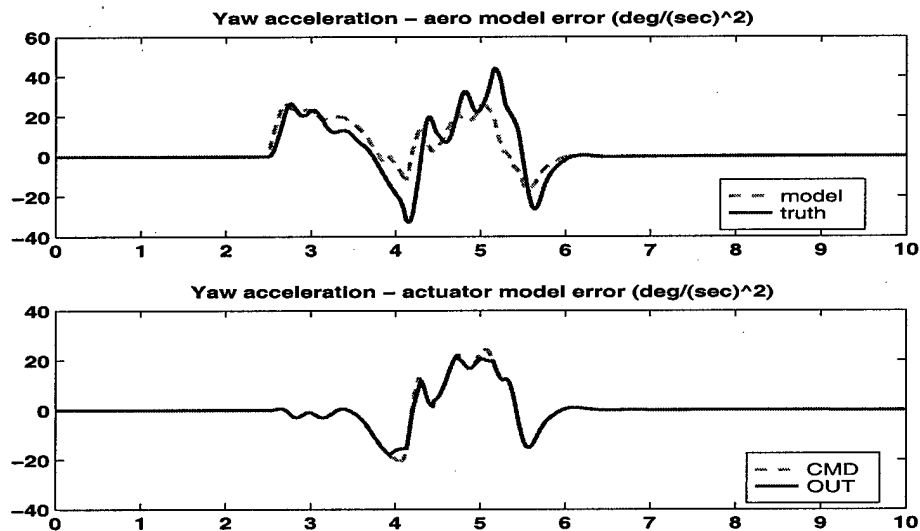


Figure 4.172: Mach 0.6, 15,000 ft. Altitude, Min Load CA Mode, Full Stick Roll

4.5 Piloted simulation

Evaluation of the control laws in a real-time environment have begun to evaluate pilot in the loop properties of the control system. The results from the piloted simulations will appear in a future document.

Chapter 5

Conclusions

A modular flight control architecture was developed that is highly re-usable and allows insertion of technology advances in different aspects of control theory such as control allocation and modeling. Dynamic inversion proved to be a intuitive flight control approach that resulted in excellent nominal stability and command augmentation. Application of dynamic inversion to a tailless fighter required only minor extensions from previous efforts in command variable definitions. The angle of slip gain in the yaw command variable had to be increased, due to the tailless configuration, for sufficient angle of slip attenuation. Robust stability of dynamic inversion was good, but robust performance was slightly deficient. Nonlinear on-board models were required to achieve acceptable control law performance. Refinements to increase on-board airframe model fidelity are still required to achieve improved control law performance. The ICE configuration 101-3 control effector suite of redundant, multi-axis, nonlinear control effectors was challenging. A multi-branch linear program based control allocation algorithm was developed that utilizes all available (affine) control power without violating actuator limits. However, the control affine assumption inherent in the control allocation problem prohibits directly accounting for nonlinearities such as control effector interactions. Spoiler slot deflector and elevon interactions were problematic and solved by limiting spoiler slot deflector deflections. Actuator bandwidth limitations are not accounted for by the control allocation algorithm due to the static nature of the control allocation problem formulation. Neglecting actuator bandwidths became problematic due to inconsistent actuator bandwidths between control effectors. Use of thrust vectoring was restricted at low dynamic pressures due to the low phase crossover frequency of its actuator compared to the aerodynamic effector actuators. The control allocation method easily integrated mission segment objectives, such as minimum drag, and optimized these objectives. Eigenvalue and simulation analysis showed that poorly designed control allocation methods may reduce stability margins or even destabilize the aircraft. An innovative null space injection method was implemented as a control allocation mode to assist in a future reconfiguration capability through adaptation. The injection mode was very successful in that it commanded decorrelated effector positions without degrading aircraft response.

Bibliography

- [1] Adams, R. J., J. M. Buffington, and S. S. Banda, "Design of Nonlinear Control Laws for High Angle-of-Attack Flight," *Journal of Guidance, Control, and Dynamics*, Vol.17, No.4, 1994, pp. 737-746.
- [2] Barron Associates Inc., "Self-Designing Controller Design, Simulation and Flight Test Evaluation," WL-TR-97-3095, May 1996.
- [3] Bennani, S. and Looye, G. H. N., "Design of Flight Control Laws for a Civil Aircraft using μ -synthesis," *AIAA 1998 Guidance, Navigation, and Control Conference*, Boston, MA, Aug 1998, AIAA 98-4133.
- [4] Bodson, M. and Pohlchuck, W. A., "Command Limiting in Reconfigurable Flight Control", *Journal of Guidance, Control, and Dynamics*, Vol 21, No. 4, July-August 1998, pp. 639-646.
- [5] Boeing Phantom Works, "Reconfigurable Systems for Tailless Fighter Aircraft - RESTORE," to appear as Air Force Research Laboratory Technical Report.
- [6] Bowlus, J. A., Multhopp, D. and Banda, S. S., "Challenges and Opportunities in Tailless Aircraft Stability and Control," *AIAA 1997 Guidance, Navigation, and Control Conference*, New Orleans, LA, Aug 1997.
- [7] Brinker, J. S. and Wise K. A., "Reconfigurable Flight Controller for a Tailless Advanced Fighter Aircraft," *AIAA 1998 Guidance, Navigation, and Control Conference*, Boston, MA, Aug 1998, AIAA 98-4107.
- [8] Buffington, J. M., Chandler, P. R. and Pachter, M., "Integration of On-line System Identification and Optimization-based Control Allocation," *AIAA 1998 Guidance, Navigation, and Control Conference*, Boston, MA, Aug 1998, AIAA 98-4487.
- [9] Buffington, J. M. and Sparks A. G., "Synthesis and Analysis of Dynamic Inversion and LPV Tailless Flight Control Law Designs," *AIAA 1998 Guidance, Navigation, and Control Conference*, Boston, MA, Aug 1998, AIAA 98-4248.
- [10] Buffington, J. M., "Tailless Aircraft Control Allocation," *1997 AIAA Guidance, Navigation, and Control Conference*, New Orleans, LA, August 1997, AIAA 97-3605.

- [11] Buffington, J. M., "Control Design and Analysis for Systems with Redundant Limited Controls," Ph.D. Thesis, University of Minnesota, 1996.
- [12] Calise, A. J. and Lee, S., "Direct Adaptive Reconfigurable Control of a Tailless Fighter Aircraft," *AIAA 1998 Guidance, Navigation, and Control Conference*, Boston, MA, Aug 1998, AIAA 98-4108.
- [13] Chandler, P. R., Pachter, M., and Mears, M., "System Identification for Adaptive and Reconfigurable Control", *Journal of Guidance, Control, and Dynamics*, Vol 18, No. 3, May-June 1995, pp. 516-524.
- [14] Doman, D. B., "Interactive Flying Qualities Toolbox for MATLAB User's Guide," WL-TR-95-3070, August 1995.
- [15] Dorsett, K. M. and Mehl, D. R., "Innovative Control Effectors (ICE)," WL-TR-96-3043, January 1996.
- [16] Durham, W. C., "Efficient, Near-Optimal Control Allocation", *Journal of Guidance, Control, and Dynamics*, Vol 22, No. 2, March-April 1999, pp. 369-371.
- [17] Durham, W., J. Bolling, and K. Bordignon, "Minimum Drag Control Allocation," *1996 AIAA Atmospheric Flight Mechanics Conference Proceedings*, San Diego, CA, July 1996, pp.399-407.
- [18] Durham, W. C., "Constrained Control Allocation: Three-Moment Problem," *Journal of Guidance, Control, and Dynamics*, Vol.17, No.2, 1994, pp. 330-336.
- [19] Elgersma, M. and Enns, D., "Parameter Identification for Systems with Redundant Actuators," *AIAA 1998 Guidance, Navigation, and Control Conference*, Boston, MA, Aug 1998, AIAA 98-4110.
- [20] Enns, D., "Control Allocation Approaches," *AIAA 1998 Guidance, Navigation, and Control Conference*, Boston, MA, Aug 1998, AIAA 98-4109.
- [21] Enns, D. F., Bugajski, D. J., Pahle, J. W., Carter, J. F., Antoniewicz, R. F., Regenie, V., "Control Design and Flight Hardware Implementation Experience with Nonlinear Dynamic Inversion Control Laws (NASA-2) for the F/A-18 HARV," *NASA High Angle-of-Attack Technology Proceedings*, June 1998.
- [22] Enns, D., Bugajski, D., Hendrick, R., Stein, G., "Dynamic Inversion: An Evolving Methodology for Flight Control Design," *International Journal of Control*, 1994, Vol. 59, pp. 71-91.
- [23] Fulghum, D. A., "Tailless Designs Touted For New Combat Aircraft," *Aviation Week & Space Technology*, November 11, 1996, McGraw-Hill Companies.

- [24] Glaze, M. and Durham, W. C., "Design and Implementation of a Control Allocation Toolbox for MATLAB V.5.0," *AIAA 1998 Guidance, Navigation, and Control Conference*, Boston, MA, Aug 1998, AIAA 98-4436.
- [25] Honeywell Technology Center, "Application of Multivariable Control Theory to Aircraft Control Laws, Final Report: Multivariable Control Design Guidelines," WL-TR-96-3099, May 1996.
- [26] Khalil, H. K., Nonlinear Systems, Macmillan Publishing Company, New York, 1992.
- [27] Kim, S. G and Tahk, M. J., "Output-redefinition Based on Robust Zero Dynamics," *AIAA 1998 Guidance, Navigation, and Control Conference*, Boston, MA, Aug 1998, AIAA 98-4493.
- [28] Schumacher, C. J., "Adaptive Flight Control Using Dynamic Inversion and Neural Networks", *Proceedings from the 1999 AIAA Guidance, Navigation, and Control Conference*, Portland, OR, August 1999, to appear.
- [29] Smith, Capt. L., Chandler, P. and Pachter, M., "Regularization Techniques for Real-Time Identification of Aircraft Parameters," *AIAA 1997 Guidance, Navigation, and Control Conference*, New Orleans, LA, Aug 1997.
- [30] Virnig, J. C. and D. S. Bodden, "Multivariable Control Allocation and Control Law Conditioning when Control Effectors Limit," *Proceedings from the 1994 AIAA Guidance, Navigation, and Control Conference*, Scottsdale, AZ, August 1994, pp.572-582.